ISSN 0915-633X

NATIONAL INSTITUTE FOR FUSION SCIENCE

Turbulence Theories and Modelling of Fluids and Plasmas

A. Yoshizawa, S.-I. Itoh, K. Itoh and N. Yokoi

(Received - Apr. 10, 2001)

NIFS-691 Apr. 2001

RESEARCH REPORT
NIFS Series

TOKI, JAPAN

Turbulence Theories and Modelling of Fluids and Plasmas

Akira Yoshizawa†, Sanae-I Itoh‡. Kimitaka Itoh¶, and Nobumitsu Yokoi†

† Institute of Industrial Science. University of Tokyo, Komaba. Meguro-ku, Tokyo 153-8505, Japan

‡ Research Institute for Applied Mechanics. Kyushu University, 87, Kasuga 816-8580, Japan

¶ National Institute for Fusion Science. Toki. Gifu 509-529, Japan

Abstract. Theoretical and heuristic modelling methods are reviewed for studying turbulence phenomena of fluids and plasmas. Emphasis is put on understanding of effects on turbulent characteristics due to inhomogeneities of field and plasma parameters. The similarity and dissimilarity between the methods for fluids and plasmas are sought in order to shed light on the properties that are shared or not by fluid and plasma turbulence.

Keywords: turbulence, MHD turbulence, statistical theory, turbulence modelling, dynamo, MHD flow, plasma turbulence, anomalous transport, structural formation, bifurcation,improved confinement, nonlinear waves, zonal flow and streamer, turbulence suppression, far-nonequilibrium physics

Contents

1. General Introduction

The theoretical study of turbulence in electrically non-conducting fluids has been undergone a development very different from its counterpart of plasma turbulence. In fluid flows, the growth of disturbances imposed on the laminar state of each flow is investigated on the basis of linear and nonlinear stability analyses [1.1, 1.2]. In those analyses, the effects of global boundary conditions such as wall boundaries often play an important role. compared with stability analyses of plasma micro-instabilities. In the case that the laminar state is unstable, it is not rare that initial small disturbances rapidly revolve into a fully-developed turbulent state. In the presence of a solid wall, a steep gradient of velocity is generated there, and this inhomogeneity of the velocity field plays an important role of supplying small-scale components of flow with energy [1.3, 1.4]. The fully developed state of turbulence is sustained by the continuous supply of energy, for instance, through the imposition of pressure. In this situation, the fully developed state of turbulence may be studied in distinct separation from the initial stage of growing disturbances.

In the history of the theoretical study of turbulence. much attention has been paid to homogeneous, isotropic turbulence free from a spatially-varying mean flow [1.5, 1.6]. Such turbulence is ideal and is difficult to realize in laboratory experiments. The flow state similar to isotropic turbulence may be observed in the small-scale components of motion in atmospheric and oceanic flows. Especially. the famous $-5/3$ power law for the energy spectrum, which is derived with the aid of the concept of the inertial range, is a primary target of the theoretical study of turbulence, greatly contributing to the formulation of statistical theoretical approaches. In other words, the structural simplicity intrinsic to isotropic fluid turbulence has greatly helped the development of turbulence theory.

A big incentive for developing an inhomogeneous-turbulence theory on the basis of the accomplishments of isotropic-turbulence theories is turbulence modelling [1.7]. In the study of real-world turbulent flows, the non-dimensional parameters such as the Reynolds number are very large, and a computer experiment based on the direct use of the fluid equations is not possible. As a result, the small-scale components of turbulent motion are eliminated, and their effects are taken into account through the concept of turbulent or renormalized viscosity etc. This procedure is called turbulence modelling, which is a very useful tool in the study of flows encountered in engineering and sciences, but its applicability is not sufficient in the presence of a three-dimensional mean flow. A systematic approach to the study of inhomogeneous turbulence is indispensable for improving the current turbulence models and constructing new turbulence models. This situation has stimulated the study of inhomogeneous-turbulence theory.

In contrast to fluid turbulence, the fully-developed state of plasma turbulence is

not always a matter of theoretical concern, specifically, in fusion plasma, for such a state is what is to be avoided for efficient plasma confinement. Then the primary target of the theoretical study of plasma turbulence is the stage of instability growth and the following highly nonlinear regime subject to strong inhomogeneity. Turbulence in plasmas has several characteristic features. One is that the fluctuation level becomes high through the instabilities driven due to the inhomogeneity. The turbulent level and spectrum are highly influenced by the spatial inhomogeneity and plasma configuration. Inhomogeneities exist for plasma parameters (e.g., density and temperature) as well as for the fields (e.g., magnetic field and radial electric field). These inhomogeneities couple so as to drive and/or suppress instabilities and turbulent fluctuations. In particular, the anisotropy along and perpendicular to the strong magnetic field induces a variety in the nature of possible fluctuations: fluctuations often have a very long correlation length along the magnetic-field line and are quasi-two-dimensional. In addition, mobilities of electrons and ions differ prominently. The inhomogeneities, the anisotropy due to the strong magnetic field, and the difference of ion and electron mobilities have strong influences on the linear properties of plasma waves as well as on the turbulent transport in the plasma. In many cases, instabilities develop into strong turbulence, so that the decorrelation rate caused by the nonlinear interactions is usually of the same order of or much larger than the damping rate (growth rate) of the linear eigenmode. A theoretical method developed for fluid turbulence is helpful for the study of these phenomena. In some cases, on the other hand, only a few modes are excited, and an analysis based on the weak turbulence suffices.

In the quest of understanding anomalous transport in confined plasmas, investigation of turbulent fluctuations has been a central theme [1.8-1.13]. In particular, after finding the H-mode in ASDEX tokamak [1.14], it has been widely recognized that the plasma profile could have a variety of forms, and changes between them occur as sudden transitions (see reviews of experimental observations [1.15-1.21]). One of the keys to understanding the structural formation and transitions in plasmas is the study of mutual interactions of the plasma inhomogeneity, electric-field structure, and fluctuations. Advances of theories in this direction have been reported in a series of reviews [1.22-1.34] and in a monograph [1.35]. It is emphasized that this theoretical progress is based upon the development of turbulence theories in fluids and plasmas. It is necessary and timely to survey the basis and recent development of turbulence theories in order to establish a perspective for the future research of turbulence, turbulent transport and structural formation.

In this review article, we illustrate both the characteristics that fluid and plasma turbulence have in common and those that are different. The article is organized as follows. In §2, we give the fundamental equations for electrically non-conducting and conducting fluids and for plasma, as well as their reduced sets. In §3, we

give a review of the theoretical approaches to homogeneous turbulence and the phenomenological methods for inhomogeneous turbulence, that is, turbulence modelling. An inhomogeneous turbulence theory is explained in relation to the theoretical derivation of turbulence models. The approach to electrically non-conducting fluid is extended to magnetohydrodynamic flow, and the turbulent dynamo is discussed in the context of astronomy and fusion. In §4, various theoretical approaches to plasma turbulence are illustrated with examples of applications. Emphasis is put on the way in which turbulence theory is applied to systems composed of components with different mobility due to strong inhomogeneity and anisotropy. The connection with the current fluid-turbulence theories is also sought for shedding light on the similarity and differences between fluid and plasma turbulence. A summary is presented in §5.

References

[1.1] Chandrasekhar S 1961 *Hydrodynamic and Hydrodynamic Stability* (New York: Dover)

[1.2] Drazin P G and Reid W H 1981 *Hydrodynamic Stability* (Cambridge: Cambridge University)

[1.3] Hinze J O 1975 *Turbulence* (New York: McGraw-Hill)

[1.4] Tennekes H and Lumley J L 1972 *A first Course in Turbulence* (Cambridge: The MIT)

[1.5] Leslie D C 1973 *Developments in the Theory of Turbulence* (Oxford: Clarendon)

[1.6] McComb W D 1990 *The Physics of Fluid Turbulence* (Oxford: Clarendon)

[1.7] Yoshizawa A 1998 *Hydrodynamic and Magnetohydrodynamic Turbulent Flows: Modelling and Statistical Theory* (Dordrecht: Kluwer)

[1.8] Yoshikawa S 1970 in *Methods of Experimental Physics* (ed. Griem H R, Loveberg R H, New York: Academic) vol 9, chap 8

[1.9] Liewer P C 1985 Nucl. Fusion **25** 543

[1.10] Fonck R J et al. 1992 Plasma Phys. Contr. Fusion **34** 1993

[1.11] Wootton A et al. 1992 Plasma Phys. Contr. Fusion **34** 2030

[1.12] Wagner F and Stroth U 1993 Plasma Phys. Contr. Fusion **35** 1321

[1.13] Stroth U 1998 Plasma Phys. Contr. Fusion **40** 9

[1.14] Wagner F et al. 1982 Phys. Rev. Lett. **49** 1408

[1.15] ASDEX Team 1989 Nucl. Fusion **29** 1959

[1.16] Stambaugh R D et al. 1990 Phys. Fluids B **2** 2941

[1.17] Groebner R J 1993 Phys. Fluids B **5** 2343

[1.18] Zohm H 1996 Plasma Phys. Contr. Fusion **38** 105

[1.19] Burrel K H 1997 Phys. Plasmas **4** 1499

[1.20] Ida K 1998 Plasma Phys. Contr. Fusion **40** 1429

[1.21] Fujisawa A 2000 J. Plasma Fusion Res. **76** 335 (in Japanese)

[1.22] Itoh K 1994 Plasma Phys. Contr. Fusion **36** A307

[1.23] Itoh S-I et al. 1995 J. Nucl. Materials **220-222** 117

[1.24] Connor J W 1995 Plasma Phys. Contr. Fusion **37** A119

[1.25] Itoh K and Itoh S-I 1996 Plasma Phys. Contr. Fusion **38** 1

[1.26] Rozhansky Y and Tendler M 1996 Plasma Rotation in Tokamaks in *Reviews of Plasma Physics* (ed. Kadomtsev B B, New York: Consultants Bureau) vol 19, p 147

[1.27] Carreras B A 1997 IEEE Trans. on Plasma Science **25** 1281
[1.28] Staebler G M 1998 Plasma Phys. Contr. Fusion **40** 569
[1.29] Wakatani M 1998 Plasma Phys. Contr. Fusion **40** 597
[1.30] Connor J W 1998 Plasma Phys. Contr. Fusion **40** 531
[1.31] Krommes J A 1999 Plasma Phys. Contr. Fusion **41** A641
[1.32] Connor J W and Wilson H R 2000 Plasma Phys Contr. Fusion **42** R1
[1.33] Terry P W 2000 Rev. Mod. Phys. **72** 109
[1.34] Krommes J A 2001 "Fundamental statistical theories of plasma turbulence in magnetic fields." Phys. Reports in press
[1.35] Itoh K, Itoh S-I and Fukuyama A 1999 *Transport and Structural Formation in Plasmas* (Bristol: IOP)

2. Fundamentals of Fluid and Plasma Motion

2.1. Fluid Equations

2.1.1. Equations for electrically non-conducting fluids The motion of an electrically non-conducting fluid may be described by the conservation laws for the mass, momentum, and internal energy [2.1]:

$$\frac{\partial \rho}{\partial t} + \nabla \cdot (\rho \mathbf{V}) = 0, \tag{2.1}$$

$$\frac{\partial}{\partial t}\rho V_i + \frac{\partial}{\partial x_j}\rho V_i V_j = \rho K_i - \frac{\partial p}{\partial x_i} + \frac{\partial}{\partial x_j}\left[\mu_{\mathrm{f}}\left(\frac{\partial V_j}{\partial x_i} + \frac{\partial V_i}{\partial x_j} - \frac{2}{3}\nabla \cdot \mathbf{V}\delta_{ij}\right) + \mu_{\mathrm{b}}\nabla \cdot \mathbf{V}\delta_{ij}\right]. \tag{2.2}$$

$$\frac{\partial}{\partial t}\rho C_V \theta + \nabla \cdot (\rho C_V \theta \mathbf{V}) = \nabla \cdot (\mu_\theta \nabla \theta) - p\nabla \cdot \mathbf{V} + \Phi_{\mathrm{D}}. \tag{2.3}$$

Here ρ is the mass density, $\mathbf{V}$ is the velocity, $\mathbf{K}$ is the external force per unit mass, p is the pressure, μ_{f} is the viscosity, μ_{b} is the bulk viscosity, θ is the temperature, C_V is the specific heat at constant volume, μ_θ is the heat conductivity, and Φ_{D} is the dissipation function expressing the conversion rate of kinetic to thermodynamic energy per unit volume (its details are omitted here). The summation convention is applied to repeated subscripts. Equation (2.2) is specifically called the Navier–Stokes equation. In order to close the system of Eqs. (2.1)-(2.3), we need a thermodynamic relation connecting ρ, p, and θ. For a perfect gas, it is given by

$$p = \rho(\gamma - 1) C_V \theta, \tag{2.4}$$

where γ is the ratio of C_P (the specific heat at constant pressure) to C_V.

In §3 devoted to fluid turbulence, we shall focus attention on the incompressible case and neglect the spatial variation of ρ, μ_{f}, and μ_θ. In this case, the foregoing system of equations is reduced to

$$\nabla \cdot \mathbf{V} = 0. \tag{2.5}$$

$$\left(\frac{\partial}{\partial t} + \mathbf{V} \cdot \nabla\right)\mathbf{V} = \mathbf{K} - \nabla p + \nu \nabla^2 \mathbf{V}, \tag{2.6}$$

$$\left(\frac{\partial}{\partial t} + \mathbf{V} \cdot \nabla\right)\theta = \kappa \nabla^2 \theta, \tag{2.7}$$

where $\nu (= \mu_{\mathrm{f}}/\rho)$ is the kinematic viscosity, and $\kappa [= \mu_\theta/(\rho C_V)]$ is the thermal diffusivity. Here and hereafter, p/ρ in incompressible flow is simply denoted by p.

In the presence of the buoyancy force $\rho\mathbf{g}$ as an external force, Eq. (2.6) is replaced with

$$\left(\frac{\partial}{\partial t}+\mathbf{V}\cdot\nabla\right)\mathbf{V}=-\nabla\left(p+\varphi\right)-\alpha_{\rm th}\left(\theta-\theta_R\right)\mathbf{g}+\nu\nabla^2\mathbf{V}, \tag{2.8}$$

under the Boussinesq approximation in which the change of density is taken into account through the buoyancy force only [2.2]. Here φ is the gravitational potential ($\mathbf{g}=-\nabla\varphi$), $\alpha_{\rm th}$ is the thermal expansion coefficient, and θ_R is the reference temperature. The Boussinesq approximation may be interpreted from a different viewpoint. For $\rho=\rho(\theta,p)$, we have $\delta\rho=(\partial\rho/\partial\theta)_p\delta\theta+(\partial\rho/\partial p)_\theta\delta p$, which indicates that the approximation corresponds to the case of large Young's modulus.

2.1.2. Magnetohydrodynamic equations As an application of the theoretical approach to magnetohydrodynamic flow, we shall discuss the turbulent dynamo or the generation mechanism of magnetic fields due to electrically conducting turbulent flow. We shall also refer to the occurrence of flow by magnetic effects. In these discussions, we shall neglect effects of fluid compressibility to concentrate on the fundamental aspects of dynamo processes, and adopt Alfvén velocity units.

The magnetohydrodynamic (MHD) system of equations consists of the incompressible Navier-Stokes equation with the Lorentz force added [2.3],

$$\left(\frac{\partial}{\partial t}+\mathbf{V}\cdot\nabla\right)\mathbf{V}=-\nabla p+\mathbf{J}\times\mathbf{B}+\nu\nabla^2\mathbf{V}, \tag{2.9}$$

the magnetic induction

$$\frac{\partial\mathbf{B}}{\partial t}=-\nabla\times\mathbf{E}, \tag{2.10}$$

and the Ampère law combined with the Ohm's law,

$$\mathbf{J}=\nabla\times\mathbf{B}=(1/\eta)\left(\mathbf{E}+\mathbf{V}\times\mathbf{B}\right). \tag{2.11}$$

where $\mathbf{B}$ is the magnetic field, $\mathbf{J}$ is the electric current density, $\mathbf{E}$ is the electric field, and $\eta[=1/(\sigma\mu_0)]$ is the magnetic diffusivity (σ is the electric conductivity, and μ_0 is the magnetic permeability). In Alfvén velocity units, the original magnetic field, electric current, and electric field are divided by $\sqrt{\rho\mu_0}$, $\sqrt{\rho/\mu_0}$, and $\sqrt{\rho\mu_0}$, respectively.

2.2. Plasma Equations

2.2.1. Fluid picture One distinct feature of plasma as a continuous media is that the responses of electrons and ions are not identical so as to induce a collective electromagnetic field in it. The dynamical equations of plasma in the fluid limit are usually constructed by use of the two-fluid picture. In addition, inhomogeneities

often exist in plasma number density, pressure and velocity, and they have important roles in the evolution of turbulence. Therefore various plasma quantities together with electromagnetic fields must be simultaneously calculated to understand the turbulence dynamics in plasmas. The number of relevant variables is much larger than in the case of neutral-fluid turbulence. The large number of independent variables is one of the reason why a variety of processes could occur in turbulent plasmas.

A representative set of equations is the Braginskii equations [2.4]. In this set of equations, variables are chosen as density n_s, velocity $\mathbf{v}_s$ and temperature T_s for each species ($s = \mathrm{i}, \mathrm{e}$). The higher order moments, i.e., the fluxes of number density, momentum, and energy [$\mathbf{\Gamma}_s$, $\mathbf{\Pi}_s^{\mathrm{d}}$, and $\mathbf{q}_s$, where the superscript d stands for the deviatric part (traceless part)] and the exchanges of momentum and energy between different species, $\mathbf{R}_{\mathrm{ei}}$ and Q_s, are expressed in terms of n_s, $\mathbf{V}_s$ and T_s, i.e., the flux–gradient relations are given. Explicit formula for the flux–gradient relation are given in [2.4] and are not reproduced here. These flux–gradient relations are the closure equations for deducing the fluid equations from kinetic equations. Two-fluid equations are:

$$\frac{\partial}{\partial t} n_s + \nabla \cdot (n_s \mathbf{V}_s) = 0 \quad (s = \mathrm{i}, \mathrm{e}), \tag{2.12a}$$

$$n_{\mathrm{i}} m_{\mathrm{i}} \frac{d}{dt} \mathbf{V}_{\mathrm{i}} - e_{\mathrm{i}} n_{\mathrm{i}} (\mathbf{E} + \mathbf{V}_{\mathrm{i}} \times \mathbf{B}) + \nabla p_{\mathrm{i}} + \nabla \cdot \mathbf{\Pi}_{\mathrm{i}}^{\mathrm{d}} = -\mathbf{R}_{\mathrm{ei}}, \tag{2.12b}$$

$$n_{\mathrm{e}} m_{\mathrm{e}} \frac{d}{dt} \mathbf{V}_{\mathrm{e}} + e n_{\mathrm{e}} (\mathbf{E} + \mathbf{V}_{\mathrm{e}} \times \mathbf{B}) + \nabla p_{\mathrm{e}} + \nabla \cdot \mathbf{\Pi}_{\mathrm{e}}^{\mathrm{d}} = \mathbf{R}_{\mathrm{ei}}, \tag{2.12c}$$

$$\frac{3}{2} n_s \frac{d}{dt} T_s + p_s \nabla \cdot \mathbf{V}_s = -\nabla \cdot \mathbf{q}_s - \mathbf{\Pi}_s^{\mathrm{d}} : \nabla \mathbf{V}_s + Q_s \quad (s = \mathrm{i}, \mathrm{e}) \tag{2.12d}$$

(see [2.5] for details). Combining these equations with the Maxwell equations

$$\epsilon_0 \nabla \cdot \mathbf{E} = \sum_{s=\mathrm{i,e}} e_s n_s, \tag{2.13}$$

$$\nabla \times \mathbf{B} - \frac{1}{c^2} \frac{\partial}{\partial t} \mathbf{E} = \mu_0 \mathbf{J} = \mu_0 \sum_{s=\mathrm{i.e}} e_s n_s \mathbf{V}_s, \tag{2.14}$$

$$\frac{\partial}{\partial t} \mathbf{B} = -\nabla \times \mathbf{E}, \tag{2.15}$$

the dynamics of plasma and electromagnetic field are described.

As will be seen in the following, there are a variety of plasma dynamics with different characteristic time scales and length scales. Therefore, the choice of normalization unit [e.g., the Alfvén unit in MHD equations Eqs. (2.9)-(2.11)] may not be unique for plasma turbulence. Instead, characteristic scales are chosen case by case in order to easily understand complicated plasma dynamics. Therefore plasma equations in this review will be either expressed with explicit dimensions or normalized to convenient units depending on the problems.

2.2.2. Reduced set of equations The set of two-fluid equations is deduced from kinetic equation in a collisional limit. Some processes, which could be important in real plasmas, e.g., Landau damping, are neglected. Nevertheless, it is a set of nonlinear equations with thirteen independent variables and is still too complicated. For further analytic transparency in investigations, various efforts have been made for a further reduction of variables. There are several characteristic wave frequencies in MHD equations: the compressional Alfvén wave, the shear Alfvén wave, and the ion sound wave. The compressional Alfvén wave has high frequency, so that it is decoupled by use of the time-scale separation. (The temporal change of magnitude of the strong magnetic field is neglected.) Eliminating the high frequency oscillation associated with the compressional Alfvén wave, simplified models have been proposed to analyze the nonlinear evolution of global MHD instabilities in tokamaks [2.6-2.8]. This method is also extended to cover the cases of pressure-gradient-driven turbulence, electrostatic perturbations, or microscale fluctuations. Various reduced sets of equations have been derived. Some of them are:

(1) Yagi–Horton; seven-field model [2.9]

(2) Romaneli–Zonca; six-field model [2.10]

(3) Drake–Antonsen; five-field model [2.11]

(4) Hazeltine; four-field model [§7.4 of 2.12]

(5) Strauss; three-field model [2.13], [2.14]

(6) Itoh et al.; electron inertial three-field model [2.15]

(7) Rosenbluth et al.; MHD two-field model [2.8]

(8) Hasegawa–Wakatani; two-field model [2.16]

(9) Hasegawa–Mima; one-field model [2.17]

Examples of reduced sets of equations are briefly illustrated. The conservation properties of equations are discussed in §4.1.4.

A Yagi–Horton equations For the study of low frequency and pressure-gradient driven turbulence, Yagi et al. have proposed a seven-field model of plasma dynamics [2.9]. As independent variables, density ($n = n_e = e_i e^{-1} n_i$ is assumed), electrostatic potential ϕ, stream function Φ, ion velocity in the direction of the magnetic field $v_\parallel$, vector potential in the direction of the magnetic field, $A_\parallel$, electron and ion pressures, p_e and p_i, are chosen. A set of equations for variables $(n, \phi, \Phi, v_\parallel, p_e, p_i, A_\parallel)$ are given as

$$\frac{d}{dt} n + n \nabla \cdot \mathbf{V} = 0, \qquad \text{continuity} \qquad (2.16a)$$

$$\nabla_\perp \cdot \left(\frac{n m_\mathrm{i}}{B} \frac{d}{dt} \frac{1}{B} \nabla_\perp \Phi \right) = \nabla_\parallel J_\parallel + \nabla_\perp \cdot \left\{ \frac{\mathbf{B}}{B} \times \left[\nabla_\perp (p_\mathrm{e} + p_\mathrm{i}) + \nabla_\perp \cdot \mathbf{\Pi}_\mathrm{i}^\mathrm{d} \right\} \right),$$

equation of motion (2.16b)

$$n m_\mathrm{i} \frac{d}{dt} v_\parallel + \nabla_\parallel (p_\mathrm{e} + p_\mathrm{i}) + \hat{\mathbf{b}} \cdot \nabla_\perp \cdot \mathbf{\Pi}_\mathrm{i}^\mathrm{d} = 0,$$

equation of motion (2.16c)

$$-\frac{\partial}{\partial t} A_\parallel - \nabla_\parallel \varphi + \frac{1}{en} \nabla_\parallel p_\mathrm{e} = \eta_\parallel J_\parallel - \frac{0.71}{e} \nabla_\parallel T_\mathrm{e},$$

Ohm's law (2.16d)

$$\mathbf{J}_\perp = \frac{\mathbf{B}}{B} \times \left[\nabla (p_\mathrm{e} + p_\mathrm{i}) + \nabla \cdot \mathbf{\Pi}_\mathrm{i}^\mathrm{d} \right] - \frac{n m_\mathrm{i}}{B} \frac{d}{dt} \nabla_\perp \Phi,$$

drift motion (2.16e)

$$\frac{3}{2} \frac{\partial}{\partial t} p_\mathrm{i} + \frac{3}{2} \nabla_\perp \cdot (p_\mathrm{i} \mathbf{V}) + p_\mathrm{i} \nabla \cdot \mathbf{V} = -\nabla \cdot \mathbf{q}_\mathrm{i} + Q_\mathrm{i} - \mathbf{\Pi}_\mathrm{i}^\mathrm{d} : \nabla \mathbf{V},$$

ion energy balance (2.16f)

$$\frac{3}{2} \frac{\partial}{\partial t} p_\mathrm{e} + \frac{3}{2} \nabla_\perp \cdot \left[p_\mathrm{e} \left(\mathbf{V} - \frac{1}{en} \mathbf{J} \right) \right] + p_\mathrm{e} \nabla \cdot \left(\mathbf{V} - \frac{1}{en} \mathbf{J} \right) = -\nabla \cdot \mathbf{q}_\mathrm{e} + Q_\mathrm{e},$$

electron energy balance (2.16g)

where the Lagrange derivative

$$\frac{d}{dt} = \frac{\partial}{\partial t} + \mathbf{V} \cdot \nabla \tag{2.17}$$

is used, $\hat{\mathbf{b}} = \mathbf{B}/B$ ($B = |\mathbf{B}|$). In this set of equations, the velocity and current are expressed in terms of $(n, \phi, \Phi, v_\parallel, p_\mathrm{e}, p_\mathrm{i}, A_\parallel)$ as

$$\mathbf{V} = \frac{\hat{\mathbf{b}} \times \nabla_\perp \Phi}{B} + v_\parallel \hat{\mathbf{b}}, \tag{2.18a}$$

$$J_\parallel = -\nabla_\perp^2 A_\parallel, \tag{2.18b}$$

and the relation between stream function Φ and potential ϕ is given as

$$\nabla_\perp \Phi - \nabla_\perp \phi - \frac{1}{en} (\mathbf{J}_\perp \times \mathbf{B} - \nabla_\perp p_\mathrm{e}) = \eta_\perp \mathbf{J}_\perp + \frac{3}{2} \frac{1}{e \omega_\mathrm{ce} \tau_\mathrm{e}} \hat{\mathbf{b}} \times \nabla_\perp T_\mathrm{e}.$$

perpendicular Ohm's law (2.18c)

With the help of the flux-gradient relations, that describe $\mathbf{\Pi}_\mathrm{i}^\mathrm{d}$, $\mathbf{q}_\mathrm{e}$, $\mathbf{q}_\mathrm{i}$, Q_e, Q_i, $\eta_\parallel$ and $\eta_\perp$ [2.4], Eqs. (2.16)-(2.18) form a closed set of equations that describes low frequency turbulence in inhomogeneous plasmas. ($\eta_\parallel$ and $\eta_\perp$: resistivity in the direction to $\hat{\mathbf{b}}$ and

that perpendicular to $\hat{\mathbf{b}}$, respectively. ω_{ce}: electron cyclotron frequency, τ_e: electron collision frequency).

The Yagi–Horton equation could describe a wide variety of plasma turbulence. Depending on the subject of the analysis, a much simpler version of reduced set of equations is employed.

B Hasegawa–Mima equation The investigation of nonlinearity of $E \times B$ motion is the central subject of plasma turbulence. The study has been performed for electrostatic perturbations by keeping only one variable. The static potential ϕ is chosen as the relevant variable.

A simple model of a two-dimensional magnetized plasma is that charged elements move with the guiding center velocity $\mathbf{V}_{E\times B} = \mathbf{E} \times \mathbf{B}/B^2$ in a constant magnetic field [2.18]. This is expressed by

$$\frac{d}{dt}\nabla_\perp^2 \phi = 0, \tag{2.19}$$

which expresses the conservation of the z-component of vorticity $\boldsymbol{\omega} = \nabla \times \mathbf{V}_{E\times B}$. The convective derivative is given by the $E \times B$ drift velocity as

$$\frac{d}{dt} = \frac{\partial}{\partial t} + \mathbf{V}_{E\times B} \cdot \nabla \qquad \text{i.e.,} \tag{2.20a}$$

$$\frac{d}{dt} = \frac{\partial}{\partial t} + \frac{1}{B}[\phi,\ ], \tag{2.20b}$$

where the Poisson bracket is defined as

$$[\phi, F] = (\nabla_\perp \phi \times \nabla_\perp F) \cdot \hat{\mathbf{b}}. \tag{2.21}$$

The nonlinear term is expressed in terms of the Poisson bracket. Model equation (2.19) describes the advection change of vortex, and does not include plasma responses that generate electric field. In plasmas, various mechanisms cause the screening (or anti-screening) of the electric field.

The simplest model equation that describes the electrostatic turbulence in inhomogeneous plasmas is the Hasegawa–Mima (HM) equation [or Hasegawa–Mima–Charney (HMC) equation]. In this model, the density response is assumed to be adiabatic, $n = e\phi/T_e$, and pressure and magnetic perturbations are assumed to be small. The Hasegawa–Mima equation (or HMC equation) is a dissipationless system for two-dimensional $E \times B$ motion [2.17],

$$\frac{d}{dt}\rho_i^2 \nabla_\perp^2 \phi - \frac{\partial}{\partial t}\phi = 0. \tag{2.22}$$

The plasma property is included in the HM equation Eq. (2.22) through the polarization drift effect, which is due to the finite inertia of ions, and adiabatic response of electrons.

The latter appears as the second term of Eq. (2.22). In the presence of density inhomogeneity in the x-direction, the density perturbation is caused by the $E \times B$ advection of the background profile. In this case, Eq. (2.22) takes the form

$$\frac{d}{dt}\rho_{\mathrm{i}}^2\nabla_\perp^2\phi - \frac{\partial}{\partial t}\phi - V_{\mathrm{de}}\frac{\partial}{\partial y}\phi = 0, \tag{2.23}$$

where V_{de} is the electron drift velocity,

$$V_{\mathrm{de}} = T_{\mathrm{e}}/(eBL_n) \quad \text{and} \quad L_n^{-1} = \left|-\nabla\bar{n}/\bar{n}\right|, \tag{2.24}$$

and $\omega_* = V_{\mathrm{de}}k_y$ is the drift frequency. The HM equation is an analog to the vorticity equation which is deduced from the Navier–Stokes equation. In the neutral-fluid dynamics, an equation with the same structure has been derived [2.19]. Note that HM equation can also derived via gyrokinetics, which is sketched in [2.20].

C Hasegawa–Wakatani equations Global scale transport is described by cross-correlation functions. For instance, the cross-correlation function between the internal energy and velocity controls the fluctuation-driven energy flux. Analysis of a cross-correlation function requires at least two variables. The simplest set of model equations which allows the study of cross-field transport by electrostatic drift wave is the Hasegawa–Wakatani (HW) equations [2.16]. These model equations describe $E \times B$ motion and density perturbation, in order to investigate the collisional drift waves. A set of dynamical equations for the normalized potential and normalized density ($\phi \equiv e\tilde{\phi}/T_{\mathrm{e}}, n \equiv \tilde{n}/\bar{n}$) is given for the collisional drift wave in the electrostatic limit as

$$\frac{\partial}{\partial t}\nabla_\perp^2\phi + \left[\phi, \nabla_\perp^2\right] = d_\parallel(\phi - n) + \mu_{\mathrm{c}}\nabla_\perp^4\phi, \tag{2.25a}$$

$$\frac{\partial}{\partial t}n + [\phi, n] = d_\parallel(\phi - n) - \frac{\partial\phi}{\partial y} + D_{\mathrm{c}}\nabla_\perp^2 n, \tag{2.25b}$$

where $d_\parallel \equiv k_\parallel^2 D_\parallel \omega_{\mathrm{ci}}^{-1} L_n \rho_{\mathrm{s}}^{-1}$ and $D_\parallel = v_{\mathrm{the}}^2 \nu_{\mathrm{ei}}^{-1}$. ($v_{\mathrm{the}}$: electron thermal velocity, ν_{ei}: electron-ion collision frequency, ω_{ci}: ion cyclotron frequency, μ_{c} and D_{c}: collisional viscosity and diffusivity, respectively. Time and length are normalized to $\rho_{\mathrm{s}}/V_{\mathrm{d}} = L_n/c_{\mathrm{s}}$ and ρ_{s}, respectively.) The parameter $d_\parallel$, being the ratio between the parallel diffusion rate and the drift frequency, controls the phase difference between potential and density. In the collisionless limit of $\nu_{\mathrm{ei}}/\omega_* \to 0$, i.e., $d_\parallel^{-1} \to 0$, the electron motion is not impeded and the plasma response tends to be adiabatic, i.e.,$n \sim \phi$. This limit, with $\mu_{\mathrm{c}}, D_{\mathrm{c}} \to 0$, Eq. (2.25b) gives

$$d_\parallel(\phi - n) = \frac{\partial}{\partial t}\phi + \frac{\partial\phi}{\partial y} + O(d_\parallel^{-1}).$$

Substitution of this relation into Eq. (2.25a) leads to the HM equation Eq. (2.23).

In the opposite limit, $d_{\parallel} \to 0$, Eqs. (2.25a) and (2.25b) are decoupled. The density perturbation then becomes a passive scalar quantity. It must be noted that the variable n is not a perturbed density in its rigorous meaning [2.20]. This set of equations is the simplest one which allows the study of both the auto-correlation function and cross-correlation function. Not only the cascade of the turbulence spectrum, but also the transport, which is induced by the inhomogeneity-driven turbulence, can be studied. An intensive study has been performed.

D Reduced MHD equations For the study of the evolution of MHD instabilities, which are caused by the inhomogeneity of plasma current and/or pressure gradient, another set of variables is chosen, namely the electrostatic potential and the vector potential in the direction of magnetic field $\bar{\mathbf{B}}$, $(\phi, A_{\parallel})$. A reduced set of equations is:

$$\frac{\partial}{\partial t}\nabla_{\perp}^2\varphi + \left[\phi, \nabla_{\perp}^2\phi\right] - \nabla_{\parallel}J_{\parallel} = 0. \tag{2.26a}$$

$$\frac{\partial}{\partial t}A_{\parallel} + \nabla_{\parallel}\phi = \eta_{\parallel}J_{\parallel}, \tag{2.26b}$$

with $J_{\parallel} = -\nabla_{\perp}^2 A_{\parallel}$. In this set of equations, the length, time, electrostatic potential, and vector potential are normalized to the plasma radius a, the poloidal Alfvén transit time $\tau_{\mathrm{Ap}} = a/v_{\mathrm{Ap}} = R/v_{\mathrm{A}}$, Ba^2/R, and $Bv_{\mathrm{A}}a^2/R$, respectively.

2.2.3. Kinetic equations

A Vlasov equation When the motion of individual particles is essential, a kinetic equation must be used. A typical example of the kinetic equation is:

$$\left[\frac{\partial}{\partial t} + \mathbf{v}\cdot\nabla + \frac{e_s}{m_s}(\mathbf{E} + \mathbf{v}\times\mathbf{B})\cdot\nabla_{\mathbf{v}}\right] f_s(\mathbf{v}:t) = C \tag{2.27}$$

where C is the collision operator. In the case of $C = 0$, it is the Vlasov equation. Solving Eq. (2.27) and attaining the plasma density and current, and using Maxwell's equations Eqs. (2.13)-(2.15), plasma turbulence can be investigated.

B Gyro-average equations In many cases, the scale length of fluctuations is in the range of the gyroradius, but the time scale is much longer than the cyclotron frequency. In such a case, resonances associated with the gyromotion are unimportant, and the distribution function becomes a function of $(v_{\perp}, v_{\parallel})$, $f(\mathbf{v}:t) = \hat{f}(v_{\perp}, v_{\parallel}:t)$, so that the kinetic equation is deduced to

$$\begin{aligned}\frac{\partial}{\partial t}\hat{f}_s &+ (v_{\parallel}\hat{\mathbf{b}} + \mathbf{v}_{\mathrm{D}})\cdot\nabla\hat{f}_s \\ &+ \left(e_s\frac{\partial\phi}{\partial t} + \mu_s\frac{\partial B}{\partial t} - e_s\mathbf{v}_{\parallel}\cdot\frac{\partial\mathbf{A}}{\partial t}\right)\frac{\partial}{\partial U}\hat{f}_s = C,\end{aligned} \tag{2.28}$$

where

$$\mathbf{v}_{\parallel} = v_{\parallel}\hat{\mathbf{b}},$$

$\mathbf{v}_{\mathrm{D}}$ is the particle drift velocity defined by

$$\mathbf{v}_{\mathrm{D}} = B^{-1}\mathbf{E} \times \hat{\mathbf{b}} + \omega_{\mathrm{cs}}^{-1}\hat{\mathbf{b}} \times (m_s^{-1}\mu_s \nabla B + v_{\parallel}^2 \boldsymbol{\kappa} + v_{\parallel}\partial\hat{\mathbf{b}}/\partial t).$$

$$U = m_s v_{\parallel}^2/2 + e_s\phi + \mu_s B,$$

μ_s is the magnetic moment, and $\boldsymbol{\kappa}$ is the curvature of magnetic field. An explicit form for non-uniform plasmas is seen in, e.g., §4.3 of [2.12] and [2.21, 2.22].

References

[2.1] Lagerstrom, P A 1964 in *Theory of Laminar Flows* (ed. Moore F K, Princeton: Princeton University)

[2.2] Phillips O M 1977 *The Dynamics of the Upper Ocean* (Cambridge: Cambridge University)

[2.3] Moreau R 1990 *Magnetohydrodynamics* (Dordrecht: Kluwer)

[2.4] Braginskii S I 1965 in *Reviews of Plasma Physics* (ed. M. A. Leontovich, New York: Consultants Bureau) vol 1 p 205

[2.5] Miyamoto K 1976 *Plasma Physics for Nuclear Fusion* (Cambridge: The MIT)

[2.6] Kadomtsev B B and Pogutse O P 1974 Sov. Phys. -JETP **38** 283 [Zh. Eksp. Teor. Fiz. **65** 575 (1973)]

[2.7] Sykes A and Wesson J A 1976 Phys. Rev. Lett. **37** 140

[2.8] Rosenbluth M N, Monticello D A, Strauss H R and White R B 1976 Phys. Fluids **19** 198

[2.9] Yagi M and Horton C W 1994 Phys. Plasmas **1** 2135

[2.10] Romaneli F and Zonca F 1989 Plasma Phys. Contr. Fusion **31** 1365

[2.11] Drake J F and Antonsen T M Jr 1984 Phys. Fluids **27** 898

[2.12] Hazeltine R D and Meiss J D 1992 *Plasma Confinement* (Reading: Addison Wesley)

[2.13] Strauss H R 1976 Phys. Fluids **19** 134
— 1977 Phys. Fluids **20** 1354

[2.14] Hazeltine R D 1983 Phys. Fluids **26** 3242

[2.15] Itoh K, Yagi M, Itoh S-I, Fukuyama A and Azumi M 1993 Plasma Phys. Contr. Fusion **35** 543

[2.16] Hasegawa A and Wakatani M 1983 Phys. Rev. Lett. **50** 682

[2.17] Hasegawa A and Mima K 1977 Phys. Rev. Lett. **39** 205

[2.18] Taylor J B and McNamara B 1971 Phys. Fluids **14** 1492

[2.19] See [2.14] for comparison Original work is given as Charney J G 1948 Geophys. Public. Kosjones Nors. Videnshap. - Akad. Oslo **17** 3

[2.20] Hu G. Krommes J A and Bowman J C 1997 Phys. Plasmas **4** 2116

[2.21] Frieman E A and Chen L 1982 Phys. Fluids **25** 502

[2.22] Antonsen T M Jr and Lane B 1980 Phys. Fluids **23** 1205

3. Fluid Turbulence and Dynamo

3.1. Towards Mode Reduction

In turbulent flow at high Reynolds number (Re), the spatial scale of included modes ranges from the reference scale characterizing the global geometry of each flow, L, to the energy-dissipation scale $\ell_{\rm D}[= O(LRe^{-3/4})]$, as will be shown in §3.2.2. From this result, the total number of modes included in the flow is $N = O[(L/\ell_{\rm D})^3] = O(Re^{9/4})$. In the case of large Re, a method for reducing the modes is the use of an ensemble averaging procedure. Under this procedure, the modes whose spatial symmetry coincides with the geometrical one are retained, and highly time-dependent, asymmetric properties of motion are masked.

In the numerical computation of fluid equations, the ratio of each grid size to $\ell_{\rm D}$ becomes critical. In the case that the ratio is much larger than unity, as is often encountered in turbulent flow at high Re, we need to use spatial filtering and smooth out the fluctuations whose scales are smaller than the grid size. To compensate for this mode reduction, we supplement the eliminated energy dissipation mechanism with the aid of the so-called subgrid-scale (SGS) modelling.

3.1.1. Ensemble averaging We divide a quantity f into the ensemble mean $\bar{f} = \langle f \rangle$ and the fluctuation around it, $\tilde{f} = f - \bar{f}$. The ensemble averaging of Eqs. (2.5)-(2.7) results in

$$\nabla \cdot \bar{\mathbf{V}} = 0. \tag{3.1}$$

$$\frac{D\bar{V}_i}{Dt} \equiv \left(\frac{\partial}{\partial t} + \bar{\mathbf{V}} \cdot \nabla \right) \bar{V}_i = -\frac{\partial \bar{p}}{\partial x_i} + \frac{\partial}{\partial x_j} \left(-R_{ij} \right) + \nu \nabla^2 \bar{V}_i, \tag{3.2}$$

$$\frac{D\bar{\theta}}{Dt} = \nabla \cdot (-\mathbf{H}) + \kappa \nabla^2 \bar{\theta}. \tag{3.3}$$

Here R_{ij} and $\mathbf{H}$, which are defined as

$$R_{ij} = \langle \tilde{v}_i \tilde{v}_j \rangle, \tag{3.4}$$

$$\mathbf{H} = \left\langle \tilde{\theta} \tilde{\mathbf{v}} \right\rangle, \tag{3.5}$$

express the turbulent momentum and heat fluxes, respectively. The former is specifically called the Reynolds stress.

The fluctuation $\tilde{\mathbf{v}}$ obeys

$$\frac{D\tilde{v}_i}{Dt} + (\tilde{\mathbf{v}} \cdot \nabla) \bar{V}_i + \frac{\partial}{\partial x_j} \left(\tilde{v}_i \tilde{v}_j - R_{ij} \right) = -\frac{\partial \tilde{p}}{\partial x_i} + \nu \nabla^2 \tilde{v}_i. \tag{3.6}$$

with the solenoidal condition $\nabla \cdot \tilde{\mathbf{v}} = 0$. From Eq. (3.6), we have

$$\frac{DR_{ij}}{Dt} = P_{ij} + \Pi_{ij} - \varepsilon_{ij} + \frac{\partial T_{ij\ell}}{\partial x_\ell} + \nu \nabla^2 R_{ij}, \tag{3.7}$$

where

$$P_{ij} = -R_{i\ell}\frac{\partial \bar{V}_j}{\partial x_\ell} - R_{j\ell}\frac{\partial \bar{V}_i}{\partial x_\ell}, \tag{3.8}$$

$$\Pi_{ij} = \left\langle \tilde{p}\left(\frac{\partial \tilde{v}_j}{\partial x_i} + \frac{\partial \tilde{v}_i}{\partial x_j}\right)\right\rangle. \tag{3.9}$$

$$\varepsilon_{ij} = 2\nu \left\langle \frac{\partial \tilde{v}_i}{\partial x_\ell}\frac{\partial \tilde{v}_j}{\partial x_\ell}\right\rangle, \tag{3.10}$$

$$T_{ij\ell} = -\left(\langle \tilde{v}_i \tilde{v}_j \tilde{v}_\ell\rangle + \langle \tilde{p}\tilde{v}_i\rangle \delta_{j\ell} + \langle \tilde{p}\tilde{v}_j\rangle \delta_{i\ell}\right). \tag{3.11}$$

The turbulent energy K is related to R_{ij} by

$$K \equiv \left\langle \tilde{\mathbf{v}}^2/2\right\rangle = R_{ii}/2. \tag{3.12}$$

Taking the contraction of Eq. (3.7), we have

$$\frac{DK}{Dt} = P_K - \varepsilon + \nabla \cdot \mathbf{T}_K + \nu \nabla^2 K, \tag{3.13}$$

where

$$P_K = -R_{ij}\frac{\partial \bar{V}_j}{\partial x_i}, \tag{3.14}$$

$$\varepsilon = \nu \left\langle \left(\frac{\partial \tilde{v}_j}{\partial x_i}\right)^2\right\rangle, \tag{3.15}$$

$$\mathbf{T}_K = -\left\langle \left(\frac{\tilde{\mathbf{v}}^2}{2} + \tilde{p}\right)\tilde{\mathbf{v}}\right\rangle. \tag{3.16}$$

Let us see the role of R_{ij} in the generation process for K. We integrate Eq. (3.13) and the mean-field counterpart obtained from Eq. (3.2) over the whole fluid region V, and have

$$\frac{\partial}{\partial t}\int_V K dV = \int_V P_K dV - \int_V \varepsilon dV - \int_S (\mathbf{T}_K + \nu \nabla K)\cdot \mathbf{n} dS, \tag{3.17}$$

$$\begin{aligned}\frac{\partial}{\partial t}\int_V \frac{\bar{\mathbf{V}}^2}{2} dV = &-\int_V P_K dV - \int_V \nu \left(\frac{\partial \bar{V}_i}{\partial x_i}\right)^2 dV \\ &+ \int_S \left(-\bar{p}\bar{\mathbf{V}} - \frac{\bar{\mathbf{V}}^2}{2}\bar{\mathbf{V}} - \mathbf{R}\bar{\mathbf{V}} + \nu \nabla \frac{\bar{\mathbf{V}}^2}{2}\right)\cdot \mathbf{n} dS,\end{aligned} \tag{3.18}$$

where $\mathbf{R} = (R_{ij})$, S is the surface of V, and $\mathbf{n}$ is the outward unit vector normal to S. On the right-hand side of Eq. (3.17), the second part is always non-positive. The third part is the energy inflow or outflow rate across S due to turbulence effects. In the absence of the mean velocity $\bar{\mathbf{V}}$, P_K vanishes, and K decays so long as there is no specific mechanism for keeping such energy flows. Thus, a turbulent state is maintained by P_K, which is usually called the turbulent energy production rate.

On the right-hand side of Eq. (3.18), the first or P_K-related term plays the opposite role, compared with its counterpart in Eq. (3.17). The former expresses the rate of the energy that is drained from $\bar{\mathbf{V}}$ and is supplied eventually to $\tilde{\mathbf{v}}$. The primary energy source of $\bar{\mathbf{V}}$ is the $\bar{p}$-related term in the last part of Eq. (3.18), which expresses the energy supply through the imposition of pressure. In these processes, R_{ij} is the intermediary of the energy exchange between the mean and fluctuating motions. The clear mathematical relationship between Eqs. (3.17) and (3.18) arises from the fact that the total amount of energy, $\int_V (\mathbf{V}^2/2) dV$, is conserved in the absence of ν.

A prominent difference between Eqs. (3.7) and (3.13) is the pressure/velocity-strain correlation Π_{ij}, which disappears in the latter, owing to the solenoidal condition $\nabla \cdot \tilde{\mathbf{v}} = 0$. This fact indicates that Π_{ij} contributes to the exchange of energy among three turbulence intensities $\langle \tilde{v}_x^2 \rangle$, $\langle \tilde{v}_y^2 \rangle$, and $\langle \tilde{v}_z^2 \rangle$, but not to the change of K. From this property, Π_{ij} is also called the energy redistribution rate.

3.1.2. Filtering We introduce a filter function G and smooth out a flow quantity f as

$$\hat{f} \equiv \overline{f}^G = \int G(\mathbf{y} - \mathbf{x}) f(\mathbf{y}) d\mathbf{y}. \tag{3.19}$$

The deviation around $\hat{f}$ is denoted by $f' = f - \hat{f}$. We apply the filtering to Eq. (2.6) with $\mathbf{K}$ dropped, and have

$$\frac{\partial \hat{V}_i}{\partial t} + \frac{\partial}{\partial x_j} \hat{V}_i \hat{V}_j = -\frac{\partial \hat{p}}{\partial x_i} + \frac{\partial}{\partial x_j} \left(-\tau_{ij}^{(1)} - \tau_{ij}^{(2)} - \tau_{ij}^{(3)} \right) + \nu \nabla^2 \hat{V}_i, \tag{3.20}$$

where the subgrid-scale (SGS) stresses $\tau_{ij}^{(n)}$ (n = 1-3) are defined as

$$\tau_{ij}^{(1)} = \overline{\hat{V}_i \hat{V}_j}^G - \hat{V}_i \hat{V}_j, \tag{3.21}$$

$$\tau_{ij}^{(2)} = \overline{\hat{V}_i v_j' + v_i' \hat{V}_j}^G, \tag{3.22}$$

$$\tau_{ij}^{(3)} = \overline{v_i' v_j'}^G. \tag{3.23}$$

Here $\tau_{ij}^{(3)}$ corresponds to the Reynolds stress in the ensemble-mean system, R_{ij}, whereas the other two have no counterparts and arise from the relations intrinsic to the filtering procedure,

$$\overline{\overline{f}^G}^G \neq \overline{f}^G, \quad \overline{f}^G \neq 0. \tag{3.24}$$

In order to close Eq. (3.20), we need to relate $\tau_{ij}^{(2)}$ and $\tau_{ij}^{(3)}$ to the grid-scale (GS) velocity $\hat{\mathbf{V}}$ (note that $\tau_{ij}^{(1)}$ is written in terms of $\hat{\mathbf{V}}$). The use of either $\tau_{ij}^{(2)}$ or $\tau_{ij}^{(3)}$ leads to the breaking of the Galilean invariance as we will refer to later.

3.1.3. Fourier representation Some important turbulence properties still remain in the absence of a mean flow. In this case, it is useful to introduce the Fourier representation and its inverse

$$\tilde{f}(\mathbf{x}) = \int \tilde{f}(\mathbf{k}) \exp(-i\mathbf{k}\cdot\mathbf{x}) d\mathbf{k}, \tag{3.25a}$$

$$\tilde{f}(\mathbf{k}) = (2\pi)^{-3} \int \tilde{f}(\mathbf{x}) \exp(i\mathbf{k}\cdot\mathbf{x}) d\mathbf{x}. \tag{3.25b}$$

with the counterpart for the Dirac delta function

$$\delta(\mathbf{x}) = (2\pi)^{-3} \int \exp(\pm i\mathbf{k}\cdot\mathbf{x}) d\mathbf{k}. \tag{3.26}$$

We apply Eq. (3.25) to Eq. (2.6) with vanishing $\bar{\mathbf{V}}$, and eliminate $\tilde{p}(\mathbf{k})$ with the aid of the solenoidal condition $\mathbf{k}\cdot\tilde{\mathbf{v}}(\mathbf{k}) = 0$. Then we have [1.5-1.7]

$$\left(\frac{\partial}{\partial t} + \nu k^2\right) \tilde{v}_i(\mathbf{k}) = iM_{ij\ell}(\mathbf{k}) \iint \tilde{v}_j(\mathbf{p})\tilde{v}_\ell(\mathbf{q})\delta(\mathbf{k}-\mathbf{p}-\mathbf{q}) d\mathbf{p} d\mathbf{q}, \tag{3.27}$$

with

$$M_{ij\ell}(\mathbf{k}) = M_{i\ell j}(\mathbf{k}) = (1/2)\left[k_j D_{i\ell}(\mathbf{k}) + k_\ell D_{ij}(\mathbf{k})\right]. \tag{3.28}$$

Here $D_{ij}(\mathbf{k})$ is the solenoidal operator defined by $D_{ij}(\mathbf{k}) = \delta_{ij} - (k_i k_j / k^2)$, leading to $k_i M_{ij\ell}(\mathbf{k}) = 0$.

An abbreviated form of Eq. (3.27), which keeps its second-order nonlinearity, is given by [1.5, 3.1]

$$\left[\frac{\partial}{\partial t} + \gamma(i)\right] X_i = N_{ij\ell} X_j X_\ell, \tag{3.29}$$

where $\gamma(i)$ is the damping rate of mode X_i, and the coupling coefficient $N_{ij\ell}$ is prescribed to be symmetric with respect to j and ℓ, just as for $M_{ij\ell}(\mathbf{k})$ (note that the summation convention is applied to repeated subscripts only). This simplified expression is useful in the study of statistical approaches to Eq. (3.27).

3.2. Homogeneous Turbulence

3.2.1. Fundamental concepts By homogeneity, we mean that the correlation functions of any order are independent of the choice of the origin of coordinates. For instance, the second-order velocity correlation obeys

$$\langle \tilde{v}_i(\mathbf{x})\tilde{v}_j(\mathbf{x}')\rangle = \langle \tilde{v}_i(\mathbf{x}-\mathbf{x}')\tilde{v}_j(\mathbf{0})\rangle. \tag{3.30}$$

The homogeneity holds only in an infinite fluid region, and the velocity profile of the mean flow is greatly limited. Such a representative flow is the homogeneous-shear turbulence, in which the mean velocity is unidirectional and varies linearly in the direction normal to the mean flow. Under the homogeneity assumption, R_{ij} [Eq. (3.4)] and $\mathbf{H}$ [Eq. (3.5)] may survive, but they have no influence on $\bar{\mathbf{V}}$ and $\bar{\theta}$ since $\nabla \cdot \mathbf{R}$ and $\nabla \cdot \mathbf{H}$ vanish in Eqs. (3.2) and (3.3). The simplest homogenous turbulence is isotropic turbulence without any preferred direction. In current theoretical studies of homogeneous turbulence, much attention has been paid to the isotropic case.

In three-dimensional homogeneous turbulence lacking a mean flow, the mechanism of energy supply due to P_K is lost, and the energy-containing component of motion plays the role of the energy reservoir for smaller-scale ones. In this situation, the primary targets of homogeneous turbulence theory are the energy transfer mechanism among modes and the energy dissipation mechanism at fine scales. The turbulent transport mechanism related to the occurrence of R_{ij} etc. is beyond our scope and is left for the study of inhomogeneous turbulence theory.

Using Eqs. (3.25) and (3.26), we have

$$\begin{aligned}\langle \tilde{v}_i(\mathbf{k})\tilde{v}_j(\mathbf{k}')\rangle &= (2\pi)^{-6}\iint Q_{ij}(\mathbf{x}-\mathbf{x}')\exp[i(\mathbf{k}\cdot\mathbf{x}+\mathbf{k}'\cdot\mathbf{x}')]d\mathbf{x}d\mathbf{x}' \\ &= (2\pi)^{-3}\delta(\mathbf{k}+\mathbf{k}')\int Q_{ij}(\mathbf{r})\exp(i\mathbf{k}'\cdot\mathbf{r})d\mathbf{r}, \end{aligned} \tag{3.31}$$

with

$$Q_{ij}(\mathbf{x}-\mathbf{x}') = Q_{ij}(\mathbf{r}) = \langle \tilde{v}_i(\mathbf{x})\tilde{v}_j(\mathbf{x}')\rangle, \tag{3.32}$$

where $\mathbf{r} = \mathbf{x} - \mathbf{x}'$. In Eq. (3.31), Dirac's delta function appears. This is due to the assumption that the fluid region is infinite. In the case that the cubic region is adopted with the cyclic boundary condition, $\delta(\mathbf{k}+\mathbf{k}')$ is replaced by Kronecker's delta symbol. The inverse of Eq. (3.31) leads to

$$K = \frac{1}{2}Q_{ii}(\mathbf{0}) = \frac{1}{2}\int \frac{\langle \tilde{v}_i(\mathbf{k})\tilde{v}_i(\mathbf{k}')\rangle}{\delta(\mathbf{k}+\mathbf{k}')}d\mathbf{k}. \tag{3.33}$$

Here the expression $1/\delta(\mathbf{k}+\mathbf{k}')$ is not correct in the strict mathematical sense of a generalized function [3.2]. The use of Eq. (3.33) with the foregoing point in mind introduces no errors to the final results even if it is treated as a normal function.

The most general isotropic expression for $\langle \tilde{v}_i(\mathbf{k})\tilde{v}_j(\mathbf{k}')\rangle$, which obeys the solenoidal condition $\mathbf{k}\cdot\tilde{\mathbf{v}}(\mathbf{k}) = 0$, is

$$\frac{\langle \tilde{v}_i(\mathbf{k})\tilde{v}_j(\mathbf{k}')\rangle}{\delta(\mathbf{k}+\mathbf{k}')} = D_{ij}(\mathbf{k})Q(k) + \frac{i}{2}H(\mathbf{k})\frac{k_\ell}{k^2}\epsilon_{ij\ell}, \tag{3.34}$$

with $k = |\mathbf{k}|$, where Q and H are functions of k and $\epsilon_{ij\ell}$ is the alternating tensor. From Eq. (3.34), we have

$$K = \int E(k)dk, \tag{3.35}$$

with the energy spectrum $E(k)$ defined by

$$E(k) = 4\pi k^2 Q(k). \tag{3.36}$$

In Eq. (3.34), the pseudo-scalar $H(k)$ does not contribute to K and is related to the turbulent helicity $\langle \tilde{\mathbf{v}} \cdot \tilde{\boldsymbol{\omega}} \rangle$ as

$$\langle \tilde{\mathbf{v}} \cdot \tilde{\boldsymbol{\omega}} \rangle = \int 4\pi k^2 H(k) dk, \tag{3.37}$$

where $\tilde{\boldsymbol{\omega}} (= \nabla \times \tilde{\mathbf{v}})$ is the fluctuation vorticity.

From Eq. (3.27), $E(k)$ obeys

$$\frac{\partial E(k)}{\partial t} + 2\nu k^2 E(k) = S(k), \tag{3.38}$$

where the transfer function $S(k)$ expresses the contribution from the nonlinear term and plays the role of transferring the energy among the modes $\tilde{\mathbf{v}}(\mathbf{k})$. Because energy is conserved by the nonlinearity, $S(k)$ is subject to the constraint

$$\int_0^\infty S(k) dk = 0, \tag{3.39}$$

resulting in

$$\frac{dK}{dt} = -\varepsilon \equiv -\int D(k) dk, \tag{3.40}$$

where $D(k)$ is the dissipation function defined as

$$D(k) = 2\nu k^2 E(k). \tag{3.41}$$

3.2.2. Kolmogorov scaling In homogeneous turbulence with no mean flow, the low-wavenumber range of the energy spectrum plays the role of an energy reservoir for smaller eddies. At high Re (Reynolds number), the contribution of the low-wavenumber range to the energy dissipation rate ε is negligible, and the fine-scale or high-wavenumber components of motion is totally responsible for ε. In this situation, a clear spectral gap may occur between the dominant ranges of $E(k)$ and $D(k)$, and a universal property free from the energy input and dissipation mechanisms is expected to exist in the intermediate range. The range is usually called the inertial range.

The extent of the spectral gap may be stated in more mathematical terms. We denote the characteristic scale of the energy-containing range (energy reservoir) and the intensity of related velocity fluctuations by ℓ_C and v_C, respectively. The dissipation rate is characterized by ν and ε, in terms of which ℓ_D (the energy-dissipation scale) and the corresponding wavenumber k_D may be written. From dimensional analysis, we have

$$\ell_D = k_D^{-1} = \left(\nu^3/\varepsilon\right)^{1/4}, \tag{3.42}$$

apart from numerical factors. This relation may be derived from the consideration that ε is the energy in the dissipation range, $(\nu k)^2$, divided by the time-scale counterpart $(\nu k^2)^{-1}$.

In the equilibrium state, ε may be also regarded as equivalent to the energy outflow rate from the reservoir, and ℓ_C is estimated as

$$\ell_C = v_C^3/\varepsilon. \tag{3.43}$$

From Eqs. (3.42) and (3.43), we have

$$\ell_D/\ell_C = R_T^{-3/4}, \tag{3.44}$$

where R_T is the Reynolds number characterizing the energy reservoir. It is defined by

$$R_T = v_C \ell_C/\nu, \tag{3.45}$$

which also expresses the relative magnitude of the inertial term $(\tilde{\mathbf{v}} \cdot \nabla)\tilde{\mathbf{v}}$ to the viscous term $\nu\nabla^2\tilde{\mathbf{v}}$ on the basis of v_C and ℓ_C. Equation (3.44) gives a measure for the degree of separation between the energy reservoir and the dissipation range. It is more proper to call ε the energy transfer rate passing through the inertial range since it is associated with both the energy-input and -dissipation processes.

We adopt ε as the primary quantity characterizing the inertial range, and write

$$E(k) = K_O \varepsilon^{2/3} k^{-5/3}, \tag{3.46}$$

from dimensional analysis. This is the Kolmogorov's $-5/3$ power law [3.3-3.5], and the Kolmogorov constant K_O is around 1.5 in observations [3.6, 3.7]. In close relation to Eq. (3.46), the characteristic time scale intrinsic to the inertial range is

$$\tau \propto \varepsilon^{-1/3} k^{-2/3}, \tag{3.47}$$

which signifies that smaller eddies have shorter life times.

In physical space, the Kolmogorov law may be written as

$$\left\langle |\Delta\tilde{\mathbf{v}}(\mathbf{r})|^2 \right\rangle \equiv \left\langle |\tilde{\mathbf{v}}(\mathbf{x}+\mathbf{r}) - \tilde{\mathbf{v}}(\mathbf{x})|^2 \right\rangle \propto (\varepsilon r)^{2/3}. \tag{3.48}$$

with the aid of the velocity difference at two locations ($r = |\mathbf{r}|$). Equation (3.48) may be extended to the moment of an arbitrary order n as

$$C_n\{\tilde{\mathbf{v}}\} \equiv \langle |\Delta\tilde{\mathbf{v}}(\mathbf{r})|^n \rangle \propto (\varepsilon r)^{n/3}. \tag{3.49}$$

which should be compared with $(\varepsilon/\nu)r^2$ for small r.

The Kolmogorov spectrum is directly related to neither the energy production nor the energy dissipation. Such a fact seems to suggest the minor importance of the spectrum in the study of real turbulent flows. However, this is not the case. The lower end of the spectrum joints to the higher-wavenumber part of the energy-containing spectrum. This property indicates that parts of the characteristics of the energy-containing region may be abstracted from the Kolmogorov spectrum. This merit will be fully utilized in the inhomogeneous-turbulence theory presented in §3.3.4.

3.2.3. Breaking of Kolmogorov scaling The Kolmogorov scaling (3.49) has been subject to extensive tests based on observations. Atmospheric and oceanic observations have provided important information about the validity of the scaling, for flows at high R_T guaranteeing the separation between the energy-containing and -dissipation ranges are realized there.

Through the comparison with observations, Eq. (3.46) or Eq. (3.49) with $n = 2$ is affirmed, but the small deviation from it is also detectable, resulting in

$$E(k) = K'_O \varepsilon^{2/3} k^{-5/3} (kL)^{-\mu_2}. \tag{3.50}$$

with K'_O a non-dimensional coefficient. The exponent μ_2 is about 0.02 [3.5, 3.8]. What is important here is the occurrence of the other length scale L. In the equilibrium state arising from the balance between the energy input and dissipation, the details of the energy input mechanism has little influence on the inertial range, but their memory may still occur in $E(k)$. In this sense, L should be regarded as

$$L \propto \ell_C, \tag{3.51}$$

and K'_O is not a universal constant since the choice of L is not unique.

The breakdown of the Kolmogorov scaling for the energy spectrum is minor from the practical viewpoint, but it becomes serious with increasing n. The moments $C_n\{\tilde{\mathbf{v}}\}$ for higher n are linked more tightly with the small-scale components of motion. This tendency may be also seen from Eq. (3.50), which shows that the deviation from the $-5/3$ power law becomes clearer for $k \gg L^{-1}$. The breakdown of the Kolmogorov scaling, however, does not always arise from only the small-scale components only. The scaling (3.49) is founded on the validity of the equilibrium state in which the energy dissipation balances the input one. A breakdown in such a balance is another cause for deviation from Eq. (3.46).

A Intermittency effects In order to see a cause of the breaking of the Kolmogorov scaling in the light of small-scale properties, we write

$$|\Delta\tilde{\mathbf{v}}(\mathbf{r})|^2 = |\tilde{\mathbf{v}}(\mathbf{x}+\mathbf{r}) - \tilde{\mathbf{v}}(\mathbf{x})|^2 \propto (\varepsilon r)^{2/3}, \tag{3.52}$$

where ε' is the instantaneous energy dissipation rate given by

$$\varepsilon = \nu \left(\frac{\partial \tilde{v}_j}{\partial x_i} \right)^2 \tag{3.53}$$

($\varepsilon = \langle \varepsilon' \rangle$). The moment $C_n\{\tilde{\mathbf{v}}\}$ is

$$C_n\{\tilde{\mathbf{v}}\} \propto \left\langle \varepsilon^{n/3} \right\rangle r^{n/3}. \tag{3.54}$$

Equation (3.54) is reduced to Eq. (3.49) as long as $\langle \varepsilon'^{n/3} \rangle \cong \varepsilon^{n/3}$ holds, that is, the fluctuation of ε' around ε is negligible. In turbulent flows at high R_C (turbulence

Reynolds number), both observations and computer experiments show that larger ε' is spotty in the spatial and temporary senses. From Eq. (3.54), the deviation of $C_n\{\tilde{\mathbf{v}}\}$ from the Kolmogorov scaling (3.49) is highly dependent on the probability distribution of ε', $P\{\varepsilon'\}$ [3.9, 3.10]. In order to obtain a scaling law consistent with observations, various elaborate models for $P\{\varepsilon'\}$ have been proposed and are still under intensive study. Readers may consult [3.5, 3.8] for such recent developments, and [3.11] for quite a new attempt using the Tsallis statistics.

B Shell model In the foregoing discussions on the Kolmogorov scaling and its breaking, no direct use is made of the Navier–Stokes equation (3.27), although the concept of the energy cascade is an important property. As a dynamic approach to intermittency effects, we may mention shell models. There we divide the wavenumber space into successive spherical shells, whose radii are denoted by $k_n(=k_0q^n)$ (k_0 is the reference wavenumber, $q>1$, and n is a positive integer). By V_n in the range $k_n<k<k_{n+1}$, we denote a one-dimensional model for $\tilde{\mathbf{v}}(\mathbf{k})$ in Eq. (3.27). Under the constraint $\mathbf{k}=\mathbf{p}+\mathbf{q}$, $\tilde{\mathbf{v}}(\mathbf{k})$ interacts with all other modes. In shell models, however, the interaction is usually restricted to the nearest and second-nearest ones [3.12-3.15]. A representative example is

$$\frac{dV_n}{dt}+\nu k^2V_n = i\left(C_{n1}V_{n+1}V_{n+2}+C_{n2}V_{n-1}V_{n+1}+C_{n3}V_{n-1}V_{n-2}\right)^*+f_n. \tag{3.55}$$

where C_{nm}'s are real constants, f_n is the external force maintaining a turbulent state, and A^* denotes the complex conjugate of A [3.15].

Equation (3.55) does not correspond to Eq. (3.27) straightforwardly, but the former possesses some properties similar to the latter. For instance, the energy, which is defined by $\sum_n V_n^2/2$, is conserved in the absence of ν and f_n, under the proper choice of C_{nm}. One of the interesting consequences of Eq. (3.55) is the intermittency effect on the structure function

$$S_p(k_n)=\langle|V_n|^p\rangle, \tag{3.56}$$

which is the shell-model counterpart of $C_n\{\tilde{\mathbf{v}}\}$ in Eq. (3.49). For small p, Eq. (3.55) gives a scaling property close to the Kolmogorov one, but the so-called intermittent behavior becomes prominent with increasing p.

C Non-equilibrium effects A typical non-equilibrium effect on the energy spectrum may be seen in the homogeneous-shear turbulence with the mean velocity $\bar{\mathbf{V}}=(Sy,0,0)$ in Cartesian coordinates. In this case, Eq. (3.13) is reduced to

$$\frac{\partial K}{\partial t}= \langle\tilde{v}_x\tilde{v}_y\rangle S-\varepsilon. \tag{3.57}$$

The first term plays a role of abstracting energy from the mean field. In homogeneous turbulence, the fluctuating field has no feedback effect on the mean field. As a result, K continues to grow without limit, and Eq. (3.57) does not have a stationary solution. This fact signifies that the energy input from the mean to the fluctuating field is not in the equilibrium state, unlike the premise of the Kolmogorov scaling.

A parameter characterizing such a non-equilibrium effect is the temporary variation of the energy input rate that is defined by $\dot{\varepsilon}(=\partial\varepsilon/\partial t)$. An instance of the $\dot{\varepsilon}$-related effect on the energy spectrum is

$$E(k) = K_{\mathrm{O}}\varepsilon^{2/3}k^{-5/3}\left[1 - C_{\mathrm{N}}\mathrm{sgn}(\dot{\varepsilon})(k\ell_{\mathrm{N}})^{-2/3}\right], \tag{3.58}$$

where the length scale $\ell_{\mathrm{N}} = \varepsilon^{2/3}/\dot{\varepsilon}^{3/2}$ is associated with the non-equilibrium effect, and $\mathrm{sgn}(\dot{\varepsilon})$ is defined as 1 and -1 for $\dot{\varepsilon} > 0$ and $\dot{\varepsilon} < 0$, respectively [3.16]. In the case of $\dot{\varepsilon} > 0$, Eq. (3.58) signifies that the energy dissipation cannot catch up with the growing energy input, resulting in the eventual decrease in the transfer rate. This effect becomes important only for low wavenumbers, in contrast to the foregoing intermittency effect.

3.2.4. Two-dimensional turbulence As the other example of scaling in homogeneous turbulence, we may mention two-dimensional turbulence with special reference to the inverse energy cascade and the formation of coherent vortices. Besides its tractability in a numerical simulation, two-dimensional turbulence is considered to provide an idealized model for geophysical and atmospheric flow phenomena. Such flows, subject to a rotation, are often confined in a thin layer, where the fluid motion is characterized by a horizontal scale length much larger than the vertical counterpart. Even in the case that the mean or large-scale flow is two dimensional, the fluctuation or turbulent motion is still three dimensional. In this sense, purely two-dimensional turbulence is not realized in nature. Nevertheless, the presence of a strong rotation around the vertical axis may suppress the vertical variation of fluid motion. Then the two-dimensional treatment may serve as a first step to the modelling of geophysical and atmospheric turbulence subject to strong rotation [3.17].

From Eq. (2.6), the equation for the vorticity $\boldsymbol{\omega}(=\nabla\times\mathbf{V})$ is given as

$$\frac{d\boldsymbol{\omega}}{dt} \equiv \left(\frac{\partial}{\partial t} + \mathbf{V}\cdot\nabla\right)\boldsymbol{\omega} = (\boldsymbol{\omega}\cdot\nabla)\,\mathbf{V} + \nu\nabla^2\boldsymbol{\omega}, \tag{3.59}$$

with the solenoidal condition $\nabla\cdot\boldsymbol{\omega} = 0$. Here and in this section, the external force $\mathbf{K}$ in Eq. (2.6) is dropped for simplicity of discussion. The first term in Eq. (3.59) represents the vorticity-amplification (-reduction) effect due to the stretching (shrinking) of the vorticity and is called vortex stretching. Vortex stretching is strongly connected to the vorticity-maintenance and energy-transfer mechanisms in turbulent motions. In two dimensions, however, vortex stretching always vanishes;

$$(\boldsymbol{\omega}\cdot\nabla)\,\mathbf{V} = 0. \tag{3.60}$$

It follows from Eq. (3.59) that in two dimensions the vorticity is conserved along the fluid motion in the inviscid limit ($\nu \to 0$). The absence of vortex stretching and resultant vorticity conservation constitute prominent features of two-dimensional fluid motion as compared to three-dimensional motion.

The conservation of vorticity leads to the conservation of any function of vorticity. In the following argument, we consider the squared vorticity called enstrophy since the detailed-balance relation between the spectral modes is simplest for such a quadratic invariant. From Eqs. (2.5) and (3.59), the equations for the energy $\mathbf{V}^2/2$ and the enstrophy $\boldsymbol{\omega}^2/2$ are given as

$$\frac{d}{dt}\frac{1}{2}\mathbf{V}^2 = -\nu\left(\frac{\partial V_b}{\partial x_a}\right)^2 + \nabla\cdot\left[-p\mathbf{V} + \nu\nabla\left(\frac{1}{2}\mathbf{V}^2\right)\right]. \tag{3.61}$$

$$\frac{d}{dt}\frac{1}{2}\boldsymbol{\omega}^2 = -\nu\left(\nabla\boldsymbol{\omega}\right)^2 + \nabla\cdot\left[\nu\nabla\left(\frac{1}{2}\boldsymbol{\omega}^2\right)\right]. \tag{3.62}$$

Equations (3.61) and (3.62) show that in two dimensions the enstrophy as well as the energy is conserved in the inviscid limit.

The dual conservation of the energy and the enstrophy in two dimensions gives rise to the possibility of an inverse energy cascade from smaller scales to larger ones [3.18, 3.19]. In wave-number space, the conservation of the energy and enstrophy correspond to the constancy of

$$K_E \equiv \left\langle \frac{1}{2}\tilde{\mathbf{v}}^2 \right\rangle = \int E_{2\mathrm{D}}(k)dk, \tag{3.63}$$

$$K_\Omega \equiv \left\langle \frac{1}{2}\tilde{\boldsymbol{\omega}}^2 \right\rangle = \int E^\Omega_{2\mathrm{D}}(k)dk = \int k^2 E_{2\mathrm{D}}(k)dk, \tag{3.64}$$

respectively. Under the nonlinear interaction, the profile of $E_{2\mathrm{D}}(k)$ in wave-number space changes as the energy is transferred between larger and smaller scales with the total energy or K_E being constant. If some portion of energy is transferred towards the small scales (large k), it results in an increase of the enstrophy [note that the enstrophy spectrum is $E_{2\mathrm{D}}(k)$ multiplied by k^2 in Eq. (3.64)]. In order for the total enstrophy to be conserved, a larger portion of energy should be transferred towards the large scales (small k), and balance the increase of the enstrophy due to the energy transfer towards the small scales. As a consequence, $E_{2\mathrm{D}}(k)$ is shifted to the larger scales. This is a picturesque explanation of the origins of inverse energy cascade in two-dimensional turbulence. As is seen below, however, we should note that the energy transfer identically vanishes in a large-k or enstrophy-cascade range while the enstrophy transport vanishes in a small-k or energy-inverse-cascade range [3.18].

Because of the dual conservation, the inertial-range properties in two dimensions may differ from their counterparts in three dimensions in which the energy (for non-helical flow) is the sole quadratic quantity conserved in the inviscid limit. The possibility

of the inverse energy cascade in two dimensions was first pointed out for a two-dimensional forced turbulence with the energy injected at the intermediate scale [3.18]. Since the enstrophy contains higher derivatives than the energy does, the enstrophy has a stronger k dependence than the energy. Thus, the enstrophy cascade is expected to play a dominant role in determining the inertial-range characteristics in the high-wave-number range (enstrophy-cascade range). As can be seen from Eqs. (3.63) and (3.64), $E_{2D}(k)$ is related to the Fourier amplitude of velocity, $\tilde{v}_k$, as $E_{2D}(k) \sim k^{-1}\tilde{v}_k^2$, and the enstrophy spectrum is expressed as $E_{2D}^{\Omega}(k) \sim k\tilde{v}_k^2$. In the enstrophy-cascade range, the enstrophy flux in wave-number or k space, $k\tilde{v}_k[kE_{2D}^{\Omega}(k)]$. should be balanced by the enstrophy dissipation rate ε_{Ω} in the equilibrium state;

$$k^3\tilde{v}_k^3 \sim \varepsilon_{\Omega}. \tag{3.65}$$

Then the two-dimensional energy spectrum in the enstrophy-cascade range obeys

$$E_{2D}(k) \sim \varepsilon_{\Omega}^{2/3}k^{-3}. \tag{3.66}$$

On the other hand. the energy cascade plays a key role in the low-wave-number range (energy-cascade range). In the energy-cascade range, the energy flux in k space, $k\tilde{v}_k\tilde{v}_k^2$. is balanced by the energy transfer rate ε_{2D} in the equilibrium state. This situation is the same as the ordinary energy cascade in the three-dimensional inertial range and the Kolmogorov scaling Eq. (3.46) is obtained. The sole difference is the lack of the energy sink or dissipation in two dimensions. In this sense, ε_{2D} is not the dissipation rate but the energy injection rate. The injected energy inversely cascades towards the large scales until the accumulation of energy stops owing to some saturation mechanism such as the back-scattering. Consequently, the two-dimensional energy spectrum in the inverse-energy-cascade range obeys

$$E_{2D}(k) \sim \varepsilon_{2D}^{2/3}k^{-5/3}. \tag{3.67}$$

These arguments concerning the enstrophy cascade and the inverse energy cascade were confirmed through high-resolution direct numerical simulations (DNS's) of decaying two-dimensional Navier–Stokes turbulence [3.20].

The inverse energy cascade and formation of coherent vortices in two-dimensional turbulence have been extensively studied by means of numerical simulation. The systematic DNS's of the two-dimensional decaying turbulence shows that coherent vortices can be formed from random initial conditions, and that such structures are sustained for a long time as a stationary state [3.21].

In atmospheric and oceanic turbulence research, a system of shallow-water equations rather than the Navier–Stokes equation has been extensively investigated, with special emphasis on the formation of structures such as the stripe or band patterns observed at the planetary surface. One of the representative shallow-water equations is the Charney equation [3.22]. This equation is equivalent to the Hasegawa–Mima equation for the drift

wave in plasmas [Eq. (2.23)] with the electrostatic potential replaced by the variable part of fluid depth [3.23]. The pioneering work in the numerical investigations of the shallow-water equation was performed in a one-eighth region of a rotating sphere, which successfully reproduced the striped pattern on the Jovian surface [3.24]. With advances in computer capability, high-resolution DNS's for the full region of a rotating sphere at relatively high Reynolds numbers have been performed. With the resort to a modified viscosity or hyperviscosity, the formation of coherent vortices in the polar region and the emergence of zonal jets in the low-latitude region have been reproduced [3.25].

3.2.5. Statistical theories In this article, we view the study of homogeneous isotropic turbulence as the first step towards understanding realistic complicated flows, and give a brief account of some representative statistical turbulence theories that are usually called closure theories. In this context, we shall put an emphasis on the direct-interaction approximation (DIA) for the following two reasons. One is that the mathematical procedures in the DIA are the basis of other theories, and the other is that the inhomogeneous-turbulence theory explained in §3.3 is founded on the DIA. The intermittency effects remarked on in §3.2.3A are small on turbulent fluxes such as R_{ij}. Thus no reference will be made to them.

A Direct-interaction approximation The statistical theory which has a profound influence on the study of turbulence, specifically, homogeneous isotropic turbulence, is the DIA [3.26, 3.27]. We first give a simple overview, and then proceed to its relationship with other approaches. Detailed discussions on the DIA are given in [1.5-1.7, 3.28].

A1 Formal procedure The instantaneous second-order correlation function $\langle \tilde{v}_i(\mathbf{k},t)\tilde{v}_j(\mathbf{k}',t)\rangle$ is a primary turbulence quantity in homogeneous flow, in relation to the energy spectrum $E(k)$. We bear a characteristic time such as Eq. (3.47) in mind, and introduce the two-time counterpart $\langle \tilde{v}_i(\mathbf{k},t)\tilde{v}_j(\mathbf{k}',t')\rangle$, which is denoted by $\chi_{ij}(t,t') = \langle X_i(t)X_j(t')\rangle$ in the abbreviated form based on Eq. (3.29). Then $\chi_{ij}(t,t')$ obeys

$$\left[\frac{\partial}{\partial t} + \gamma(i)\right]\chi_{ij}(t,t') = N_{i\ell m}\langle X_\ell(t)X_m(t)X_j(t')\rangle \equiv N_{i\ell m}\chi_{\ell mj}(t,t,t'). \quad (3.68)$$

In order to relate the two-time triple correlation function $\chi_{\ell mj}(t,t,t')$ on the right-hand side of Eq. (3.68) to the two-time second-order one, we start from the simple perturbational solution of Eq. (3.29). We assume that a random force $g(t)$ was imposed on the fluid motion in the past, that is, for $-\infty < t \ll 0$. This effect is removed from Eq. (3.68), for we are concerned with the turbulent state for $t > 0$. The formal solution

with the nonlinear part as an inhomogeneous source is given by

$$X_i(t) = X_i^{\mathrm{L}}(t) + N_{i\ell m}\int_{-\infty}^{t} \exp\left[-\gamma(i)(t-t_1)\right] X_\ell(t_1) X_m(t_1) dt_1, \tag{3.69}$$

with the linear solution $X_i^{\mathrm{L}}t)$ defined by

$$X_i^{\mathrm{L}}(t) = \int_{-\infty}^{t} \exp\left[-\gamma(i)(t-t_1)\right] g(t_1) dt_1; \tag{3.70}$$

namely, X_i^{L} obeys Gaussian statistics. We expect that this assumption brings no critical inconsistency into the final result since the past memory of turbulence is lost rapidly owing to intense mixing effects. In reality, the numerical simulation of turbulent flow indeed shows the independence of the fully-developed state from initial conditions.

In Eq. (3.69), we perform an iteration with the linear solution $X_i^{\mathrm{L}}(t)$ as the leading term and have

$$\begin{aligned} X_i(t) = {} & X_i^{\mathrm{L}}(t) + N_{i\ell m}\int_{-\infty}^{t} \exp\left[-\gamma(i)(t-t_1)\right] X_\ell^{\mathrm{L}}(t_1) X_m^{\mathrm{L}}(t_1) dt_1 \\ & + 2N_{i\ell m}N_{\ell ab}\int_{-\infty}^{t}\int_{-\infty}^{t_1} \exp\left[-\gamma(i)(t-t_1) - \gamma(\ell)(t_1-t_2)\right] \\ & \times X_a^{\mathrm{L}}(t_2) X_b^{\mathrm{L}}(t_2) X_m^{\mathrm{L}}(t_1) dt_1 dt_2 + \cdots \end{aligned} \tag{3.71}$$

where use has been made of the symmetry of $N_{i\ell m}$ concerning ℓ and m. Equation (3.71) may be regarded as an asymptotic expansion of $X_i(t)$ in the turbulence Reynolds number R_{C}, and the order of $N_{i\ell m}$ corresponds to that of R_{C}. The truncated solution at a finite order in $N_{i\ell m}$ is not straightforwardly applicable to turbulent flows at high R_{C}. A method for alleviating this difficulty is renormalization. In this method, we make use of the first few terms in Eq. (3.71) and incorporate parts of the contributions of infinite order in R_C into $\chi_{\ell mj}(t,t,t')$. Reader may see [1.34] for detailed discussions on renormalization.

From the assumption about the Gaussian distribution of $X_i^{\mathrm{L}}(t)$, we have

$$\begin{aligned} & \left\langle X_1^{\mathrm{L}}(t_1) X_2^{\mathrm{L}}(t_2) X_3^{\mathrm{L}}(t_3) \cdots X_n^{\mathrm{L}}(t_n) \right\rangle \\ & \quad = \begin{cases} \sum \left\langle X_a^{\mathrm{L}}(t_a) X_b^{\mathrm{L}}(t_b) \right\rangle \cdots \left\langle X_p^{\mathrm{L}}(t_p) X_q^{\mathrm{L}}(t_q) \right\rangle & \text{for even } n; \\ 0 & \text{for odd } n, \end{cases} \end{aligned} \tag{3.72}$$

where the summation is made over all the combinations concerning the second-order correlation functions.

From Eqs. (3.71) and (3.72), we have

$$\begin{aligned} & \left[\frac{\partial}{\partial t} + \gamma(i)\right] \chi_{ij}(t,t') \\ & \quad = 2N_{i\ell m}N_{jab}\int_{-\infty}^{t'} \exp\left[-\gamma(j)(t'-t_1)\right] \chi_{\ell a}^{\mathrm{L}}(t,t_1) \chi_{mb}^{\mathrm{L}}(t,t_1) dt_1 \end{aligned}$$

$$+ 4N_{i\ell m}N_{\ell ab}\int_{-\infty}^{t}\exp\left[-\gamma(m)(t-t_1)\right]\chi^{\mathrm{L}}_{ma}(t,t_1)\chi^{\mathrm{L}}_{bj}(t_1,t')dt_1$$
$$+ O\left(|N|^4\right), \tag{3.73}$$

where $\chi^{\mathrm{L}}_{ij}(t,t') = \langle X^{\mathrm{L}}_i(t)X^{\mathrm{L}}_j(t')\rangle$ expresses the contribution of the linear solution to $\chi_{ij}(t,t')$, and the numerical factors 2 and 4 arise from the symmetry of $N_{ij\ell}$ concerning j and ℓ.

To perform a renormalization, we now replace the linear part $\chi^{\ell}_{ij}(t,t')$ in Eq. (3.73) with its full counterpart $\chi_{ij}(t,t')$, and have

$$\left[\frac{\partial}{\partial t}+\gamma(i)\right]\chi_{ij}(t,t')$$
$$= 2N_{i\ell m}N_{jab}\int_{-\infty}^{t'}\exp[-\gamma(j)(t'-t_1)]\chi_{\ell a}(t,t_1)\chi_{mb}(t,t_1)dt_1$$
$$+ 4N_{i\ell m}N_{\ell ab}\int_{-\infty}^{t}\exp[-\gamma(m)(t-t_1)]\chi_{ma}(t,t_1)\chi_{bj}(t_1,t')dt_1. \tag{3.74}$$

In the light of the perturbation solution (3.71), Eq. (3.73) corresponds to a truncation at the second order in $N_{i\ell m}$, whereas Eq. (3.74) contains contributions of infinite order in $N_{i\ell m}$, although their inclusion is partial.

On the right-hand side of Eq. (3.74), $\exp[-\gamma(j)(t'-t_1)]$, in which $\gamma(j)$ corresponds to νk^2 in the original expression, represents the extent of the duration of past turbulent effects on $\chi_{ij}(t,t')$. At high R_{C}, $\gamma(j)$ becomes very small since it is proportional to ν. In Eq. (3.74), the effects of past events have an equal influence on $\chi_{ij}(t,t')$, unlike the expected effects due to turbulent mixing. The explicit occurrence of $\exp[-\gamma(j)(t'-t_1)]$ is not adequate for expressing those effects.

For the proper treatment of past turbulence events, we introduce the response or Green's function for Eq. (3.29), $G_{ij}(t,t')$, which obeys

$$\left[\frac{\partial}{\partial t}+\gamma(i)\right]G_{ij}(t,t')-\delta_{ij}\delta(t-t') = 2N_{i\ell m}X_\ell(t)G_{mj}(t,t'). \tag{3.75}$$

This equation expresses the response to an infinitesimal disturbance applied to Eq. (3.29) at time t'. Averaging of Eq. (3.75) results in

$$\left[\frac{\partial}{\partial t}+\gamma(i)\right]\bar{G}_{ij}(t,t')-\delta_{ij}\delta(t-t') = 2N_{i\ell m}\left\langle X_\ell(t)G_{mj}(t,t')\right\rangle, \tag{3.76}$$

with $\bar{G}_{ij}(t,t') = \langle G_{ij}(t,t')\rangle$. Its formal integration leads to

$$\bar{G}_{ij}(t,t') = \bar{G}^{\mathrm{L}}_{ij}(t,t')$$
$$+ 2N_{i\ell m}\int_{t'}^{t}\exp[-\gamma(i)(t-t_1)]\left\langle X_\ell(t_1)G_{mj}(t_1,t')\right\rangle dt_1, \tag{3.77}$$

where $\bar{G}^{\mathrm{L}}_{ij}(t,t')$ is a deterministic function and is given by

$$G^{\mathrm{L}}_{ij}(t,t') = \delta_{ij}\exp[-\gamma(i)(t-t')]\Theta(t-t'), \tag{3.78}$$

with the Heviside step function

$$\Theta(t) = \begin{cases} 1 & \text{for} \quad t > 0, \\ 0 & \text{for} \quad t < 0. \end{cases} \tag{3.79}$$

Here we should note that what represents as the memory effect on Eq. (3.74) is $\bar{G}^{\rm L}_{ij}(t,t')$ rather than $\bar{G}_{ij}(t,t')$.

The right-hand side of Eq. (3.76) may be calculated in exactly the same manner as for Eq. (3.68). We construct the perturbational solution of Eq. (3.77) with $\bar{G}^{\rm L}_{ij}(t,t')$ as the leading term, and substitute it into the right-hand side. We use Eq. (3.72), and then renormalize the resulting expression; namely, we replace $\chi^{\rm L}_{ij}(t,t')$ and $\bar{G}^{\rm L}_{ij}(t,t')$ with their full counterparts $\chi_{ij}(t,t')$ and $\bar{G}_{ij}(t,t')$. Finally, we have

$$\left[\frac{\partial}{\partial t} + \gamma(i)\right] \bar{G}_{ij}(t,t') - \delta_{ij}\delta(t-t') = 4N_{i\ell m}N_{nab}\int_{t'}^{t} \bar{G}_{mn}(t,t_1)\bar{G}_{bj}(t_1,t')\chi_{\ell a}(t,t_1)dt_1. \tag{3.80}$$

At the same time, we renormalize Eq. (3.74) concerning $\exp[-\gamma(j)(t'-t_1)]$ and $\exp[-\gamma(m)(t'-t_1)]$. and obtain

$$\left[\frac{\partial}{\partial t} + \gamma(i)\right] \chi_{ij}(t,t') = 2N_{i\ell m}N_{nab}\int_{-\infty}^{t'} \bar{G}_{jn}(t',t_1)\chi_{\ell a}(t,t_1)\chi_{mb}(t,t_1)dt_1 + 4N_{i\ell m}N_{nab}\int_{-\infty}^{t} \bar{G}_{en}(t,t_1)\chi_{ma}(t,t_1)\chi_{bj}(t_1,t')dt_1. \tag{3.81}$$

Equations (3.80) and (3.81) constitute the so-called DIA system.

A2 Isotropic form The abbreviated DIA system, Eqs. (3.80) and (3.81), may be translated simply into the full version based on Eq. (3.27). In this context, the full version of the response equation (3.75) is given by

$$\left(\frac{\partial}{\partial t} + \nu k^2\right) G_{ij}(\mathbf{k};t,t') - D_{ij}(\mathbf{k})\delta(t-t') = iM_{i\ell m}(\mathbf{k}) \iint \tilde{v}_\ell(\mathbf{p};t)G_{mj}(\mathbf{q};t,t')\delta(\mathbf{k}-\mathbf{p}-\mathbf{q})d\mathbf{p}d\mathbf{q}. \tag{3.82}$$

In Eq. (3.34), we drop the helicity-related part, and extend it to the two-time expression

$$\frac{\langle \tilde{v}_i(\mathbf{k};t)\tilde{v}_j(\mathbf{k}';t')\rangle}{\delta(\mathbf{k}+\mathbf{k}')} \equiv Q_{ij}(\mathbf{k};t,t') = D_{ij}(\mathbf{k})Q(k;t,t'). \tag{3.83}$$

The counterpart of $G_{ij}(\mathbf{k};t,t')$ is

$$\bar{G}_{ij}(\mathbf{k};t,t') = D_{ij}(\mathbf{k})\bar{G}(k;t,t'). \tag{3.84}$$

The DIA system of equations for $Q(k;t,t')$ and $\bar{G}_{ij}(k;t,t')$ is written as

$$\left(\frac{\partial}{\partial t}+\nu k^2\right)Q(k;t,t') = k^2\iint\delta(\mathbf{k}-\mathbf{p}-\mathbf{q})d\mathbf{p}d\mathbf{q} \times\left[N_{Q1}(k,p,q)\int_{-\infty}^{t'}\bar{G}(k;t',t_1)Q(p;t,t_1)Q(q;t,t_1)dt_1 - N_{Q2}(k,p,q)\int_{-\infty}^{t}\bar{G}(q;t,t_1)Q(p;t,t_1)Q(k;t_1,t')dt_1\right], \tag{3.85}$$

$$\left(\frac{\partial}{\partial t}+\nu k^2\right)\bar{G}(k;t,t') = \delta(t-t') - k^2\iint\delta(\mathbf{k}-\mathbf{p}-\mathbf{q})d\mathbf{p}d\mathbf{q} \times N_G(k,p,q)\int_{t'}^{t}\bar{G}(q;t,t_1)\bar{G}(k;t_1,t')Q(p;t,t_1)dt_1. \tag{3.86}$$

The geometrical factors N_{Q1} etc. are defined as

$$N_{Q1}(k,p,q) = N_{Q2}(k,p,q) = N_G(k,p,q) \equiv N(k,p,q) = (q/k)\left(xz+y^3\right), \tag{3.87}$$

where x, y, and z are the cosines of the angles opposite to the sides k, p, and q of a triangle, respectively.

The one-time covariance $Q(k;t)[=Q(k;t,t)]$ obeys

$$\left(\frac{\partial}{\partial t}+2\nu k^2\right)Q(k;t) = 2k^2\iint\delta(\mathbf{k}-\mathbf{p}-\mathbf{q})d\mathbf{p}d\mathbf{q} \times N(k,p,q)\left[\int_{-\infty}^{t}\bar{G}(k;t,t_1)Q(p;t,t_1)Q(k;t,t_1)dt_1 - \int_{-\infty}^{t}\bar{G}(q;t,t_1)Q(p;t,t_1)Q(k;t,t_1)dt_1\right]. \tag{3.88}$$

We should note that the symmetry of the DIA system guarantees statistical energy conservation by nonlinear terms of Eq. (3.88).

A3 Quasi-normal approximation In the history of turbulence theory, the predecessor of the DIA is the quasi-normal approximation (QNA) [3.29], whose primary concern is $Q(k;t)$. The QNA system may be derived from Eq. (3.88) through the replacement

$$Q(k;t,t') = \exp(-\nu k^2|t-t'|)Q(k;t'), \tag{3.89a}$$

$$\bar{G}(k;t,t') = \exp[-\nu k^2(t-t')]\Theta(t-t'), \tag{3.89b}$$

At high R_C (turbulence Reynolds number), $\exp(-\nu k^2|t-t'|)$ becomes nearly one, and the past effects of $Q(k;t,t')$ give equal contributions to the development of $Q(k;t,t')$, in spite that those effects in the distant past are smaller than their near-past counterparts. As a result, the QNA tends to overestimate the memory of past events or the energy transfer to small scales, resulting in the occurrence of negative $E(k)$.

A4 Relationship with the Kolmogorov energy spectrum In order to examine the relationship of the DIA system with the Kolmogorov energy spectrum, we seek an approximate solution of the system in the form

$$Q(k;t,t') = \sigma(k)\exp[-\omega(k)|t-t'|], \tag{3.90a}$$

$$G(k;t,t') = \exp[-\omega(k)(t-t')]\Theta(t-t'), \tag{3.90b}$$

where $\sigma(k)$ and $\omega(k)$ will be specified below. We substitute Eq. (3.90) into Eq. (3.88), and integrate the resulting expression under the condition that k falls in the inertial range, that is, $\ell_{\rm C}^{-1} \ll k \ll \ell_{\rm D}^{-1}$ [for $\ell_{\rm C}$ and $\ell_{\rm D}$, see Eqs. (3.42) and (3.43)]. Then we have

$$\varepsilon = 2\int_{r>k} r^2 d\mathbf{r} \iint N(k,p,q)\frac{\sigma(p)[\sigma(q)-\sigma(r)]}{\omega(k)+\omega(p)+\omega(q)}\delta(\mathbf{k}-\mathbf{p}-\mathbf{q})d\mathbf{p}d\mathbf{q}, \tag{3.91}$$

where use has been made of

$$2\nu\int_{r>k} r^2\sigma(r)d\mathbf{r} \cong 2\nu\int_{r\geq O(k_{\rm D})} r^2 E(r)dr = \varepsilon. \tag{3.92}$$

Next, we consider the response equation (3.86). The approximate solution (3.90) cannot satisfy it exactly. Since these expressions are proper for $t-t'$ not small, we adopt it in the sense of a weak solution; namely, we integrate Eq. (3.86) from $t'+0$ to infinity in time, and have

$$\omega(k) = \nu k^2 + \iint N(k,p,q)\frac{\sigma(p)}{\omega(p)+\omega(q)}\delta(\mathbf{k}-\mathbf{p}-\mathbf{q})d\mathbf{p}d\mathbf{q}. \tag{3.93}$$

From the Kolmogorov spectrum (3.46) and the related time scale (3.47), we write

$$\sigma(k) = \sigma\varepsilon^{2/3}k^{-11/3}, \quad \omega(k) = \omega\varepsilon^{1/3}k^{2/3}, \tag{3.94}$$

where σ and ω are numerical factors. We substitute Eq. (3.94) into Eq. (3.91), and have

$$\omega/\sigma^2 = 30.1. \tag{3.95}$$

The response equation (3.93) leads to

$$\frac{\omega^2}{\sigma} = \iint N(k,p,q)\frac{p^{-11/3}}{p^{2/3}+q^{2/3}}\delta(\mathbf{k}-\mathbf{p}-\mathbf{q})d\mathbf{p}d\mathbf{q}, \tag{3.96}$$

with the ν effect dropped. In Eq. (3.96), we encounter a serious difficulty in that the integral diverges at the lower limit or $p \to 0$. In physical terms, this divergence may be interpreted as an overestimate of the effects of the energy-containing motion on the inertial-range one. This point is a critical weakness of the DIA or, more exactly speaking, that of the DIA in the Eulerian frame.

In mathematical terms, the cause of the above sweakness of the Eulerian DIA system may be explained as follows. In the nonlinear part of Eq. (3.27), the contributions from p or q of $O(\ell_{\rm C}^{-1})(\ll k)$ gives

$$\tilde{\mathbf{v}}(\mathbf{k};t) \propto \exp(-i\mathbf{k}\cdot\tilde{\mathbf{v}}_{\rm C}t). \tag{3.97}$$

Here $\tilde{\mathbf{v}}_C$ is the velocity arising from energy-containing eddies defined by

$$\tilde{\mathbf{v}}_C = \int_{|\mathbf{p}| \le O(1/\ell_C)} \tilde{\mathbf{v}}(\mathbf{p}; t) d\mathbf{p}. \tag{3.98}$$

whose temporal variation is considered to be much slower than that of $\tilde{\mathbf{v}}(\mathbf{k}; t)$. From Eq. (3.97), we have

$$Q(k; t, t') \propto \langle \exp[-\imath \mathbf{k} \cdot \tilde{\mathbf{v}}_C (t - t')] \rangle . \tag{3.99}$$

Equation (3.99) suggests that the characteristic time scale of $Q(k; t, t')$ is proportional to k^{-1} which differs from the Kolmogorov counterpart (3.47) [3.30-3.32].

B Alternative approaches to the Kolmogorov scaling We have seen that the cause of the inconsistency of the DIA with the Kolmogorov energy spectrum is the overestimate of the effect of energy-containing eddies on inertial-range ones. In what follows, we shall give a brief account of the methods for recovering the spectrum.

B1 Eddy-damped quasi-normal Markovian (EDQNM) approximation The difficulty encountered by the DIA arises from the two-point quantities such as $Q(k; t, t')$ and $\bar{G}(k; t, t')$, whereas $Q(k; t)$ is free from it, as is seen from Eq. (3.95). The method using only $Q(k; t)$ is the eddy-damped quasi-normal Markovian (EDQNM) approximation [3.33, 3.34]. There we approximate

$$Q(k; t, t') = \bar{G}(k; t, t') Q(k; t), \tag{3.100}$$

for $t > t'$. Instead of solving the equation for $\bar{G}(k; t, t')$, we write $\omega(k)$ in Eq. (3.90) as

$$\omega(k) = C'_\omega \left[\int_0^k r^4 Q(r; t) dr \right]^{1/2} + \nu k^2, \tag{3.101}$$

from dimensional considerations. Here the numerical factor C'_ω is determined so that Eq. (3.88) combined with Eqs. (3.100) and (3.101) gives the Kolmogorov constant K_O around 1.5.

The choice of $\omega(k)$ is not unique, and the EDQNM approximation is subject to some theoretical ambiguity. Its merit, however, lies in its simplicity and applicability. This method has already been applied to the study of homogeneous-shear turbulence, effects of frame rotation on turbulence properties, etc. [3.35, 3.36]. In the latter case, the rotation effect on $\omega(k)$ needs to be included.

B2 Lagrangian formalism In order to properly treat the effect of energy-containing eddies sweeping away smaller eddies, we consider the evolution of a fluid blob or an eddy at time s, which was located at $\mathbf{x}$ at a previous time t. The velocity of the blob is denoted

by $\tilde{\mathbf{v}}(\mathbf{x}, t|s)$. The Eulerian velocity $\tilde{\mathbf{v}}(\mathbf{x}, t)$ is given by $\tilde{\mathbf{v}}(\mathbf{x}, t|t)$ [3.27, 3.37, 3.38]. The condition that this blob also passes the location $\mathbf{x}'$ at time $t'(t < t' < s)$ gives

$$\mathbf{x}' = \mathbf{x} + \int_t^{t'} \tilde{\mathbf{v}}(\mathbf{x}, t|t_1) dt_1, \tag{3.102}$$

$$\tilde{\mathbf{v}}(\mathbf{x}', t'|s) = \tilde{\mathbf{v}}(\mathbf{x}, t|s), \tag{3.103}$$

For infinitesimal $|t - t'|$, Eq. (3.103) is reduced to

$$\frac{\partial \tilde{\mathbf{v}}(\mathbf{x}, t|s)}{\partial t} + [\tilde{\mathbf{v}}(\mathbf{x}, t) \cdot \nabla] \tilde{\mathbf{v}}(\mathbf{x}, t|s) = 0. \tag{3.104}$$

In the Eulerian frame, $\langle \tilde{v}_i(\mathbf{x}, t) \tilde{v}_j(\mathbf{x}, t') \rangle$ for $(t > t')$ corresponds to the correlation between one blob located at $\mathbf{x}$ at time t' and another blob that was located at $\mathbf{x} - \int_t^{t'} \tilde{\mathbf{v}} dt_1$ at time t' and occupies the location $\mathbf{x}$ at time t. The Kolmogorov energy spectrum is linked with the energy cascade process in which one eddy is split into a number of smaller ones, and our concern is the historical development of those eddies. This process may be pursued properly with the aid of the Lagrangian correlation function

$$Q_{ij}^{\mathrm{LA}}(\mathbf{x}, t; \mathbf{x}, t') = \overline{\tilde{v}_i(\mathbf{x}, t|t) \tilde{v}_j(\mathbf{x}', t')}. \tag{3.105}$$

Here $\tilde{\mathbf{v}}(\mathbf{x}, t'|t)$ expresses such a historical evolution of eddies.

In correspondence to $Q_{ij}^{\mathrm{LA}}(\mathbf{x}, t; \mathbf{x}, t')$, we introduce the response function for $\tilde{\mathbf{v}}(\mathbf{x}, t'|t)$, $G_{ij}^{\mathrm{LA}}(\mathbf{x}, t; \mathbf{x}', t')$ and apply the renormalization procedures that are used in the Eulerian DIA. The Lagrangian method succeeds in reproducing the Kolmogorov spectrum with a reasonable estimate of the numerical constant.

B3 Renormalization-group method The renormalization-group (RNG) method was originally developed in the study of critical phenomena such as the phase transition of many-body systems [3.39]. The basic concept of the method may be summarized as follows. We consider the wavenumber range $(0 < k < \Lambda)$, and divide it into two ranges, $(0 < k < b\Lambda)$ (Range I) and $(b\Lambda < k < \Lambda)$ (Range II), where $0 < b < 1$ and b is usually chosen to be close to 1. In correspondence to Range I and Range II, the velocity $\tilde{\mathbf{v}}(\mathbf{k})$ is expressed as

$$\tilde{\mathbf{v}}(\mathbf{k}) = \tilde{\mathbf{v}}^{\mathrm{I}}(\mathbf{k}) + \tilde{\mathbf{v}}^{\mathrm{II}}(\mathbf{k}), \tag{3.106}$$

where $\tilde{\mathbf{v}}^{\mathrm{I}}(\mathbf{k}) = \tilde{\mathbf{v}}(\mathbf{k}) \Theta(b\Lambda - k)$ and $\tilde{\mathbf{v}}^{\mathrm{II}}(\mathbf{k}) = \tilde{\mathbf{v}}(\mathbf{k}) \Theta(k - b\Lambda)$. Following Eq. (3.27), we write

$$\left[\frac{\partial}{\partial t} + \nu(k) k^2 \right] \tilde{v}_i(k) = f_i(\mathbf{k}) + i M_{ij\ell}(\mathbf{k}) \iint \tilde{v}_j(\mathbf{p}) \tilde{v}_\ell(\mathbf{q}) \delta(\mathbf{k} - \mathbf{p} - \mathbf{q}) d\mathbf{p} d\mathbf{q}. \tag{3.107}$$

In the original equation (3.27), $\nu(k)$ is equal to the molecular viscosity ν, and a random force $\mathbf{f}(\mathbf{k})$ has been newly inserted [3.40].

We substitute Eq. (3.106) into Eq. (3.107), and obtain

$$\left[\frac{\partial}{\partial t}+\nu(k)k^2\right]\left[\tilde{v}_i^{\mathrm{I}}(\mathbf{k})+\tilde{v}_i^{\mathrm{II}}(\mathbf{k})\right] = f_i(\mathbf{k})+iM_{ij\ell}(\mathbf{k})\iint\delta(\mathbf{k}-\mathbf{p}-\mathbf{q})d\mathbf{p}d\mathbf{q} \times\left[\tilde{v}_j^{\mathrm{I}}(\mathbf{p})\tilde{v}_\ell^{\mathrm{I}}(\mathbf{q})+2\tilde{v}_j^{\mathrm{I}}(\mathbf{p})\tilde{v}_\ell^{\mathrm{II}}(\mathbf{q})+\tilde{v}_j^{\mathrm{II}}(\mathbf{p})\tilde{v}_\ell^{\mathrm{II}}(\mathbf{q})\right]. \tag{3.108}$$

We focus attention on the interaction among the $\tilde{\mathbf{v}}^{\mathrm{II}}$'s, dropping the interaction between the $\tilde{\mathbf{v}}^{\mathrm{I}}$ and $\tilde{\mathbf{v}}^{\mathrm{II}}$ because the main interest of the RNG lies in the effects of the interaction among small-scale fluctuations on large-scale fluctuations. Using the perturbational solution of $\tilde{\mathbf{v}}^{\mathrm{II}}(\mathbf{k})$ of the type (3.71), we evaluate the interaction among $\tilde{\mathbf{v}}^{\mathrm{II}}$'s, and incorporate the effect into the $\nu(k)$-related part, obtaining new $\nu_N(k)$. In this evaluation, the dimension of the $\mathbf{k}$ space is extended to $d(\neq 3)$. Next, we extend Range I into the full one, that is, $0<k<\Lambda$, through the transformation $k\longrightarrow b^{-1}k$. Considering that Eq. (3.98) is the equation obtained by repeating this procedure many times, we may seek the fixed point of the resulting equation from the condition

$$\nu(k)=\nu_N(k). \tag{3.109}$$

In this mathematical manipulation, the lower limit of the integral is $b\Lambda$, leading to the escape of the infrared divergence encountered in the Eulerian DIA [3.40].

The RNG method is originally intended to abstract the power laws concerning k, as is suggested by the transformation $k\longrightarrow b^{-1}k$. The deduction of the Kolmogorov $-5/3$ power spectrum is within the scope of this method, but the estimate of the proportionality constant, that is, K_{O} in Eq. (3.46), is not so. A method of estimating it is the use of the energy equation in the DIA system, Eq. (3.91). The original application of the RNG method to turbulence has been subject to quite a few corrections and criticisms since its first attempt [1.6, 3.41-3.44]. The method has also been applied to the study of inhomogeneous turbulence, specifically, the analysis of the Reynolds stress R_{ij} [3.45, 3.46].

C Probability-distribution formalism In methods such as the DIA and RNG ones, the direct concern is the correlation functions of velocity. The closure formalism has also been sought on the basis of the probability distribution functional. In what follow, we shall refer to a self-consistent approach based on the Fokker–Planck equation.

C1 Liouville equation We denote the set of $(X_1, X_2, X_3, \cdots)$ by $\mathbf{X}$, and consider the probability distribution functional $P\{\mathbf{X}, t\}$ for $\mathbf{X}$. The probability distribution

functional $P\{\mathbf{X};t\}$ obeys the Liouville equation

$$\frac{\partial P\{\mathbf{X};t\}}{\partial t}+\frac{\partial}{\partial X_\ell}\left(\frac{\partial X_\ell}{\partial t}P\{\mathbf{X};t\}\right)=0, \tag{3.110}$$

which expresses the conservation of the probability density in phase space.

We first consider a simple system

$$\frac{\partial X_i}{\partial t}=-\gamma(i)X_i+w_i, \tag{3.111}$$

where $\mathbf{w}$ is a random white noise fulfilling the constraint

$$\overline{w_i w_j}^w=2\eta(i)\delta_{ij}\delta(t-t'). \tag{3.112}$$

In what follows, the w-attached overbar denotes the ensemble averaging concerning $\mathbf{w}$. We substitute Eq. (3.111) into Eq. (3.110), and take the average concerning $\mathbf{w}$. Then we have

$$\frac{\partial\overline{P}^w\{\mathbf{X};t\}}{\partial t}-\frac{\partial}{\partial X_\ell}\left[\gamma(\ell)X_\ell\overline{P}^w\{\mathbf{X};t\}\right]-\eta(\ell)\frac{\partial^2\overline{P}^w\{\mathbf{X};t\}}{\partial X_\ell^2}=0. \tag{3.113}$$

This equation is called the Fokker–Planck equation, and the random noise corresponds to the diffusion effect in light of the probability distribution function (PDF). The time-independent solution of Eq. (3.113) expresses the Gaussian state, as will be seen below.

The Liouville equation for Eq. (3.29) is

$$\frac{\partial P\{\mathbf{X};t\}}{\partial t}-\frac{\partial}{\partial X_\ell}\left[\gamma(\ell)X_\ell P\{\mathbf{X};t\}\right]+\frac{\partial}{\partial X_\ell}\left(N_{\ell mn}X_m X_n P\{\mathbf{X};t\}\right)=0. \tag{3.114}$$

C2 Characteristic functional The characteristic functional $\Psi\{\mathbf{Y};t\}$ is defined as

$$\Psi\{\mathbf{Y};t\}\equiv\langle\exp(i\mathbf{X}\cdot\mathbf{Y})\rangle=\int\exp(i\mathbf{X}\cdot\mathbf{Y})P\{\mathbf{X};t\}d\mathbf{X}. \tag{3.115}$$

The relationship between $P\{\mathbf{X};t\}$ and $\Psi\{\mathbf{Y};t\}$ is similar to the Fourier representation (3.25). In terms of $\Psi\{\mathbf{Y};t\}$, the correlation function $\langle X_i X_j\rangle$ may be calculated more simply as

$$\langle X_i X_j\rangle=\int X_i X_j P\{\mathbf{X};t\}d\mathbf{X}=-\left(\frac{\partial^2\Psi\{\mathbf{Y};t\}}{\partial Y_i\partial Y_j}\right)_{\mathbf{Y}=0}, \tag{3.116}$$

compared with $P\{\mathbf{X};t\}$.

From Eq. (3.113), $\Psi\{\mathbf{Y};t\}$ obeys

$$\frac{\partial\overline{\Psi}^w\{\mathbf{Y};t\}}{\partial t}+\gamma(\ell)Y_\ell\frac{\partial\overline{\Psi}^w\{\mathbf{Y};t\}}{\partial Y_\ell}+\eta(\ell)Y_\ell^2\overline{\Psi}^w\{\mathbf{Y};t\}=0. \tag{3.117}$$

The stationary solution of Eq. (3.117) is given by

$$\overline{\Psi}^w\{\mathbf{Y};t\}=\exp\left[-\sum_\ell\frac{\sigma(\ell)}{2}Y_{(\ell)}^2\right], \tag{3.118}$$

which obeys the condition $\overline{\Psi}^{w}\{\mathbf{0};t\} = 1$ that arises from Eq (3.115). Here the summation convention is not applied to parenthesized subscripts, and

$$\sigma(\ell) = \eta(\ell)/\gamma(\ell). \tag{3.119}$$

From Eq. (3.119), we have

$$\langle X_i X_j \rangle = \sigma(i)\delta_{ij}, \tag{3.120}$$

$$\langle X_i X_j X_\ell X_m \rangle = \sigma(i)\sigma(\ell)\delta_{ij}\delta_{\ell m} + \sigma(i)\sigma(j)\delta_{i\ell}\delta_{jm} + \sigma(i)\sigma(j)\delta_{im}\delta_{j\ell}, \tag{3.121}$$

and vanishing $\langle X_i X_j X_\ell \rangle$ etc. Namely, Eq. (3.118) is the characteristic functional for the Gaussian probability density functional leading to Eq. (3.72).

For Eq. (3.114), we have

$$\frac{\partial \Psi\{\mathbf{Y};t\}}{\partial t} - \gamma(\ell)Y_\ell \frac{\partial \Psi\{\mathbf{Y};t\}}{\partial Y_\ell} - iN_{\ell mn}Y_\ell \frac{\partial^2 \Psi\{\mathbf{Y};t\}}{\partial Y_m \partial Y_n} = 0. \tag{3.122}$$

This equation is linear in $\Psi\{\mathbf{Y};t\}$ and seems to be more manageable, compared with the original equation (3.29). The latter mathematical difficulty, however, is merely transformed to the difficulty in treating the second-order derivatives in Eq. (3.122).

C3 Self-consistent approach of Fokker–Planck type In methods such as the DIA, Gaussian statistics is used at the stage before the renormalization is performed. In the context of a characteristic functional, the Gaussian-distribution approximation corresponds to the use of an equation of Fokker–Planck type such as Eq. (3.113). As a method in this line, we may mention a self-consistent Fokker–Planck/type approach [3.1, 3.47].

For investigating the stationary state of Eq. (3.114), we first rewrite it as

$$\begin{aligned} L\Psi &\equiv \left[\omega(\ell)Y_\ell \frac{\partial}{\partial Y_\ell} + \eta_{\mathrm{T}}(\ell)Y_\ell^2\right]\Psi \\ &= \left[\omega(\ell) - \gamma(\ell)\right] Y_\ell \frac{\partial \Psi}{\partial Y_\ell} + iN_{\ell mn}Y_\ell \frac{\partial^2 \Psi}{\partial Y_m \partial Y_n} + \eta_{\mathrm{T}}(\ell)Y_\ell^2\Psi, \end{aligned} \tag{3.123}$$

on the basis of newly introduced functions $\omega(i)$ and $\eta_{\mathrm{T}}(i)$. Here $\omega(i)$ corresponds to $\gamma(i)$ in Eq. (3.29) or (3.111), and represents the nonlinear modification of the molecular-viscosity effect. The other function $\eta_{\mathrm{T}}(i)$ corresponds to $\eta(i)$ in Eq. (3.112), and indicates that the property of turbulence which cannot be described by only the effects of $\omega(i)$, is approximated by the random noise. In short, we try to renormalize the nonlinear effects of turbulence in terms of these two factors, and shall treat the right-hand side of Eq. (3.123) as a perturbation term to the left-hand side.

We expand Ψ around the Gaussian characteristic functional Ψ_0 as

$$\Psi = \sum_{i=0}^{\infty} \Psi_i. \tag{3.124}$$

where Ψ_0 obeys

$$L\Psi_0 = 0. \tag{3.125}$$

Namely, Ψ_0 is given by Eq. (3.118) with $\sigma(\ell)$ replaced with

$$\sigma(\ell) = \eta_T(\ell)/\omega(\ell). \tag{3.126}$$

The higher-order solutions $\Psi_n (n \geq 1)$ may be obtained using formulae such as

$$L\left(Y_i Y_j Y_\ell \Psi_0\right) = \left[\sigma(i) + \sigma(j) + \sigma(\ell)\right] Y_i Y_j Y_\ell \Psi_0. \tag{3.127}$$

In order to determine $\omega(i)$ and $\eta_T(i)$ [or $\sigma(i)$], we need two relations. As one relation, we require that the turbulent energy $\langle X_i^2/2\rangle$ may be evaluated using only the leading term Ψ_0 [3.47]; namely, we write

$$\left(\frac{\partial^2}{\partial Y_i^2} \sum_{n=1}^{\infty} \Psi_n\right)_{\mathbf{Y}=0} = 0. \tag{3.128}$$

This requirement is reasonable from the viewpoint that the lowest approximation is most significant in the perturbation expansion. Using the solution up to the second-order in $N_{ij\ell}$ and to the first order in ω and η_T, we evaluate Eq. (3.128), and reach the same equation as Eq. (3.91) in the representation based on Eq. (3.27).

The unknown $\omega(i)$ represents the enhancement of resistive or memory-loss effects due to the nonlinear interaction, as was noted below Eq. (3.123). In the context of Eq. (3.29), $N_{ij\ell} X_j X_\ell$ is replaced with $-\omega(i) X_i$. In order to guarantee that this approximation is optimal, we require

$$\frac{\delta}{\delta\omega(i)} \left\langle \left\{ N_{\ell mn} X_m X_n - \left[-\omega(\ell) X_\ell\right] \right\}^2 \right\rangle = 0, \tag{3.129}$$

which leads to

$$\omega(i) = -N_{(i)mn} \langle X_{(i)} X_m X_n \rangle / \langle X_{(i)}^2 \rangle \tag{3.130}$$

(the summation convention is not applied to parenthesized i). As the simplest approximation to the estimate of $\langle X_{(i)} X_m X_n \rangle$, we may use the first-order solution Ψ_1 [3.48].

Equations (3.128) and (3.130) are based on the one-time correlations such as $\langle X_{(i)}^2 \rangle$ and $\langle X_{(i)} X_m X_n \rangle$, and are free from the infrared divergence that the Eulerian DIA encounters. As a result, the Kolmogorov $-5/3$ power law may be reproduced in the full version based on the Navier–Stokes equation (3.27).

3.3. Inhomogeneous Turbulence

3.3.1. Inhomogeneity effects In §3.2, attention was focused on homogeneous turbulence, specifically, an isotropic one. Homogeneous turbulence lacks the feedback

effect of fluctuations on the mean field since $\partial(-R_{ij})/\partial x_j$ vanishes in Eq. (3.2). Real-world turbulent flows are always inhomogeneous, and the mean field and the fluctuation around it interact with each other inseparably. It is difficult to analyze those flows by a resort to computer experiments only. In the presence of mean flow, ℓ_C and v_C in Eqs. (3.43) and (3.44) are replaced by the reference length and velocity characterizing each flow, L_R and V_R, respectively. Equation (3.44) is rewritten as

$$\ell_D/L_C = Re^{-3/4}, \tag{3.131}$$

with

$$Re = V_R L_R/\nu. \tag{3.132}$$

In the numerical computation of Eqs. (2.5) and (2.6), a flow region is divided into a number of grids. In order to resolve the energy-dissipation process essential in turbulent flow, the number of necessary grids is

$$N = O\left(Re^{9/4}\right), \tag{3.133}$$

from Eq. (3.131). In real-world flows, it is not rare that Re is of $O(10^6)$, resulting in $N = O(10^{13})$. The computer that can meet this requirement is not probable in the foreseeable future.

Inhomogeneity effects on turbulence arise from the mean-velocity tensor $\partial\bar{V}_j/\partial x_i$ in the second term on the left-hand side of Eq. (3.6). The tensor may be divided into the mean-strain and -vorticity tensors, $\bar{s}_{ij}$ and $\bar{\omega}_{ij}$, as

$$\frac{\partial\bar{V}_j}{\partial x_i} = \frac{1}{2}\left(\bar{s}_{ij} + \bar{\omega}_{ij}\right), \tag{3.134}$$

with

$$\bar{s}_{ij} = \frac{\partial\bar{V}_j}{\partial x_i} + \frac{\partial\bar{V}_i}{\partial x_j}, \quad \bar{\omega}_{ij} = \frac{\partial\bar{V}_j}{\partial x_i} - \frac{\partial\bar{V}_i}{\partial x_j}. \tag{3.135}$$

The time scale characterizing the mean straining motion is given by

$$\tau_S = \|\bar{s}\|^{-1}, \tag{3.136}$$

where the magnitude of tensor A_{ij} is defined by $\|A\|(\equiv \sqrt{A_{ij}^2})$. As representative quantities characterizing the fluctuating motion, we may mention the turbulent energy K [Eq. (3.12)] and its dissipation rate ε [Eq. (3.15)], which constitute a characteristic turbulence time scale

$$\tau_T = K/\varepsilon. \tag{3.137}$$

On the left-hand side of Eq. (3.6), we estimate the relative magnitude of the second linear term to the third nonlinear one. We scale $\tilde{\mathbf{v}}$ by $\sqrt{K}$, and $\mathbf{x}$ in the nonlinear term by ℓ_C, where ℓ_C is written as

$$\ell_C = K^{3/2}/\varepsilon, \tag{3.138}$$

from Eq. (3.43). The relative magnitude is estimated as

$$\vartheta \equiv \frac{[[(\tilde{\mathbf{v}} \cdot \nabla)\bar{\mathbf{V}}]]}{[[\nabla \cdot (\tilde{\mathbf{v}}\tilde{\mathbf{v}})]]} = \frac{K\|\bar{s}\|}{\varepsilon}, \tag{3.139}$$

where $[[X]]$ denotes the magnitude of X based on the above order of magnitude estimate.

For strong inhomogeneity or large ϑ, the nonlinear term in Eq. (3.6) may be discarded, leading to a linear equation. This approximation is called the rapid-distortion theory (RDT), which is useful in the analysis of the fluctuating motion in the presence of the steep change of mean flow [3.49]. Such a change is often generated by boundaries. As the initial large distortion of the fluctuating motion relaxes, the nonlinear term gradually becomes important. As a result, the validity of the RDT is limited to a short time interval after the imposition of inhomogeneity on the fluctuating motion. The extension of the RDT to the nonlinear regime is a challenging task. In a situation with weak inhomogeneity or small ϑ, the linear term plays the role of bringing anisotropic properties into the isotropic fluctuating motion. Heuristic modelling based on small ϑ will be explained in §3.3.2.

3.3.2. Heuristic modelling The numerical computation of the Navier–Stokes equations is very difficult for real-world flows at high Reynolds numbers, as was stated in §3.3.1. Under the situation, we have two approaches to the analysis of those flows. One is to focus attention on global properties represented by the mean flow, under the use of Eq. (3.2). Another is the use of Eq. (3.20) that is founded on the filtering procedure. In the latter approach, we eliminate only the fluctuating motion whose spatial scale is smaller than the computational grid size, at the cost of increasing computational burden. The eliminated effects are compensated for through Eqs. (3.21)-(3.23). This procedure is called the subgrid-scale (SGS) modelling, whereas the former approach based on the ensemble averaging is named the Reynolds-mean modelling.

The Reynolds-mean model is further divided into two categories. In one category, we model the Reynolds stress R_{ij} [Eq. (3.4)] and the turbulent heat flux $\mathbf{H}$ [Eq. (3.5)], and relate them directly to the mean velocity and temperature, $\bar{\mathbf{V}}$ and $\bar{\theta}$. This type of modelling is called turbulent-viscosity and -diffusivity modelling. In another category, we deal with the transport equation (3.7) for R_{ij} and the counterpart for $\mathbf{H}$. There the modelling of Π_{ij} etc. is a central task. This category is called second-order modelling.

A K–ε model The simplest model of R_{ij} is the K–ε model based on the concept of turbulent viscosity or enhanced momentum diffusivity [3.50]. It is written as

$$R_{ij} = \frac{2}{3}K\delta_{ij} - \nu_{\mathrm{T}}\bar{s}_{ij}, \tag{3.140}$$

with ν_{T} as the turbulent viscosity. Considering the energy-containing components of fluctuations to contribute mainly to the momentum transport, we adopt K as the

quantity statistically characterizing those components. Moreover we use occurring in the K equation (3.13). In terms of them, we express

$$\nu_{\mathrm{T}} = C_\nu K^2/\varepsilon, \tag{3.141}$$

where $C_\nu = 0.09$. Here and hereafter, we give a typical choice of model constants for understanding their approximate magnitudes. In correspondence to Eqs. (3.140) and (3.141), the turbulent heat flux $\mathbf{H}$ [Eq. (3.5)] is modelled as

$$\mathbf{H} = -(\nu_{\mathrm{T}}/\sigma_H)\nabla\bar{\theta}, \tag{3.142}$$

with $\sigma_H = 0.7$.

In order to close Eqs. (3.1), (3.2) and (3.140), we need transport equations for K and ε. The mathematical basis of Eq. (3.13) for K is clear in relation to the kinetic-energy conservation law in the case of solenoidal inviscid flow (recall the discussion in §3.1.1). The sole term to be modelled is $\mathbf{T}_K$. Apart from the $\tilde{p}$-related part, $\mathbf{T}_K$ is the energy transport rate of the fluctuating motion by itself, and the energy may be considered to be transported from the high-K region to the low-K one, as is similar to heat transport, leading to

$$\mathbf{T}_K = -(\nu_{\mathrm{T}}/\sigma_K)\nabla K, \tag{3.143}$$

with $\sigma_K = 1$.

All that remains is equation for ε. The mathematical structure of the ε equation derived from Eq. (3.6) is much less clear, compared with Eq. (3.13), for we have no conservation relation for ε. The model equation for ε is constructed in quite a heuristic way. This point is one of the bottlenecks in the development of turbulence models. The simplest model is given by

$$\frac{D\varepsilon}{Dt} = C_{\varepsilon 1}\frac{\varepsilon}{K}P_K - C_{\varepsilon 2}\frac{\varepsilon^2}{K} + \nabla\cdot\left(\frac{\nu_{\mathrm{T}}}{\sigma_\varepsilon}\nabla\varepsilon\right), \tag{3.144}$$

with $(C_{\varepsilon 1}, C_{\varepsilon 2}, \sigma_\varepsilon) = (1.4, 1.9, 1.3)$. The basic concept of Eq. (3.144) is that K and ε should obey similar equations since large K and ε often occur togather spatially.

The foregoing model is called the K-ε one, and is the prototype of all the current turbulence models.

In inhomogeneous turbulent flows, the energy-input process due to P_K is always important, as well as the dissipation process. Hence we pay attention to these two, and write

$$P_K \cong \varepsilon. \tag{3.145}$$

This situation corresponds to the equilibrium state assumed in the discussion on the inertial range. Equation (3.145) is combined with Eqs. (3.138), (3.140), and (3.141), giving

$$K \propto (\ell_{\mathrm{C}}\|\bar{s}\|)^2, \tag{3.146}$$

resulting in

$$\nu_{\mathrm{T}} \propto \ell_{\mathrm{C}}^2 \|\bar{s}\|. \tag{3.147}$$

This is the mixing-length representation for ν_{T}, although it was derived originally in an entirely different way. The present derivation indicates that it is deeply based on the assumption of the equilibrium state. Physically, ℓ_{C} is the spatial scale characterizing the energy-containing eddies contributing to the momentum transport.

A deficiency of the turbulent-viscosity representation (3.140) occurs typically in wall flows. In a channel flow between two parallel walls whose mean velocity is given by $(\bar{v}_x(y), 0, 0)$, we have

$$\left\langle \tilde{v}_x^2 \right\rangle = \left\langle \tilde{v}_y^2 \right\rangle = \left\langle \tilde{v}_z^2 \right\rangle, \tag{3.148}$$

where x and z are the streamwise and spanwise directions while y is normal to the wall. Observation, however, indicates the anisotropy of turbulent intensities

$$\left\langle \tilde{v}_x^2 \right\rangle > \left\langle \tilde{v}_z^2 \right\rangle > \left\langle \tilde{v}_y^2 \right\rangle, \tag{3.149}$$

and the intensity normal to the wall is highly suppressed. Thus, the normal intensity is overestimated under Eq. (3.140). The overestimate is a defect intrinsic to the turbulent-viscosity model, which arises from the fact that P_K is always positive in the model. This defect gives rise to a serious problem in the analysis of engineering turbulent flows in which the mean flow impinges on a solid wall.

B Second-order modelling The representative method of alleviating the shortfall of the K–ε model is the use of the transport equation (3.7) for R_{ij}. The method is called the second-order modelling [3.51, 3.52]. There the primary term to be modelled is the pressure-strain correlation function Π_{ij}, which does not occur in the K equation (3.13). Rather, it contributes to the energy exchange among three turbulent intensities, as was noted in §3.1.1.

In the K–ε model, R_{ij} was modelled using K and ε in addition to the mean-velocity strain $\bar{s}_{ij}$ (note that $\bar{\omega}_{ij}$ does not enter R_{ij} from the symmetry of the tensor). In the second-order modelling, the counterparts of these quantities are

$$K, \quad \varepsilon, \quad B_{ij}, \quad \bar{s}_{ij}, \quad \bar{\omega}_{ij}, \tag{3.150}$$

where B_{ij} denotes the deviatoric part of R_{ij} defined as

$$B_{ij} = [R_{ij}]_{\mathrm{D}} \equiv R_{ij} - \frac{1}{3} R_{\ell\ell} \delta_{ij}, \tag{3.151}$$

and indicates the degree of anisotropy of R_{ij} (note that $B_{ij} = 0$).

In order to see the primary role of Π_{ij}, we consider the situation that the turbulent state has no mean flow and is highly anisotropic at the initial stage. In this case,

Eq. (3.7) is simplified to

$$\frac{\partial B_{ij}}{\partial t} = \Pi_{ij} - [\varepsilon_{ij}]_{\mathrm{D}} . \tag{3.152}$$

We adopt the simplest model for Π_{ij}

$$\Pi_{ij} = -C_{\Pi 1} (\varepsilon/K) B_{ij}. \tag{3.153}$$

with $C_{\Pi 1} = 1.8$. In the absence of the mean flow that is the cause of the anisotropy of fluctuations, the turbulent state will relax to the isotropic one as time elapses. Equation (3.152) fulfills this property for positive $C\Pi 1$ (note that ε_{ij} associated with viscous effects does not contribute to the occurrence of anisotropy).

For incorporating the effects of mean flow into Eq. (3.153), we retain the terms of first order in each of B_{ij}, $\bar{s}_{ij}$, and $\bar{\omega}_{ij}$, and model Π_{ij} as

$$\begin{aligned}\Pi_{ij} = & -C_{\Pi 1}\frac{\varepsilon}{K}B_{ij} + C_{\Pi 2}K\bar{s}_{ij} + C_{\Pi 3}\left[B_{i\ell}\bar{s}_{\ell j} + B_{j\ell}\bar{s}_{\ell i}\right]_D \\ & + C_{\Pi 4}\left(B_{i\ell}\bar{\omega}_{\ell j} + B_{j\ell}\bar{\omega}_{\ell i}\right).\end{aligned} \tag{3.154}$$

with $(C_{\Pi 2}, C_{\Pi 3}, C_{\Pi 4}) = (0.4, 0.3, 0.1)$ [3.53]. We usually rettain the terms up to the first order in $\bar{s}_{ij}$ and $\bar{\omega}_{ij}$ because the Poisson equation for $\tilde{p}$, which is derived by taking the divergence of Eq. (3.6), is linearly dependent on $\bar{s}_{ij}$ and $\bar{\omega}_{ij}$. However it is not mathematically guaranteed that Π_{ij} is really free from nonlinear dependence on those quantities.

Concerning the dependence of Π_{ij} on B_{ij}, the maximum order is the second order from the Caley–Hamilton formula

$$B_{i\ell}B_{\ell m}B_{mj} = \frac{1}{2}B_{\ell m}^2 B_{ij} - \frac{1}{3}B_{\ell m}B_{mn}B_{n\ell}\delta_{ij}. \tag{3.155}$$

From this result, the effects of the third or higher order in B_{ij} are incorporated into the non-dimensional coefficients, and $C_{\Pi n}$'s become functionals of $B_{\ell m}^2$ and $B_{\ell m}B_{mn}B_{n\ell}$ [3.54].

What remained to be modelled in Eq. (3.7) is the destruction term ε_{ij} [Eq. (3.10)] and the transport term $T_{ij\ell}$ [Eq. (3.11)]. For ε_{ij}, we may make the same discussion as for Π_{ij} and reach a similar mathematical expression. Then we may extend the foregoing modelling to Π_{ij} for $\Pi_{ij} - \varepsilon_{ij}$.

In Eq. (3.11), we pay attention to $\langle \tilde{v}_i \tilde{v}_j \tilde{v}_\ell \rangle$, as is similar to the modelling of $\mathbf{T}_K$ [Eq. (3.16)]. It expresses the transport rate of the stress $\tilde{v}_j \tilde{v}_\ell$ by $\tilde{v}_i$. Further we consider the symmetry concerning suffices, and write

$$T_{ij\ell} = -\frac{\nu_{\mathrm{T}}}{\sigma_{\mathrm{T}}}\left(\frac{\partial R_{j\ell}}{\partial x_i} + \frac{\partial R_{\ell i}}{\partial x_j} + \frac{\partial R_{ij}}{\partial x_\ell}\right), \tag{3.156}$$

with σ_{T} as a positive constant (note that $R_{j\ell} = \langle \tilde{v}_j \tilde{v}_\ell \rangle$). A more complicated model

$$T_{ij\ell} = -C_{\mathrm{T}}\frac{K}{\varepsilon}\left(R_{im}\frac{\partial R_{j\ell}}{\partial x_m} + R_{jm}\frac{\partial R_{\ell i}}{\partial x_m} + R_{\ell m}\frac{\partial R_{ij}}{\partial x_m}\right) \tag{3.157}$$

has also been proposed (C_{T} is a positive constant) [3.53]. Equation (3.156) may be obtained from Eq. (3.157) by replacing R_{ij} with its isotropic part $(2/3)K\delta_{ij}$.

Compared with the turbulent-viscosity modelling, the foregoing second-order modelling may give better results in the analysis of inhomogeneous turbulence, specifically, in the case of a simple flow geometry. In complicated flows in engineering devices, one often encounters computational difficulties such as numerical instabilities. They are related to the fact that those models do not always obey realizability conditions such as

$$R_{(i)(i)} > 0, \quad R_{(i)(i)}R_{(j)(j)} > R^2_{(i)(j)}, \quad \text{etc.} \tag{3.158}$$

(the summation convention is not applied to parenthesized subscripts).

C Nonlinear algebraic modelling The turbulent-viscosity modelling often fails to recover some basic properties of turbulent flow, whereas the second-order modelling leads to a heavy computational burden in analyzing turbulence subject to complex flow geometry. As an intermediate form of modelling, we may mention the nonlinear algebraic one.

We first rewrite Eq. (3.7) as

$$\frac{\partial B_{ij}}{\partial t} = [P_{ij}]_{\mathrm{D}} + \Pi_{ij} - [\varepsilon_{ij}]_{\mathrm{D}} + \frac{\partial [T_{ij\ell}]_{\mathrm{D}}}{\partial x_\ell}, \tag{3.159}$$

where the ν-related part has been dropped, and

$$[P_{ij}]_{\mathrm{D}} = -\frac{2}{3}K\bar{s}_{ij} - \frac{1}{2}\left[B_{i\ell}\bar{s}_{\ell j} + B_{j\ell}\bar{s}_{\ell i}\right]_{\mathrm{D}} - \frac{1}{2}\left(B_{i\ell}\bar{\omega}_{\ell j} + B_{j\ell}\bar{\omega}_{\ell i}\right). \tag{3.160}$$

We substitute Eq. (3.154) into Eq. (3.159), and regard the resulting expression as an equation for B_{ij}

$$\begin{aligned} B_{ij} = & -\left(\frac{2}{3C_{\Pi 1}} - \frac{C_{\Pi 2}}{C_{\Pi 1}}\right)\frac{K^2}{\varepsilon}\bar{s}_{ij} + \left(-\frac{1}{2C_{\Pi 1}} + \frac{C_{\Pi 3}}{C_{\Pi 1}}\right)\frac{K}{\varepsilon}\left[B_{i\ell}\bar{s}_{\ell j} + B_{j\ell}\bar{s}_{\ell i}\right]_{\mathrm{D}} \\ & + \left(-\frac{1}{2C_{\Pi 1}} + \frac{C_{\Pi 4}}{C_{\Pi 1}}\right)\frac{K}{\varepsilon}\left(B_{i\ell}\bar{\omega}_{\ell j} + B_{j\ell}\bar{\omega}_{\ell i}\right) \\ & - \frac{1}{C_{\Pi 1}}\frac{K}{\varepsilon}\frac{DB_{ij}}{Dt} - \frac{1}{C_{\Pi 1}}\frac{K}{\varepsilon}\frac{\partial [T_{ij\ell}]_{\mathrm{D}}}{\partial x_\ell}. \end{aligned} \tag{3.161}$$

We solve Eq. (3.161) by an iteration method with the first term as the leading one. In the first iteration, the first three parts on the right hand result in the nonlinear algebraic model

$$B_{ij} = -C_\nu\frac{K^2}{\varepsilon}\bar{s}_{ij} + C_{\mathrm{N}1}\frac{K^3}{\varepsilon^2}\left[\bar{s}_{i\ell}\bar{s}_{\ell j}\right]_{\mathrm{D}} + C_{\mathrm{N}2}\frac{K^3}{\varepsilon^2}\left(\bar{s}_{i\ell}\bar{\omega}_{\ell j} + \bar{s}_{j\ell}\bar{\omega}_{\ell i}\right), \tag{3.162}$$

with C_ν and $C_{\mathrm{N}n}(n = 1, 2)$ related to $C_{\Pi n}$ (n = 1-4) [1.7, 3.50, 3.55, 3.56]. This model may alleviate the difficulties of the K–ε model such as Eq. (3.148) [3.50, 3.57].

3.3.3. Subgrid-scale modelling One of the prominent features of mode elimination due to filtering procedures is the occurrence of the computational length scale, that is, the width of a filter, Δ_F, in addition to the length scales intrinsic to turbulent motion such as ℓ_C in Eq. (3.43). The numerical computation of turbulent flow using Eq. (3.20) is called large eddy simulation (LES). In LES, the grid-scale (GS) components, that is, the components of motion whose scale is larger than Δ_F, are treated directly, and what needs to be modelled is the subgrid-scale (SGS) stresses. The critical difference between the SGS and ensemble-mean modelling is that in the former, Δ_F becomes more important than ℓ_C as long as $\Delta_F \ll \ell_C$.

A Smagorinsky model We first consider Eq. (3.23), and then refer to Eqs. (3.21) and (3.22). We define the SGS velocity intensity

$$K_S = v_S^2/2 \equiv \overline{\mathbf{v}'^2}^G/2. \tag{3.163}$$

Under the SGS-viscosity (ν_S) approximation, $\tau_{ij}^{(3)}$ is modelled as

$$\tau_{ij}^{(3)} = \frac{1}{3}v_S^2\delta_{ij} - \nu_S\hat{s}_{ij}, \tag{3.164}$$

with

$$\hat{s}_{ij} = \frac{\partial \hat{V}_j}{\partial x_i} + \frac{\partial \hat{V}_i}{\partial x_j}. \tag{3.165}$$

Considering that Δ_F is an important factor in the SGS modelling, we write

$$\nu_S = C_{\nu_S}\Delta_F v_S \tag{3.166}$$

where C_{ν_S} is a positive model constant.

For estimating v_S in Eq. (3.166), we make use of the equation for K_S, which is given by

$$\frac{\partial K_S}{\partial t} + \overline{\left(\hat{\mathbf{V}}\cdot\nabla\right)\frac{1}{2}\mathbf{v}'^2}^G = P_{K_S} - \varepsilon_S + R_S. \tag{3.167}$$

Here P_{K_S} and ε_S are the SGS counterparts of P_K and ε in the ensemble-averaging procedure. They are given by

$$P_{K_S} = -\overline{v_i'v_j'\frac{\partial \hat{V}_i}{\partial x_j}}^G \cong -\overline{v_i'v_j'}^G\frac{\partial \hat{V}_i}{\partial x_j} \cong -\tau_{ij}^{(3)}\frac{\partial \hat{V}_i}{\partial x_j}, \tag{3.168}$$

$$\varepsilon_S = \nu\overline{\left(\frac{\partial v_j'}{\partial x_i}\right)^2}^G. \tag{3.169}$$

In obtaining the second relation in Eq. (3.168), use has been made of the approximation

$$\overline{fg}^G \cong \overline{f}^G\overline{g}^G. \tag{3.170}$$

The mathematical basis of this approximation is not so firm, but it is often used in SGS modelling and is usually called the scale similarity relation [3.58]. The residual part R_S is not used below, and its details are omitted.

In the ensemble-mean modelling explained in §3.3.2, P_K and ε are always the important ingredients in the K equation (3.13). The retension of these two terms, that is, Eq. (3.145) results in the so-called mixing-length expression for the turbulent viscosity, Eq. (3.147). In Eq. (3.167), we adopt a similar approximation and equate P_{K_S} and ε_S. We model ε_S using v_S and Δ_F, as

$$\varepsilon_S = C_{\varepsilon_S} v_S^3 / \Delta_F, \tag{3.171}$$

with a positive model constant C_{ε_S} [see Eq. (3.43)]. We combine the approximation with Eqs. (3.164), (3.166), and (3.171), and have

$$v_S = \sqrt{C_{\nu_S} / (2C_{\varepsilon_S})}\, \|\hat{s}\|\, \Delta_F, \tag{3.172}$$

where $\|\hat{s}\| = \sqrt{\hat{s}_{ij}^2}$. From Eq. (3.166) with Eq. (3.172), we have

$$\nu_S = (C_S \Delta_F)^2 \sqrt{\hat{s}_{ij}^2 / 2}, \tag{3.173}$$

with $C_S = (C_{\nu_S}^3 / C_{\varepsilon_S})^{1/4}$. Equation (3.173) is the so-called Smagorinsky model and is still the representative model in LES of engineering flows [3.59. 3.60]. The most familiar choice of the Smagorinsky constant is $C_S = 0.1$.

The Smagorinsky model is not applicable in the vicinity of a solid wall since Eq. (3.173) is not dependent directly on ν. In order to include this effect, we usually introduce Van Driest's wall damping function

$$F_{D_V} = 1 - \exp\left(-y^+/A\right), \tag{3.174}$$

where $A = 25$, and $y^+ (= u_\tau y/\nu)$ is the wall-unit coordinate [y is the distance from the wall, and u_τ is the friction velocity defined by $u_\tau = \sqrt{\nu (\partial \hat{V}/\partial y)_{y=0}}$].

The features of the Smagorinsky model combined with Van Driest's wall-damping function may be summarized as follows.

(i) The balance of the SGS-energy production and dissipation processes is assumed, which means that the advection effect represented by the second term on the left-hand side of Eq. (3.167) is negligible.

(ii) The wall-unit distance y^+ is introduced. As its typical failing, we may mention the following two points. One is that Eq. (3.174) is not proper at the separation point of flow leading to vanishing u_τ, and another is that the identification of the distance from a wall is not unique in the case of a corner and a highly curved wall.

(iii) The effect of a filter function occurs only through its width Δ_F, and the difference of filter functions does not enter the computational results.

B Non-equilibrium model In the application of the Smagorinsky model combined with Van Driest's wall-damping function, the distance in wall units, y^+, may be a stumbling block, as was noted above. In order to construct a non-equilibrium SGS model alleviating this problem, we first examine the correct behavior of ν_S near a solid wall. We choose the coordinates x and y along and normal to the wall, respectively, and denote the corresponding velocity components by V_x and V_y. In the vicinity of a solid wall, we have $V_x = O(y)$ and $V_y = O(y^3)$, which suggests $\tau_{ij}^{(3)} = O(y^3)$. As a model obeying this requirement, we write

$$\nu_S \propto v_S^3 / \left(\|\hat{s}\|^2 \Delta_F \right). \tag{3.175}$$

A simple expression connecting Eq. (3.166) with Eq. (3.175) is [3.61]

$$\nu_S = C_{\nu_S} \Delta_F v_S \left(1 - \exp\left\{ - \left[C_w v_S \left(\|\hat{s}\| \Delta_F \right)^{-1} \right]^2 \right\} \right) \tag{3.176}$$

with C_w being a constant. What remains to be modelled is v_S. For its estimate, we make use of the approximation (3.170) in place of the SGS equilibrium assumption, and have

$$v_S \equiv \sqrt{\overline{\mathbf{v}'^2}^G} \cong \sqrt{\left(\hat{\mathbf{V}} - \hat{\overline{\mathbf{V}}} \right)^2}. \tag{3.177}$$

The two model constants are chosen as $C_{\nu_S} = 0.03$ and $C_W = 20$. This model makes no use of the wall-unit coordinate and is applicable to flows subject to separation. For channel flows, Eq. (3.176) gives results better or comparable to those by the Smagorinsky/Van-Driest model (3.173) and (3.174) [3.61].

C Dynamic modelling In the SGS models described in §3.3.3A and B, the model parameters are fixed and optimized through applications to some typical turbulent flows. A method of estimating those parameters in a self-consistent manner is the dynamic SGS modelling [3.62, 3.63].

We introduce two filter functions G_A and G_B, whose characteristic filter widths are denoted by Δ_A and Δ_B, respectively. We apply G_A to Eq. (2.6). The counterpart of Eq. (3.20) is

$$\frac{\partial \overline{V_i}^A}{\partial t} + \frac{\partial}{\partial x_j} \overline{V_i}^A \overline{V_j}^A = - \frac{\partial \overline{p}^A}{\partial x_i} + \frac{\partial}{\partial x_j} \left(-T_{ij}^A \right) + \nu \nabla^2 \overline{V_i}^A, \tag{3.178}$$

where the SGS stress T_{ij}^A is given by

$$T_{ij}^A = \overline{V_i V_j}^A - \overline{V_i}^A \overline{V_j}^A. \tag{3.179}$$

The consecutive filtering due to G_A and G_B is defined as

$$\overline{f}^{AB} = \int G_B(\mathbf{x} - \mathbf{y}) \overline{f}^A(\mathbf{y}) d\mathbf{y} \tag{3.180}$$

($\Delta_B > \Delta_A$). We apply Eq. (3.180) to Eq. (2.6), and have

$$\frac{\partial \overline{V}_i^{AB}}{\partial t} + \frac{\partial}{\partial x_j}\overline{V}_i^{AB}\overline{V}_j^{AB} = -\frac{\partial \overline{p}^{AB}}{\partial x_i} + \frac{\partial}{\partial x_j}\left(-T_{ij}^{AB}\right) + \nu\nabla^2\overline{V}_i^{AB}. \tag{3.181}$$

with the SGS stress T_{ij}^{A} entirely similar to Eq. (3.179). The two SGS stresses T_{ij}^{A} and T_{ij}^{AB} are connected through the so-called Germano identity

$$L_{ij} \equiv T_{ij}^{AB} - \overline{T_{ij}^{A}}^{B} = \overline{\overline{V}_i^{A}\overline{V}_j^{A}}^{B} - \overline{V}_i^{AB}\overline{V}_j^{AB}. \tag{3.182}$$

The last part of Eq. (3.182) is composed of GS quantities and may be calculated without any modelling in the course of LES. This identity may be used for the estimate of model coefficients in SGS models.

Following the Smagorinsky model, Eqs. (3.164) and (3.173), we write

$$\left[T_{ij}^{A}\right]_D = -C_S^A\Delta_A^2\|\bar{s}^A\|\bar{s}_{ij}^A, \quad \left[T_{ij}^{AB}\right]_D = -C_S^{AB}\Delta_{AB}^2\|\bar{s}^{AB}\|\bar{s}_{ij}^{AB}, \tag{3.183}$$

with two non-dimensional coefficients C_S^A and C_S^{AB}. As a simple method of estimating these coefficients, we assume $C_S^A \cong C_S^{AB}$. We substitute Eq. (3.183) into the Germano identity (3.182). The identity is a six-component relation, but the only unknown coefficient is C_S^A. Then we use the least-square method [3.64], and estimate C_S^A as

$$\frac{\partial}{\partial C_S^A}\left([L_{ij}]_D - C_S^A M_{ij}\right)^2 = 0, \tag{3.184}$$

where

$$M_{ij} = \Delta_A^2\overline{\|\bar{s}^A\|\,\bar{s}_{ij}^A}^B - \Delta_B^2\|\bar{s}^{AB}\|\bar{s}_{ij}^{AB}. \tag{3.185}$$

Equation (3.184) gives

$$C_S^A = M_{ij}\left[L_{ij}\right]_D / M_{ij}^2. \tag{3.186}$$

A great merit of the dynamic SGS modelling based on Eq. (3.186) is the avoidance of a wall damping function of Van Driest's type. In actual application of Eq. (3.186), however, the dynamic model is not always superior to the Smagorinsky one, at least in a channel flow between two solid walls. A method for alleviating this difficulty is the inclusion of Eqs. (3.21) and (3.22). Here it should be stressed that the retention of either Eq. (3.21) or (3.22) is not allowable since Eq. (3.20) does not become invariant under the Galilean transformation $\mathbf{x} \to \mathbf{x} + \mathbf{V}t$ and $t \to t$ [3.65]. In retaining Eq. (3.21), Eq. (3.22) also needs to be retained and modelled. For instance, we make use of the approximation (3.170), and model

$$\overline{\overline{V}_i^{A} v_j'}^{A} \cong \overline{V}_i^{AA}\left(\overline{V}_i^{A} - \overline{V}_j^{AA}\right). \tag{3.187}$$

The model combining Eqs. (3.21) and (3.22) with Eq. (3.174) is called a mixed SGS model [3.66-3.68].

3.3.4. Statistical theory and turbulence modelling In §3.2.5, we gave a review of some homogeneous-turbulence theories. In §3.3.2, we discussed heuristic models that are useful in analyzing realistic turbulent flows such as engineering flows. There is a wide gap between these two methods. A prominent feature of inhomogeneous turbulence is the concurrence of slowly-varying mean and rapidly-varying fluctuating motions. Their simultaneous treatment is a primary cause of the difficulty encountered in the formalism of inhomogeneous-turbulence theory.

A Two-scale direct-interaction approximation (TSDIA) A theoretical method for bridging the gap between turbulence theories and heuristic models is the two-scale direct-interaction approximation (TSDIA), which is the combination of the DIA explained in §3.2.5A with the multi-scale approach in a singular perturbation method [1.7, 3.49]. In the TSDIA, emphasis is put on the nonlinear interaction among fluctuations, and the effect of inhomogeneity is taken into account in a perturbative manner based on small ϑ [Eq. (3.139)].

A1 Mathematical formalism In order to distinguish the rapid variation of a fluctuating motion from the slow variation of a mean field, we introduce a small artificial parameter δ, define two space and time scales as

$$\boldsymbol{\xi}(=\mathbf{x}),\ \tau(=t);\ \mathbf{X}(=\delta\mathbf{x}),\ T(=\delta t), \tag{3.188}$$

and write

$$f = \bar{f}(\mathbf{X};T) + \tilde{f}(\boldsymbol{\xi},\tau;\mathbf{X},T). \tag{3.189}$$

The $O(\delta^0)$ change of $\mathbf{x}$ corresponds to the $O(\delta)$ change of $\mathbf{X}$, which indicates that $\mathbf{X}$ is appropriate for expressing the slow variation of $\bar{f}$. The same situation holds for T. The fluctuating field $\tilde{f}$ depends on both the slow and fast variables, $(\mathbf{X},T)$ and $(\boldsymbol{\xi},\tau)$, since it is connected to $\bar{f}$ through the equations for R_{ij} and K, Eqs. (3.7) and (3.13).

We apply the two-scale variables to Eqs. (2.5) and (2.6), and have

$$\nabla_\xi \cdot \tilde{\mathbf{v}} = \delta(-\nabla_X \cdot \tilde{\mathbf{v}}), \tag{3.190}$$

$$\begin{aligned}\frac{\partial \tilde{v}_i}{\partial \tau} + \left(\bar{\mathbf{V}}\cdot\nabla_X\right)\tilde{v}_i + \frac{\partial}{\partial \xi_j}\tilde{v}_i\tilde{v}_j + \frac{\partial \tilde{p}}{\partial \xi_i} - \nu\nabla_\xi^2\tilde{v}_i \\ = \delta\left[-\left(\tilde{\mathbf{v}}\cdot\nabla_X\right)\bar{V}_i - \frac{D\tilde{v}_i}{DT}\right],\end{aligned} \tag{3.191}$$

where $\nabla_\xi = (\partial/\partial\xi_i)$, $\nabla_X = (\partial/\partial X_i)$, and $D/DT = \partial/\partial T + \bar{\mathbf{V}}\cdot\nabla_X$. In order to clearly see the key procedures of the TSDIA, we retained two typical terms on the right-hand side of Eq. (3.191), and discarded the terms such as $\partial(\tilde{v}_i\tilde{v}_j - R_{ij})/\partial X_j$ as well as the ν-dependent ones.

In homogeneous-turbulence theory, we make full use of the Fourier representation (3.25). In the presence of the mean flow $\bar{\mathbf{V}}$, we introduce a somewhat different representation concerning the fast variable $\boldsymbol{\xi}$, as

$$\tilde{f}(\boldsymbol{\xi}, \mathbf{X}; \tau, T) = \int \tilde{f}(\mathbf{k}, \mathbf{X}; \tau, T) \exp\left[-i\mathbf{k} \cdot (\boldsymbol{\xi} - \bar{\mathbf{V}}\tau)\right] d\mathbf{k}. \tag{3.192}$$

This is the Fourier representation in the frame moving with the velocity of the mean flow, $\bar{\mathbf{V}}$, and the fluctuating motion is expressed as the aggregate of eddies or waves observed there. We apply Eq. (3.192) to Eqs. (3.190) and (3.191), and have

$$\mathbf{k} \cdot \tilde{\mathbf{v}}(\mathbf{k}; \tau) = \delta\left[-i\nabla_{\mathrm{I}X} \cdot \tilde{\mathbf{v}}(\mathbf{k}; \tau)\right], \tag{3.193}$$

$$\begin{aligned} &\frac{\partial \tilde{v}_i(\mathbf{k}; \tau)}{\partial \tau} + \nu k^2 \tilde{v}_i(\mathbf{k}; \tau) - ik_i \tilde{p}(\mathbf{k}; \tau) \\ &\quad - ik_j \iint \tilde{v}_i(\mathbf{p}; \tau) \tilde{v}_j(\mathbf{q}; \tau) \delta(\mathbf{k} - \mathbf{p} - \mathbf{q}) d\mathbf{p} d\mathbf{q} \\ &\quad = \delta\left\{-\left[\tilde{\mathbf{v}}(\mathbf{k}; \tau) \cdot \nabla_X\right] \bar{V}_i - \frac{D\tilde{v}_i(\mathbf{k}; \tau)}{DT_{\mathrm{I}}}\right\}. \end{aligned} \tag{3.194}$$

with

$$(D/DT_{\mathrm{I}}, \nabla_{\mathrm{I}X}) = \exp\left(-i\mathbf{k} \cdot \bar{\mathbf{V}}\tau\right) (D/DT, \nabla_X) \exp\left(i\mathbf{k} \cdot \bar{\mathbf{V}}\tau\right). \tag{3.195}$$

Here and hereafter, the dependence of $\tilde{f}$ on $\mathbf{X}$ and T is not written explicitly, except when necessary.

In Eq. (3.193), we note that $\tilde{\mathbf{v}}$ does not obey the solenoidal condition concerning $\mathbf{k}$, unlike the homogeneous case. We rewrite

$$\tilde{\mathbf{v}}(\mathbf{k}; \tau) = \tilde{\mathbf{v}}_{\mathrm{S}}(\mathbf{k}; \tau) + \delta\left[-i\frac{\mathbf{k}}{k^2} \nabla_{\mathrm{I}X} \cdot \tilde{\mathbf{v}}(\mathbf{k}; \tau)\right]. \tag{3.196}$$

The first term obeys [3.69]

$$\mathbf{k} \cdot \tilde{\mathbf{v}}_{\mathrm{S}}(\mathbf{k}; \tau) = 0. \tag{3.197}$$

We expand the fluctuating field in δ, as

$$\tilde{\mathbf{v}}(\mathbf{k}; \tau) = \sum_{n=0}^{\infty} \delta^n \tilde{v}_n(\mathbf{k}; \tau), \tag{3.198}$$

and similar expressions for $\tilde{\mathbf{v}}_{\mathrm{S}}(\mathbf{k}; \tau)$ and $\tilde{p}(\mathbf{k}; \tau)$.

We substitute Eq. (3.188) into Eqs. (3.193) and (3.194). The $O(\delta^0)$ system of equations is given by

$$\begin{aligned} &\frac{\partial \tilde{v}_{0i}(\mathbf{k}; \tau)}{\partial \tau} + \nu k^2 \tilde{v}_{0i}(\mathbf{k}; \tau) - ik_i \tilde{p}_0(\mathbf{k}; \tau) \\ &\quad - ik_j \iint \delta(\mathbf{k} - \mathbf{p} - \mathbf{q}) d\mathbf{p} d\mathbf{q} \tilde{v}_{0i}(\mathbf{p}; \tau) \tilde{v}_{0j}(\mathbf{q}; \tau) = 0, \end{aligned} \tag{3.199}$$

with $\mathbf{k}\cdot\tilde{\mathbf{v}}_0(\mathbf{k};\tau)=0$. where we should note that $\tilde{\mathbf{v}}_0(\mathbf{k};\tau)=\tilde{\mathbf{v}}_{S0}(\mathbf{k};\tau)$. The elimination of $\tilde{p}_0(\mathbf{k};\tau)$ results in

$$\frac{\partial\tilde{v}_{0i}(\mathbf{k};\tau)}{\partial\tau}+\nu k^2\tilde{v}_{0i}(\mathbf{k};\tau) - iM_{ij\ell}(\mathbf{k})\iint\tilde{v}_{0j}(\mathbf{p};\tau)\tilde{v}_{0\ell}(\mathbf{q};\tau)\delta(\mathbf{k}-\mathbf{p}-\mathbf{q})d\mathbf{p}d\mathbf{q}=0. \tag{3.200}$$

where $M_{ij\ell}(\mathbf{k})$ is defined by Eq. (3.28). Equation (3.200) is the same as for the homogeneous counterpart (3.27), apart from the implicit dependence of $\tilde{\mathbf{v}}_0$ on $\mathbf{X}$ and T.

The $O(\delta)$ system of equations is given by

$$\tilde{\mathbf{v}}_1(\mathbf{k};\tau)=\tilde{\mathbf{v}}_{S1}(\mathbf{k};\tau)-i\frac{\mathbf{k}}{k^2}\nabla_X\cdot\tilde{\mathbf{v}}_0(\mathbf{k};\tau), \tag{3.201}$$

$$\begin{aligned}&\frac{\partial\tilde{v}_{1i}(\mathbf{k};\tau)}{\partial\tau}+\nu k^2\tilde{v}_{1i}(\mathbf{k};\tau)-ik_i\tilde{p}_1(\mathbf{k};\tau)\\&\quad-ik_j\iint\left[\tilde{v}_{1i}(\mathbf{p};\tau)\tilde{v}_{0j}(\mathbf{q};\tau)+\tilde{v}_{0i}(\mathbf{p};\tau)\tilde{v}_{1j}(\mathbf{q};\tau)\right]\delta(\mathbf{k}-\mathbf{p}-\mathbf{q})d\mathbf{p}d\mathbf{q}\\&\quad=-\left[\tilde{v}_0(\mathbf{k};\tau)\cdot\nabla_X\right]\bar{V}_i-\frac{D\tilde{v}_{0i}(\mathbf{k};\tau)}{DT_{\mathrm{I}}},\end{aligned} \tag{3.202}$$

with $\mathbf{k}\cdot\tilde{\mathbf{v}}_{S1}=0$. After eliminating $\tilde{p}_1$ from Eq. (3.202), we have

$$\begin{aligned}&\frac{\partial\tilde{v}_{S1i}(\mathbf{k};\tau)}{\partial\tau}+\nu k^2\tilde{v}_{S1i}(\mathbf{k};\tau)\\&\quad-2iM_{ij\ell}(k)\iint\tilde{v}_{0j}(\mathbf{p};\tau)\tilde{v}_{S1\ell}(\mathbf{q};\tau)\delta(\mathbf{k}-\mathbf{p}-\mathbf{q})d\mathbf{p}d\mathbf{q}\\&\quad=-D_{i\ell}(\mathbf{k})\left[\tilde{v}_0(\mathbf{k};\tau)\cdot\nabla_X\right]\bar{V}_\ell-D_{ij}(\mathbf{k})\frac{D\tilde{v}_{0j}(\mathbf{k};\tau)}{DT_{\mathrm{I}}}.\end{aligned} \tag{3.203}$$

The formal solution of Eq. (3.203) may be obtained using the Green's or response function for the $O(\delta^0)$ equation (3.200). $G_{ij}(\mathbf{k},\mathbf{X};\tau,\tau',T)$, which is simply written as $G_{ij}(\mathbf{k};\tau,\tau')$. It obeys the same equation as for Eq. (3.82), except the implicit dependence on $\mathbf{X}$ and T, which is given by

$$\begin{aligned}&\left(\frac{\partial}{\partial t}+\nu k^2\right)G_{ij}(\mathbf{k};\tau,\tau')-D_{ij}(\mathbf{k})\delta(\tau-\tau')\\&\quad=iM_{i\ell m}(\mathbf{k})\iint\tilde{v}_{0\ell}(\mathbf{p};\tau)G_{mj}(\mathbf{q};\tau,\tau')\delta(\mathbf{k}-\mathbf{p}-\mathbf{q})d\mathbf{p}d\mathbf{q}.\end{aligned} \tag{3.204}$$

The $O(\delta)$ solution is given by

$$\tilde{\mathbf{v}}_1(\mathbf{k};\tau)=\tilde{\mathbf{v}}_{S1}(\mathbf{k};\tau)-i\frac{\mathbf{k}}{k^2}\nabla_{IX}\cdot\tilde{\mathbf{v}}_0(\mathbf{k};\tau), \tag{3.205}$$

with

$$\begin{aligned}\tilde{v}_{S1i}(\mathbf{k};\tau)=&-\frac{\partial\bar{V}_\ell}{\partial X_j}\int_{-\infty}^{\tau}G_{i\ell}(\mathbf{k};\tau,\tau_1)\tilde{v}_{0j}(\mathbf{k};\tau_1)d\tau_1\\&-\int_{\infty}^{\tau}G_{ij}(\mathbf{k};\tau,\tau_1)\frac{D\tilde{v}_{0j}(\mathbf{k};\tau_1)}{DT_{\mathrm{I}}}d\tau_1.\end{aligned} \tag{3.206}$$

A2 Evaluation of correlation functions In the TSDIA, the Reynolds stress R_{ij} is written as

$$R_{ij} \equiv \langle \tilde{v}_i(\mathbf{x};t)\tilde{v}_j(\mathbf{x};t)\rangle = \langle \tilde{v}_i(\boldsymbol{\xi},\mathbf{X};\tau,T)\tilde{v}_j(\boldsymbol{\xi},\mathbf{X};\tau,T)\rangle$$
$$= \int R_{ij}(k,X;\tau,\tau,T)d\mathbf{k}, \tag{3.207}$$

where

$$R_{ij}(\mathbf{k},\mathbf{X};\tau,\tau,T) = \frac{\langle \tilde{v}_i(\mathbf{k},\mathbf{X};\tau,T)\tilde{v}_j(\mathbf{k}',\mathbf{X};\tau,T)\rangle}{\delta(\mathbf{k}+\mathbf{k}')}. \tag{3.208}$$

Hereafter $R_{ij}(\mathbf{k},\mathbf{X};\tau,\tau,T)$ will be abbreviated as $R_{ij}(\mathbf{k})$.

We define the Reynolds-stress spectrum E_{ij} by the average of $R_{ij}(\mathbf{k})$ at the spherical surface of radius k, $S(k)$:

$$E_{ij}(k) = \frac{1}{4\pi k^2}\int_{S(k)} R_{ij}(\mathbf{k})dS. \tag{3.209}$$

Using Eq. (3.198), $R_{ij}(\mathbf{k})$ up to $O(\delta)$ is

$$R_{ij}(\mathbf{k}) = \frac{\langle \tilde{v}_{0i}(\mathbf{k};\tau)\tilde{v}_{0j}(\mathbf{k}';\tau)\rangle}{\delta(\mathbf{k}+\mathbf{k}')}$$
$$+ \delta\left[\frac{\langle \tilde{v}_{1i}(\mathbf{k};\tau)\tilde{v}_{0j}(\mathbf{k}';\tau)\rangle}{\delta(\mathbf{k}+\mathbf{k}')} + \frac{\langle \tilde{v}_{0i}(\mathbf{k};\tau)\tilde{v}_{1j}(\mathbf{k}';\tau)\rangle}{\delta(\mathbf{k}+\mathbf{k}')}\right]. \tag{3.210}$$

The first term in Eq. (3.210) is essentially the same as Eq. (3.83) for homogeneous isotropic turbulence, and is written as

$$\frac{\langle \tilde{v}_{0i}(\mathbf{k};\tau)\tilde{v}_{0j}(\mathbf{k}';\tau)\rangle}{\delta(\mathbf{k}+\mathbf{k}')} = D_{ij}(\mathbf{k})Q(k;\tau,\tau). \tag{3.211}$$

In correspondence to Eq. (3.211), the mean Green's function $\bar{G}_{ij}(\mathbf{k};\tau,\tau')$ is

$$\bar{G}_{ij}(\mathbf{k};\tau,\tau') = \langle G_{ij}(\mathbf{k};\tau,\tau')\rangle = D_{ij}(\mathbf{k})G(k;\tau,\tau'). \tag{3.212}$$

From Eq. (3.205), the first part of the $O(\delta)$ terms in Eq. (3.210) is

$$\frac{\langle \tilde{v}_{1i}(\mathbf{k};\tau)\tilde{v}_{0j}(\mathbf{k}';\tau)\rangle}{\delta(\mathbf{k}+\mathbf{k}')} = -\frac{\partial \bar{V}_\ell}{\partial X_m}\int_{-\infty}^{\tau} \frac{\langle G_{i\ell}(\mathbf{k};\tau,\tau_1)\tilde{v}_{0m}(\mathbf{k};\tau_1)\tilde{v}_{0j}(\mathbf{k}';\tau)\rangle}{\delta(\mathbf{k}+\mathbf{k}')}d\tau_1$$
$$- \int_{-\infty}^{\tau} \frac{\left\langle G_{i\ell}(k;\tau,\tau_1)\frac{D\tilde{v}_{0\ell}(\mathbf{k};\tau_1)}{D\tau_1}\tilde{v}_{0j}(\mathbf{k}';\tau)\right\rangle}{\delta(\mathbf{k}+\mathbf{k}')}d\tau_1. \tag{3.213}$$

Under the DIA formalism explained in §3.2.5A, the first part in Eq. (3.213) may be evaluated as

$$\frac{\partial \bar{V}_\ell}{\partial X_m}\int_{-\infty}^{\tau} \frac{\langle G_{i\ell}(\mathbf{k};\tau,\tau_1)\tilde{v}_{0m}(\mathbf{k};\tau_1)\tilde{v}_{0j}(\mathbf{k}';\tau)\rangle}{\delta(\mathbf{k}+\mathbf{k}')}d\tau_1$$
$$= \frac{\partial \bar{V}_\ell}{\partial X_m}\int_{-\infty}^{\tau} \bar{G}_{i\ell}(\mathbf{k};\tau,\tau_1)Q_{mj}(\mathbf{k};\tau,\tau_1)d\tau_1. \tag{3.214}$$

Here we expanded $\tilde{\mathbf{v}}_0(\mathbf{k};\tau)$ and $G_{ij}(\mathbf{k};\tau,\tau')$ in the form of Eq. (3.71), substituted them into the left-hand side of Eq. (3.214), and kept only the lowest-order contributions. By renormalization, we attained the right-hand side. The second part of the $O(\delta)$ terms in Eq. (3.213) may be evaluated similarly.

Finally, we have

$$R_{ij}(\mathbf{k}) = D_{ij}(\mathbf{k})\left[Q(k;\tau,\tau) - \int_{-\infty}^{\tau} \bar{G}(k;\tau,\tau_1)\frac{DQ(k;\tau,\tau_1)}{Dt}d\tau_1\right] - \left[D_{i\ell}(\mathbf{k})D_{mj}(\mathbf{k}) + D_{j\ell}(\mathbf{k})D_{mi}(\mathbf{k})\right]\frac{\partial \bar{V}_\ell}{\partial x_m} \times \int_{-\infty}^{\tau} \bar{G}(k;\tau,\tau_1)Q(k;\tau,\tau_1)d\tau_1. \tag{3.215}$$

Here the dependence on the scale parameter δ disappears automatically through the replacement of $(\mathbf{X},T)$ with $(\delta\mathbf{x},\delta t)$. From Eq. (3.209), we have

$$E_{ij}(k) = \frac{2}{3}\left[Q(k;\tau,\tau) - \int_{-\infty}^{\tau} d\tau_1 \bar{G}(k;\tau,\tau_1)\frac{DQ(k;\tau,\tau_1)}{Dt}\right]\delta_{ij} - \left[\frac{7}{15}\int_{-\infty}^{\tau} \bar{G}(k;\tau,\tau_1)Q(k;\tau,\tau_1)d\tau_1\right]\bar{s}_{ij}. \tag{3.216}$$

Here use has been made of the formulae

$$\int \frac{k_i k_j}{k^2}d\mathbf{k} = \frac{1}{3}\delta_{ij}\int d\mathbf{k}, \tag{3.217a}$$

$$\int \frac{k_i k_j k_\ell k_m}{k^4}d\mathbf{k} = \frac{1}{15}\left(\delta_{ij}\delta_{\ell m} + \delta_{i\ell}\delta_{jm} + \delta_{im}\delta_{j\ell}\right)\int d\mathbf{k}. \tag{3.217b}$$

The energy spectrum $E(k)$ is

$$E(k) = 4\pi k^2\left[Q(k;\tau,\tau) - \int_{-\infty}^{\tau} \bar{G}(k;\tau,\tau_1)\frac{DQ(k;\tau,\tau_1)}{Dt}d\tau_1\right], \tag{3.218}$$

from the relation $E(k) = E_{ii}(k)/2$. Finally, we use Eqs. (3.207) and (3.215), and have

$$R_{ij} = \frac{2}{3}K\delta_{ij} - \nu_{\mathrm{T}}\bar{s}_{ij}, \tag{3.219}$$

where

$$K = \int Q(k;\tau,\tau)d\mathbf{k} - \int d\mathbf{k}\int_{-\infty}^{\tau} \bar{G}(k;\tau,\tau_1)\frac{DQ(k;\tau,\tau_1)}{Dt}d\tau_1, \tag{3.220}$$

$$\nu_{\mathrm{T}} = \frac{7}{15}\int d\mathbf{k}\int_{-\infty}^{\tau} \bar{G}(k;\tau,\tau_1)Q(k;\tau,\tau_1)d\tau_1. \tag{3.221}$$

Equation (3.219) is the so-called turbulent-viscosity representation for the Reynolds stress from the viewpoint of the TSDIA.

Equation (3.219) for R_{ij} is expressed using the two-time statistical quantities in wavenumber space, $Q(k;\tau,\tau')$ and $\bar{G}(k;\tau,\tau')$. It is of interest to know how it is related to the counterpart in the K–ε model, Eqs. (3.140) and (3.141). Through the elucidation of this relationship, we can derive various types of turbulence models and extend them to magnetohydrodynamic flows for the study of astrophysical and fusion-plasma phenomena.

A method of estimating Eq. (3.219) without delving into the details of $Q(k;\tau,\tau')$ and $\bar{G}(k;\tau,\tau')$, is the full use of the inertial-range concept. For simple inertial-range expressions, we adopt

$$Q(k,\mathbf{x};\tau,\tau',t) = \sigma(k,\mathbf{x};t)\exp\left[-\omega(k,\mathbf{x};t)|\tau-\tau'|\right], \tag{3.222}$$

$$\bar{G}(k,\mathbf{x};\tau,\tau',t) = \Theta(\tau-\tau')\exp\left[-\omega(k,\mathbf{x};t)(\tau-\tau')\right], \tag{3.223}$$

where

$$\sigma(k,\mathbf{x};t) = \sigma\varepsilon(\mathbf{x};t)^{2/3}k^{-11/3}, \quad \omega(k,\mathbf{x};t) = \omega\varepsilon(\mathbf{x};t)^{1/3}k^{2/3}. \tag{3.224}$$

We should note the dependence of Eqs. (3.222)-(3.224) on $\mathbf{x}$, compared with the homogeneous counterparts (3.90) and (3.94).

As long as the response equation is dealt with in the Eulerian frame, we encounter the overestimate of effects of much larger eddies on small ones, as was detailed in §3.2.5A3. In order to avoid this difficulty, we make use of the observational result for the Kolmogorov constant K_{O} in Eq. (3.46), which is related to σ through $K_{\mathrm{O}} = 4\pi\sigma$. From observations, K_{O} is around 1.5, whereas we have Eq. (3.95) between σ and ω. Then we have

$$\sigma = 0.12, \quad \omega = 0.42. \tag{3.225}$$

We substitute Eqs. (3.222)-(3.225) into Eq. (3.218), and have

$$E(k) = K_{\mathrm{O}}\varepsilon^{2/3}k^{-5/3} - K_{\mathrm{N}}\varepsilon^{-2/3}\frac{D\varepsilon}{Dt}k^{-7/3}. \tag{3.226}$$

Equation (3.226) corresponds to Eq. (3.58) in the case of homogeneous-shear flow, and the second part represents the non-equilibrium effect on the energy spectrum.

Next, we substitute Eqs. (3.222)-(3.225) into Eqs. (3.220) and (3.221). In the TSDIA, the low-wavenumber components of turbulent motion mainly belong to the mean field. Then we may consider that the contribution of those components to R_{ij} is small. Then we terminate the integral as

$$\int d\mathbf{k} \;\to\; \int_{k\geq k_{\mathrm{C}}} d\mathbf{k}. \tag{3.227}$$

Here k_{C} is the wavenumber characterizing the largest eddies of the fluctuating motion, and it is related to their size ℓ_{C} as

$$k_{\mathrm{C}}(\mathbf{x};t) = 2\pi/\ell_{\mathrm{C}}(\mathbf{x};t). \tag{3.228}$$

Here we should note the dependence of k_C and ℓ_C on $\mathbf{x}$ and t.

We perform the integration in Eq. (3.220) under the constraint (3.226) to obtain

$$K = C_{K1}\varepsilon^{2/3}\ell_C^{2/3} - C_{K2}\varepsilon^{-2/3}\ell_C^{4/3}\frac{D\varepsilon}{Dt} - C_{K3}\varepsilon^{1/3}\ell_C^{1/3}\frac{D\ell_C}{Dt}, \tag{3.229}$$

$$\nu_T = C_{\nu\ell}\varepsilon^{1/3}\ell_C^{4/3}, \tag{3.230}$$

where $(K_O, K_N) = (1.5, 0.90)$. $(C_{K1}, C_{K2}, C_{K3}) = (0.67, 0.058, 0.47)$ and $C_{\nu\ell} = 0.054$.

Equation (3.229) was derived in a perturbative manner with the first part as the leading term. We solve it for ℓ_C in such a manner, and have

$$\ell_C = C_{\ell 1}K^{3/2}\varepsilon^{-1} + C_{\ell 2}K^{3/2}\varepsilon^{-2}\frac{DK}{Dt} - C_{\ell 3}K^{5/2}\varepsilon^{-3}\frac{D\varepsilon}{Dt}, \tag{3.231}$$

where $(C_{\ell 1}, C_{\ell 2}, C_{\ell 3}) = (1.8, 4.4, 2.6)$.

We substitute Eq. (3.231) into Eq. (3.230), and have

$$\nu_T = C_\nu\frac{K^2}{\varepsilon} - C_{\nu K}\frac{K^2}{\varepsilon^2}\frac{DK}{Dt} + C_{\nu\varepsilon}\frac{K^3}{\varepsilon^3}\frac{D\varepsilon}{Dt}, \tag{3.232}$$

with $(C_\nu, C_{\nu K}, C_{\nu\varepsilon}) = (0.12. 0.15, 0.093)$. The first part in Eq. (3.232) is the turbulent viscosity in the K–ε model, which is given by Eq. (3.141). The second and third parts correspond to the expressions that may be obtained from the DB_{ij}/DT-related term in Eq. (3.161), in the perturbation expansion with the turbulent-viscosity term as the leading one. The nonlinear model (3.162) is derived from the $O(\delta^2)$ analysis of the TSDIA, although the mathematical manipulation is a little tedious [1.7, 3.49. 3.65].

The TSDIA may be used for the theoretical derivation of various types of turbulence models. Some of those findings may give a mathematical basis to the models that were proposed in a heuristic manner. The others may be used for constructing new models in complicated turbulent flows. A typical instance is the dynamo model that is needed specially for the study of astronomical magnetic fields. This point will be discussed in §3.4.

B Turbulence model and flow-structure generation In homogeneous turbulence with no mean flow, the most prominent feature is the enhanced energy transfer from large to small eddies; namely, large eddies break up into small ones, and the memory or specific structure of large eddies is rapidly lost in this process. From this feature, we are apt to consider that effects of fluctuations always destroy ordered structures of flow. On the contrary, some ordered structures can exist only in the presence of strong fluctuations. As an interesting example of structure generation in fluid turbulence, we may mention the flow in a long square-duct pipe, which is driven by an axial pressure gradient. In a long circular pipe, the uniform axial pressure gradient generates a turbulent flow with mean velocity in the axial direction, although the velocity profile is much flatter,

compared to the laminar case. In a square-duct flow, on the other hand, a secondary flow occurs in the cross section (Fig. 3.1). The magnitude of its velocity is at most a few percent of the mean axial velocity, but the occurrence of the secondary flow has a drastic influence on the profile of the mean axial velocity.

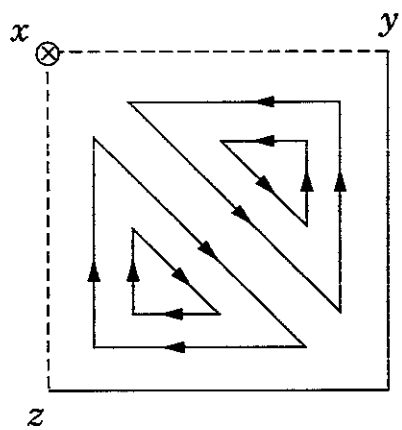

Figure 3.1. Illustration of secondary flows in the one-fourth cross section of a square duct (the primary flow is in the x direction).

In the application of the K–ε model to a square-duct flow, the initially-imposed secondary flow is rapidly lost, and the mean flow relaxes to a simple flow in the axial direction. This finding contradicts observations. This fact indicates that the observed secondary flow in a square duct survives the structure-destruction process arising from the turbulent-viscosity effect. As in §3.3.2C, we referred to the nonlinear algebraic model given by Eq. (3.162), in which the Reynolds stress R_{ij} includes the nonlinear effect of a mean velocity gradient. The balance between the nonlinear effect and the one from the linear turbulent-viscosity leads to the generation of the secondary flow in a square duct [3.50, 3.71]. This point may be actually confirmed through numerical computation of the nonlinear model.

3.4. Dynamo and Structure Occurrence in Magnetohydrodynamic Turbulence

The mechanism for the generation of magnetic fields due to the motion of electrically conducting fluids is called a dynamo. In astro/geophysical phenomena, the Reynolds number is always very large, and the related flows are highly turbulent. The magnetic-field generation process in such a turbulent state is specifically named the turbulent dynamo. The present section is devoted to a review of the turbulent dynamo [1.7, 3.72-3.74]. In this context, special attention will be paid to the geomagnetic field, the solar magnetic field occurring as sunspots, and the high collimation of astronomical bipolar jets ejected from an accretion disk around a high-mass astronomical object.

The magnetohydrodynamic (MHD) system of equations is the starting point for the study of these phenomena. Throughout §3.4, Alfvén velocity units are adopted for the magnetic field, electric current, and electric field, as was noted in §2.1.2.

The generators of magnetic fields in thermo-nuclear fusion devices are an external coil and an external coil and the plasma current generated by the loop voltage. An interesting phenomenon in this situation is the occurrence of global plasma flows. Recently, such flows have been shown to be closely related to a dramatic improvement in plasma confinement. This phenomenon may be called the flow dynamo in contrast to the foregoing magnetic dynamo. Phenomena in fusion plasma are very complicated, and many of their properties are beyond the scope of the MHD system of equations. The system, however, is expected to shed light on some restricted aspects of the flow dynamo in plasma confinement.

3.4.1. Magnetohydrodynamic turbulence modelling The change of mass density often plays a critical role in various phenomena due to electrically conducting fluid flows. The importance of compressibility is recognized in the study of turbulent flows of electrically non-conducting fluids. A typical instance is compressibility effects on the suppression of the growth rate of a free-shear-layer flow caused by the merger of two parallel flows with different velocities. A study of the suppression mechanism in the flow is in progress and is still at a premature stage. No definite conclusion has yet been drawn on the mechanism. Considering this situation, this section will be devoted to discussions based on the solenoidal or constant-density system of the MHD equations.

A Elsässer's variables From Eqs. (2.10) and (2.11), we eliminate the electric field $\mathbf{E}$, and have the magnetic induction equation

$$\frac{\partial \mathbf{B}}{\partial t} = \nabla \times (\mathbf{V} \times \mathbf{B}) + \eta \nabla^2 \mathbf{B}. \tag{3.233}$$

Considering that $\mathbf{B}$ in Alfvén-velocity units has the same dimension as $\mathbf{V}$, we introduce Elsässer's variables

$$\boldsymbol{\phi} = \mathbf{V} + \mathbf{B}, \quad \boldsymbol{\psi} = \mathbf{V} - \mathbf{B}. \tag{3.234}$$

With the use of Eq. (3.234), the MHD system of equations is written in a highly symmetric form

$$\frac{\partial \phi_i}{\partial t} + \frac{\partial}{\partial x_j}\phi_i \psi_j = -\frac{\partial p_{\mathrm{M}}}{\partial x_i} + \frac{\nu + \eta}{2}\nabla^2 \phi_i + \frac{\nu - \eta}{2}\nabla^2 \psi_i, \tag{3.235}$$

$$\frac{\partial \psi_i}{\partial t} + \frac{\partial}{\partial x_j}\psi_i \phi_j = -\frac{\partial p_{\mathrm{M}}}{\partial x_i} + \frac{\nu + \eta}{2}\nabla^2 \psi_i + \frac{\nu - \eta}{2}\nabla^2 \phi_i, \tag{3.236}$$

with $p_{\rm M} = p + (\mathbf{B}^2/2)$ and the solenoidal conditions $\nabla \cdot \boldsymbol{\phi} = \nabla \cdot \boldsymbol{\psi} = 0$. The important property of Elsässer's MHD system, Eqs. (3.235) and (3.236), is that $\int \boldsymbol{\phi}^2 dV$ and $\int \boldsymbol{\psi}^2 dV$ are conserved in the absence of ν and η.

In correspondence to Eq. (3.132), the magnetic Reynolds number $R_{\rm M}$ is defined by

$$R_{\rm M} = V_{\rm R} L_{\rm R}/\eta. \tag{3.237}$$

In astronomical and fusion-plasma phenomena, both Re and $R_{\rm M}$ are very large. Specifically, in the case that the difference between them is not so critical, Eqs. (3.235) and (3.236) are reduced to the quite symmetric system

$$\frac{\partial \phi_i}{\partial t} + \frac{\partial}{\partial x_j}\phi_i \psi_j = -\frac{\partial p_{\rm M}}{\partial x_i} + \nu \nabla^2 \phi_i, \tag{3.238}$$

$$\frac{\partial \psi_i}{\partial t} + \frac{\partial}{\partial x_j}\psi_i \phi_j = -\frac{\partial p_{\rm M}}{\partial x_i} + \nu \nabla^2 \psi_i. \tag{3.239}$$

This system of equations is helpful to the understanding of turbulence effects.

B Primary turbulence effects We apply the ensemble averaging in §3.1.1 to the MHD system, Eqs. (2.9) and (3.233), and have

$$\frac{D\bar{V}_i}{Dt} = -\frac{\partial}{\partial x_i}\left(\bar{p} + \frac{1}{2}\tilde{\mathbf{B}}^2\right) + \left(\bar{\mathbf{J}} \times \bar{\mathbf{B}}\right)_i - \frac{\partial R_{{\rm M}ij}}{\partial x_j} + \nu \nabla^2 \bar{V}_i, \tag{3.240}$$

$$\frac{\partial \bar{\mathbf{B}}}{\partial t} = \nabla \times (\bar{\mathbf{V}} \times \bar{\mathbf{B}} + \mathbf{E}_{\rm M}) + \eta \nabla^2 \bar{\mathbf{B}}, \tag{3.241}$$

where $R_{{\rm M}ij}$ and $\mathbf{E}_{\rm M}$ are the MHD Reynolds stress and the turbulent electromotive force, defined by

$$R_{{\rm M}ij} = \left\langle \tilde{v}_i \tilde{v}_j - \tilde{B}_i \tilde{B}_j \right\rangle, \tag{3.242}$$

$$\mathbf{E}_{\rm M} = \left\langle \tilde{\mathbf{v}} \times \tilde{\mathbf{B}} \right\rangle. \tag{3.243}$$

The latter is also related to the mean electric current $\bar{\mathbf{J}}$ as

$$\bar{\mathbf{J}} = (1/\eta)\left(\bar{\mathbf{E}} + \bar{\mathbf{V}} \times \bar{\mathbf{B}} + \mathbf{E}_{\rm M}\right). \tag{3.244}$$

In Elsässer's MHD system, the counterpart of $R_{{\rm M}ij}$ and $\mathbf{E}_{\rm M}$ is given by

$$R_{{\rm E}ij} = \left\langle \tilde{\phi}_i \tilde{\psi}_j \right\rangle. \tag{3.245}$$

In terms of $R_{{\rm E}ij}$, $R_{{\rm M}ij}$ and $\mathbf{E}_{\rm M}$ may be written as

$$R_{{\rm M}ij} = (1/2)\left(R_{{\rm E}ij} + R_{{\rm E}ji}\right), \tag{3.246}$$

$$E_{{\rm M}i} = -(1/2)\varepsilon_{ij\ell} R_{Ej\ell}. \tag{3.247}$$

This fact indicates that R_{Eij} is the quantity more fundamental than R_{Mij} and $\mathbf{E}_M$.

As some scalar relationships, we have

$$K_M \equiv \left\langle \tilde{\mathbf{v}}^2 + \tilde{\mathbf{B}}^2 \right\rangle /2 = \left\langle \tilde{\phi}^2 + \tilde{\psi}^2 \right\rangle /4, \tag{3.248}$$

$$W \equiv \left\langle \tilde{\mathbf{v}} \cdot \tilde{\mathbf{B}} \right\rangle = \left\langle \tilde{\phi}^2 - \tilde{\psi}^2 \right\rangle /4. \tag{3.249}$$

Here K_M and W are called the turbulent MHD energy and the turbulent cross helicity, respectively. The importance of W is clear since ϕ and ψ are independent of each other except in the special case. The role of the cross helicity has long been missing in the history of dynamo research.

From the fact that $\int (1/2)(\mathbf{V}^2 + \mathbf{B}^2) dV$ and $\int \mathbf{V} \cdot \mathbf{B} dV$ are conserved in the absence of ν and η, K_M and W obey equations whose mathematical structures are firm and clear:

$$\frac{DG}{Dt} = P_G - \varepsilon_G + \nabla \cdot \mathbf{T}_G \quad (G = K_M \text{ or } W), \tag{3.250}$$

where

$$P_{K_M} = -\mathbf{E}_M \cdot \bar{\mathbf{J}} - R_{Mij} \frac{\partial \bar{V}_j}{\partial x_i}, \tag{3.251}$$

$$\varepsilon_{K_M} \equiv \varepsilon_M = \nu \left\langle \left(\frac{\partial \tilde{v}_j}{\partial x_i} \right)^2 \right\rangle + \eta \left\langle \left(\frac{\partial \tilde{B}_j}{\partial x_i} \right)^2 \right\rangle, \tag{3.252}$$

$$\mathbf{T}_{K_M} = W\mathbf{B} + \tilde{\mathbf{T}}_{K_M} + \nu \nabla K_M, \tag{3.253}$$

$$P_W = -\mathbf{E}_M \cdot \bar{\boldsymbol{\omega}} - R_{Eij} \frac{\partial \bar{B}_j}{\partial x_i}, \tag{3.254}$$

$$\varepsilon_W = (\nu + \eta) \left\langle \frac{\partial \tilde{v}_j}{\partial x_i} \frac{\partial \tilde{B}_j}{\partial x_i} \right\rangle, \tag{3.255}$$

$$\mathbf{T}_W = K_M \mathbf{B} + \tilde{\mathbf{T}}_W + \eta \nabla W, \tag{3.256}$$

with the mean vorticity $\bar{\boldsymbol{\omega}} = \nabla \times \bar{\mathbf{V}}$. Equations (3.251)-(3.253) and (3.254)-(3.256) correspond to Eqs. (3.14)-(3.16) for an electrically nonconducting flow. In Eqs. (3.253) and (3.256), $\tilde{\mathbf{T}}_{K_M}$ and $\tilde{\mathbf{T}}_W$ consist of third-order correlation functions concerning $\tilde{\mathbf{v}}$ and $\tilde{\mathbf{B}}$, whose details are omitted here.

C Modelling of turbulence effects based on the TSDIA For closing the MHD system, Eqs. (3.240) and (3.241), we need to relate R_{Mij} and $\mathbf{E}_M$ to the mean field and the quantities characterizing the MHD turbulent state. A systematic method of finding such relations is the use of the two-scale direct-interaction approximation (TSDIA) explained

in §3.3.4. In what follows, we shall omit the details of the TSDIA analysis of Elsässer's MHD system [1.7, 3.75], and give the simplest dynamo model in the physical-space representation applicable to various interesting realistic phenomena.

The important procedure in dynamo modelling is the choice of proper characteristic turbulence quantities, entirely the same as for the electrically nonconducting case in §3.3.2. Turbulence theories such as the TSDIA suggest that the most fundamental turbulence quantities are

$$K_{\mathrm{M}},\ \ W,\ \ H_{\mathrm{R}}\left(\equiv\left\langle-\tilde{\mathbf{v}}\cdot\tilde{\boldsymbol{\omega}}+\tilde{\mathbf{B}}\cdot\tilde{\mathbf{J}}\right\rangle\right),\ \ \varepsilon_{\mathrm{M}}, \tag{3.257}$$

where H_{R} is called the turbulent residual helicity ($\tilde{\boldsymbol{\omega}}=\nabla\times\tilde{\mathbf{v}}$). Of these four, W and H_{R} are pseudo-scalars. At least, two pure scalars such as K_{M} and ε_{M} are indispensable for the construction of a characteristic time scale. The important inequality

$$|W|/K_{\mathrm{M}}\leq 1 \tag{3.258}$$

holds between K_{M} and W.

The simplest modelling of $R_{\mathrm{M}ij}$ and $\mathbf{E}_{\mathrm{M}}$ is

$$R_{\mathrm{M}ij}=(2/3)K_{\mathrm{R}}\delta_{ij}-\nu_{\mathrm{T}}\bar{s}_{ij}+\nu_{\mathrm{M}}\bar{m}_{ij}, \tag{3.259}$$

$$\mathbf{E}_{\mathrm{M}}=\alpha\bar{\mathbf{B}}-\beta\bar{\mathbf{J}}+\gamma\bar{\boldsymbol{\omega}}, \tag{3.260}$$

where $K_{\mathrm{R}}(=\langle\tilde{\mathbf{v}}^2-\tilde{\mathbf{B}}^2\rangle/2)$ is the turbulent residual energy, and the mean velocity-strain tensor $\bar{s}_{ij}$ is defined by Eq. (3.135), and the magnetic-counterpart $\bar{m}_{ij}$ is obtained by replacing $\bar{\mathbf{V}}$ in $\bar{s}_{ij}$ with $\bar{B}$. Among the coefficients ν_{T}, ν_{M}, β, and γ, the TSDIA gives the simple relationship

$$\nu_{\mathrm{T}}=(7/5)\beta,\ \ \nu_{\mathrm{M}}=(7/5)\gamma. \tag{3.261}$$

Using expression (3.257), α, β, and γ may be modelled as

$$\alpha=C_{\alpha}\tau H_{\mathrm{R}}, \tag{3.262}$$

$$\beta=C_{\beta}\tau K_{\mathrm{M}}, \tag{3.263}$$

$$\gamma=C_{\gamma}\tau W. \tag{3.264}$$

with the characteristic time scale $\tau=K_{\mathrm{M}}/\varepsilon_{\mathrm{M}}$. Here the numerical coefficients C_{α}, C_{β}, and C_{γ} have already been estimated as [3.76]

$$C_{\alpha}\cong 0.02,\ \ C_{\beta}\cong 0.05,\ \ C_{\gamma}\cong 0.04. \tag{3.265}$$

In what follows, no use will be made of the details of the magnitude of these coefficients.

In Eq. (3.250), we need to model $\tilde{\mathbf{T}}_{K_{\mathrm{M}}}$ [Eq. (3.253)], ε_W [Eq. (3.255)], and $\tilde{\mathbf{T}}_W$ [Eq. (3.256)]. Their simplest models are

$$\tilde{\mathbf{T}}_{K_{\mathrm{M}}}=(\nu_{\mathrm{T}}/\sigma_K)\,\nabla K, \tag{3.266}$$

$$\varepsilon_W = C_W W/\tau, \tag{3.267}$$

$$\tilde{\mathbf{T}}_W = (\nu_T/\sigma_W)\,\nabla W, \tag{3.268}$$

where the numerical factors σ_K etc. are chosen as

$$\sigma_K = \sigma_W = 1, \quad C_W = 1.1. \tag{3.269}$$

As for the remaining two quantities ε_M and H_R, we have no conservation rules corresponding to $\int (1/2)(\mathbf{V}^2 + \mathbf{B}^2)dV$ and $\int \mathbf{V}\cdot\mathbf{B}dV$ or $\int \phi^2 dV$ and $\int \psi^2 dV$. As a result, the modelling of their equations is inevitably phenomenological. The following discussion will not be based on the details of their modelling.

D Physical meanings of turbulence effects MHD turbulence effects occur through R_{Mij} and $\mathbf{E}_M$. We are in position to understand the generation mechanism of those effects in physical terms.

D1 Effects on the magnetic field We substitute Eq. (3.260) into Eqs. (3.241) and (3.244), and have

$$\frac{\partial \bar{\mathbf{B}}}{\partial t} = \nabla \times \left[\bar{\mathbf{V}} \times \bar{\mathbf{B}} + \alpha \bar{\mathbf{B}} - (\eta + \beta)\bar{\mathbf{J}} + \gamma \bar{\boldsymbol{\omega}}\right], \tag{3.270}$$

$$\bar{\mathbf{J}} = \frac{1}{\eta + \beta}\left(\bar{\mathbf{E}} + \bar{\mathbf{V}} \times \bar{\mathbf{B}} + \alpha \bar{\mathbf{B}} + \gamma \bar{\boldsymbol{\omega}}\right). \tag{3.271}$$

First, the physical meaning of β is clear from Eq. (3.270) or (3.271). It expresses the enhanced effect of the resistivity due to fluctuations, which is called the turbulent or anomalous resistivity. The effect tends to destroy ordered structures of the magnetic fields. In order that the structures continue to survive, some other effects need to balance the β effect and effectively suppress it.

As such factors, we have two effects in Eq. (3.270) or (3.271). One is the α-related term. It generates $\bar{\mathbf{J}}$ aligned with $\bar{\mathbf{B}}$ in sharp contrast to the original term $\bar{\mathbf{V}} \times \bar{\mathbf{B}}$. This mechanism, which is called the alpha effect, is very familiar in the long history of the turbulent dynamo [3.72-3.74]. The coefficient α consists of two effects. One is the contribution from the turbulent kinetic helicity $\langle \tilde{\mathbf{v}} \cdot \tilde{\boldsymbol{\omega}} \rangle$. The mechanism is illustrated in Fig. 3.2. The other is from the turbulent current helicity $\langle \tilde{\mathbf{B}} \cdot \tilde{\mathbf{J}} \rangle$ [3.77]. Nonvanishing $\langle \tilde{\mathbf{B}} \cdot \tilde{\mathbf{J}} \rangle$ is an indicator of nonvanishing $\bar{\mathbf{B}} \cdot \bar{\mathbf{J}}$.

A prominent feature of the alpha effect is that the resulting equation, that is, Eq. (3.270) with the γ-related term discarded, is linear and homogeneous. As a result, the saturation level of $\bar{\mathbf{B}}$ is not determined from the equation alone. The saturation process of $\bar{\mathbf{B}}$ is a major problem in the alpha dynamo. A method of investigating the process is the incorporation of nonlinear effects of $\bar{\mathbf{B}}$ into the alpha coefficient α [3.78].

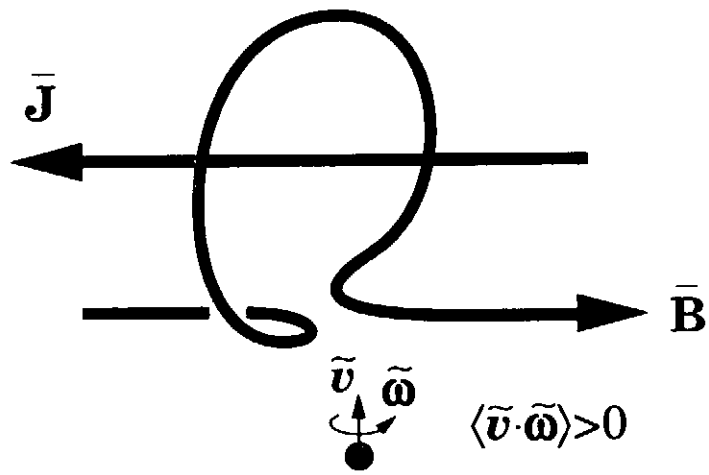

Figure 3.2. Alpha or helicity dynamo.

This method is also extended to the inclusion of the similar effects in the turbulent resistivity (β) and the turbulent diffusivity of a passive scalar [3.79, 3.80].

Another ingredient possessing the potential to balance the turbulent-resistivity effect is the γ-related part in Eq. (3.270) or (3.271) [1.7, 3.75]. In this effect, a $\bar{\mathbf{J}}$ aligned with $\bar{\omega}$ is generated, which is equivalent to the occurrence of a $\bar{\mathbf{B}}$ aligned with $\bar{\mathbf{V}}$. This process is shown schematically in Fig. 3.3. The balance between the cross-helicity and turbulent-resistivity effects may determine the saturation level of $\bar{\mathbf{B}}$ within the framework of the induction equation, unlike the method based on the alpha effect.

The cross-helicity effect $\gamma\bar{\omega}$ is sensitive to the effect of frame rotation. In the frame rotating with the angular velocity $\mathbf{\Omega}_\mathrm{F}$, $\bar{\omega}$ is subject to the transformation

$$\bar{\omega} \rightarrow \bar{\omega} + 2\mathbf{\Omega}_\mathrm{F}. \tag{3.272}$$

This fact indicates that the cross-helicity effect may play an important role in the study of the astronomical dynamo that is associated with rotational motion.

D2 Effects on fluid motion We substitute Eq. (3.259) into Eq. (3.240), and discard the spatial variation of the coefficients ν_T and ν_M for the understanding of basic turbulence effects. Then we have

$$\begin{aligned}\frac{D\bar{V}_i}{Dt} = &-\frac{\partial}{\partial x_i}\left(\bar{p} + \left\langle\frac{\tilde{\mathbf{B}}^2}{2}\right\rangle + \frac{2}{3}K_\mathrm{R}\right) + (\bar{\mathbf{J}}\times\bar{\mathbf{B}})_i \\ &+ \nu_\mathrm{T}\nabla^2\bar{V}_i - \nu_\mathrm{M}\nabla^2\bar{B}_i.\end{aligned} \tag{3.273}$$

Here the turbulent-viscosity (ν_T) effect is entirely the same as for electrically non-conducting flows. Ordered magnetic structures are usually linked with ordered flow structures. In such a case, the eventual cancellation of diffusion effects due to ν_T is

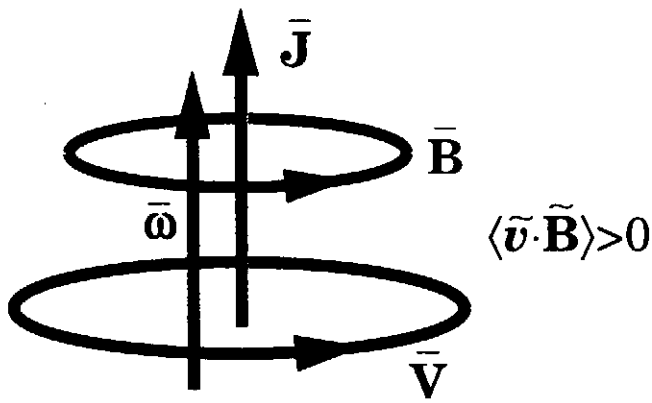

Figure 3.3. Cross-helicity dynamo.

essential for the persistence of ordered magnetic structures. The last term on the right-hand side of Eq. (3.273) is a promising candidate as the ingredient giving rise to such a cancellation.

The ν_M-related term in Eq. (3.273) arises from the tension intrinsic to magnetic-field lines. In the case that a fluid blob moves in the direction normal to magnetic-field lines at high magnetic Reynolds numbers, the field lines move locally with the blob from the frozen-in property, and bending of the lines occurs. The further movement of the blob is suppressed by the tension of the bent magnetic field lines. This process is the cause of the ν_M-related term.

The alpha effect has no direct influence on the fluid motion since $\bar{\mathbf{J}}$ generated by the effect results in vanishing $\bar{\mathbf{J}} \times \bar{\mathbf{B}}$. In the absence of the ν_M-related term, we often encounter the difficulty that the saturation level of $\bar{\mathbf{B}}$ cannot be determined, as was noted in §3.4.1D1.

3.4.2. Astro/geophysical dynamo Dynamo researches were started originally for understanding the generation and sustainment mechanisms of the geomagnetic field [3.72-3.74], the solar magnetic fields represented by sunspots [3.81], and galactic magnetic fields [3.82, 3.83]. Magnetic effects have also attracted much attention in close relation to the occurrence of high-speed jets observed ubiquitously around protostars, active galactic nuclei, binary X-ray sources, etc. and the high collimation of such jets [3.84].

A Geomagnetic and solar magnetic fields

A1 Characteristic magnetic behavior The interiors of the earth and the sun are depicted schematically in Figs. 3.4 and 3.5. The earth interior consists of the mantle,

the outer core, and the inner core, whose main constituents are silicon, molton iron, and solid iron, respectively. The geomagnetic field originates from the motion of molton iron, specifically, its turbulent motion, as will be mentioned below. The interior of the sun is divided into the convective zone, the radiative zone, and the core. The origin of the solar magnetic field lies in the convective zone that is in the fluid state of hydrogen.

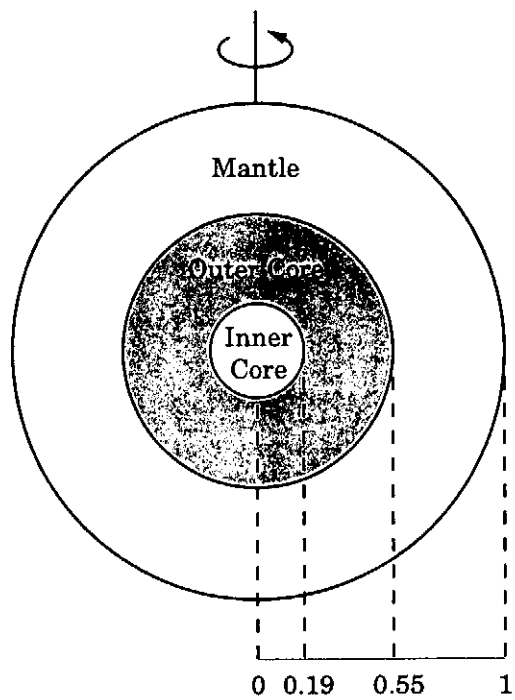

Figure 3.4. Earth's interior with the outer core as the magnetic generator.

The outer core of the earth is covered with the electrically non-conducting mantle. As a result, the toroidal component of the geometric field that is normal to the rotation axis is masked, and only the poloidal component is directly observable. On the other hand, more detailed observational data are accumulating on the solar magnetic field since the field is generated in the outermost zone.

Both the geomagnetic and solar fields are generated in a spherical shell region, apart from a difference in the location of the shells. The properties of the generated magnetic fields, however, differ much from each other. Some typical features of the geomagnetic field are summarized as follows [3.85, 3.86]:

(G1) Of the poloidal field, the dipole component whose axis is nearly along the rotation axis is strongest, and its magnitude is a few Gauss (G) at the surface.

(G2) The velocity of the molton iron is not observable, but it is inferred to be $O(10^{-4})$

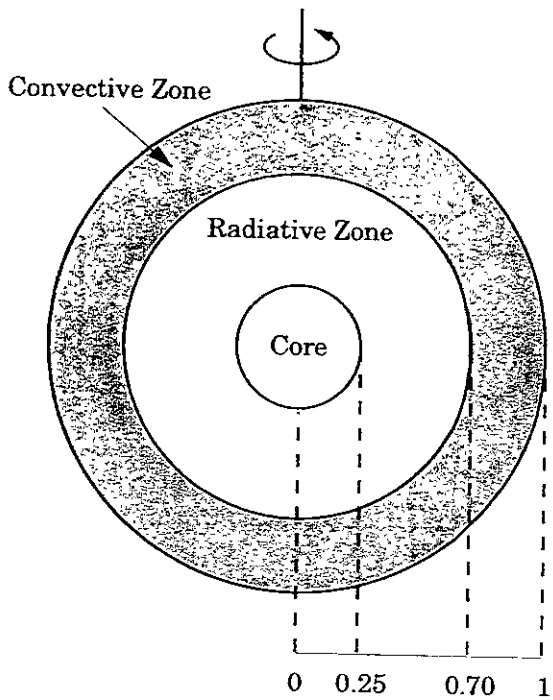

Figure 3.5. Solar interior with the convective zone as the magnetic generator.

ms^{-1} in a frame fixed at the earth. This inference indicates that the Reynolds number in the outer core is $O(10^7)$, and that the fluid motion is highly turbulent.

(G3) The polarity of the dipole component repeats a reversal in an irregular manner. The typical period of the duration of one polarity is $O(10^5) \sim O(10^6)$ years, whereas the transition from one polarity to the other occurs in a period within $O(10^4)$ years.

The intense toroidal component of the solar magnetic field is observed as sunspots. The toroidal magnetic flux tubes in the convective zone rise up under buoyancy effects and break through the photosphere adjacent to the zone. Sunspots represent the cross sections of these tubes and appear in pairs. Many important features of the solar-field generation process can be understood from the sunspot behavior. The primary behavior of sunspots is summarized as the following sunspot rule [3.81, 3.87]:

(S1) The occurrence of sunspots is limited to the middle- to low-latitude region. The polarity of sunspots reverses quite regularly, that is, in about 11 years.

(S2) At the start of the sunspot cycle, the polarity of the leading sunspot of the pair in one hemisphere is coincident with the polarity of the polar field or the poloidal field near the pole of the hemisphere (Fig. 3.6). The latter is of a few G and is very weak, compared with the magnetic field of sunspots whose intensity may become a few kilogauss (KG).

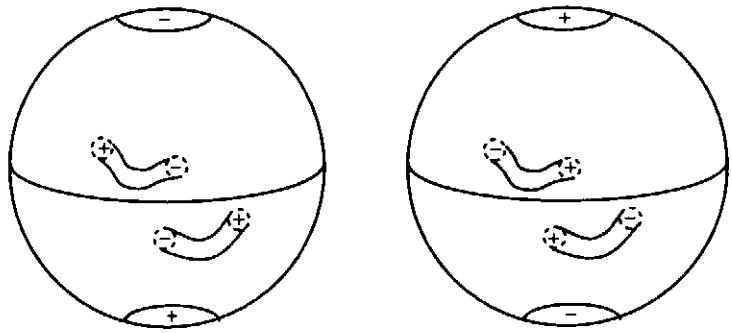

Figure 3.6. Sunspot's polarity rule.

From the foregoing characteristics of geomagnetic and sunspot fields, we may see a large difference between the irregular geomagnetic reversal period and the regular sunspot-polarity counterpart, $O(10^5) \sim O(10^6)$ and 11 years, although both the magnetic fields are generated in a spherical shell region. It is appropriate to say that the geomagnetic field with a dipole axis nearly along the rotation axis is quite stable, compared with the solar field.

In the case of molton iron, 1 G corresponds to a velocity $O(10^{-3})$ ms^{-1}. From the geomagnetic feature (G2), the energy of the dipole field alone is some hundred times the kinetic energy of the fluid motion. The toroidal field is not observable, but it is inferred to be of $O(10) \sim O(10^2)$ G. Then the geomagnetic field may store an energy that is $O(10^4) \sim O(10^6)$ times that of the fluid motion generating it. It is probable that the stability of the geomagnetic field is linked with the storage of such high energy. The elucidation of this linkage is a major target of the turbulent geodynamo.

The origin of sunspots is the toroidal magnetic field generated in the convective zone. The intensity of large sunspots is $O(10^3)$ G, and it is inferred to reach $O(10^4)$ G near the bottom. The poloidal component is weak and is of a few G, which is comparable to the geomagnetic dipole field. This weak poloidal field is considered to be associated with the periodic reversal of the solar polarity. In the context of fluid motion, the rotation of the convective zone is highly differential. The deviation of the angular velocity from a solid rotation reaches about thirty percent near the bottom of the zone [3.88]. Such high differential rotation is inferred to generate a very strong field near the bottom.

A2 Turbulent geodynamo The differential rotation in the outer core is very weak, compared with the solar convective zone. From Eqs. (3.270) and (3.272), a sufficient condition on the stationary magnetic field is given by

$$\bar{\mathbf{V}} \times \bar{\mathbf{B}} + \alpha \bar{\mathbf{B}} - \beta \bar{\mathbf{J}} + \gamma \left(\bar{\omega} + 2\Omega_{\mathrm{F}} \right) = 0. \tag{3.274}$$

The helicity effect is closely associated with the formation of convection columns along the rotation axis. We place an emphasis on the helicity effect [3.89], and rewrite

Eq. (3.274) as

$$\bar{\mathbf{J}} - \frac{\alpha}{\beta}\bar{\mathbf{B}} = \frac{\gamma}{\beta}(\bar{\boldsymbol{\omega}} + 2\boldsymbol{\Omega}_{\mathrm{F}}) + \frac{1}{\beta}\bar{\mathbf{V}} \times \bar{\mathbf{B}} \cong \frac{2\gamma}{\beta}\boldsymbol{\Omega}_{\mathrm{F}} + \frac{1}{\beta}\bar{\mathbf{V}} \times \bar{\mathbf{B}}. \tag{3.275}$$

We discard the last term on the right-hand side of Eq. (3.275), which will be justified below. We substitute Eq. (3.275) into the frame-rotation counterpart of Eq. (3.273), and obtain

$$\begin{aligned}\frac{\partial \bar{\mathbf{V}}}{\partial t} = & -\nabla\left(\bar{p} + \frac{\bar{\mathbf{V}}^2}{2} + \left\langle\frac{\tilde{\mathbf{B}}^2}{2}\right\rangle + \frac{2}{3}K_{\mathrm{R}}\right) \\ & + 2\left(\bar{\mathbf{V}} - \frac{\gamma}{\beta}\bar{\mathbf{B}}\right) \times \boldsymbol{\Omega}_{\mathrm{F}} + \nu_{\mathrm{T}}\nabla^2\left(\bar{\mathbf{V}} - \frac{\gamma}{\beta}\bar{\mathbf{B}}\right).\end{aligned} \tag{3.276}$$

The duration of the ordered magnetic structure is equivalent to that of the flow structure, for the change of the latter distorts the former. On the right-hand side of Eq. (3.276), the last part destroys such a flow structure as long as the $\bar{\mathbf{B}}$-related part is absent. The near balance between the turbulent-viscosity and cross-helicity effects, that is,

$$\bar{\mathbf{V}} - \frac{\gamma}{\beta}\bar{\mathbf{B}} \cong 0 \ \text{ or } \ \bar{\mathbf{B}} \cong \frac{C_\beta}{C_\gamma}\frac{K_{\mathrm{M}}}{W}\bar{\mathbf{V}}, \tag{3.277}$$

may alleviate the structure destruction due to the ν_{T} effect. Equation (3.277) justifies the approximation of dropping $\bar{\mathbf{V}} \times \bar{\mathbf{B}}$ in Eq. (3.275). Equation (3.277) also indicates that the frame-rotation or Colioris effect is reduced effectively.

In Eq. (3.275) with $\bar{\mathbf{V}} \times \bar{\mathbf{B}}$ discarded, the frame-rotation effect occurs as the ingredient perturbing the so-called force-free state

$$\bar{\mathbf{J}} = (\alpha/\beta)\,\bar{\mathbf{B}}. \tag{3.278}$$

In the geodynamo, this force-free state corresponds to the α^2 dynamo. There the toroidal field generates the toroidal current through Eq. (3.278), and the current induces the poloidal field according to Ampère law. The poloidal field generates the poloidal current from Eq. (3.278), regenerating the toroidal field through Ampère law. From expression (3.258), Eq. (3.277) indicates that the energy of the induced magnetic field is larger than that of the fluid motion. For the probable parameter range of $|W|/K_{\mathrm{M}} = O(10^{-2}) \sim O(10^{-1})$, the magnetic field may become much larger, as in the geomagnetic case.

A recent computer experiment of the MHD system of equations mimicking the geomagnetic field indicates that the dynamo resembles the α^2 dynamo, and the frame-rotation or $\boldsymbol{\Omega}_{\mathrm{F}}$-related effect is effectively reduced to the level of the other terms [3.90]. These findings are consistent with the foregoing dynamo that is the combination of helicity and cross-helicity effects. The reversal of the dipole field is now under intensive study based on computer experiments in the context of the geomagnetic reversal [3.91, 3.92].

A3 Turbulent sunspot dynamo The solar polarity rule has been investigated intensively with the aid of the so-called α–ω dynamo [3.93, 3.94]. In this dynamo, a properly chosen differential rotation generates the toroidal field from the poloidal field. The toroidal electric current occurs from the toroidal field under the alpha effect, resulting in the regeneration of the poloidal field. The stretching of magnetic lines by the differential rotation is the cause of the oscillatory behavior of this dynamo.

The solar convection zone is rather thin, compared with the outer core of the earth. This fact suggests that the helicity effect resulting from the formation of convection columns along the rotation axis is weaker in the sun, compared to the geodynamo. In contrast to the α–ω dynamo, let us suppose that the magnetic-field structure occurs from the balance between the β- and γ-related terms in Eq. (3.274) [3.95], resulting in

$$\bar{\mathbf{B}} = \frac{\gamma}{\beta}\bar{\mathbf{V}} = \frac{C_\gamma}{C_\beta}\frac{W}{K_{\mathrm{M}}}\bar{\mathbf{V}}. \tag{3.279}$$

In the convective zone, the primary motion is the toroidal differential rotation. Equation (3.279) indicates that the toroidal field is induced in the convective zone, and that it is in the opposite direction in the northern and southern hemispheres since the cross helicity W is a pseudoscalar. Such a magnetic field leads to the sunspots depicted in Fig. 3.6.

From the toroidal field given by Eq. (3.279), the alpha effect in Eq. (3.271) induces the poloidal field, whose primary component is of the dipole type. This field is shown to contribute to the annihilation of W that is indispensable for the generation of the toroidal field through Eq. (3.279). Instead of giving the details of this process, we explain the polarity reversal with the aid of an illustrative model

$$\bar{B}_{\mathrm{T}} = \gamma^* \bar{V}_{\mathrm{T}}, \tag{3.280}$$

$$\frac{d\bar{B}_{\mathrm{P}}}{dt} = \alpha^* \bar{B}_{\mathrm{T}}, \tag{3.281}$$

$$\frac{d\gamma^*}{dt} = -\delta \bar{B}_{\mathrm{P}}. \tag{3.282}$$

Here Eq. (3.280) expresses the generation of the toroidal field $\bar{B}_{\mathrm{T}}$ due to the rotational motion $\bar{V}_{\mathrm{T}}$, and γ^* plays the role of the turbulent cross helicity W. Equation (3.281) shows the occurrence of the poloidal field $\bar{B}_{\mathrm{P}}$ from $\bar{B}_{\mathrm{T}}$ under the alpha effect. Equation (3.282) expresses the annihilation of the turbulent cross helicity through the poloidal field.

In Eqs. (3.280)-(3.282), we neglect the temporal variation of α^* in addition to $\bar{V}_{\mathrm{T}}$ and δ, and focus attention on that of $\bar{B}_{\mathrm{T}}$, $\bar{B}_{\mathrm{P}}$, and γ^*. We retain $\bar{B}_{\mathrm{T}}$, and have

$$\frac{d^2\bar{B}_{\mathrm{T}}}{dt^2} = -\omega_{B_{\mathrm{T}}}^2 \bar{B}_{\mathrm{T}}, \tag{3.283}$$

with $\omega_{B_T} = \sqrt{\alpha^* \delta \bar{V}_T}$. Equation (3.283) shows the periodic oscillation of $\bar{B}_T$ with the reversal frequency ω_{B_T}. In this model, the phase difference between $\bar{B}_T$ and $\bar{B}_P$ is $\pi/2$. It is noteworthy that some phase difference is confirmed in the observations concerning sunspots and the poloidal field near the poles.

B Collimation of astronomical jets Around a high-mass body such as active galactic nuclei, protostars, etc., gases exist in a disk form and accrete onto them while rotating (Fig. 3.7) [3.84]. The angular momentum of gases needs to be released for the accretion. One possible mechanism is the transfer of the angular momentum towards the outer part of the disk through the turbulence transport effects, and the other is the release through the rotating jets that are observed ubiquitously around an accretion disk. They are bipolar and normal to the disk, and are highly collimated; namely, they go straight on without diffusing, in sharp contrast to the jets observed in laboratories.

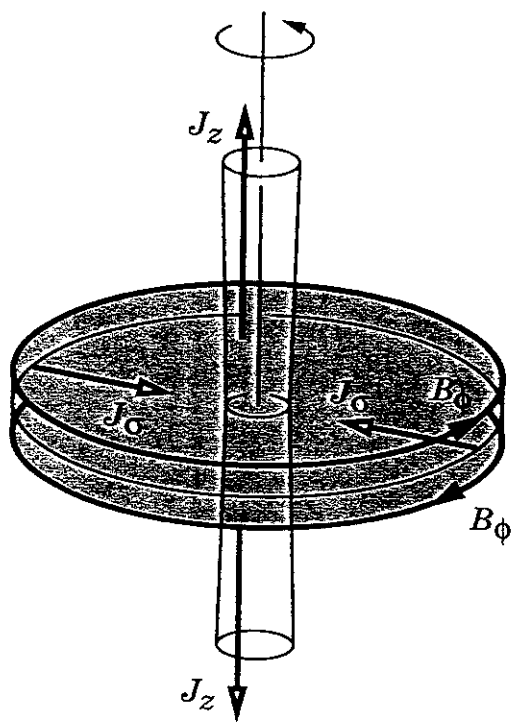

Figure 3.7. Illustration of an accretion disk and an accompanying jet.

The primary factors to be clarified concerning accretion-disk jets are the driving and collimation mechanisms. The driving mechanism has been investigated by computer experiments on the MHD system of equations [3.96, 3.97]. The turbulent dynamo based on the cross helicity was also applied to the study of the generation mechanism of a magnetic field that is intense enough to release gases against the gravitational energy [3.98, 3.99].

In what follows, we shall seek the collimation mechanism on the basis of the MHD system. The velocity of the jets from active galactic nuclei may reach some ten percent of velocity of light. In such a case, it is probable that the relativistic effect has a large influence on the collimation mechanism. Here we focus attention on the non-relativistic jets that are observed for protostars. In this case, we may consider two factors as the cause of the collimation [3.100]. One is the effect of magnetic fields, and the other is the effects of fluid compressibility. In electrically non-conducting flows, it is wellknown that fluid compressibility reduces the growth of turbulence. A typical example is the suppression of the growth rate of laboratory flows such as mixing-layer flows and jets. The astronomical jets, however, are often collimated over a long distance of $O(10^4)$ light years. For such extreme collimation, effects of magnetic fields are considered to play a great part in addition to effects of fluid compressibility.

In the light of magnetic-field effects on the jet collimation, we seek the stationary state of Eq. (3.270) [3.101], which is guaranteed by

$$\bar{\mathbf{V}} \times \bar{\mathbf{B}} + \alpha \bar{\mathbf{B}} - \beta \bar{\mathbf{J}} + \gamma \bar{\boldsymbol{\omega}} = 0, \tag{3.284}$$

with the molecular resistivity η discarded. From Eq. (3.284), we have

$$\bar{\mathbf{J}} \times \bar{\mathbf{B}} = -\frac{\gamma}{\beta} \bar{\mathbf{B}} \times \bar{\boldsymbol{\omega}} + \frac{1}{\beta} \left(\bar{\mathbf{V}} \times \bar{\mathbf{B}} \right) \times \bar{\mathbf{B}}. \tag{3.285}$$

We substitute Eq. (3.285) into the equation for $\bar{\boldsymbol{\omega}}$ that is derived from Eq. (3.273). Here we drop the second part in Eq. (3.285) (this procedure will be justified below). Then we have

$$\frac{\partial \bar{\boldsymbol{\omega}}}{\partial t} = \nabla \times \left[\left(\bar{\mathbf{V}} - \frac{\gamma}{\beta} \bar{\mathbf{B}} \right) \times \bar{\boldsymbol{\omega}} + \nu_{\mathrm{T}} \nabla^2 \left(\bar{\mathbf{V}} - \frac{\gamma}{\beta} \bar{\mathbf{B}} \right) \right]. \tag{3.286}$$

The stationary state of $\bar{\boldsymbol{\omega}}$ exists under the condition

$$\bar{\mathbf{V}} = \frac{\gamma}{\beta} \bar{\mathbf{B}}, \tag{3.287}$$

which justifies the foregoing discard of the second part in Eq. (3.285).

Equations (3.287) indicates

$$\bar{\mathbf{B}}^2/2 > \bar{\mathbf{V}}^2/2, \tag{3.288}$$

from Eq. (3.258). Specifically, the magnetic energy becomes much larger under the probable condition that $|W|/K_{\mathrm{M}} \leq O(10^{-1})$, just as for the geomagnetic field. One of the prominent features of a magnetic field is the tension force, under which magnetic field lines resist their distortion due to fluid motion. A jet possessing an intense magnetic field inside may strongly resist the bending and go straight on. This is the collimation mechanism deduced from the turbulent dynamo based on both cross-helicity and helicity effects.

3.4.3. Turbulent dynamo and fusion plasma We consider the relationship of the turbulent dynamo with plasma confinement based on reversed-field pinches (RFP's) and tokamaks. Here we should stress that the MHD approximation is applicable to a limited range of fusion plasma behaviour.

RFP's and tokamaks belong to the category of magnetic confinement in symmetric tori. These confinement methods are characterized typically by the safety factor

$$q = (a/R)\,(B_{\mathrm{TR}}/B_{\mathrm{PR}})\,. \tag{3.289}$$

Here R and a are the major and minor radii of the torus, and B_{TR} and B_{PR} express reference magnitudes of the toroidal and poloidal components of the magnetic field. The primary part of the toroidal field is sustained by an external coil, whereas the poloidal counterpart is due to the plasma current generated by a loop voltage etc. In the light of MHD stability analysis, RFP's and tokamaks are characterized by $q \ll 1$ and $q > 1$, respectively.

A Magnetic dynamo and RFP's The confinement of plasma in RFP's is realized in the situation

$$R \gg a, \quad |B_{\mathrm{TR}}/B_{\mathrm{PR}}| \cong 1. \tag{3.290}$$

The latter condition gives rise to a turbulent state of plasma, owing to strong pinch effects due to B_{PR}. A prominent property of RFP's is the reversal of the toroidal field in the outer part of plasma [3.102, 3.103]. As a result, the long duration of RFP's hinges on the sustainment of the reversed toroidal field by the toroidal plasma current. This toroidal alignment between the electric current and the magnetic field is the most typical manifestation of the alpha effect.

In RFP's, we have no global plasma flow. In Eq. (3.270), we drop the $\bar{\mathbf{V}}$-related terms, and have

$$\beta\bar{\mathbf{J}} - \alpha\bar{\mathbf{B}} - \bar{\mathbf{E}} = 0. \tag{3.291}$$

The loop voltage driving the plasma current comes from the toroidal component of $\bar{\mathbf{E}}$. We assume that the first two terms in Eq. (3.291) are primary, and that their difference balances $\bar{\mathbf{E}}$. Then we approximate Eq. (3.291) as

$$\bar{\mathbf{J}} = \chi\bar{\mathbf{B}}, \tag{3.292}$$

with $\chi = \alpha/\beta$ [1.7, 3.96].

From the first relation of Eq. (3.290), we adopt the cylindrical approximation to a torus, with the coordinates (r, θ, z) (θ and z correspond to the poloidal and toroidal directions, respectively). We take the curl of Eq. (3.292), and have

$$\left(\nabla^2 + \chi^2\right)\bar{\mathbf{B}} = 0. \tag{3.293}$$

The axisymmetric solution of Eq. (3.293) is given by

$$B_z(r)/B_z(0) = J_0(|\chi|r), \quad B_\theta(r)/B_z(0) = J_1(|\chi|r), \tag{3.294}$$

where J_n is the Bessel function of the nth order. The Bessel function J_0 behaves like $\cos(|\chi|r)$ for small r, and the sign of B_z reverses at the outer edge of plasma under the condition

$$|\chi|a > 2.4. \tag{3.295}$$

Equation (3.292) was originally derived by an entirely different approach [3.105]. There $\mathbf{A} \cdot \mathbf{B}$ is adopted as the quantity expressing the helical property of the magnetic field, where $\mathbf{A}$ is the magnetic potential and is related to $\mathbf{B}$ as $\mathbf{B} = \nabla \times \mathbf{A}$. In the absence of the resistivity, $\int \mathbf{A} \cdot \mathbf{B} dV$ is conserved. Equation (3.292) is obtained using the variational method under the condition that $\int (\mathbf{B}^2/2) dV$ is minimum with constant $\int \mathbf{A} \cdot \mathbf{B} dV$. This property of $\mathbf{A} \cdot \mathbf{B}$ seems to indicate that it is more adequate than $\mathbf{B} \cdot \mathbf{J}$, in turbulent dynamo. From the dimensional viewpoint of Alfvén velocity units, however, $\mathbf{B} \cdot \mathbf{J}$ is linked more tightly with the kinetic helicity $\mathbf{v} \cdot \boldsymbol{\omega}$. The indication of the importance of $\mathbf{B} \cdot \mathbf{J}$ from turbulence theories such as the TSDIA is the manifestation of this point.

In the variational derivation of RFP's, we have no theoretical way to estimate the value of χ. In the turbulent dynamo, it is possible to construct model equations for K_{M}, H_{R}, and ε_{M} in α, and discuss the properties of both $\bar{\mathbf{B}}$ and the turbulence characteristics [3.106].

B Flow dynamo and tokamaks Plasma confinement in a tokamak has been improved through the discovery of two types of transport barriers, that is, edge and internal ones. One type is observed in the so-called high-confinement (H) modes, and the transport barrier is formed in the close vicinity of plasma edge [1.14]. The occurrence of H modes is spontaneous. The modes are characterized by a localized radial electric field [1.17, 1.19, 1.25] and poloidal plasma rotation. H modes are considered to arise from the plasma behavior intrinsic to the edge, as is explained in §4, and are beyond the scope of the MHD approximation.

The formation of internal transport barriers is observed in reversed-shear (RS), negative-central-shear (NCS), and enhanced-reversed-shear (ERS) modes (hereafter, they are simply called RS modes) [1.20, 3.107-3.109]. Those modes are characterized by the local safety factor

$$q_{\mathrm{L}} = (r/R)\,[B_z(r)/B_\theta(r)]\,, \tag{3.296}$$

under the cylindrical approximation (this approximation is used only for a simple explanation of phenomena, and the toroidicity is an important ingredient in tokamaks).

In RS modes, the $q_{\rm L}$ profile has a local minimum in the core region, and the heat transport barrier is formed there. The poloidal rotation and the radial electric field are also observed simultaneously, as is similar to H modes.

We consider the generation of poloidal plasma flow in RS modes from the viewpoint of turbulent dynamo [3.110]. In Eq. (3.273), we may discard $\bar{\mathbf{V}}$ in the initial stage. The candidates for the force driving plasma flow are $\bar{\mathbf{J}} \times \bar{\mathbf{B}}$ and the $\nu_{\rm M}$-related term since the $\nu_{\rm T}$-related term always contributes to the retardation of such a flow. In $\bar{\mathbf{J}} \times \bar{\mathbf{B}}$, the main component of $\bar{\mathbf{J}}$ is toroidal, and the counterparts of $\bar{\mathbf{B}}$ are toroidal and poloidal. Thus $\bar{\mathbf{J}} \times \bar{\mathbf{B}}$ may not give rise to the poloidal flow. The remaining candidate is the $\nu_{\rm M}$-related term.

We take the curl of Eq. (3.273). The z component of the mean vorticity, $\bar{\omega}_z$, expresses the poloidal plasma rotation, and obeys

$$\frac{\partial \bar{\omega}_z}{\partial t} = \nu_{\rm T} \nabla^2 \bar{\omega}_z - \nu_{\rm M} \nabla^2 \bar{J}_z. \tag{3.297}$$

In order to see the $\bar{\omega}_z$ generation process due to the $\nu_{\rm M}$-related effect, we write

$$\frac{\partial \bar{\omega}_z}{\partial t} = -\frac{5 C_\gamma}{7} \frac{K_{\rm M}}{\varepsilon_{\rm M}} W \nabla^2 \bar{J}_z + R_{\omega 1}, \tag{3.298}$$

where use has been made of Eqs. (3.261) and (3.264), and $R_{\omega 1}$ denotes the remaining contribution.

The quantity W is generated by P_W [Eq. (3.254)]. At the onset of $\bar{\omega}_z$, the second term in Eq. (3.260) is dominant, resulting in

$$\mathbf{E}_{\rm M} \cong -\beta \bar{\mathbf{J}}. \tag{3.299}$$

We combine Eq. (3.299) with P_W and have

$$P_W \cong \beta \bar{J}_z \bar{\omega}_z. \tag{3.300}$$

We focus attention on the contribution of Eq. (3.300) to the W equation (3.250), and have

$$\frac{\partial W}{\partial t} = \beta \bar{J}_z \bar{\omega}_z + R_W = C_\beta \frac{K_{\rm M}^2}{\varepsilon_{\rm M}} \bar{J}_z \bar{\omega}_z + R_W, \tag{3.301}$$

where Eq. (3.263) was used, and R_W denotes the remaining contribution.

We eliminate W from Eqs. (3.298) and (3.301), and connect $\bar{\omega}_z$ directly with $\bar{J}_z$. Here we focus attention on the temporal variation of W, and discard that of $\bar{J}_z$, $K_{\rm M}$ and $\varepsilon_{\rm M}$. Then we have

$$\frac{\partial^2 \bar{\omega}_z}{\partial t^2} - \chi_\omega^2 \bar{\omega}_z = R_{\omega 2}, \tag{3.302}$$

where

$$\chi_\omega \equiv \sqrt{-\frac{5 C_\beta C_\gamma}{7} \frac{K_{\rm M}^3}{\varepsilon_{\rm M}^2} \bar{J}_z \nabla^2 \bar{J}_z}. \tag{3.303}$$

and $R_{\omega 2}$ represents all the remaining contributions. Equation (3.302) indicates that $\bar{\omega}_z$ may grow under the condition

$$-\frac{5C_\beta C_\gamma}{7}\frac{K_{\rm M}^3}{\varepsilon_{\rm M}^2}\bar{J}_z\nabla^2\bar{J}_z > 0. \tag{3.304}$$

A typical example of the plasma current $\bar{J}_z$ in RS modes is shown in Fig. 3.8 [3.111]. The location of large negative $\bar{J}_z\nabla^2\bar{J}_z$ may be confirmed to coincide with that of a minimum $q_{\rm L}$. Equation (3.304) suggests that the poloidal rotation starts to be driven there. This finding is consistent with the fact that a poloidal flow in RS modes is observed near the minimum-$q_{\rm L}$ point where the transport barrier is formed. In short, there is a close relationship between the plasma rotation and the spatial profile of the plasma current, specifically, its curvature.

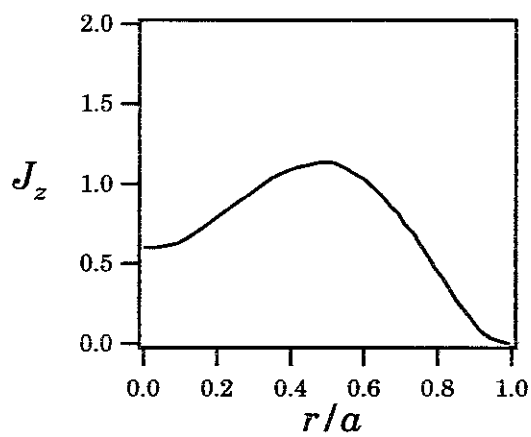

Figure 3.8. Typical plasma current in the RS mode.

References

[3.1] Herring J R 1965 Phys. Fluids **8** 2219
[3.2] Lighthill M J 1970 *Fourier Representation and Generalized Functions* (Cambridge: Cambridge University)
[3.3] Kolmogorov A N 1941 C. R. Acad. Sci. USSR **30** 301
[3.4] Kolmogorov A N 1941 C. R. Acad. Sci. USSR **32** 16
[3.5] Frisch U 1995 *Turbulence* (Cambridge: Cambridge University)
[3.6] Paquin J E and Pond S 1971 J. Fluid Mech. **50** 257
[3.7] Williams R W and Paulson C A 1977 J. Fluid Mech. **83** 547
[3.8] Meneveau C and Screenivasan K R 1991 J. Fluid Mech. **224** 429
[3.9] Oboukhov A M 1962 J. Fluid Mech. **13** 77
[3.10] Kolmogorov A N 1962 J. Fluid Mech. **13** 82

[3.11] Arimitsu T and Arimitsu N 2000 J. Phys. A **33** L1
[3.12] Desnyansky V N and Novikov E A 1974 Akad. Nauk. SSSR Fiz. Atoms. Okeana **10** 127
[3.13] Gledzer E B 1973 Phys. Dokl. **18** 216
[3.14] Yamada M and Ohkitani K 1987 J Phys. Soc. Jpn. **56** 4210
[3.15] Ohkitani K and Yamada M 1989 Prog. Theor. Phys. **81** 329
[3.16] Yoshizawa A 1994 Phys. Rev. E **49** 4065
[3.17] Kraichnan R H and Montgomery D 1980 Rep. Prog. Phys. **43** 547
[3.18] Kraichnan R H 1967 Phys. Fluids **10** 1417
[3.19] Batchelor G I 1969 Phys. Fluids Suppl. **12** II-233
[3.20] Brachet M E, Meneguzzi M, Politano H, Sulem P L 1988 J. Fluid Mech. **194** 333
[3.21] McWilliams J C 1984 J. Fluid Mech. **146** 21
[3.22] Pedlosky J 1979 *Geophysical Fluid Dynamics* (New York: Springer)
[3.23] Horton W and Hasegawa A 1994 Chaos **4** 227
[3.24] Williams G P 1978 J Atmos. Sci. **35** 1399
[3.25] Yoden S and Yamada M 1993 J. Atmos. Sci. **50** 631
[3.26] Kraichnan R H 1959 J. Fluid Mech. **5** 497
[3.27] Kraichnan R H 1977 J. Fluid Mech. **83** 349
[3.28] Wyld H W 1961 Ann. Phys. (NY) **14** 143
[3.29] Tatsumi T 1980 Adv. in Appl. Mech. **20** 39
[3.30] Kraichnan R H 1964 Phys. Fluids **7** 1723
[3.31] Kraichnan R H 1965 Phys. Fluids **8** 575
[3.32] Nakano T 1972 Ann. Phys. (NY) **73** 326
[3.33] Orszag S A 1970 J. Fluid Mech. **41** 363
[3.34] Lesieur M 1997 *Turbulence in Fluids* (Dordrecht: Kluwer)
[3.35] Cambon C, Jeandel D and Mathieu J 1981 J. Fluid Mech. **104** 247
[3.36] Cambon C and Jacquin L 1989 J. Fluid Mech. **202** 295
[3.37] Kaneda Y 1981 J. Fluid Mech. **107** 131
[3.38] Kaneda Y and Gotoh T 1991 Phys. Fluids A **3** 1924
[3.39] Wilson K G and Kogut J 1974 Phys. Rep. C **12** 75
[3.40] Yakhot V and Orszag S 1986 J. Sci. Comput. **1** 3
[3.41] Dannevik W P, Yakhot V and Orszag S 1987 Phys. Fluids **30** 2021
[3.42] Smith L M and Reynolds W C 1992 Phys. Fluids A **4** 364
[3.43] Nakano T 1992 J. Phys. Soc. Jpn. **61** 3994
[3.44] Eyink G L 1994 Phys. Fluids **6** 3063
[3.45] Rubinstein R and Barton J M 1990 Phys. Fluids A **2** 1472
[3.46] Rubinstein R and Barton J M 1992 Phys. Fluids A **4** 759
[3.47] Edwards S F 1964 J. Fluid Mech. **18** 239
[3.48] Quian J 1983 Phys. Fluids **26** 2098
[3.49] Hunt J C R and Carruthers D J 1990 J. Fluid Mech. **212** 497
[3.50] Speziale C G 1991 Annu. Rev. Fluid. Mech. **23** 107
[3.51] Lumley J L 1978 Adv. in Appl. Mech. **18** 123
[3.52] Shih T -H 1996 in *Turbulence and Transition Modeling* (ed. Halläck M, Henningson D S, Johansson A V and Alfredson P H, Dordrecht: Kluwer)
[3.53] Launder B E, Reece G and Rodi W 1975 J. Fluid Mech. **68** 537

[3.54] Speziale C G, Sarkar S and Gatski T 1991 J. Fluid Mech. **227** 245
[3.55] Yoshizawa A 1984 Phys. Fluids **27** 1377
[3.56] Speziale C G 1987 J. Fluid Mech. **178** 459
[3.57] Nisizima S and Yoshizawa A 1987 AIAA J. **25** 414
[3.58] Bardina J 1983 Ph. D. Dissertation, Stanford University
[3.59] Smagorinsky J S 1963 Mon. Weather Rev. **91** 99
[3.60] Deardorff J W 1970 J. Fluid. Mech. **41** 453
[3.61] Yoshizawa A, Kobayashi K, Kobayashi T and Taniguchi, N 2000 Phys. Fluids **12** 2338
[3.62] Germano M, Piomelli U, Moin P and Cabot W H 1991 Phys. Fluids A **3** 1760
[3.63] Germano M 1992 J. Fluid. Mech. **238** 325
[3.64] Lilly D 1992 Phys. Fluids A **4** 633
[3.65] Speziale C G 1985 J. Fluid Mech. **156** 55
[3.66] Zang Y, Street R L and Koseff J R 1993 Phys. Fluids A **5** 3186
[3.67] Vreman B, Geurts B and Kuerten H 1993 Phys. Fluids A **6** 4057
[3.68] Horiuti K 1997 Phys. Fluids **9** 3443
[3.69] Hamba F 1987 J. Phys. Soc. Jpn. **56** 2721
[3.70] Okamoto M 1994 J. Phys. Soc. Jpn. **63** 2102
[3.71] Nisizima S 1990 Theor. Comput. Fluid Dyn. **2** 61
[3.72] Moffatt, H K 1978 *Magnetic Field Generation in Electrically Conducting Fluids* (Cambridge: Cambridge Unversity)
[3.73] Krause F and Rädler K -H 1980 *Mean-Field Magnetohydrodynamics and Dynamo Theory* (Oxford: Pergamon)
[3.74] Roberts P H 1993 in *Astrophysical Fluid Dynamics* (ed. Zahn J -P and Zinn-Justin J, Amsterdam: Elsevier) p 229
[3.75] Yoshizawa A 1990 Phys. Fluids B **2** 1589
[3.76] Hamba F 1992 Phys. Fluids A **4** 441
[3.77] Pouquet A, Frisch U and Léorat J 1976 J. Fluid Mech. **77** 321
[3.78] Gruizinov A V and Diamond P H 1994 Phys. Rev. Lett. **72** 1651
[3.79] Gruizinov A V and Diamond P H 1996 Phys. Plasmas **3** 1853
[3.80] Gruizinov A V and Diamond P H 1994 Phys. Rev. Lett. **78** 3306
[3.81] Priest E 1982 *Solar Magnetohydrodynamics* (Dordrecht: D. Reidel)
[3.82] Parker E N 1979 *Cosmical Magnetic Fields* (Oxford: Clarendon)
[3.83] Ruzumaikin A A, Shukurov A M and Sokoloff D D 1988 *Magnetic Fields of Galaxies* (Dordrecht: Kluwer)
[3.84] Begelman M C, Blandford R D and Rees M J 1984, Rev. Mod. Phys. **56** 255
[3.85] Melchior P 1986 *The Physics of the Earth's Core* (Oxford: Pergamon)
[3.86] Merrill R T, McElhinny M W and McFaden P L 1996 *The Magnetic Field of the Earth* (San Diego: Academic)
[3.87] Wilson P W 1994 *Solar and Stellar Activity Cycles* (Cambridge: Cambridge University)
[3.88] Schou J, Antia H M, Basu S, et al. 1998 Astrophys. J. **505** 390
[3.89] Yoshizawa A, Yokoi N and Kato H 1999 Phys. Plasmas **6** 4586
[3.90] Olson P, Christensen U and Glatzmaier G A 1999 J. Geophys. Res. **104** 10383
[3.91] Ochi M M, Kageyama A and Sato T 1999 Phys. Plasmas **6** 777
[3.92] Glatzmaier G A, Coe R S, Hongre L and Roberts P H 1999 Nature **401** 885

[3 93] Stix M 1981 Solar Phys. **74** 79
[3.94] Yoshimura H 1984 Astrophys. J. Supplement **52** 36
[3.95] Yoshizawa A. Kato H and Yokoi N 2000 Astrophys. J. **537**. 1039
[3.96] Uchida Y and Shibata K 1985 Publ. Astron. Soc. Jpn. **37** 515
[3.97] Matsumoto R, Uchida Y, Hirose S. et al. 1996 Astrophys. J. **461** 115
[3.98] Yoshizawa A and Yokoi N 1993 Astrophys. J **407** 540
[3.99] Nishino S and Yokoi N 1998 Publ. Astron. Soc. Jpn. **50** 653
[3.100] Ferrari A 1998 Annu. Rev. Astron. Astrophys **36** 539
[3.101] Yoshizawa A. Yokoi N and Kato H 2000 Phys. Plasmas **7** 2646
[3.102] Bodin H A B and Newton A A 1980 Nucl. Fusion **20** 1255
[3.103] Ji H. Prager S C, Almagiri A F. et al. 1996 Phys. Plasmas **3** 1935
[3.104] Gimblett C G and Watkins M L 1975 in *Proceedings of the Seventh European Conference on Controlled Fusion and Plasma Physics* (Lausanne: Ecole de Polytechnique Fédéral de Lausanne) vol 1 p 103
[3.105] Taylor J B 1974 Phys. Rev. Lett. **33** 1139
[3.106] Hamba F 1990 Phys Fluids B **2** 3064
[3.107] Koide Y. Kikuchi M. Mori M, et al. 1994 Phys. Rev. Lett. **72** 3662
[3.108] Levinton M, Zarnstroff M C, Batha S H. et al. 1995 Phys. Rev. Lett. **75** 4417
[3.109] Strait E J. Lao L L. Mauel M E, et al. 1995 Phys. Rev. Lett. **75** 4421
[3.110] Yoshizawa A. Yokoi N, Itoh S -I and Itoh K 1999 Phys. Plasmas **6** 3194
[3.111] Fujita T 1997 J. Plasma Fusion Res. **73** 549

4. Plasma Turbulence

Turbulence in plasmas have several characteristic features. One is that the fluctuation level becomes high through the instabilities which are driven owing to the strong inhomogeneity. The turbulent level and spectrum is strongly influenced by the spatial inhomogeneity and plasma configuration. Inhomogeneities exist for plasma parameters (e.g., density and temperature) as well as for the fields (e.g., magnetic field and radial electric field). These inhomogeneities couple so as to drive and/or suppress instabilities and turbulent fluctuations. In particular, the anisotropy along and perpendicular to the strong magnetic field induces the varieties of nature of possible fluctuations: Fluctuations often have a very long correlation length along the magnetic field line and are quasi-two-dimensional. In addition, mobilities of electrons and ions differ prominently. The inhomogeneities, anisotropy due to the strong magnetic field, and the difference of ion and electron mobilities have strong influences on plasma turbulence as well as on the linear properties of plasma waves. In many cases, instabilities develop into strong turbulence, so that the decorrelation rate caused by the nonlinear interactions is usually of the same order of or much larger than, the damping rate (growth rate) of the linear eigenmode: the theoretical method like the fluid turbulence is required. In some cases, only few modes are excited, and an analysis based on the weak turbulence suffices. (General discussion is given in, e.g., [4.1-4.4].)

In order to illustrate the common features and different characteristics between neutral-fluid and plasma turbulence, various theoretical approaches are illustrated with examples of applications in §4. Emphasis is put on how the theory of turbulence is applied to a strongly inhomogeneous and anisotropic system which is composed of components with different mobility.

One important difference of plasma turbulence from neutral-fluid turbulence is that plasma particles sometimes respond as 'collisionless' particles. In neutral fluids, like liquids or gasses, molecules and atoms collide each other in a short distance. (These collisions are the origin of molecular viscosity that causes real dissipation in the energy dissipation scale ℓ_D.) The mean-free-path of atomic and molecular collisions in neutral fluid is usually much shorter than the characteristic 'wavelength' of fluctuations. In contrast, the Coulombic collisions between ions or electrons, which are the origins of the real dissipation, are rare in high temperature plasmas. The mean-free-path can be longer than the typical wavelength. In such cases, particles can traverse many wave periods along the magnetic field line without losing the memory by collisions. The wave-particle interaction occurs, and the internal freedom of particle distribution can influence the plasma turbulence.

The objective of this review is to illustrate the methods which could be common to neutral-fluid turbulence and to plasma turbulence. Therefore emphasis is made on the

analyses based on fluid (moment) equations.

4.1. Inhomogeneity and Turbulent Intensity

In this subsection, linear waves are described first. A few characteristic examples of linear modes are introduced. Next, the methods of weak turbulence are explained, and conditions for strong turbulence are illustrated. Some cases are discussed on the basis of reduced sets of equations.

4.1.1. Linear stability There are many characteristic waves in magnetized plasmas. In this article, the discussion is limited to those perturbations whose frequencies are lower than the ion-cyclotron frequency.

A Dispersion relation The spatio-temporal patterns to appear (either stationary or propagating) are called *modes*. The property of mode is a characterizing information in the continuous media. If one imposes an external perturbation of the form $\tilde{\mathbf{E}}_{\text{ext}} \exp(i\mathbf{k}\cdot\mathbf{x} - i\omega t)$ (where $\mathbf{k}$, ω can be complex), then the charged elements of plasma are displaced so as to generate a response field $\tilde{\mathbf{E}}_{\text{ind}} \exp(i\mathbf{k}\cdot\mathbf{x} - i\omega t)$. If there is a relation of $(\mathbf{k}, \omega)$ as

$$\omega = \omega(\mathbf{k}), \tag{4.1}$$

for which the ratio $\tilde{E}_{\text{ind}}/\tilde{E}_{\text{ext}}$ becomes very large, then a pattern $\exp[i\mathbf{k}\cdot\mathbf{x} - i\omega(\mathbf{k})t]$ is expected to have a large amplitude and to be selectively observed. Such a pattern is called *mode*, and the relation (4.1) is called *dispersion relation*.

The dispersion relation is determined by the electric conductivity tensor, $\boldsymbol{\sigma}_{s,k\omega}$, where the suffix s stands for the species of plasma elements, i.e., electrons and ions (s = e, i). The perturbed current which is carried by the s-th component, $\tilde{\mathbf{J}}_{s,k\omega}$, is expressed as

$$\tilde{\mathbf{J}}_{s,k\omega} = \boldsymbol{\sigma}_{s,k\omega}\tilde{\mathbf{E}}_{k\omega}. \tag{4.2}$$

The perturbed current is given as $\tilde{\mathbf{J}}_{k\omega} = (\sum_s \boldsymbol{\sigma}_{s,k\omega})\tilde{\mathbf{E}}_{k\omega}$, and the dielectric tensor is introduced (according to the convention) as

$$\boldsymbol{\varepsilon}(\mathbf{k}, \omega) = \mathbf{I} - \frac{ic^2\mu_0}{\omega}\left(\sum_s \boldsymbol{\sigma}_{s,k\omega}\right), \tag{4.3}$$

where $\mathbf{I}$ is the unit tensor, μ_0 is the magnetic permeability of vacuum, and c is the velocity of light. Substituting Eq. (4.3) into the Maxwell equations, i.e., Eqs. (2.14) and (2.15), one has the relation

$$\left[\boldsymbol{\varepsilon}(\mathbf{k}, \omega) - \left(\frac{kc}{\omega}\right)^2\left(\mathbf{I} - \frac{\mathbf{kk}}{k^2}\right)\right]\mathbf{E}_{k\omega} = \frac{c\mu_0}{i\omega}\mathbf{j}_{\text{ext};k\omega}, \tag{4.4}$$

where $\mathbf{j}_{\mathrm{ext};k\omega}$ is an externally-imposed current perturbation of the Fourier component $(\mathbf{k},\omega)$. Equation (4.4) predicts that the perturbed field $\mathbf{E}_{k\omega}$ can take a finite amplitude even without the external perturbation, if the condition

$$\det\left[\boldsymbol{\varepsilon}(\mathbf{k},\omega)-\left(\frac{kc}{\omega}\right)^2\left(\mathbf{I}-\frac{\mathbf{kk}}{k^2}\right)\right]=0 \tag{4.5}$$

is satisfied. The dispersion relation (4.1) is given as a solution of Eq. (4.5).

Plasma dielectric tensor is discussed in text books [4.3, 4.5-4.7]. The study of the linear instability in plasmas is reduced to the calculation of the conductivity tensor and the solution of the dispersion relation. Varieties of low-frequency instabilities are reviewed in the literature [4.1, 4.2, 4.8-4.18].

B Vlasov equation and linear dielectric tensor The perturbed distribution function is calculated within a framework of linear response theory. The distribution function is written as the sum of the average and the fluctuating parts as

$$f_s(\mathbf{x},\mathbf{v},t)=\bar{f}_s(\mathbf{x},\mathbf{v},t)+\tilde{f}_s(\mathbf{x},\mathbf{v},t), \tag{4.6}$$

where the time dependence is slow for $\bar{f}_s$ and fast for $\tilde{f}_s$. The fluctuating part is given by a path integral of the Vlasov equation [Eq. (2.27) with $C=0$] as

$$\tilde{f}_s(\mathbf{x},\mathbf{v},t)=\frac{e_s}{m_s}\int_{-\infty}^{t}dt'\left[\tilde{\mathbf{E}}(\mathbf{x}',t')+\mathbf{v}'\times\tilde{\mathbf{B}}(\mathbf{x}',t')\right]\frac{\partial}{\partial\mathbf{v}'}\bar{f}_s(\mathbf{x}',\mathbf{v}',t), \tag{4.7}$$

where $\mathbf{x}'(t')$ and $\mathbf{v}'(t')$ are the particle position and velocity along the unperturbed orbit of particles with the boundary condition

$$\mathbf{x}=\mathbf{x}'(t)\quad\text{and}\quad\mathbf{v}=\mathbf{v}'(t)\quad\text{at}\quad t'=t. \tag{4.8}$$

The $(\mathbf{k},\omega)$-Fourier component of the perturbed distribution function, $\tilde{f}_{s,k\omega}(\mathbf{v})\exp(i\mathbf{k}\cdot\mathbf{x}-i\omega t)$, is given from Eq. (4.7) as

$$\begin{aligned}\tilde{f}_{s,k\omega}(\mathbf{v})=\frac{e_s}{m_s}\int_{-\infty}^{t}dt'\exp\left\{i\mathbf{k}\cdot(\mathbf{x}'-\mathbf{x})-i\omega(t'-t)\right\}\\ \times\frac{\partial}{\partial\mathbf{v}'}\bar{f}_s(\mathbf{x}',\mathbf{v}')\cdot\left(\mathbf{I}+\frac{\mathbf{v}'}{\omega}\times\mathbf{k}\times\right)\tilde{\mathbf{E}}_{k\omega}.\end{aligned} \tag{4.9}$$

The perturbed current $\tilde{\mathbf{J}}_{s.k\omega}$ is calculated as

$$\tilde{\mathbf{J}}_{s,k\omega}=e_s\int\mathbf{v}\tilde{f}_{s,k\omega}(\mathbf{v})d\mathbf{v}. \tag{4.10}$$

Once the distribution function of the average part $\bar{f}_s(\mathbf{x}',\mathbf{v}')$ is given, then the dispersion relation is obtained from a direct manipulation.

Before illustrating some of typical examples, we briefly discuss the relation between the analyses based on fluid equations (like the MHD equations) and those on kinetic equations.

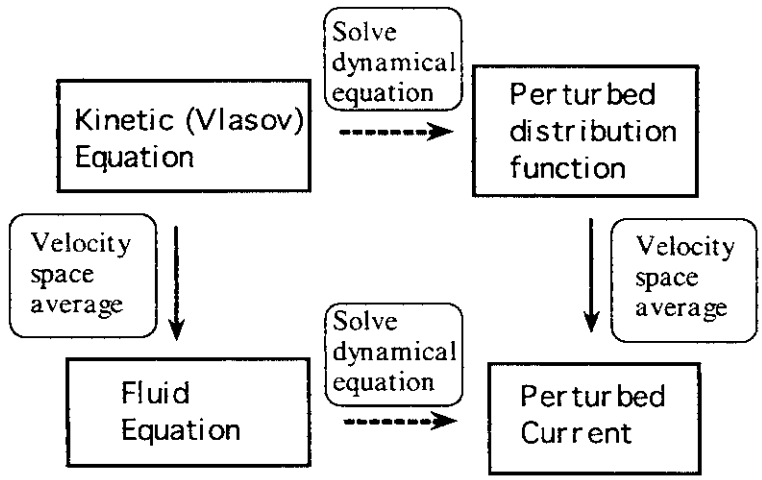

Figure 4.1. Comparison between fluid approach and kinetic approach. Solutions of dynamical equations in the presence of perturbing electromagnetic field and the velocity-space average are shown by the dashed arrow and solid arrow, respectively. Solution of dynamical equation and velocity space average are not necessarily commutable.

Figure 4.1 illustrates the difference between fluid and kinetic approaches. Dynamical equations can be employed as fluid equations as in §3. In the fluid approach, the kinetic equation (the Boltzmann equation or the Vlasov equation or others) is first integrated over the velocity space, and the higher-order moments are modelled. The velocity-space integral gives equations of moments (e.g., mass density or number density, velocity, pressure, etc.). Then the fluid equations are solved in the presence of the symmetry-breaking perturbations. The perturbed current is calculated, and dispersion relation is obtained. In the kinetic approach, the dynamical equation is solved first, and the perturbed distribution is obtained. Then the velocity-space integral is performed to yield the perturbed current.

The process of 'solution of dynamical equation' and 'velocity-space average' is not necessarily commutable. The propagator in Eq. (4.9) contains a term like $(k_\parallel v_\parallel - \omega)^{-1}$. The weighted average of it is not recovered, if the velocity-space average is taken before solving the dynamical equation. The contribution for the average of $(k_\parallel v_\parallel - \omega)^{-1}$ comes from the particles, the velocity of which satisfies the relation $k_\parallel v_\parallel \cong \omega$, i.e., the resonant particles. The fluid approach ignores the information that the resonant particles have. The Braginskii equations, Eqs. (2.12a)-(2.12d), which use the lowest-order closure for the flux–gradient relation, are derived in a collisional limit. In order to extend an applicability range of the fluid equations to less collisional cases, efforts have been made by employing higher-order closure models. See, e.g., discussions in [4.19-4.23]. Such approaches are called *gyro-fluid models*. As long as the linear response of the plasma is

the issue, the kinetic approach is a more precise one. Nevertheless, the fluid approach is relevant and useful on many occasions to study turbulent plasmas. A basis of the relevance is discussed for the study of strong turbulence in the later subsections.

C Examples of modes We consider a strongly magnetized plasma slab, and show typical examples of modes in the presence of inhomogeneity. We take the z-axis in the direction of the main magnetic field. Plasma parameters (number density, temperature) are inhomogeneous in the x-direction.

C1 Ion sound wave, drift wave, and convective cell Sound wave in the plasma,

$$\omega^2 = c_{\rm s}^2 k_\parallel^2, \tag{4.11}$$

with the ion sound speed $c_{\rm s}^2 = (Z_{\rm i}T_{\rm e0} + \gamma T_{\rm i0})m_{\rm i}^{-1}$, where γ is a specific heat ratio of ions, is modified by a density gradient. The drift wave appears with the dispersion relation

$$\omega^2 - \omega\omega_* - k_\parallel^2 c_{\rm s}^2 = 0, \tag{4.12a}$$

where

$$\omega_* = -\frac{k_y T_{\rm e}}{eB}\frac{d\bar{n}/dx}{\bar{n}} \tag{4.12b}$$

is the drift frequency. The drift mode, $\omega \cong \omega_*$, exists under the condition of $|k_\parallel v_{\rm thi}| \ll \omega \ll |k_\parallel v_{\rm the}|$. The dispersion relation is shown in Fig. 4.2(a).

From Fig. 4.2(a), one sees that there is other low-frequency branch satisfying

$$\omega \cong -\frac{k_\parallel^2 c_{\rm s}^2}{\omega_*}. \tag{4.13}$$

In the long-wavelength limit, the real frequency in Eq. (4.13) vanishes, i.e., this mode is not propagating. This branch of perturbation is called the 'convective cell' [4.2, 4.24, 4.25]. In the linear theory, the convective cell is a damped mode with damping rate of $\mu_\perp k_\perp^2$, where $\mu_\perp$ is the viscosity for motions in the perpendicular direction. A convective cell for an electromagnetic perturbation is discussed in [4.26].

C2 Shear Alfvén wave and drift Alfvén mode Shear Alfvén wave $\omega^2 = k_\parallel^2 v_{\rm A}^2$, with the Alfvén velocity $v_{\rm A}^2 = \bar{B}^2/m_{\rm i}\bar{n}_{\rm i}\mu_0$, is modified by a density gradient. The drift Alfvén mode is generated. Its dispersion relation is

$$\omega^2 - \omega\omega_* - k_\parallel^2 c_{\rm s}^2 = \frac{\omega^2(\omega - \omega_*)\left(\omega + |\omega_{*\rm i}|\right)}{k_\parallel^2 v_{\rm A}^2}, \tag{4.14}$$

where $\omega_{*\rm i} = -(T_{\rm i}/T_{\rm e})\omega_*$. The dispersion relation is illustrated in Fig. 4.2(b).

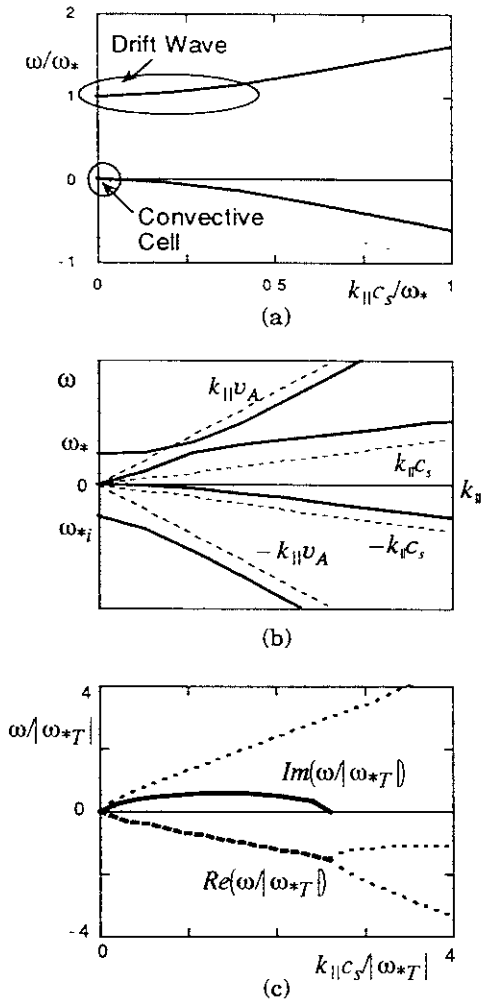

Figure 4.2. Dispersion relations for drift wave and convective cell (a), drift Alfvén waves together with drift wave (b) and ion temperature gradient mode (c).

C3 Interchange mode When both the pressure and magnetic-field strength are inhomogeneous in the x-direction, the drift Alfvén mode is modified to yield the reactive instability. The dispersion relation is given as

$$-\omega^2 = \gamma_0^2 \equiv \frac{c_s^2}{L_p L_M}, \tag{4.15}$$

where $1/L_p = |-\nabla\bar{p}/\bar{p}|$ and $1/L_M = |-\nabla\bar{B}/\bar{B}|$. The combination of the inhomogeneities of the plasma pressure and magnetic pressure causes an instability [2.12, 4.8]. This instability is an MHD analogue to the Rayleigh–Bénard instability. In toroidal geometry. its counterpart is the ballooning instability [4.27-4.30].

C4 Ion temperature gradient mode The influence of the temperature gradient of ions is coupled to the parallel ion motion. The ion-sound term $k_\parallel^2 v_{\rm thi}^2/\omega^2$ is modified in the ion response as [4.8]

$$\frac{\tilde{n}_{\rm i}}{\bar{n}} \cong \frac{k_\parallel^2 c_{\rm s}^2}{\omega^2}\left(1 - \frac{\omega_{*T_{\rm i}}}{\omega}\right)\frac{e\tilde{\phi}}{T_{\rm e}}, \tag{4.16}$$

where

$$\omega_{*T_{\rm i}} = k_y (dT_{\rm i}/dx)/(eB) \tag{4.17}$$

is the ion temperature gradient drift frequency. Electrons have the Boltzmann response, $\tilde{n}_{\rm e}/\bar{n} \cong e\tilde{\phi}/T_{\rm e}$. The dispersion relation of the ion sound wave is modified as

$$1 = \frac{k_\parallel^2 c_{\rm s}^2}{\omega^2}\left(1 - \frac{\omega_{*T_{\rm i}}}{\omega}\right). \tag{4.18}$$

The motion of ions drive instability in the regime of long parallel wavelength as is shown in Fig. 4.2(c). This instability is called the ion temperature gradient (ITG) mode [4.8].

C5 Dissipative drift mode A drift wave becomes unstable if dissipation exists. The electron response to the electrostatic perturbation is close to the Boltzmann distribution, i.e., $\tilde{n}_{\rm e}/\bar{n}_{\rm e} \cong e\tilde{\phi}/T_{\rm e}$, but is not completely so. If there is a small but finite phase difference in the electron response as

$$\frac{\tilde{n}_{\rm e}}{\bar{n}_{\rm e}} = (1 - i\delta_{\rm d})\frac{e\tilde{\phi}}{T_{\rm e}}, \tag{4.19}$$

the drift wave becomes unstable as

$$\omega = \omega_* (1 + i\delta_{\rm d}). \tag{4.20}$$

4.1.2. Weak turbulence theory

A Ansatz of weak turbulence A simple approach in the nonlinear theory is to assume that the nonlinearity is weak so that the excited fluctuations are composed of the linear eigenmodes, e.g.,

$$\left\langle \tilde{E}_y(\mathbf{k},\omega)\tilde{E}_y(\mathbf{k}',\omega')\right\rangle = 2\pi\delta_{\mathbf{k},-\mathbf{k}'}\delta(\omega+\omega')\delta[\omega - \omega(\mathbf{k})]I_{\mathbf{k}}, \tag{4.21}$$

where ω satisfies the dispersion relation $\omega = \omega(\mathbf{k})$. The spectral function (auto-correlation function) is non-zero on the hyper-surface $\omega = \omega(\mathbf{k})$ in the four-dimensional space $(\mathbf{k},\omega)$. In other words, the nonlinear terms in the dynamical equation of the wave mode [e.g., the $(\partial/\partial x_j)(\tilde{v}_i\tilde{v}_j - R_{ij})$ term in Eq. (3.6)] are assumed to be much smaller than the linear terms. Nonlinear interactions are often truncated at the lowest-order

correction. In the dynamical equation for the $[\mathbf{k}, \omega(\mathbf{k})]$ mode, nonlinear interactions with the $[\mathbf{k}', \omega(\mathbf{k}')]$ and $[\mathbf{k}'', \omega(\mathbf{k}'')]$ modes are retained only if the relation

$$\mathbf{k} = \mathbf{k}' + \mathbf{k}'' \quad \text{and} \quad \omega(\mathbf{k}) = \omega(\mathbf{k}') + \omega(\mathbf{k}'') \tag{4.22}$$

holds. In calculating the nonlinear terms of $[\mathbf{k}, \omega(\mathbf{k})]$ modes, linear eigenmodes are substituted for the $[\mathbf{k}', \omega(\mathbf{k}')]$ and $[\mathbf{k}'', \omega(\mathbf{k}'')]$ modes. This belongs to the methods of the truncation of nonlinearlities.

B Wave kinetic equation The wave kinetic equation is derived by the ansatz of weak plasma turbulence. It takes the form [4.1, 4.31, 4.32]

$$\frac{1}{2}\left[\frac{\partial}{\partial\omega}\Re\varepsilon_1(\mathbf{k},\omega)\right]\frac{d}{dt}I_{\mathbf{k}} = -\Im\varepsilon_1(\mathbf{k},\omega)I_{\mathbf{k}} + \sum_{\mathbf{k}'} A_{\mathbf{k}\mathbf{k}'} I_{\mathbf{k}'} I_{\mathbf{k}} + \sum_{\substack{\mathbf{k}'+\mathbf{k}''=\mathbf{k} \\ \omega'+\omega''=\omega}} B_{\mathbf{k}'\mathbf{k}''} I_{\mathbf{k}'\mathbf{k}''}, \tag{4.23}$$

where $\varepsilon_1(\mathbf{k}, \omega)$ is the linear dielectric constant, and the linear growth rate is given as

$$\gamma_{\mathbf{k}} = -\Im\varepsilon_1(\mathbf{k},\omega)[(\partial/\partial\omega)\Re\varepsilon_1(\mathbf{k},\omega)]^{-1}. \tag{4.24}$$

The relation $\omega(\mathbf{k}) = \omega(\mathbf{k}') + \omega(\mathbf{k}'')$ is abbreviated as $\omega = \omega' + \omega''$.

Equation (4.23), which is derived based on a strong assumption of the weak turbulence, has been used to study the statistical property of plasma turbulence. If one calculates the stationary state, $dI_{\mathbf{k}}/dt = 0$, an order of magnitude estimate of the solution is

$$I_{\mathbf{k}} \sim O\left[A^{-1}_{\mathbf{k}\mathbf{k}'}\Im\varepsilon_1(\mathbf{k}',\omega')\right]. \tag{4.25}$$

The ansatz of weak turbulence means that the nonlinear interactions are weak and the linear dispersion relation is not modified. That is, the condition

$$\left|\sum_{\mathbf{k}'} A_{\mathbf{k}\mathbf{k}'} I_{\mathbf{k}'}\right| \ll |\omega(\mathbf{k})| \tag{4.26}$$

must be satisfied. Therefore, one of the necessary conditions for the applicability of the weak turbulence theory is

$$\gamma_{\mathbf{k}} \ll |\omega(\mathbf{k})|. \tag{4.27}$$

C Integral, Lyapunov function, and thermodynamics Although the applicable region of the weak turbulence theory might be narrow, it has been successfully applied to such problems as one-dimensional turbulence [4.33] or excitation of toroidal Alfvén-wave eigenmodes (TAE modes) [4.34]. It also gives some perspective on the analysis of plasma turbulence [4.31, 4.35, 4.36].

The second term in the right-hand side of Eq. (4.23) is linear in $I_{\mathbf{k}}$, and acts as the change of growth rate for the mode (like an eddy-viscosity term). The relation of anti-symmetry holds as

$$A_{\mathbf{k}\mathbf{k}'} = -A_{\mathbf{k}'\mathbf{k}}, \tag{4.28}$$

reflecting detailed balance in, e.g., the induced scattering process. The induced wave scattering is the process with $\omega_{\mathbf{k}} - \omega_{\mathbf{k}'} = (\mathbf{k} - \mathbf{k}') \cdot \mathbf{v}$ where $\mathbf{v}$ is a particle velocity. Details are explained in [4.31]. The third term, $B_{\mathbf{k}'\mathbf{k}''} I_{\mathbf{k}'} I_{\mathbf{k}''}$, is considered to be the 'noise-source term' when many linear modes are independently excited, as is explained in [4.32]. An integral and Lyapunov function could be constructed within the framework of a quasi-linear theory [4.35, 4.36].

If one first neglects the $B_{\mathbf{k}'\mathbf{k}''} I_{\mathbf{k}'} I_{\mathbf{k}''}$ term (noise source), Eq. (4.23) has the integral. From the anti-symmetry of the coefficient $A_{\mathbf{k}\mathbf{k}'}$, one can derive an integral of motion

$$\frac{d}{dt}\hat{\mathcal{F}} = 0, \tag{4.29}$$

where $\hat{\mathcal{F}}$ is defined as

$$\hat{\mathcal{F}} = \frac{1}{2}\sum_{\mathbf{k}} \left[\frac{\partial}{\partial\omega}\Re\varepsilon_1(\mathbf{k},\omega)\right]\left(I_{\mathbf{k}} - \hat{I}_{0,\mathbf{k}} \ln I_{\mathbf{k}}\right), \tag{4.30}$$

and $\hat{I}_{0,\mathbf{k}}$ is the solution of the stationary equation $\sum_{\mathbf{k}'} A_{\mathbf{k}\mathbf{k}'} \hat{I}_{0,\mathbf{k}'} = \Im\varepsilon_1(\mathbf{k},\omega)$ without noise. The trajectory of $\{I_{\mathbf{k}}\}$ in its phase space is confined on the hyper-surface $\hat{\mathcal{F}} = \text{const}$.

The 'noise-source term' $B_{\mathbf{k}'\mathbf{k}''} I_{\mathbf{k}'} I_{\mathbf{k}''}$ modifies the trajectory of $\{I_{\mathbf{k}}\}$ in the phase space. Writing the source term symbolically, $\sum_{\mathbf{k}'} B_{\mathbf{k}'\mathbf{k}''} I_{\mathbf{k}'} I_{\mathbf{k}''} \to \varepsilon_{\text{noise},\mathbf{k}}$, one defines

$$\mathcal{F} = \frac{1}{2}\sum_{\mathbf{k}} \left[\frac{\partial}{\partial\omega}\Re\varepsilon_1(\mathbf{k},\omega)\right]\left(I_{\mathbf{k}} - I_{0,\mathbf{k}} \ln I_{\mathbf{k}}\right) \tag{4.31}$$

with the stationary solution $I_{0,\mathbf{k}}$ in the presence of the noise-source term as

$$-\Im\varepsilon_1(\mathbf{k},\omega) I_{0,\mathbf{k}} + \sum_{\mathbf{k}'} A_{\mathbf{k}\mathbf{k}'} I_{0,\mathbf{k}'} I_{0,\mathbf{k}} + \varepsilon_{\text{noise},\mathbf{k}} = 0. \tag{4.32}$$

For this $\mathcal{F}$ one has

$$\frac{d}{dt}\mathcal{F} = -\sum_{\mathbf{k}} \varepsilon_{\text{noise},\mathbf{k}} \frac{(I_{\mathbf{k}} - I_{0,\mathbf{k}})^2}{I_{\mathbf{k}} I_{0,\mathbf{k}}} \leq 0 \tag{4.33}$$

for positive or zero noise sources. Now $\mathcal{F}$ is the Lyapunov functional of the dynamics of $\{I_{\mathbf{k}}\}$, and is minimum if $I_{\mathbf{k}} = I_{0,\mathbf{k}}$ holds for all $\mathbf{k}$. The noise-source term $\varepsilon_{\text{noise},\mathbf{k}}$ acts as a friction, and all trajectories finally approach, as an average,

$$\{I_{\mathbf{k}}\} \to \left\{I_{0,\mathbf{k}}\right\}. \tag{4.34}$$

The thermodynamical relationship is now explained. The number density of the mode, $N_{\mathbf{k}}$, is introduced as

$$N_{\mathbf{k}} = (\partial/\partial\omega)\Re\varepsilon_1(\mathbf{k},\omega)I_{\mathbf{k}}/8\pi. \tag{4.35}$$

By adding a constant value $-\sum_{\mathbf{k}}\omega_{\mathbf{k}}N_{0.\mathbf{k}}$ to Eq. (4.31), $\mathcal{F}$ is transformed to $\mathcal{F}_{\mathrm{H}}$ as

$$\mathcal{F}_H = \mathcal{F} - \sum_{\mathbf{k}}\omega_{\mathbf{k}}N_{0.\mathbf{k}} = \sum_{\mathbf{k}}\omega_{\mathbf{k}}\left[N_{\mathbf{k}} - N_{0.\mathbf{k}}\left(\ln N_{\mathbf{k}} + 1\right)\right]. \tag{4.36}$$

The internal energy of the wave is $\mathcal{E} = \sum_{\mathbf{k}}\omega_{\mathbf{k}}N_{\mathbf{k}}$, and the wave entropy is defined as

$$S_{\mathrm{wave}} \sim k_B\sum_{\mathbf{k}}\left(\ln N_{\mathbf{k}} + 1\right) \tag{4.37}$$

in the large-$N_{\mathbf{k}}$ limit. If $\omega_{\mathbf{k}}N_{0.\mathbf{k}}$ is common to all $\mathbf{k}$ (i.e., equipartition holds), it is written as a 'temperature',

$$\omega_{\mathbf{k}}N_{0.\mathbf{k}} = k_{\mathrm{B}}T_{\mathrm{wave}} \quad (\text{for all } \mathbf{k}) \tag{4.38}$$

and $\mathcal{F}_{\mathrm{H}}$ is written as

$$\mathcal{F}_{\mathrm{H}} = \mathcal{E} - k_{\mathrm{B}}T_{\mathrm{wave}}S_{\mathrm{wave}}. \tag{4.39}$$

In this case, the quantity $\mathcal{F}_{\mathrm{H}}$ corresponds to the Helmholtz' free energy [4.36]. Equation (4.34) is considered as the approach to the minimum of the Helmholtz' free energy of the fluctuation state, if equipartition (4.38) holds. In realistic cases, however, the stationary solution Eq. (4.32) does not satisfy the equipartition law [Eq. (4.38)].

D Transport matrix and symmetry The evolution of averaged distribution function is caused by the back-interactions of fluctuations. The quasilinear diffusion of the distribution function is induced. The cross-correlation functions are related to the flux of global quantities, which are expressed in terms of the gradient and fluctuation spectrum $\{I_{\mathbf{k}}\}$. The transport matrix of fluxes and gradients is symmetric in the framework of quasilinear theory [4.37-4.41]. Details are explained in Appendix A.

4.1.3. Regime of strong plasma turbulence In the presence of fluctuating fields, plasma elements (particles) are subject to $E \times B$ motion. The Doppler shift of mode $\mathbf{k}$ due to a fluctuating velocity $\tilde{\mathbf{v}}_{E\times B}$, $\omega_{E\times B} = \tilde{\mathbf{v}}_{E\times B}\cdot\mathbf{k}_{\perp}$, can substantially influence the mode characteristics if the condition

$$\omega_{E\times B} \cong |\boldsymbol{\omega}_{\mathbf{k}}| \tag{4.40}$$

holds ($\mathbf{k}_{\perp}$: wave vector perpendicular to a main magnetic field). When the fluctuations are quasi-electrostatic, (which is a relevant assumption for the low-β plasmas, β being the ratio of the plasma pressure to the magnetic pressure), the perturbed velocity is

given in terms of the potential perturbation as $\tilde{\mathbf{v}}_{E\times B} = -i\mathbf{k}'_\perp\tilde{\phi}/B$ ($\mathbf{k}'_\perp$ and $\tilde{\phi}$ being the wave vector and potential for the background fluctuations, respectively) and the condition (4.40) is rewritten as

$$\frac{e\tilde{\phi}}{T} \sim \frac{1}{kL_n} \tag{4.41}$$

for the range of the drift frequency. Condition (4.41) is easily satisfied for the foregoing fluctuations listed in §4.1.1 as is discussed later. In this section, 'strong turbulence' is used for the case when Eq. (4.40) is satisfied.

It is noted that strong plasma turbulence occurs even if the 'Reynolds number' remains of order unity. The Reynolds number Re might be evaluated as the ratio between the convective nonlinear term $(\mathbf{V}\cdot\nabla)\mathbf{V}$ and the viscous damping term. The molecular viscosity μ_c is of the order $\mu_c \sim \nu_{ii}\rho_i^2$, where ν_{ii} is the ion-ion collision frequency and ρ_i is the ion gyroradius. Note that μ_c could be enhanced by an order of magnitude in toroidal plasmas [4.42-4.44]. Such details are, however, not the subject of this heuristic argument. For turbulence which is pumped by the instabilities in the rage of $k\rho_i \sim 1$, one has an estimate for Re as

$$Re = \frac{v_{E\times B}k}{\nu_{ii}\rho_i^2k^2} \cong \frac{\omega_*}{\nu_{ii}}, \tag{4.42}$$

where the fluctuating $E\times B$ velocity was estimated for the fluctuation level of Eq. (4.41) as $k\tilde{\phi}/B \sim T/eL_nB$. The value of Re can remain of the order of unity (e.g., example of resistive drift-wave turbulence is given in [4.45]). The strong plasma turbulence, characterized by the condition (4.40), develops without requiring the large Reynolds number. For fluctuations on the global scale length, $k \sim 1/L_n$, one has

$$Re \cong \frac{\omega_*}{\nu_{ii}}\frac{L_n^2}{\rho_i^2} \tag{4.43}$$

for the level of Eq. (4.41). For such a case, Re becomes greater than unity.

In the regime of the strong turbulence, nonlinear interactions of various gradients become noticeable in the formula of a flux. The transport matrix is no longer linear in the wave spectrum. The symmetry of the transport matrix does not necessarily hold.

4.1.4. Reduced sets of equations and conservation property In order to analyze the nonlinear interactions in strong plasma turbulence, various reduced sets of equations have been used. Representative ones are listed in §2.2.2. Some basic properties of these reduced sets of equations are explained below.

A Hasegawa–Mima equation The simplest model equation that describes electrostatic turbulence in inhomogeneous plasmas, i.e., the Hasegawa–Mima equation (or the

Hasegawa–Mima–Charney equation), is derived for two-dimensional $E \times B$ motion as Eq. (2.23), which is given in dimensionless form as

$$\frac{\partial}{\partial t}\nabla_\perp^2\phi + \left[\phi, \nabla_\perp^2\phi\right] - \frac{\partial}{\partial t}\phi - \frac{\partial}{\partial y}\phi = 0. \tag{4.44}$$

Here, time, length and potential are normalized using $\rho_s/V_d = L_n/c_s$, the ion gyroradius at the electron temperature, ρ_s, and T_e/e respectively. Plasma properties are included in a form of the polarization-drift effect due to the finite ion-inertia (the first term), the electron adiabatic response (the third term), and the density inhomogeneity (the fourth term). The adiabatic limit of response for dissipationless plasmas, $\tilde{n}/\bar{n} = e\tilde{\phi}/T_e$, is studied.

When the Debye length becomes longer, an equation similar to Eq. (4.44) can be derived for fluctuations in the range of the Debye length. In this case, the length is regulated by the Debye length, not by the ion gyroradius [4.46].

The HM equation conserves the 'energy', 'enstrophy', and 'mass' of the vortices which are defined as

$$\mathcal{E} = (1/2)\int d\mathbf{x}\left[\phi^2 + (\nabla\phi)^2\right], \tag{4.45a}$$

$$\mathcal{U} = (1/2)\int d\mathbf{x}\left[(\nabla_\perp\phi)^2 + (\Delta_\perp\phi)^2\right], \tag{4.45b}$$

$$\mathcal{M} = \int d\mathbf{x}\left(\phi - \nabla_\perp^2\phi\right). \tag{4.45c}$$

Note that the integral $\int d\mathbf{x} f[f, g]$ vanishes for the periodic boundary conditions. One can deduce that the inverse cascade is possible from Eq. (4.44) [4.13, 4.47]. This is one of the most important contributions of the HM equation for the understanding of plasma turbulence. That is, micro-scale fluctuations can generate a structure which has much longer scale length in comparison with the fluctuations. The structure with longer scales can also be induced by turbulence. Effects of turbulence on the formation and destruction of global structures are recognized clearly in the study of the HM equation. This aspect of turbulence is discussed in §4.3.3. The thermodynamical equilibrium limit is discussed in the Appendix B.

The HM equation is an analogue to the vorticity equation in a neutral fluid, which can be applied to the case of atmospheric dynamics on a rotating planet. The atmospheric flow on the horizontal plane is governed by the equation

$$\frac{\partial}{\partial t}\mathbf{V} = -g\nabla h + R_C\mathbf{V} \times \hat{\mathbf{z}}, \tag{4.46}$$

where g is the gravitational acceleration, h is the atmospheric depth, and $R_C\mathbf{V} \times \hat{\mathbf{z}}$ is the Coriolis force. The gradient (in the latitudinal direction) of the vertical component of the Coriolis force plays the role of the density gradient in Eq. (4.44). The Rossby wave

in a neutral fluid corresponds to the drift wave (see, e.g., [4.47]). The inverse cascade has been discussed in fluid dynamics; See, e.g., the discussion in [4.24] and related references therein [4.48, 4.49].

B Three-field equations Plasma turbulence is often investigated in more general circumstances, i.e., for the case of electromagnetic turbulence, or the case subject to multiple gradients (those of temperature, density, and magnetic field, etc.). Fluctuations like the drift wave, ion temperature gradient mode, resistive MHD mode, interchange mode, ballooning mode, current-diffusive interchange mode, etc., are studied by three- or four-fields models.

As an example, a set of three-field equations is given as [1.35]

$$\frac{\partial}{\partial t}\nabla_\perp^2\tilde{\phi} + \left[\tilde{\phi}, \nabla_\perp^2\tilde{\phi}\right] = \nabla_\parallel \tilde{J}_\parallel + (\mathbf{b}\times\boldsymbol{\kappa})\cdot\nabla\tilde{p} + \mu_c\nabla_\perp^4\tilde{\phi}. \tag{4.47a}$$

$$\frac{\partial}{\partial t}\tilde{A}_\parallel + \frac{c^2}{\omega_p^2 a^2}\left(\frac{\partial}{\partial t}\tilde{J}_\parallel + \left[\tilde{\phi}, \tilde{J}_\parallel\right]\right) = -\nabla_\parallel\tilde{\phi} - \eta_\parallel\tilde{J}_\parallel + \lambda_c\nabla_\perp^2\tilde{J}_\parallel, \tag{4.47b}$$

$$\frac{\partial}{\partial t}\tilde{p} + \left[\tilde{\phi}, \tilde{p}\right] + \left[\tilde{\phi}, \bar{p}\right] = \chi_c\nabla_\perp^2\tilde{p}, \tag{4.47c}$$

where $\boldsymbol{\kappa}$ denotes the gradient of magnetic-field strength, and ω_p is the plasma frequency. The suffix c in the transport coefficients stands for the collisional dissipation process. In this set of equations, length, time, static potential, and vector potential are normalized using the plasma radius a, the poloidal Alfvén transit time $\tau_{Ap} = a/v_{Ap} = R/v_A$, Bv_Aa^2/R, and Ba^2/R, respectively.

A conservation relation is derived as

$$\begin{aligned}\frac{\partial}{\partial t}\frac{1}{2}&\left[\int dV\left|\nabla_\perp\tilde{\phi}\right|^2 + \left(1+\frac{c^2}{\omega_p^2a^2}\right)\int dV\left|\tilde{J}_\parallel\right|^2 + \int dV\tilde{p}^2\right] \\ &= \mu_c\int dV\left(\kappa_x + \frac{d\bar{p}}{dx}\right)\int dV\left(\tilde{p}^*\nabla_y\tilde{\phi}\right) - \mu_c\int dV\left|\nabla_\perp^2\tilde{\phi}\right|^2 \\ &- \eta_\parallel\int dV\left|\hat{J}_\parallel\right|^2 - \lambda_c\int dV\left|\nabla_\perp\tilde{J}_\parallel\right|^2 - \chi_c\int dV|\nabla_\perp\tilde{p}|^2.\end{aligned} \tag{4.48}$$

In addition to the dissipation by collisional transport coefficients (viscosity, resistivity, current diffusivity, thermal conductivity), the fluctuation energy is induced by the energy release associated with the global turbulent-driven flux $q_x = -\tilde{p}^*\nabla_y\tilde{\phi}$. In a stationary state,

$$\begin{aligned}\left(\kappa_x + \frac{d\bar{p}}{dx}\right)\int dV q_x = \mu_c\int dV\left|\nabla_\perp^2\tilde{\phi}\right|^2 + \eta_\parallel\int dV\left|\hat{J}_\parallel\right|^2 \\ + \lambda_c\int dV\left|\nabla_\perp\tilde{J}_\parallel\right|^2 + \chi_c\int dV|\nabla_\perp\tilde{p}|^2\end{aligned} \tag{4.49}$$

holds. The right-hand side is semi-positive definite. Non-trivial solutions, i.e., finite amplitudes for fluctuations ($|\tilde{o}| \neq 0$, etc.), are induced and sustained by the turbulent-driven flux in the direction of the global inhomogeneity.

C Yagi–Horton equations In the reduced set of equations with a small number of fields (e.g., the HM equation, the HW equation, and the three-field models, etc.), 'energy' includes the quadratic terms of perturbations. The quadratic term of perturbed internal energy also appears. For instance, the integrand of 'energy' in the HM equation, Eq. (4.45a), is essentially $\tilde{n}^2 + \tilde{\mathbf{v}}_{E\times B}^2$ (with proper normalization). The perturbation of internal energy contributes to $\mathcal{E}$ in a quadratic form. By this fact, conservation relations for some reduced sets of equations are not directly comparable with the conservation of energy. Such a difficulty is resolved in a reduced set of equations with a large number of fields [2.9, 2.10]. In the case of the YH equations, the energy conservation relation is given as

$$\frac{\partial}{\partial t}\left(\left\langle\frac{3}{2}p_{\mathrm{e}}\right\rangle + \left\langle\frac{3}{2}p_{\mathrm{i}}\right\rangle + \left\langle\frac{nm_{\mathrm{i}}}{2}\frac{|\nabla_\perp\Phi|^2}{B^2}\right\rangle + \left\langle\frac{nm_{\mathrm{i}}}{2}v_\parallel^2\right\rangle + \left\langle\frac{1}{2}\left|\nabla_\perp A_\parallel\right|^2\right\rangle\right) = 0, \tag{4.50}$$

in the invicid limit (no collisional dissipation), where $\langle\ \rangle$ indicates the average within a volume, and the flow across the surface is assumed to vanish. The perturbation of internal energy appears in a linear form, as in the energy conservation relation. The conservation property of the gyro-averaged equations is discussed in [4.50].

4.2. Inhomogeneous Strong Turbulence

4.2.1. Concepts to describe turbulent plasmas Although there are many common features between the neutral-fluid turbulence and plasma turbulence, there are specific aspects in the turbulence of magnetized plasmas. Concepts that characterize turbulence in inhomogeneous plasmas are briefly surveyed below.

A Gradients and magnetic geometry Magnetized plasmas are associated with the strong anisotropy between the motion along the magnetic field and the one perpendicular to the magnetic field. Global plasma parameters, say the temperature $\bar{T}$, tend to be constant along the filed line. Plasma confinement scheme is to form nested and closed magnetic surfaces (as an average) so as to insulate the high temperature plasma from cold surrounding materials. One example is toroidal plasma confinement, for which one uses the quasi-toroidal coordinates, (r, θ, ζ) (r: minor radius, θ: poloidal angle, ζ: toroidal angle) (see Fig. 4.3). An overview of toroidal plasma is given in, e.g., [4.2, 4.4, 4.27].

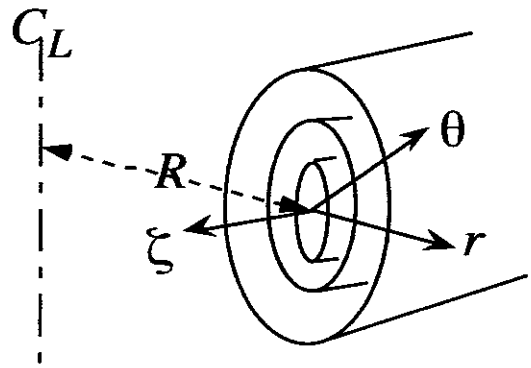

Figure 4.3. Geometry of toroidal plasma. Local Cartesian coordinates (x, y, z) are taken where x-axis is in the r-direction and z-axis is in the direction of magnetic field.

The inhomogeneities, that drive (or suppress) instabilities and turbulence, exist primarily in a perpendicular direction to the magnetic field. The gradients in the number density, pressure, and temperature, are in the direction across the magnetic surfaces. The global flow vector $\bar{\mathbf{V}}$ is on the magnetic surface. The gradient of $\bar{\mathbf{V}}$ across the magnetic surface, $d\bar{\mathbf{V}}/dr$, influences the turbulence strongly.

The inhomogeneity of the electromagnetic field is also important for plasmas. The global plasma velocity across the magnetic field is related to the radial electric field through the relation

$$-e\bar{n}_{\rm i}(\bar{\mathbf{E}} + \bar{\mathbf{V}} \times \bar{\mathbf{B}}) + \nabla \bar{p}_{\rm i} + \nabla \cdot \bar{\mathbf{\Pi}}^{\rm d}_{\rm i} = 0, \tag{4.51}$$

where $\mathbf{\Pi}^{\rm d}$ is the traceless part (deviatoric part) of the stress tensor. The inhomogeneity of $\bar{\mathbf{E}}$ is related to that of $\bar{\mathbf{V}}$ and changes the turbulence. Details are discussed in §4.3.4. The gradient of the magnetic field structure $\nabla|\bar{\mathbf{B}}|$ also influences the free energy, which generates instability and turbulence as is shown in Eq. (4.15). There $\nabla|\bar{\mathbf{B}}|$ plays the role of effective gravity, being an analogue to a buoyancy force in fluid dynamics. It is a convention to name 'magnetic hill' if

$$\nabla|\bar{\mathbf{B}}|\nabla\bar{p} > 0 \tag{4.52}$$

holds so that the $\nabla|\bar{\mathbf{B}}|$ term contributes to instability. If $\nabla|\bar{\mathbf{B}}|\nabla\bar{p} < 0$, it is called a 'magnetic well'. The pitch of the magnetic field line, $1/q = RB_\theta/(rB_\zeta)$ plays a role in selecting the wave vector, where R is the major radius of the torus. The wave vector in the direction of $\bar{\mathbf{B}}$, $k_\parallel = \mathbf{k}\cdot\bar{\mathbf{B}}/\bar{B}$, has the form $k_\parallel \propto [k_\zeta + k_\theta r/(qR)]$. For the combination of $k_\theta/k_\zeta = -qR/r$, it vanishes ($k_\parallel = 0$). A surface, on which $k_\parallel = 0$ holds, is called a mode rational surface. The variation of the magnetic field direction (in the r-direction) is called the 'magnetic shear', and

$$s = rq^{-1}dq/dr \tag{4.53}$$

is called the shear parameter. If the magnetic shear exists, the condition $k_\parallel \approx 0$ for a given values of (k_θ, k_ζ) holds, in a narrow region (whose width is in proportion to s^{-1}) near the mode rational surface.

These geometrical and inhomogeneous structures play an important role in the evolution of turbulence in confined plasmas.

B Mode, wave, and vortex As is illustrated in §4.1.1, plasma turbulence could be pumped in a scale length which is much smaller than the global gradient scale lengths. The wavelength of such instabilities can be much shorter than the system size. Therefore, fluctuations could be observed as a 'mode' or a 'wave', if the spatial correlation length is longer than the wavelength. Same arguments apply to the temporal evolution.

Example of this view is the weak-turbulence picture as is explained in §4.1.2. In the limit of Eq. (4.21), the observed correlation function takes the form

$$\langle \tilde{E}(t')^* \tilde{E}(t) \rangle = \sum_{\mathbf{k}} I(\mathbf{k}, \omega_{\mathbf{k}}) \exp[-i\omega_{\mathbf{k}}(t-t')], \tag{4.54}$$

i.e., a wave feature (a pattern that satisfies $\omega = \omega_{\mathbf{k}}$) is observed. In the case where Eq. (4.27) is satisfied, fluctuations might be observed as waves.

The wave-like feature is barely observed if the correlation length becomes shorter. When the spectrum becomes broader, so that

$$\langle \tilde{E}(\omega')^* \tilde{E}(\omega) \rangle : \delta(\omega - \omega') \to \frac{\Delta\omega}{(\omega-\omega')^2 + \Delta\omega^2}, \tag{4.55}$$

the auto-correlation time becomes shorter

$$\langle \tilde{E}(t')^* \tilde{E}(t) \rangle \to \exp\left[-i\omega_{\mathbf{k}}(t-t') - \Delta\omega|t-t'|\right]. \tag{4.56}$$

If the auto-correlation time is comparable to or shorter than $\omega_{\mathbf{k}}^{-1}$, the wave-like feature is not observed. When one measures, say, the static potential $\tilde{\phi}$, the transient peak of $\tilde{\phi}$ could disappear in a short time $\Delta\omega^{-1}$, so that the perturbation is no longer seen as a wave. When the broadening in k space becomes larger and the width Δk becomes of the order of the representative mode number, the perturbation is no longer seen as a wave but as a small-scale vortex (with short life time). When the turbulence becomes strong, the perturbation might be seen as being composed of vortices.

In some occasions, a solitary vortex appears. The life time of isolated potential structure can be much longer than the eddy turn over time. See Appendix B.

C Convective cell, zonal flow, and streamer By the words 'mode' and 'wave', one describes the patterns that change in space and in time. There is mode that is not propagating and is subject to growth or damping. The typical example is the *convective cell* which is discussed in Fig. 4.2(a). This has a very small wave number along the

magnetic-field line and is associated with the electric field across the magnetic-field line. Two limiting cases have a special importance in the turbulence of inhomogeneous plasmas.

One limit is that the perturbation is almost constant on a magnetic surface, and is localized in the vicinity of the particular magnetic surface. The perturbed electric field is in the radial direction, as

$$\mathbf{k} \cong (k_r, 0, 0) \quad \text{and} \quad \tilde{\mathbf{E}} \cong (\tilde{E}_r, 0, 0) \tag{4.57}$$

[see Fig. 4.4(a)]. The perturbed flow on the magnetic surface is associated with the field. The flow is strongly localized in the vicinity of the particular magnetic surface. This perturbation is called a *zonal flow*. The presence of the zonal flow has strong impacts on the developments of micro-scale turbulence as is explained later in §4.3.4.

The other limit is that the perturbation is rapidly changing in the poloidal direction, but is almost constant in the radial direction,

$$\mathbf{k} \cong (0, k_\theta, 0) \quad \text{and} \quad \tilde{\mathbf{E}} \cong (0, \tilde{E}_\theta, 0) \tag{4.58}$$

[see Fig. 4.4(b)]. The perturbed flow due to this electric field perturbation is in the radial direction. For this perturbation, the localized radial flow is generated in the vicinity of a particular poloidal angle. This perturbation is called a *streamer*. An analogy holds between the '*streamer*' in plasma modelling and '*streak*' in fluid dynamics. Both of them are caused by convection in the direction of the gradients of global parameters. Once a streamer is generated, the radial flow of plasma (energy, etc.) could be enhanced. This has also strong impact on the transport phenomena in plasmas.

D Reconnection, island overlapping, braiding, and mixing A topological change of the magnetic field is a key issue for plasma turbulence, because plasma particles move almost freely along magnetic-field lines. In particular, the motion of electrons along the filed line is much faster than that of ions. Once the topology of magnetic-field lines changes, there arises a sudden global variation of plasma parameters. This global change becomes complicated if a substantial velocity difference exists between the electron and ions. Not only the plasma parameters, but also the electromagnetic fields are modified rapidly.

A topological change takes place owing to the reconnection of the magnetic-field lines. When the system with nested closed magnetic surfaces is subject to the symmetry breaking perturbations, magnetic surfaces are deformed. Their topology is preserved in the beginning owing to a high electric conductivity of plasmas. By the deformation of magnetic surfaces, a strongly localized current is generated near the mode rational surface. The current is subject to the impedance (either due to the collisional resistivity, electron inertial impedance, or current diffusion within a collisionless skin depth) and a small but finite perturbed electric field is inevitable near the rational surface.

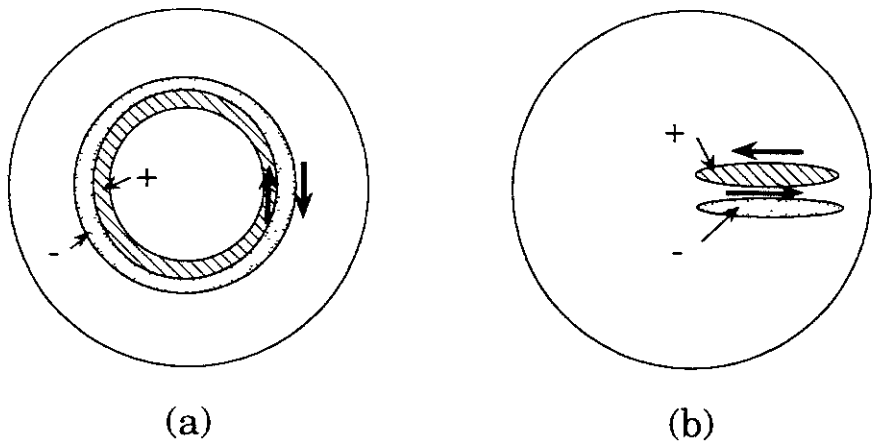

Figure 4.4. Examples of convective-cell formation are illustrated in a poloidal cross-section of toroidal plasmas. Zonal flow (left) and streamer (right). In these examples plasma is charged positive in the hatched region and negative in the dotted region. Radially-inhomogeneous poloidal flow occurs for the zonal flow (a), and poloidally-inhomogeneous radial flow happens for streamer (b).

This localized electric field (in the direction of the magnetic-field line) induces the perturbed magnetic field that causes reconnection. Through this reconnection process, the topology of magnetic-field lines and magnetic surfaces changes. Magnetic surfaces are no longer nested nor isolated, but they have many islands between isolated surfaces.

In the case that many magnetic islands are generated on various magnetic surfaces, interactions between islands on different magnetic surfaces induce the global variation of the plasma. If the width of magnetic islands, $w_{\rm is}$, becomes larger than the radial distance between magnetic islands, $d_{\rm is}$, i.e.,

$$\frac{w_{\rm is}}{d_{\rm is}} \geq 1, \tag{4.59}$$

a global stochastization of magnetic fields can take place [4.51, 4.52]. Field lines become stochastic and meander diffusively over a wide area. Mixing in the phase space occurs, and large transport are possibly occurs [4.53]. Under such circumstance, the electron temperature and pressure tend to become uniform in this region of stochasticity. Ions tend to move as well: however, the mobilities are different for electrons and ions. There could arise the difference between the electron response and ion response, so that a selective loss of electron energy and momentum can be induced. See also [4.54-4.56] for applications to plasma physics.

E Plume and avalanche (time intermittence) A perturbation like the streamer might not be constant in time but could take place intermittently. A heat flux associated with the perturbations happens abruptly from time to time. The flow across the magnetic

surfaces can occur as an avalanche. Non-stationary features of the fluxes are seen as a plume or avalanche. These are also characteristic features of inhomogeneous and strongly turbulent plasmas.

F Micro- and meso-scale structures and competition A 'meso-scale' is an intermediate scale length between the global inhomogeneity and microscopic fluctuations [1.35]. Its typical example is the electric domain interface, which is illustrated in Fig. 4.5. Two radial regions of different radial electric fields touch across a thin layer, and a steep gradient is established in this layer. It is called a domain interface. One of the central themes of recent turbulence theory in plasmas is the mutual interaction of the macro- and meso-scale inhomogeneities and turbulent fluctuations that are regulating each other, leading to the anomalous transport, transitions, and improved confinement [1.22-1.35]. Microscopic fluctuations generate the convective cells and meso-scale structures. The convective cells, including the electric-field domain interface, zonal flow, and streamer, cause the suppression and excitation of micro instabilities (Fig. 4.6). Thus, stabilizing and destabilizing influences of meso-scale structure on turbulence cause complex dynamics, including the subcritical excitation of turbulence. These nonlinear features are surveyed in the later subsections.

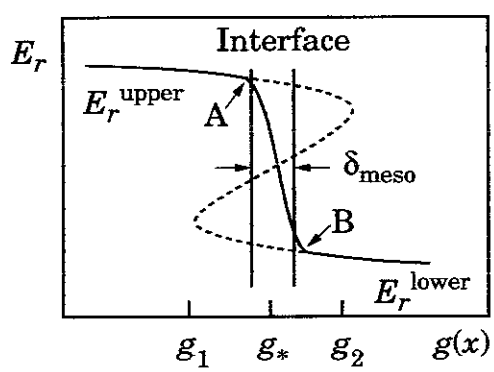

Figure 4.5. Electric-field domain interface as a typical example of meso-scale structure. (Radial electric field as a function of radial parameter is illustrated).

G Crumps The Balescu-Lenard collision operator includes the collective nature of the plasma dynamics through the form of the dielectric constant [4.3]. Thus, important plasma characteristics, which arise from the long-range interactions mediated by the electromagnetic field, could be described by this collision operator. Under some circumstances, the initial condition (ballistic term) can affect the relaxation. If the deviation of the initial condition from the equilibrium distribution is large, it can influence (accelerate) the relaxation. The ballistic effect is usually analyzed in terms

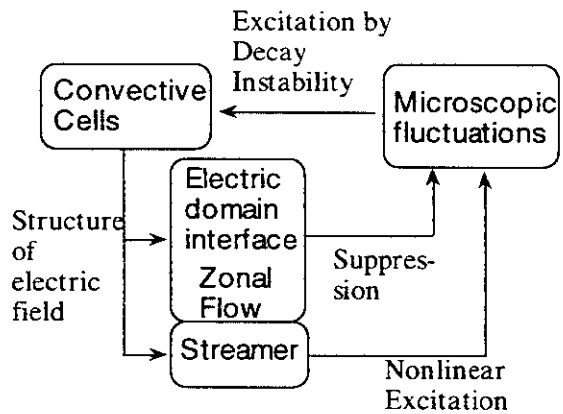

Figure 4.6. Generation–destruction mechanisms between microscopic turbulence and meso-scale structures like electric-domain interface, convective cells, zonal flow and streamer.

of the concept of a clump, because a clump (cluster) of particles behaves together as a macro particle with a finite life time [4.57, 4.58]. An explanation of the clump concept is briefly given in Appendix C. The description of clumps is limited in this article: Here we stress the fluid (moment) description of plasma turbulence, because we emphasize the mutual relationship between the plasma and neutral fluid. More detailed discussion of the clump formalism, with particular emphasis on its application to nonlinear fluid theory, can be found in, e.g., [1.34] and references therein.

4.2.2. Methods for strong turbulence The perturbed electromagnetic field in plasmas is coupled with the perturbed current as Eq. (2.14), i.e.,

$$\frac{1}{c^2}\frac{\partial^2}{\partial t^2}\tilde{\mathbf{E}} + \nabla \times (\nabla \times \tilde{\mathbf{E}}) = -\mu_0 \frac{\partial}{\partial t}\tilde{\mathbf{J}}.$$

As in Eq. (4.10), the perturbed current

$$\tilde{\mathbf{J}} = \sum_{s,k\omega} \exp(i\mathbf{k}\cdot\mathbf{x} - i\omega t) e_s \int \mathbf{v}\tilde{f}_{s,k\omega}(\mathbf{v})d\mathbf{v} \tag{4.60}$$

is determined by the dynamical equation like the Vlasov equation. The properties of fluctuations, particularly their nonlinear behaviour is solely determined by the response of the plasma-current perturbation to the perturbed electromagnetic field, $\tilde{\mathbf{J}}[\tilde{\mathbf{E}}, \tilde{\mathbf{B}}]$. Therefore the analysis of the dielectric tensors is of primary importance. The study of nonlinear dielectric tensors has been a central issue for plasma turbulence.

A Resonance broadening and renormalization in kinetic propagator

A1 Renormalization of propagator When one describes plasma dynamics through the kinetic equations, the perturbed velocity distribution function is obtained by solving the Vlasov equation. In the framework of the linear-response theory, the perturbed distribution function, against the electric perturbation of the form $\tilde{E} \propto \tilde{E}_{k\omega} \exp(i\mathbf{k}\cdot\mathbf{x} - i\omega t)$, has the form

$$\tilde{f} \propto \frac{1}{\omega - k_\parallel v_\parallel + i\nu} \tilde{E}_{k\omega}, \tag{4.61}$$

where ν is the rate at which the particles lose the memory of phase through collisions. The particles which satisfy the condition $v_\parallel \cong \omega/k_\parallel$, i.e., the resonant particles, contribute the energy exchange between waves. In the presence of background fluctuations, resonant particles are scattered by fluctuations. The mean free time Γ^{-1} can be much shorter than the Coulomb collision time. Then the resonance in the response function is broadened as

$$\tilde{f} \propto \frac{1}{\omega - k_\parallel v_\parallel + i\Gamma} \tilde{E}_{k\omega}. \tag{4.62}$$

The resonant condition is rewritten as $|\omega - k_\parallel v_\parallel| < \Gamma$.

The rate of scattering of resonant particles by the background fluctuation, Γ, depends on the magnitude of the fluctuations. One can calculate the resonance broadening by means of the renormalization. A brief sketch is presented here. Systematic description of renormalization is given in, e.g., [1.34]. When one perturbatively solves the Vlasov equation

$$\begin{aligned}\tilde{f}_k(\mathbf{v}) = {} & \frac{e_s}{m_s}\int_{-\infty}^{t} dt' \exp\left[i\mathbf{k}\cdot(\mathbf{x}'-\mathbf{x}) - i\omega(t'-t)\right] \frac{\partial}{\partial \mathbf{v}'} \bar{f}(\mathbf{x}', \mathbf{v}') \cdot \tilde{\mathbf{E}}_{\mathbf{k}} \\ & + \frac{e_s}{m_s}\int_{-\infty}^{t} dt' \exp\left[i\mathbf{k}\cdot(\mathbf{x}'-\mathbf{x}) - i\omega(t'-t)\right] \frac{\partial}{\partial \mathbf{v}'} \tilde{f}_p(\mathbf{x}', \mathbf{v}') \cdot \tilde{\mathbf{E}}_{\mathbf{k}-\mathbf{p}} \\ & + \cdots,\end{aligned} \tag{4.63}$$

one obtains $\tilde{f}_k(\mathbf{v})$ in a series of $\tilde{E}^n$. The n-th order terms with $\tilde{E}^n$ diverge like $(\omega - k_\parallel v_\parallel)^{-n}$. If one collects the most secular terms among these divergent terms at each order, one obtains a renormalized dielectric tensor. In the case of electrostatic fluctuations, $\tilde{\mathbf{E}} = -\nabla\tilde{\phi}$, an explicit formula for the dielectric constant is given as

$$\begin{aligned}\varepsilon_{k,\omega} = 1 - \sum_{s=\mathrm{e,i}} \frac{e_s^2}{k^2 m_s} \int d\mathbf{v} \\ \times \left[\frac{\partial \bar{f}_s}{\partial W} - \frac{J_0\left(k_\perp' v_\perp/\omega_{cs}\right)}{\omega - k_\parallel v_\parallel + i\Gamma_{k,\omega}} \left(\omega \frac{\partial \bar{f}_s}{\partial W} - \frac{\hat{\mathbf{b}}\cdot(\mathbf{k}\times\nabla)\bar{f}_s}{\omega_{cs}}\right)\right],\end{aligned} \tag{4.64}$$

where $W = m_s(v_\perp^2 + v_\parallel^2)/2$ is the kinetic energy of a particle, $\hat{\mathbf{b}}$ is the unit vector in the direction of the magnetic field, ω_{cs} is the cyclotron frequency, and J_0 is the 0-th order Bessel function of the first kind. The nonlinear turbulent decorrelation operator Γ is

determined by a recurrent formula [4.4. 4.59]. See also [4.60-4.63]. Formal theory and more complete form of the renormalized dielectric function than Eq. (4.64) are given in [4.60]. The recurrent formula is explicitly given as

$$\Gamma_{k,\omega}(v_\perp, v_\parallel) = -\Im \sum_{k',\omega'} \frac{J_0\left(k'_\perp v_\perp/\omega_{\rm ci}\right)}{\omega - \omega' - (k_\parallel - k'_\parallel)v_\parallel + i\Gamma_{k',\omega'}} \times \frac{\left(\mathbf{k}\times\mathbf{k}'\cdot\hat{\mathbf{b}}\right)|\phi_{k',\omega'}|^2}{B^2}. \tag{4.65}$$

In the case that a separation is made between the scales of the test mode (k,ω) and the background modes (k',ω'):

$$|k,\omega| \ll |k',\omega'|, \tag{4.66}$$

the damping rate of the (k,ω) component is expressed through the diffusion operator $\mathbf{D}$ as $\Gamma_{k,\omega} = \mathbf{k}\cdot\mathbf{D}\cdot\mathbf{k}$. The recurrent formula is then given in terms of the diffusion operator as [4.64]

$$\mathbf{D}(v_\perp, v_\parallel) = -\Im \sum_{k',\omega'} \frac{J_0\left(k'_\perp v_\perp/\omega_{\rm ci}\right)}{\omega' - k'_\parallel v_\parallel + i\mathbf{k}'\cdot\mathbf{D}\cdot\mathbf{k}'} \times \frac{(\mathbf{k}'\times\hat{\mathbf{b}})(\mathbf{k}'\times\hat{\mathbf{b}})\,|\phi_{k',\omega'}|^2}{B^2}. \tag{4.67}$$

In the absence of turbulence, Eq. (4.67) reduces to the quasi-linear formula as

$$\mathbf{D}(v_\perp, v_\parallel) = \sum_{k',\omega'} J_0\left(k'_\perp v_\perp/\omega_{\rm ci}\right) \Im\left(\frac{-1}{\omega' - k'_\parallel v_\parallel + i\nu}\right) \frac{|\tilde{E}_{\perp\,k',\omega'}|^2}{B^2}. \tag{4.68}$$

Kinetic equations could describe the wave–particle interaction. Substitution of the renormalized operator (4.65) into the formula (4.64) gives the renormalized dielectric constant. The combination of the dielectric constant with the Maxwell equation (or the charge-neutrality condition for the case of long-wavelength and electro-static perturbations) would provide a solution for the turbulent state. In this turbulent state, the orbit of plasma particles is modified by the turbulence. Main emphasis of the analysis of the renormalized propagator has been put upon the calculation of the dielectric tensor which is screened by the background turbulence. The incoherent noise has often been put aside. Modelling of the incoherent random noise is explained in §4.2.3.

A2 Strong-turbulence limit and fluid model The broadening of the resonance in response function is one of the basis for the use of fluid equations in the study of plasma turbulence. If the turbulent scattering becomes stronger and the parallel wave number is small, $|k_\parallel v_{\rm th}| < \Gamma$, all the plasma particles respond in the same way with one decorrelation rate Γ ($v_{\rm th}$: thermal velocity). In this limit, the individuality of a

particle has no influence on the dielectric tensor. A fluid description is valid in this limit. This approximation is a basis to employ a fluid approach for the problems of plasma turbulence.

A3 Strong-turbulence limit and Kubo number The Corrsin approximation [4.65] in strong turbulence is also related with this simplification. In the limit of strong turbulence, $|\omega - k_\parallel v_\parallel| < \Gamma$, the $\mathbf{k}' \cdot \mathbf{D} \cdot \mathbf{k}'$ term dominates in the denominator of Eq. (4.67). Then Eq. (4.67) gives

$$D \cong \frac{|\tilde{\phi}|}{B}. \tag{4.69}$$

In this expression, diffusivity is a linear function of the Kubo number $\mathcal{K}$ if the decorrelation rate and wavelength are specified as being independent of the diffusivity, where $\mathcal{K}$ is the ratio between the $E \times B$ velocity to the wavelength divided by the decorrelation rate, (i.e., the correlation time divided by the eddy turn-over time) as [4.66]:

$$\mathcal{K} = \frac{k^2 |\tilde{\phi}|}{\Gamma B}. \tag{4.70}$$

See also discussion on the role of the Kubo number in [1.34, 4.67].

The assumption that the nonlinear decorrelation dominates for all particles, $|\omega - k_\parallel v_\parallel| < \Gamma$, is a simplified limit. Equation (4.67), which is a closed equation for D for given fluctuations, is derived by use of Markovian approximation. These analytic simplifications (i.e., the Markovian approximation as well as the neglect of the wave–particle resonance) do not necessarily hold in all circumstances. For example, when trapping of particles exists, the $\mathcal{K}$ dependence of D becomes weaker [4.68, 4.69]. A weak dependence on $\mathcal{K}$ is also recovered in transport due to a percolation process [4.70-4.73].

Even though the renormalized formulae have these limitations, they provide a way to determine turbulence and turbulent transports self-consistently. In the case that the nonlinear decorrelation rate Γ caused by damping through the diffusivity (or viscosity of the same magnitude), $\Gamma \cong Dk^2$, Eq. (4.69) means that

$$\mathcal{K} \cong 1. \tag{4.71}$$

The strong turbulence state, which is governed by the fluctuating $E \times B$ motion, is specified by Eq. (4.71).

Noting these facts in mind, analyses based on fluid models are discussed in the following.

B Nonlinear response in fluid-like equations A system of renormalized kinetic equations is usually too complicated for the study of plasma turbulence. The renormalization

approach to moment equations (fluid equations) has been applied. By using the fluid (moment) equations, one can study in detail the property of interactions through the convective nonlinearlity, by sacrificing the wave-particle interactions. Here, the analysis of passive advection is briefly discussed in the following [4.74, 4.75]. The statistical reduction of the dynamical equation for plasmas is discussed in the next subsection.

A model equation which describes the passive advection of a scalar quantity X in the presence of a statistically-specified background velocity $\tilde{\mathbf{v}}$ with an external statistical source is given as

$$\frac{\partial \tilde{X}}{\partial t} + (\bar{\mathbf{V}} + \tilde{\mathbf{v}}) \cdot \nabla \tilde{X} - D_c \nabla^2 \tilde{X} = \tilde{S}^{\text{ext}}, \tag{4.72}$$

where D_c is the collisional diffusion coefficient. The fluctuating field quantity $\tilde{X}$ has its own characteristic scale length ℓ_c. Two categories of background fluctuation fields are considered in $\tilde{\mathbf{v}}$, i.e.,

$$\tilde{\mathbf{v}} = \tilde{\mathbf{v}}_s + \tilde{\mathbf{v}}_l, \tag{4.73}$$

where $\tilde{\mathbf{v}}_s$ has much shorter wavelength than ℓ_c, while $\tilde{\mathbf{v}}_l$ has much longer wavelength than ℓ_c. The static and inhomogeneous flow $\bar{\mathbf{V}}$ is a special limit of $\tilde{\mathbf{v}}_l$. The separation of background flows is shown in Fig. 4.7.

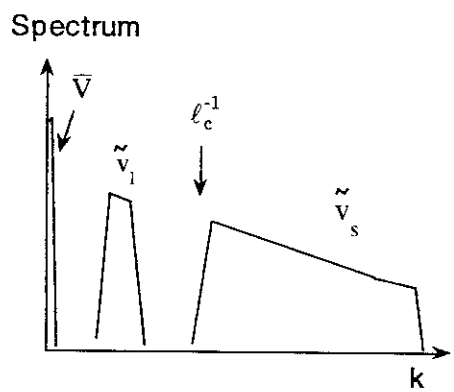

Figure 4.7. Schematic illustration of background fluctuations, $\tilde{v}_s$ and $\tilde{v}_l$, and inhomogeneous flow $\bar{V}$. They are assumed to be statistically independent.

B1 Short-wavelength fluctuations First, shorter-wavelength components are studied. When the background fluctuation velocity changes very rapidly, one takes the rapid change model (RCM) [4.76] in which the correlation functions are assumed to have the form

$$\langle \tilde{v}_s(x + \ell, t + \tau) \tilde{v}_s(x, t) \rangle = 2 \langle \tilde{v}_s \tilde{v}_s \rangle (\ell) \tau_{ac} \delta(\tau), \tag{4.74}$$

$$\langle \tilde{S}^{\rm ext}(x+\ell, t+\tau)\tilde{S}^{\rm ext}(x,t)\rangle = S^{\rm ext}(\ell)\delta(\tau). \tag{4.75}$$

The auto-correlation time of $\tilde{v}_{\rm s}$, $\tau_{\rm ac}$, is assumed to be much shorter than the eddy turnover time of the perturbation $\tilde{X}$. With the help of this model, a statistical equation for the passive scalar perturbation is derived. The correlation function

$$C(\ell,\tau) = \langle \tilde{X}(x+\ell, t+\tau)\tilde{X}(x,t)\rangle \tag{4.76}$$

is then governed by the equation

$$\frac{\partial}{\partial t}C - \frac{2}{\ell^{d-1}}\frac{\partial}{\partial \ell}\ell^{d-1}D_{-}(\ell)\frac{\partial}{\partial \ell}C = S^{\rm ext}(\ell) \tag{4.77}$$

with

$$D_{-}(\ell) = D_{\rm c} + \tau_{\rm ac}\sum_{\mathbf{k}}\left(1 - e^{i\mathbf{k}\cdot\boldsymbol{\ell}}\right)\langle|\tilde{v}_{\rm s}|^2\rangle, \tag{4.78}$$

and d stands for the space dimension.

From the relations (4.77) and (4.78), an estimate for the intensity of fluctuation, $I = \lim_{\ell\to 0} C(\ell)$, is made as

$$I \sim \tau_{\rm D}[\lim_{\ell\to 0} S^{\rm ext}(\ell)], \tag{4.79}$$

$$\tau_{\rm D} \sim \frac{\ell_{\rm c}^2}{D}, \tag{4.80}$$

and

$$D = \lim_{\ell\to\infty} D_{-}(\ell) = D_{\rm c} + \tau_{\rm ac}\sum_{\mathbf{k}}\langle|\tilde{v}_{\rm s,\mathbf{k}}|^2\rangle. \tag{4.81}$$

The diffusion time $\tau_{\rm D}$ over the scale of $\ell_{\rm c}$ is a time scale that determines the lifetime of the perturbation of the passive field [4.75]. Note that Eq. (4.79) is one form of the fluctuation–dissipation relation in turbulent plasmas. The fluctuation–dissipation relation, which is discussed in several places of this review, is an extension, to non-equilibrium plasmas, of the fluctuation–dissipation theorem (FDT) which has been established in the thermodynamical limit [4.77]. The fluctuation–dissipation relation is also called 'extended FDT'.

Equation (4.81) agrees with a limiting form of Eq. (4.67) which is derived by kinetic approach: in the limit of $k'_{\perp}\rho_{\rm i}/\omega_{\rm ci}$ and $|\omega - k_{\parallel}v_{\parallel}| \ll \Gamma$, Eq. (4.67) with $\tau_{\rm ac} = \Gamma^{-1}$ reduces to Eq. (4.81).

B2 Rapidly-changing, long-wavelength components Next the influence of longer-wavelength fluctuations is discussed. As for the case of $\tilde{\mathbf{v}}_{\rm s}$, the fluctuation velocity $\tilde{\mathbf{v}}_{\rm l}$ is also assumed to be rapidly changing in time. The influence of $\tilde{\mathbf{v}}_{\rm l}$ is introduced as a

rapidly changing Doppler-shift. $i\tilde{\omega}_k\tilde{X}_k = \tilde{\mathbf{v}}_l \cdot \nabla\tilde{X}_k$. Then, from Eq. (4.72), the forced stochastic oscillator equation

$$\frac{\partial}{\partial t}\tilde{X}_k + i\tilde{\omega}_k\tilde{X}_k - D_k\nabla^2\tilde{X}_k = \tilde{S}_k^{\text{ext}} \tag{4.82}$$

is obtained for a Fourier component. The diffusion coefficient D_k is obtained from the contribution of random shorter-wavelength components, $\tilde{\mathbf{v}}_s$ in Eq. (4.81). Its contribution is evaluated through the damping rate $\Gamma_s = D_k k_\perp^2$. The impact of the stochastic frequency shift is characterized by the parameter

$$\Gamma_l = \tau_{ac,l}\langle\tilde{\omega}_k^2\rangle, \tag{4.83}$$

where $\tau_{ac,l}$ is the auto-correlation time of the longer-wavelength fluctuations $\tilde{\mathbf{v}}_l$. The statistical property of the response function of Eq. (4.82)

$$G(t;t') = \exp\left[-\int_{t'}^{t} d\tau\,(i\tilde{\omega}_k + \Gamma_s)\right] \tag{4.84}$$

has been studied when the correlation $\langle\tilde{\omega}_k(t)\tilde{\omega}_k(0)\rangle$ decays as [4.77]

$$\langle\tilde{\omega}_k(t)\tilde{\omega}_k(0)\rangle = \langle\tilde{\omega}_k^2\rangle \exp\left(-|t|/\tau_{ac,l}\right). \tag{4.85}$$

In the limit of rapidly changing background fluctuations:

$$\tau_{ac,l} \ll \tau_D, \tag{4.86}$$

one obtains

$$\langle G(t;0)G(t';0)\rangle = \exp\left[-2(\Gamma_l + \Gamma_s)|t-t'|\right] \tag{4.87}$$

with $\Gamma_s = \tau_D^{-1}$. The decorrelation of the test field occurs at the rate $\Gamma_s + \Gamma_l = \tau_D^{-1} + \Gamma_l$. The statistical average of the fluctuating field $\tilde{X}$ is given as

$$I \sim \frac{\lim_{\ell\to 0} S^{\text{ext}}(\ell)}{\tau_D^{-1} + \Gamma_l} = \frac{1}{1+\tau_D\Gamma_l}\left[\tau_D \lim_{\ell\to 0} S^{\text{ext}}(\ell)\right]. \tag{4.88}$$

Comparing Eqs. (4.79) and (4.88). one finds that the level of fluctuations is suppressed by the stochastic Doppler shift due to the longer-wavelength fluctuations by the factor

$$\frac{1}{1+\tau_D\Gamma_l} = \frac{1}{1+\tau_D\tau_{ac,l}\langle\tilde{\omega}_k^2\rangle} \quad \text{for} \quad \tau_{ac,l} \ll \tau_D, \tag{4.89}$$

assuming that the source $\lim_{\ell\to 0} S^{\text{ext}}(\ell)$ is unchanged. In the large-amplitude limit of random oscillations (or long correlation time $\tau_{ac,l}$). $\tau_{ac,l}^2\langle\tilde{\omega}_k^2\rangle > 1$, the Gaussian response is given as

$$\langle G(t;0)G(t';0)\rangle \propto \exp\left[-2\langle\tilde{\omega}_k^2\rangle(t-t')^2\right]. \tag{4.90}$$

Equation (4.90). being compared to Eq. (4.87), is called the motional narrowing. This results in

$$I \sim \sqrt{\frac{\pi}{2}}\frac{1}{\sqrt{\langle\tilde{\omega}_k^2\rangle}} \lim_{\ell\to 0} S^{\text{ext}}(\ell). \tag{4.91}$$

Compared to Eq. (4.79), a reduction by the factor $1/\tau_D\sqrt{\langle\tilde{\omega}_k^2\rangle}$ is obtained.

The statistical quantities $\tilde{\omega}_k$ and $\tilde{S}_k^{\rm ext}$ might be independent or be correlated. The influence of a cross-correlation between $\tilde{\omega}_k$ and $\tilde{S}_k^{\rm ext}$ has also been studied [4.74]. An example of the results is

$$I \propto 1 - \alpha_1 Z^2, \tag{4.92}$$

where α_1 is a numerical coefficient, and Z is the ratio of cross-correlation to auto-correlation, $Z = \langle\tilde{\omega}_k\tilde{S}_k^{\rm ext}\rangle/\sqrt{\langle\tilde{\omega}_k^2\rangle\langle\tilde{S}_k^{\rm ext2}\rangle}$. The cross-correlation between the Doppler shift and the external noise source suppresses the fluctuation level.

B3 Static but sheared flow A Doppler shift by the sheared static velocity $\bar{\mathbf{V}}\cdot\nabla$ also influences in the level of the perturbation of the passive field. For a case of sheared flow, one takes $V = [0, V_y(x), 0]$. The contribution of short-wavelength turbulence is modelled by the turbulent transport coefficient D, and Eq. (4.72) is rewritten as

$$\frac{\partial}{\partial t}\tilde{X} + \bar{V}_y(x)\frac{\partial}{\partial y}\tilde{X} - D\nabla^2\tilde{X} = \tilde{S}^{\rm ext}. \tag{4.93}$$

The sheared static flow induces the stretching of a vortex, and the correlation time of the test field $\tilde{X}$ is modified. The influence on statistical properties is discussed, in detail, in the later subsection, §4.3.4.

B4 On rigorous upper bound Equations in §4.4.4B are useful basis for the analysis of plasma turbulence. For some cases, a rigorous upper bounds of the turbulence-driven transport could be calculated [4.67]. A rigorous upper bound might have a different parameter dependence compared to the true value. However, it would be a firm basis of the understanding of turbulence. For instance, one could find a boundary in a parameter space, below which the upper bound is zero for steady states. Such a criterion might be called 'energy-stability criterion' for turbulence: perturbation of any amplitude (either subcritical or supercritical ones) decays in time [1.31, 1.34, 4.78]. A brief description on the rigorous upper bound is given in Appendix D.

C Renormalization in reduced set of equations The nonlinear dispersion relation is derived by use of the renormalized dielectric tensor. This method is illustrated by taking the example of a reduced set of equations. The reduced set of equations (see §2.2.2) has the form

$$\frac{\partial}{\partial t}\mathbf{f} + \mathcal{L}^{(0)}\mathbf{f} = \mathcal{N}(\mathbf{f}) + \tilde{\mathbf{S}}_{\rm th}, \tag{4.94}$$

where $\mathbf{f}$ denotes the set of variables

$$\mathbf{f}^{\rm T} = (\phi, n), \tag{4.95a}$$

$$\mathbf{f}^{\mathrm{T}} = (\varphi, J, p), \tag{4.95b}$$

$$\mathbf{f}^{\mathrm{T}} = (\phi, J, v_{\parallel}, p), \tag{4.95c}$$

$$\mathbf{f}^{\mathrm{T}} = (n, \phi, \Phi, v_{\parallel}, p_{\mathrm{e}}, p_{\mathrm{i}}, A_{\parallel}), \tag{4.95d}$$

for the two-field (HW) model, three-field model, four-field model, and seven-field (YH) model, respectively. The linear operator $\mathcal{L}^{(0)}$ is the $N \times N$ matrix for the N-field model and controls the linear modes. $\mathcal{N}(\mathbf{f})$ is the nonlinear terms, e.g.,

$$\mathcal{N}(\mathbf{f}) = -\begin{pmatrix} \nabla_{\perp}^{-2}[\phi, \nabla_{\perp}^2 \phi] \\ [\phi, J] \\ [\phi, p] \end{pmatrix} \tag{4.96}$$

for the case of (4.95b). The term $\tilde{\mathbf{S}}_{\mathrm{th}}$ stands for the thermodynamical excitation induced by the interaction with a heat bath.

Theoretical models have been developed in order to separate the nonlinear interaction term into two terms as

$$\mathcal{N}(\mathbf{f}) = \mathcal{N}_{\mathrm{coherent}}(\mathbf{f}) + \tilde{\mathbf{S}}. \tag{4.97}$$

where $\mathcal{N}_{\mathrm{coherent}}(\mathbf{f})$ is a coherent part, which changes with the phase of test mode, $\mathbf{f}$, and $\tilde{\mathbf{S}}$ is the incoherent part (noise part). The noise part $\tilde{\mathbf{S}}$ could change very rapidly in time. For a basis of rapid change, see a discussion in §4.2.3C. Explicit forms of $\mathcal{N}_{\mathrm{coherent}}(\mathbf{f})$ and $\tilde{\mathbf{S}}$ are given by modelling. Various modellings for the coherent and incoherent parts have been analyzed. For detailed discussion, see, e.g., [1.34]. A sample is explained in the following.

A test mode $\mathbf{f}_k$ is chosen, and the terms $\mathcal{N}_{\mathrm{coherent}}(\mathbf{f}_k)$ and $\tilde{\mathbf{S}}_k$ for $\mathbf{f}_k$ are estimated. The coherent part is estimated by renormalization when the background fluctuations have a smaller scale length than the test perturbation. The coherent part $\mathcal{N}_{\mathrm{coherent}}(\mathbf{f})$ is modelled by a matrix form for the N-field models. In a case of two-field model (HW equation), explicit form of the matrix is given in [2.20]. A case of three-field model is discussed in [1.35]. A diagonalization approximation is often used for the analytic insight, based on a view that the parameter dependence of the obtained result is little influenced by off-diagonal terms. The contribution of the off-diagonal elements must be included for the quantitative conclusion. The diagonal terms are approximated by the the diffusion terms with the turbulent viscosity (μ_{N} for ion viscosity, μ_{Ne} for electron viscosity, and ξ_{N} for thermal diffusivity), or by the eddy-damping coefficients ($\gamma_{(1)}$ for ion momentum, $\gamma_{(2)}$ for parallel electron momentum, and $\gamma_{(3)}$ for thermal energy), as

$$\mathbf{N}_{\mathrm{coherent}}(\mathbf{f}_k) = \begin{pmatrix} \mu_{\mathrm{N}} \nabla_{\perp}^2 f_1 \\ \mu_{\mathrm{Ne}} \nabla_{\perp}^2 f_2 \\ \chi_{\mathrm{N}} \nabla_{\perp}^2 f_3 \end{pmatrix}_k = -\begin{pmatrix} \gamma_{(1)} f_1 \\ \gamma_{(2)} f_2 \\ \gamma_{(3)} f_3 \end{pmatrix}_k \tag{4.98}$$

(note that nonlinear damping rate $\gamma_{(1)}$, $\gamma_{(2)}$, and $\gamma_{(3)}$ could be different). Within this diagonal approximation, the renormalized operator $\mathcal{L}$ is given as

$$\mathcal{L}_{ij} = \mathcal{L}^{(0)}_{ij} + \gamma_{(i)}\delta_{ij}, \tag{4.99}$$

and one has a renormalized reduced set of equations (with a thermodynamical noise source) as

$$\frac{\partial}{\partial t}\mathbf{f}_k + \mathcal{L}\mathbf{f}_k = \tilde{\mathbf{S}}_k + \tilde{\mathbf{S}}_{\mathrm{th}.k}, \tag{4.100}$$

where $\mathbf{k}$ denotes the test mode.

The renormalized transfer rates are given as [1.31]

$$\gamma_{i,k} = -\sum_{\Delta} M_{i,kpq} M^*_{i.qkp} \tau^*_{i.qkp} |\tilde{f}^2_{1.p}|. \tag{4.101}$$

Here, suffix i denotes the field component, $(i = 1, 2, 3)$ for three-field models, and k, p, q stand for the interacting Fourier modes. In these expressions, the summation Δ indicates the constraint $\mathbf{k} + \mathbf{p} + \mathbf{q} = 0$. The triad-interaction time $\tau_{i.kpq}$ obeys the same linear and nonlinear physics as the test mode, as is explained in [1.31]. By employing Markovian approximation, the triad-interaction time is approximately estimated by the relation

$$\tau_{j.kpq} \cong [\mathcal{L}(k) + \mathcal{L}(p) + \mathcal{L}(q)]^{-1}\mathbf{I}, \tag{4.102}$$

where $\mathbf{I}$ is a unit vector. Note that $\tau_{j,kpq}$ might be different for different j, and is often approximately estimated by $\tau_{kpq} = \tau_{1,kpq}$. More thorough argument in a full matrix model of $\mathcal{N}_{\mathrm{coherent}}(\mathbf{f}_k)$ is given in [2.20]. The explicit form of the nonlinear interaction matrix is given as, e.g., $M_{(2,3),kpq} = (\mathbf{p} \times \mathbf{q}) \cdot \mathbf{b}$.

Equation (4.100) shows that the amplitude of the fluctuation $|\mathbf{f}_\mathbf{k}|$ becomes large in the vicinity of the pole of the renormalized operator $\mathcal{L}$. Thus the nonlinear dispersion relation

$$\det(\lambda\mathbf{I} + \mathcal{L}) = 0 \tag{4.103}$$

describes the characteristic features of the turbulence, where $\mathbf{I}$ is a unit tensor, and $-\lambda$ is the eigenvalue of the operator $\mathcal{L}$. The sign is chosen so that $\lambda < 0$ for unstable cases. In a steady state, the fluctuation level does not grow. This state could be evaluated from the condition,

$$\Re\lambda \cong 0. \tag{4.104}$$

In a case of purely growing/damping modes, one has $\lambda = 0$, i.e.,

$$\det(\mathcal{L}) = 0. \tag{4.105}$$

Equation (4.103) is a simplified nonlinear dispersion relation, in which the effects of noise source are neglected. This describes a dispersion relation of a test mode which is

screened by the eddy-damping-like effects of background turbulence [1.35]. The screened test mode is also called the *dressed test mode*. Equation (4.105) gives a rough estimate for the level of turbulence, because $\mathcal{L}$ is a functional of the turbulence spectrum through the renormalization relation, e.g., Eq. (4.101). It is used to understand the role of various non-equilibrium parameters (e.g., gradient, magnetic-field configuration, etc.) on the plasma turbulence. This analytic simplicity is given at a sacrifice of mathematical rigour. This simplified relation neglects the noise source and thus the nonlinear conservation of the quadratic invariants like energy is not guaranteed. The validity of the solution of Eq. (4.105) must be examined, *a posteriori*, by more accurate modelling in which the renormalized operator $\mathcal{L}$ and the noise source $\tilde{\mathbf{S}}$ are determined self-consistently. The modelling including the noise sources is explained in §4.2.3, and the relevance of solution is discussed there.

D Scale invariance method The method of scale invariance is an alternative approach to understanding turbulence properties. The method and applications to plasma turbulence are reviewed in [4.79].

D1 Fluid models There are two well known examples in fluid dynamics: One is the analysis of the drag force acting on a body in a flow [4.80, 4.81], and the other is the Kolmogorov spectrum [4.82].

The drag force is discussed in terms of the scale invariance property. It has been shown that the Navier-Stokes equation for an incompressible fluid;

$$\rho\left[\frac{\partial \mathbf{V}}{\partial t} + (\mathbf{V}\cdot\nabla)\mathbf{V}\right] = -\nabla p + \nu\nabla^2\mathbf{V} \tag{4.106}$$

is invariant under the following three transformations:

$$\mathcal{T}_1: \quad \mathbf{V} \to a_1\mathbf{V}, \quad t \to a_1^{-1}t, \quad p \to a_1^2 p, \quad \nu \to a_1\nu, \tag{4.107a}$$

$$\mathcal{T}_2: \quad \mathbf{x} \to a_2\mathbf{x}, \quad t \to a_2 t, \quad \nu \to a_2\nu, \tag{4.107b}$$

$$\mathcal{T}_3: \quad \rho \to a_3\rho, \quad p \to a_3 p, \quad \nu \to a_3\nu. \tag{4.107c}$$

The drag force F, which acts on a sphere of radius L in a fluid with velocity V, has the dimension of $\rho V x^3 t^{-1}$, so that $F/(\rho V^2 L^2)$ is invariant under transformations $\mathcal{T}_1$, $\mathcal{T}_2$, and $\mathcal{T}_3$ (ρ: mass density, L: system size). The Reynolds number $Re = \rho LV\nu^{-1}$ is also invariant under these transformations, so is an arbitrary function of Re, $F_{\rm a}(Re)$. Therefore the ratio $[\rho V^2 L^2 F_{\rm a}(Re)]^{-1}F$ is invariant. The drag force must be given in such a form as

$$F = \rho V^2 L^2 F_{\rm a}(Re). \tag{4.108}$$

The scale-invariance method is also useful in determining a turbulent spectrum. Let us consider a homogeneous system and assume that the dissipated power per unit volume, ε, is given. The change of scales is applied as

$$\mathcal{T}_{\mathrm{K}}: \quad x \to a_1 x \quad \text{and} \quad t \to a_2 t. \tag{4.109}$$

By noting the fact that the viscosity μ, the dissipation ε, the energy spectrum of the fluctuations, $E(k)$, and the wave number are transformed as

$$\mu \to a_1^2 a_2^{-1}\mu, \quad \varepsilon \to a_1^2 a_2^{-3}\varepsilon, \quad E(k) \to a_1^3 a_2^{-2} E(k), \quad k \to a_1^{-1} k, \tag{4.110}$$

one finds the following two ratios

$$\frac{E(k)}{\mu^{5/4}\varepsilon^{1/4}} \quad \text{and} \quad \frac{k}{\mu^{-3/4}\varepsilon^{1/4}}. \tag{4.111}$$

are invariant under this transformation $\mathcal{T}_{\mathrm{K}}$ [Eq. (4.109)]. From this result, the spectrum is independent of a choice of coordinates if it is expressed as $E(k) = \mu^{5/4}\varepsilon^{1/4} F(k\mu^{3/4}\varepsilon^{-1/4})$ where $F(z)$ is an arbitrary function. The essence of the inertial range is that the wave energy is independent of viscosity. The factor $\mu^{5/4} F(k\mu^{3/4}\varepsilon^{-1/4})$ is chosen as being independent of μ; i.e., $F \propto \mu^{-5/4}$. By use of this form factor, one finally has

$$E(k) \propto k^{-5/3}\varepsilon^{2/3}. \tag{4.112}$$

Scale invariance approach is also applicable in the presence of external forces. For instance, the counterpart of Eq. (4.112) for the gravity waves ($\omega_k \propto k^{1/2}$) and capillary waves ($\omega_k \propto k^{3/2}$) in a fluid are

$$E(k) \propto k^{-5/2} \tag{4.113}$$

and

$$E(k) \propto k^{-3}, \tag{4.114}$$

respectively [4.33].

D2 Plasma models This scale invariance method is also applied to plasma turbulence. From general cases to specific ones, representative examples are shown [4.79].

Let us first show a case of electrostatic perturbations, which is valid in the limit that the plasma pressure $\bar{p}$ is low compared to the magnetic pressure $\bar{\mathbf{B}}^2/(2\mu)$. In this case, the Vlasov equation takes the form of

$$\left[\frac{\partial}{\partial t} + \mathbf{v}\cdot\nabla + \frac{e_s}{m_s}\left(\mathbf{E} + \mathbf{v}\times\bar{\mathbf{B}}\right)\frac{\partial}{\partial \mathbf{v}}\right] f_s(\mathbf{x},\mathbf{v};t) = 0 \quad (s = \mathrm{i},\mathrm{e}), \tag{4.115}$$

where $\bar{\mathbf{B}}$ is a constant magnetic field, and the distribution function f_s and the electric field contain fluctuating components. In the limit that the scale length of the perturbation is longer than the Debye length λ_D, $|\lambda_D k| \ll 1$, the Maxwell equations are simplified under the charge-neutrality condition

$$\sum_{s=\mathrm{i,e}} e_s \int d\mathbf{v} f_s = 0. \tag{4.116}$$

There are three (and only three) independent transformations that leave these equations [Eqs. (4.115) and (4.116)] invariant:

$$\mathcal{T}_1 : \quad f_j \to a_1 f_j \tag{4.117a}$$

$$\mathcal{T}_2 : \quad \mathbf{v} \to a_2 \mathbf{v}, \quad \mathbf{B} \to a_2 \mathbf{B}, \quad t \to a_2^{-1} t, \quad \mathbf{E} \to a_2^2 \mathbf{E}, \tag{4.117b}$$

$$\mathcal{T}_3 : \quad \mathbf{x} \to a_3 \mathbf{x}, \quad \mathbf{B} \to a_3^{-1} \mathbf{B}, \quad t \to a_3 t, \quad \mathbf{E} \to a_3^{-1} \mathbf{E} \tag{4.117c}$$

(note that the temperature scales as $T \to a_2^2 T$ by $\mathcal{T}_2$). Under this set of transformations, one finds that quantities tB and $Ta^{-2}B^{-2}$ (T being the plasma temperature, a being the plasma size) are invariant under the transformations $\mathcal{T}_1$, $\mathcal{T}_2$, and $\mathcal{T}_3$. That is, the quantity such as a confinement time τ_E must satisfy

$$\tau_E B = F_\mathrm{a}\left(\frac{T}{a^2 B^2}\right) \tag{4.118}$$

(F_a: an arbitrary function). This form is a general constraint that turbulent state which is governed by Eqs. (4.115) and (4.116) with a constraint $|\lambda_D k| \ll 1$ must satisfy. Some forms of F_a have received particular interest. In the history of the plasma confinement research, importance of the Bohm diffusion, for which the diffusivity has a dependence like $D_\mathrm{B} \propto T/(eB)$, and the gyro-Bohm diffusion $D \propto (\rho_\mathrm{i} a^{-1}) D_\mathrm{B}$, has been recognized empirically (see, e.g., [4.2, 4.4]). If the function F_a has the form $F_\mathrm{a}(z) \sim z^{-1}$, one has the so-called Bohm diffusion, i.e.,

$$\tau_E \propto \frac{a^2 B}{T}. \tag{4.119}$$

For another power form of $F_\mathrm{a}(z) \sim z^{-3/2}$, one obtains

$$\tau_E \propto \frac{a^3 B^2}{T^{3/2}}, \tag{4.120}$$

which is called gyro-reduced Bohm diffusion.

It should also be noted that there could be multiple characteristic time scales. For instance, the energy confinement time (the time scale of the transport across a global scale length), auto-correlation time of microscopic fluctuations could have a different dependence in general. In such a case, F_a takes a different form depending on the choice of characteristic times.

When the electromagnetic perturbations are considered, like those in a family of MHD turbulence, the electromagnetic dynamical equations (e.g., ideal or dissipative MHD equations) are used. A different choice of dynamical equations leads to a different invariant transformation. The invariant relation is given as

$$\tau_E B = \left(n^{1/2}a\right) F_{\mathrm{a}}\left(\frac{nT}{B^2}, Ta^{1/2}\right). \tag{4.121}$$

By selecting particular type of instabilities in specific circumstances, a more explicit form of turbulence transport can be derived. See exhaustive references in [4.79]. For instance, one has the transport coefficient $\chi = a^2/\tau_E$ as

$$\chi = \frac{T^{3/2}}{aB^2}\left(\frac{na}{T^2}\right)^q. \tag{4.122}$$

The index q is summarized for various drift-wave range instabilities in [4.79]. Summary is quoted in Table 4.1.

Table 4.1. Summary of scale-invariance relations for various specific turbulence models. (Quoted from [4.79] with supplement.) Reference 1-11 corresponds to [4.83-4.85, 4.45, 4.86-4.92], respectively.

Instability modes	Index q	Reference
collisional drift	1	1, 2, 3
	0	2, 3
	2/3	4
	1/3	2
dissipative trapped electrons	-1	2, 3, 5, 6
	-4/3	7
	-2	8
collisionless trapped electron	0	2, 3, 5
dissipative trapped ion	-1	2
ion-temperature-gradient	0	3, 5, 6, 9, 10
current-diffusive turbulence	0	11

It is noted that the scale-invariance method gives the same result as the mixing-length estimate for supercritical instabilities [4.93].

A discussion of the fluctuation spectrum is also feasible for plasma turbulence. For the current diffusive interchange mode (CDIM) turbulence, a model basic equation is given as

$$\frac{d}{dt}\begin{pmatrix}\nabla_\perp^2\phi\\ j\\ p\end{pmatrix} + \begin{pmatrix}0 & -ik_y sx & ik_y G_0\\ ik_y sx & 0 & 0\\ ik_y & 0 & 0\end{pmatrix}\begin{pmatrix}\phi\\ j\\ p\end{pmatrix} = 0, \tag{4.123}$$

where $d/dt = \partial/\partial t + [o,\ ]$. Here, normalization follows MHD models [4.94]. It should be noted that the driving source of fluctuations, which is represented by parameter G_0 ($G_0 = \nabla \ln \bar{p} \cdot \nabla \ln \bar{B}$) in this problem, is also to be transformed. The system of Eq. (4.123) is found to be invariant under the transformation [4.92]

$$x \to a_1 x,\quad t \to a_1^{-1} t \tag{4.124}$$

with $(\phi, j, p) \to (a_1^3 o, a_1^2 j, a_1 p)$ and $G_0 \to a_1^2 G_0$. The turbulent transport coefficient D is transformed as $D \to a_1^3 D$, and $D/G_0^{3/2}$ is found to be invariant. We see that the dependence $D \propto G_0^{3/2}$ is satisfied.

Constraints for a spectrum is also deduced from a scale invariant property. From the scaling properties of $\tilde{\phi}$ and k, $\phi^2 G_0^{-3}$ and $k\sqrt{G_0}$ are invariant. As a result, $\phi^2 G_0^{-3}$ is expressed as a function of $k\sqrt{G_0}$ as $\tilde{\phi}^2 G_0^{-3} \sim F_{\rm CD}(\sqrt{G_0}k)$, where $F_{\rm CD}$ is an arbitrary function. For quasi two-dimensional turbulence in magnetized plasmas ($d = 2$), the energy spectrum $E(k) = [k_\perp^2 |\phi(k)|^2] k^{d-1}$ is given as

$$E(k_\perp) \sim G_0^3 F_{\rm CD}(\sqrt{G_0} k_\perp) k_\perp. \tag{4.125}$$

If the energy spectrum is expressed as a power law, $E(k) \propto k^{-\nu}$, $F_{\rm CD}(z)$ has a dependence $F_{\rm CD}(z) \propto z^{-1-\nu}$. By use of this form, Eq. (4.125) is rewritten as

$$E(k_\perp) \sim G_0^{5/2-\nu/2} k_\perp^{-\nu}. \tag{4.126}$$

The index $\nu = 3$ has been obtained for a nonlinear stationary state, in the wavelength regime where turbulence is excited [1.35].

4.2.3. Randomness and statistical picture A fundamental origin of randomness is collisions in plasmas. Parts of the nonlinear interactions of the background fluctuations are treated as a random noise source for a test mode. Modelling and effects of the random noise source are discussed in this subsection.

A Estimate of random source term Consider a generic form of equation [1.31, 4.95];

$$\left(\frac{\partial}{\partial t} + i\omega_k\right) \tilde{X}_k = \frac{1}{2} \sum_{\Delta} M_{kpq} \tilde{X}_p^* \tilde{X}_q^*, \tag{4.127}$$

where $\tilde{X}_k$ is a fluctuation quantity, ω_k is a complex linear wave frequency, M_{kpq} is the coefficient of nonlinear interactions, $(\mathbf{k}, \mathbf{p}, \mathbf{q})$ are the wave vectors of interacting modes, and $\sum_\Delta$ means the summation with the condition $\mathbf{k}+\mathbf{p}+\mathbf{q} = 0$ (notation follows [1.31]). Its counterpart in fluid dynamics is given in Eq. (3.29). This equation is modelled by the Langevin equation

$$\left[\frac{\partial}{\partial t} + i\omega_k + \Gamma_k(t)\right] \tilde{X}_k(t) = \tilde{S}_k(t), \tag{4.128}$$

where $\Gamma_k(t)$ is the nonlinear damping rate, which is discussed in §4.2.2C, and $\tilde{S}_k(t)$ is the nonlinear noise. The assumption $\langle \tilde{S}(t)\tilde{S}(t')\rangle \propto \delta(t-t')$ is often employed in order to ensure the Markovian approximation. The nonlinear noise term is treated by use of the white Gaussian model

$$\tilde{S}_k(t) = \tilde{w}(t) \sum_{\Delta} \sqrt{\tau_{kpq}}\tilde{g}_{kpq}, \tag{4.129}$$

where $\tilde{w}(t)$ denotes the white-noise function, τ_{kpq} is the Markovianized nonlinear propagator (the long-time average of τ_{pqr} gives the interaction time that plays the role of auto-correlation time), and $\tilde{g}_{kpq}$ is the average amplitude of the instantaneous noise source;

$$\langle \tilde{S}(t)\tilde{S}(t')^*\rangle = \delta(t-t')\tau_{kpq}\langle \tilde{g}_{kpq}\tilde{g}^*_{kpq}\rangle. \tag{4.130}$$

The quasi-normal picture of turbulence is that background fluctuations are almost normal. That is, when the noise amplitude $\tilde{g}_{kpq}$ is expressed by the use of a statistically-independent variable ζ (virtual field) as

$$\tilde{g}_{kpq} = M_{kpq}\zeta^*_p\zeta^*_q, \tag{4.131}$$

the correlation functions for the virtual field ζ_p is identical to the one for the fluctuating field

$$\langle \zeta_p\zeta^*_q\rangle = \langle \tilde{X}_p\tilde{X}^*_q\rangle. \tag{4.132}$$

B Dynamical equations for correlation functions A set of dynamical equations for correlation functions, called the realizable Markovian closure (RMC), has been discussed [4.96, 4.97]. A two-time correlation function

$$C_k(t,t') = \langle \tilde{X}_k(t)\tilde{X}^*_k(t')\rangle \tag{4.133}$$

is given in a form

$$C_k(t,t') = C^{1/2}_k(t)\bar{r}_k(t,t')C^{1/2}_k(t'). \tag{4.134}$$

Here, $C_k(t)$ is the one-time correlation function, and $\bar{r}_K(t,t')$ is related to the Markovianized nonlinear damping Γ_k as

$$\bar{r}_k(t,t') = \begin{cases} \exp\left[-\int_{t'}^{t} \mathcal{P}\Gamma(\tau)d\tau\right] & \text{for} \quad t > t', \\ \exp\left[-\int_{t}^{t'} \mathcal{P}\Gamma(\tau)^* d\tau\right] & \text{for} \quad t \le t', \end{cases} \tag{4.135}$$

where the operator $\mathcal{P}$ is defined as

$$\mathcal{P}\Gamma = \Re\Gamma\Theta(\Re\Gamma) + i\Im\Gamma, \tag{4.136}$$

and $\Theta(\Re\Gamma)$ is the Heaviside step function. As discussed in [4.96], the role of $\mathcal{P}$ is to ensure the realizability, i.e., to guarantee that the correlation function remains positive.

With the help of this Markovianization, a set of dynamical equations for the correlation function C and the normalized triad-interaction time $\hat{\tau}_{kpq}$ can be derived as

$$\left[\frac{\partial}{\partial t} + 2\Re\Gamma_k(t)\right] C_k(t) = 2F_k(t), \tag{4.137}$$

and

$$\left[\frac{\partial}{\partial t} + \Gamma_k(t) + \mathcal{P}\Gamma_p(t) + \mathcal{P}\Gamma_q(t)\right] \tau_{kpq}(t) = C_p^{1/2}(t) C_q^{1/2}(t), \tag{4.138}$$

where the damping rate Γ_k and the source term are given as functions of C and $\hat{\tau}_{kpq}$:

$$\Gamma_k = \gamma_{\mathrm{c},k} - \sum_{\Delta} M_{kpq} M^*_{pqk} \tau^*_{kpq} C_q^{1/2} C_k^{-1/2}, \tag{4.139}$$

$$F_k = \frac{1}{2}\Re \sum_{\Delta} |M_{kpq}|^2 \tau_{kpq} C_p^{1/2} C_q^{1/2}, \tag{4.140}$$

and $\gamma_{\mathrm{c},k}$ is the collisional damping rate. This model equation is realizable, i.e., the correlation function C_k remains positive [4.97].

In a stationary state, one has

$$C_k(t) = \frac{F_k(t)}{\Re\Gamma_k(t)}, \tag{4.141}$$

which is a fluctuation–dissipation relation (extended FDT) for the turbulent state.

C Langevin equations The Langevin equation (4.100)

$$\frac{\partial}{\partial t}\mathbf{f} + \mathcal{L}\mathbf{f} = \tilde{\mathbf{S}} + \tilde{\mathbf{S}}_{\mathrm{th}}$$

is constructed with Eqs. (4.130) and (4.131) as the model form of nonlinear noise functions [4.98, 4.99].

In order to solve Eq. (4.100), an ansatz of a large number of degrees of freedom in random modes, N, is introduced. The renormalized term γ_j in $\mathcal{L}$ arises from the statistical sum of contributions from N components, so that its variation in time becomes $O(N^{-1/2})$ times smaller in comparison with that of $\mathbf{f}_k$. Therefore, in solving the time evolution of fluctuating $\mathbf{f}_k$, $\mathcal{L}$ is approximated to be constant in time in the limit of $N \to \infty$. With the help of this ansatz, the general solution is formally given as

$$\mathbf{f}(t) = \sum_m \exp(-\lambda_m t)\mathbf{f}^{(m)}(0) + \int_0^t \exp\left[-\mathcal{L}(t-\tau)\right] \tilde{\mathbf{S}}(\tau) d\tau, \tag{4.142}$$

where $-\lambda_m$ ($m = 1, 2, 3, \cdots$ and $\Re\lambda_1 < \Re\lambda_2 < \Re\lambda_3 < \cdots$) represent the eigenvalues of the renormalized matrix $\mathcal{L}$, and are determined by Eq. (4.103). Here, $\mathbf{f}^{(m)}(0)$ is a representation of the initial value which is transformed into a diagonal basis. The eigenvector with the eigenvalue $-\lambda_1$ corresponds to the least stable branch (mode), the decay time of which is longest. Others with $(-\lambda_2, -\lambda_3, \cdots)$ denote highly-stable branches, which decay much faster. For the case of the N-field model, Eq. (4.103) is a N-th order equation of λ. Equation (4.103) provides a relation between λ_m, γ_j, and global parameters such as $G_0 \equiv \nabla(\ln\bar{p}) \cdot \nabla(\ln\bar{B})$, $\eta_{\rm i} \equiv |\nabla(\ln\bar{T}_{\rm i})|/|\nabla(\ln\bar{n}_{\rm e})|$, etc.

C1 Example of three-field model The matrix $\exp[-\mathcal{L}(t-\tau)]$ in Eq. (4.142) could be explicitly expressed in terms of parameters that specify the inhomogeneous turbulent plasmas. For example, the elements of $\exp[-\mathcal{L}(t-\tau)]$ for the three-field model of Eq. (4.47) are expressed in terms of three discrete eigenvalues of Eq. (4.103), λ_1, λ_2, and λ_3, as

$$\begin{aligned}\{\exp[-\mathcal{L}(t-\tau)]\}_{ij} &= A_{ij}^{(1)} \exp\left[-\lambda_1(t-\tau)\right] + A_{ij}^{(2)} \exp\left[-\lambda_2(t-\tau)\right] \\ &\quad + A_{ij}^{(3)} \exp\left[-\lambda_3(t-\tau)\right], \end{aligned} \tag{4.143}$$

where the elements of matrix $\mathbf{A}$ are given in Ref. [4.98]. By introducing a projected amplitude of noise source as

$$\mathcal{S}^{(m)}(\tau) = \left[1, \frac{-ik_\parallel}{k_\perp^2(\gamma_{\rm e}-\lambda_m)}, \frac{-ik_y\Omega'}{k_\perp^2(\gamma_{\rm p}-\lambda_m)}\right] \cdot \left[\tilde{\mathbf{S}}(\tau) + \tilde{\mathbf{S}}_{\rm th}(\tau)\right], \tag{4.144}$$

where $\gamma_{\rm e}$ and $\gamma_{\rm p}$ stand for $\gamma_{(2)}$ and $\gamma_{(3)}$ in Eq. (4.98), respectively. the fluctuation field is given as

$$\mathbf{f}^{(m)}(t) = A_{11}^{(m)} \begin{pmatrix} 1 \\ \frac{-ik_\parallel\xi}{\gamma_{\rm e}-\lambda_m} \\ \frac{ik_y p_0'}{\gamma_{\rm p}-\lambda_m} \end{pmatrix} \int_0^t \exp[-\lambda_m(t-\tau)]\mathcal{S}^{(m)}(\tau)d\tau \tag{4.145}$$

on neglecting the initial condition which is ineffective in determining the statistical average [4.100]. Superscript (m) denotes the m-th branch of Eq. (4.103).

The long-time average of the decomposed amplitude is obtained from Eq. (4.145). For the decomposed amplitude, one has

$$\langle f_1^{(m)*} f_1^{(m)} \rangle = \frac{1}{2\Re(\lambda_m)} |A_{11}^{(m)}|^2 \langle \mathcal{S}^{(m)*} \mathcal{S}^{(m)} \rangle. \tag{4.146}$$

This is the fluctuation–dissipation relation (extended FDT) in the case of strongly unstable plasmas. The estimate of Eq. (4.146) is made for a noise source with the magnitude

$$\langle \mathcal{S}^{(1)*} \mathcal{S}^{(1)} \rangle \cong C_0 \gamma_{\rm v} A_{11}^{-2} \langle f_{1,k}^{(1)*} f_{1,k}^{(1)} \rangle + \text{thermal excitations}, \tag{4.147}$$

where γ_v is the nonlinear damping rate of the vorticity (eddy damping rate), and C_0 is a numerical factor of the order of unity. This is a crude estimate of the noise level, and the modeling of C_0 that can preserve a conservation property of Eq. (4.146) has not been established. With this estimate, the fluctuation-dissipation relation (extended FDT) [Eq. (4.146)] is rewritten as

$$\langle f_{1,k}^{(1)*} f_{1\,k}^{(1)} \rangle = \frac{C_0 \gamma_v}{2\Re\lambda_1} \langle f_{1\,k}^{(1)*} f_{1\,k}^{(1)} \rangle + \text{thermal excitations.} \tag{4.148}$$

In the limit of strong turbulence, i.e., the fluctuation level is much larger than the thermodynamical fluctuations, Eq. (4.148) is simplified as

$$\Re\lambda_1 = \frac{C_0}{2}\gamma_v. \tag{4.149}$$

Both the nonlinear decorrelation rate λ_1 and the eddy damping rate γ_v depend on the fluctuation spectrum as Eqs. (4.101), (4.103), and (4.149); these are the equations that determine the fluctuation level together with the decorrelation rate. A schematic explanation of the foregoing mathematical procedure is given in Fig. 4.8. The fluctuation level that is determined by the fluctuation–dissipation relation (extended FDT) [Eq. (4.148)] is higher than that determined by the nonlinear marginal stability condition $\lambda_1 = 0$.

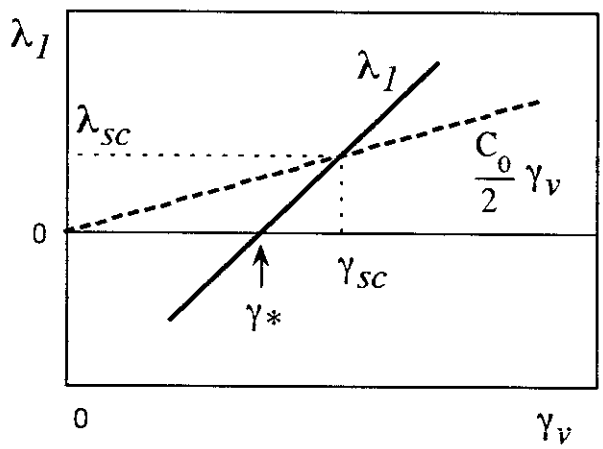

Figure 4.8. Balance between the nonlinear decorrelation rate λ_1 (solid line) and the noise source rate $C_0\gamma_1/2$ (dashed line). These two are written as a function of γ_v. The cross point determines the statistical averages of the nonlinear decorrelation rate and eddy damping rate. λ_{sc} indicates the self-consistent solution for the turbulence decorrelation rate. γ_{sc} is the eddy damping rate in the self-consistent solution.

D Fokker–Planck equation By use of the decomposed elements, a Fokker–Planck equation may be derived. A case of Eq. (4.100) is illustrated by taking an example

of the three-field model. A projected variable

$$F^{(1)}(t) = \left[1, \frac{-ik_\parallel}{(k_\perp^2+\xi)(\bar{\gamma}_e-\lambda_1)}, \frac{-ik_y\Omega'}{k_\perp^2(\bar{\gamma}_p-\lambda_1)}\right]\cdot \mathbf{f}(t) \tag{4.150}$$

is introduced. Then the Langevin equation is decomposed as

$$\frac{\partial}{\partial t}F_k^{(1)} + \lambda_1 F_k^{(1)} = \mathcal{S}_k^{(1)}, \tag{4.151}$$

where projected noise source $\mathcal{S}_k^{(1)}$ is modelled by a white noise. Statistical independence between different k components holds, and we write

$$\langle \mathcal{S}_k^{(1)}(t)\mathcal{S}_{k'}^{(1)}(t')\rangle \propto \mathcal{G}_k^{(1)2}\delta_{k,k'}\delta(t-t'). \tag{4.152}$$

From this property, the Fokker–Planck equation for the probability density function (PDF) $P(F^{(1)})$ is derived [4.101, 4.102] from this dynamical equation (4.151) as

$$\frac{\partial}{\partial t}P = \sum_k \frac{\partial}{\partial F_k^{(1)}}\left(\lambda_1 F_k^{(1)} + \frac{1}{2}\mathcal{G}_k^{(1)}\frac{\partial}{\partial F_k^{(1)}}\mathcal{G}_k^{(1)}\right)P. \tag{4.153}$$

Equation (4.153) describes the PDF for the one from three branches of fluctuation modes.

The equilibrium PDF is given as

$$P_{eq}(\{F_k^{(1)}\}) = \bar{P}\prod_k \frac{1}{\mathcal{G}_k^{(1)}}\exp\left[-\int^{F_k^{(1)}}\frac{2\lambda_{1,k}F_k^{(1)}}{\mathcal{G}_k^{(1)2}}dF_k^{(1)}\right]. \tag{4.154}$$

The presence of the nonlinear noise term, $\mathcal{G}_k^{(1)} \neq 0$, allows access to the equilibrium PDF. One defines the $\mathcal{H}$-function as

$$\mathcal{H}^{(1)}(t) = \int dF^{(1)}P(F^{(1)};t)\ln\left[\frac{P(F^{(1)};t)}{P_{eq}(F^{(1)})}\right], \tag{4.155}$$

and obtains the inequality

$$\frac{d}{dt}\mathcal{H}^{(1)}(t) \leq 0 \tag{4.156}$$

which showing that the PDF relaxes to the equilibrium one in the long-time limit. The irreversibility of evolution, Eq. (4.156), is due to the nonlinear noise term, $\mathcal{G}_k^{(1)} \neq 0$, which is enhanced by the turbulence. The microscopic origin of the irreversibility is the Coulomb collisions, and the Lyapunov exponent of individual particles has been analyzed [4.103]. The irreversibility associated with the renormalized diffusion coefficient $\mathcal{G}_k^{(1)2}$ includes the cascade of energy which leads to an enhanced irreversible dissipation by the Coulomb collisions.

A tail component in the PDF is another feature of nonlinear plasma turbulence. In the equilibrium PDF [Eq. (4.154)], the 'effective temperature' that determines the

width of $P_{\rm eq}(F_k^{(1)})$ is given by $\mathcal{G}_k^{(1)2}$. If the fluctuation amplitude becomes high, the turbulent noise amplitude $\mathcal{G}_k^{(1)}$ increases. As a result, $2\lambda_{1,k}F_k^{(1)}\mathcal{G}_k^{(1)-2}$ in the integrand of Eq. (4.154) has the $F_k^{(1)}$ dependence

$$\frac{2\lambda_{1,k}F_k^{(1)}}{\mathcal{G}_k^{(1)^2}} \propto \frac{1}{F^{(1)}} \tag{4.157}$$

in the large-amplitude limit. The integral in Eq. (4.154) has a logarithmic dependence on $F^{(1)}$, and Eq. (4.154) predicts a power-law distribution in the large-amplitude limit. This power-law dependence of the PDF originated from the fact that the diffusion coefficient $\mathcal{G}_k^{(1)2}$ is renormalized [4.98].

One may compare the above analysis with those in fluid theory. The work by [3.48] is an example of detailed analysis of neutral-fluid turbulence. In this case, however, the integrand of Eq. (4.154) is expanded with respect to the fluctuation amplitude. Once the integrand is expanded, exponential forms are deduced.

E Memory effects and non-Markovian property As is discussed for fluid turbulence, the memory effect could also be important for plasma turbulence. The statistical procedure used for the reduction of variables makes the resulting equations have a non-Markovian nature. A proper treatment of memory effects is necessary [4.104, 4.105]. For instance, the quasi-normal approximation (QNA) kept only the decorrelation due to the molecular viscosity and turned out to be inadequate owing to the too long memory effect. Analytic expressions which are used for the evaluation of inhomogeneous plasma turbulence, e.g., Eqs. (4.69) and (4.105) or (4.149), are derived by use of the Markovianization.

Memory effects could be important when the Kubo number is large. Examples are given in §4.2.2A3. If the fluctuation amplitude $\tilde{A}$ becomes large, fluid elements circumnavigate the fluctuation eddy many times during the decorrelation time of fluctuations, $\tau_{\rm c}$. The correlation function along the path of fluid elements (Lagrangian correlation function) becomes different from the correlation function at one time slice (Eulerian correlation function). A method named 'decorrelation path method' has been applied to obtain the Lagrangian correlation function [4.68]

$$C_{ij}(t_1,t_2) = \langle v_i[x(t_1);t_1]v_j[x(t_2);t_2]\rangle \qquad i,j=(x,y). \tag{4.158}$$

In stationary homogeneous turbulence, it is given as $C_{ij}(t_1,t_2) = C_{\rm L}(t_1-t_2)\delta_{ij}$. For small $\mathcal{K}$, the quasi-linear limit is recovered as

$$C_{\rm L}(\Delta t) \cong \left(\frac{\tilde{A}}{\ell_{\rm c}}\right)^2 \exp\left(-\frac{|\Delta t|}{\tau_{\rm c}}\right) \quad \text{for} \quad \mathcal{K} \ll 1, \tag{4.159}$$

where $\ell_{\rm c}$ is the correlation length of the fluctuating field, $\tilde{A}$ is an appropriately normalized amplitude, and the Kubo number is defined as $\mathcal{K} = \tilde{A}\tau_{\rm c}/\ell_{\rm c}^2$ in this case.

In the large K limit, an asymptotic formula for $C_{\mathrm{L}}(\Delta t)$ is given as [4.104]

$$C_{\mathrm{L}}(\Delta t) \sim -0.32\left(\frac{\tilde{A}}{\ell_{\mathrm{c}}}\right)^2\left(K\frac{|\Delta t|}{\tau_{\mathrm{c}}}\right)^{-1.42} \quad \text{for } K\frac{|\Delta t|}{\tau_{\mathrm{c}}} > 3 \text{ and } K \gg 1. \quad (4.160)$$

A slow power-law decay is demonstrated.

This power-law decay of the correlation function demonstrates the limitation of theories that use Markovianization. The Markovianization approximation is valid in a certain range of Kubo number, and the investigations into the non-Markovian property are surveyed in [4.104]. The appearance of the '*subdiffusive process*' and its related discussion for a transient response is given in §4.5.2. The dispersion evolves in time as [4.106]

$$\left\langle [x(t) - x(0)]^2 \right\rangle \propto t^{\alpha_{\mathrm{tail}}} \quad (4.161)$$

with the index

$$\alpha_{\mathrm{tail}} = 0.58. \quad (4.162)$$

The index α_{tail} is smaller than unity, and this process is subdiffusive. The initially-localized perturbation, however, develops a long tail in space. An application to drift-wave turbulence has been recently discussed [4.107].

4.2.4. Model based on reduced variables By a reduction of variables, specific processes in inhomogeneous turbulence may be studied. First is the influence of boundary conditions. When the wavelength of perturbation is comparable to the system size, global perturbations which are selectively chosen by boundary conditions are excited. In such a case, a truncated model is often used, and a few degree of freedoms for the global perturbations are kept. A typical example is the Lorenz model in fluid dynamics [4.108]. An application to plasma is described. The second is that a cascade plays a dominant role. In such a case, the shell model is a useful approach [3.12-3.15]. An application of the shell model to a system with linear instabilities is shown. In plasmas, the competition between the instability and cascade causes anisotropy of spectrum. An example to extend the shell model to two-dimensional systems is illustrated. The third is the K–ε model [3.49, 4.109]. In many cases the coherence length of turbulence is shorter than the system size, but the influence of the boundary condition could appear through the spatial transport of turbulence. The K–ε model based on TSDIA is used for the study of such situations.

A Lorenz model Perturbations in a thin bounded region are analyzed by keeping only a small number of Fourier modes. Higher harmonics are truncated. One of the most famous models is the Lorenz model, in which only three components are kept, i.e., the

fundamental mode (most unstable one), the second harmonics, and the background profile modification [4.108]. A closed set of equations has been derived for these three scalar quantities. Extension to a model with truncation at five modes was made to study the role of a standing wave [4.110]. A model with eight-mode truncation was proposed to introduce the effect of travelling waves [4.111].

The method of Lorenz model has also been applied to the study of plasma instabilities in a thin region. For instance, perturbations in the scrape-off layer (thin plasma region that surrounds a plasma surface) are sometimes investigated by this method [4.112-4.116]. In an application to plasmas, five variables are often taken into account: the fundamental mode (X for potential and Y for pressure perturbation), the background profile modification for plasma pressure (Z), the zonal flow component (V) and the second harmonics of the static potential (W). The equations for the truncated components are:

$$\frac{d}{dt}X = Pr(-X + Y) + VW, \tag{4.163a}$$

$$\frac{d}{dt}Y = -XZ + r_a X - Y, \tag{4.163b}$$

$$\frac{d}{dt}Z = XY - bZ, \tag{4.163c}$$

$$\frac{d}{dt}V = -XW - \gamma_V V, \tag{4.163d}$$

$$\frac{d}{dt}W = -cXV - \gamma_W W, \tag{4.163e}$$

where Pr is the Prandtl number,

$$r_a = Ra\pi^{-4}k_a^2(1 + k_a^2)^{-3}, \tag{4.164a}$$

$$b = 4(1 + k_a^2)^{-1}, \tag{4.164b}$$

$$\gamma_V = Pr(1 + k_a^2)^{-1}, \tag{4.164c}$$

$$\gamma_W = Pr(4 + k_a^2)(1 + k_a^2)^{-1}, \tag{4.164d}$$

$$c = (3/4)k_a^2(1 + k_a^2)^{-1}, \tag{4.164e}$$

and k_a is the inverse of the wavelength in the y direction being normalized by the thickness of the layer. Here, Ra is the Rayleigh number defined by

$$Ra = L^3 g\alpha_{\mathrm{th}}\frac{\theta(L) - \theta(0)}{\kappa\mu_{\mathrm{f}}} \tag{4.165}$$

with $\theta(L) - \theta(0)$ being the temperature difference. The influence of VW term in Eq. (4.163a) shows the stabilizing influence of sheared flow.

It is shown that this set of dynamical equations for five variables shows a chaotic nature. Only one positive Lyapunov number exists in a certain region of Rayleigh number [4.115]. The effective Rayleigh number for the magnetized plasmas is defined by using the magnetic gradient in stead of gravitational acceleration as is explained in §4.3.2. Even though the number of variables increases from three to five, the number of positive Lyapunov exponent remains one. This approach of truncated Fourier modes captures some feature of chaotic behaviour due to the nonlinearity, but not necessarily the turbulent feature of excited fluctuations.

B Shell model

B1 One-dimensional model The energy cascade in the Navier-Stokes equation has been studied by shell models. In particular, a choice of nonlinear terms called the Gledzer–Ohkitani–Yamada (GOY) model is often employed [3.12-3.15]. A shell model has also been discussed for passive advection [4.117]. With these shell models, a system of pressure-driven instability (like the Rayleigh–Bénard instability or flute instability) may be described [4.118]. A set of model equations for the fluid velocity and temperature is:

$$\frac{du_n}{dt} = i(a_n u^*_{n+1}u^*_{n+2} + b_n u^*_{n-1}u^*_{n+1} + c_n u^*_{n-1}u^*_{n-2}) + Pr\theta_n - Prk_n^2 u_n, \tag{4.166a}$$

$$\frac{d\theta_n}{dt} = i\left[e_n(u^*_{n-1}\theta^*_{n+1} - u^*_{n+1}\theta^*_{n-1}) + g_n(u^*_{n-2}\theta^*_{n-1} + u^*_{n-1}\theta^*_{n-2}) + h_n(u^*_{n+1}\theta^*_{n+2} - u^*_{n+2}\theta^*_{n+1})\right] + Rau_n - k_n^2\theta_n, \tag{4.166b}$$

where $*$ represents the complex conjugate, $n = 1, \ldots, N$ is the number of each shell, $k_n = C2^{n-1}$, u_n is the fluctuating velocity, θ_n is the fluctuating temperature, and Pr is the Prandtl number [see Fig. 4.9(a)]. One takes $a_n = k_n$, $b_n = -k_{n-1}/2$, $c_n = -k_{n-2}/2$, $e_n = k_n/2$, $g_n = -k_{n-1}/2$, $h_n = k_{n+1}/2$.

One may use this system to examine the linear instability with growth rate

$$\gamma_n = \frac{-k_n^2(1+Pr) + \sqrt{k_n^4(1-Pr)^2 + 4PrRa}}{2}. \tag{4.167}$$

This conservation relations for the kinetic and internal energy of fluctuations:

$$\frac{d}{dt}\left(\frac{1}{2}\sum_{n=1}^{N}|u_n|^2\right) = -Pr\sum_{n=1}^{N}k_n^2|u_n|^2 + Pr\sum_{n=1}^{N}\theta_n u_n^* \tag{4.168}$$

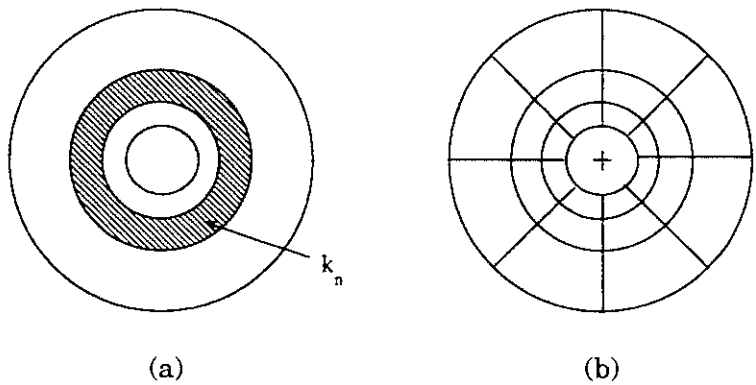

Figure 4.9. Shell in the k space for a one-dimensional model (a) and for a multiple-bin model (b).

and

$$\frac{d}{dt}\left(\frac{1}{2}\sum_{n=1}^{N}|\theta_n|^2\right) = -\sum_{n=1}^{N}k_n^2|\theta_n|^2 + Ra\sum_{n=1}^{N}u_n\theta_n^* \tag{4.169}$$

show that competition takes place between the viscosity damping and excitation through the cross-correlation between velocity and temperature. The latter is related to the transport of the net heat. A power-law solution of the form

$$u_n = Ak_n^{-1/3} \quad \text{and} \quad \theta_n = \sqrt{Ra}Ak_n^{-1/3} \tag{4.170}$$

is obtained for the steady state.

This set of model equations (4.166) has a large degree of freedom with the positive Lyapunov experiment, and describes the chaos. In a nonlinear steady state, quantities are fluctuating around their long-time average, resulting in the power spectrum

$$\left\langle |u_n|^2 + |\theta_n|^2 \right\rangle \propto k_n^{-2/3}, \tag{4.171}$$

and a dependence on the Rayleigh number as

$$\left\langle \sum_{n=1}^{N}|u_n|^2 \right\rangle \propto Ra \quad \text{and} \quad \left\langle \sum_{n=1}^{N}|\theta_n|^2 \right\rangle \propto Ra^2 \tag{4.172}$$

Figure 4.10 shows an example of the fluctuation spectrum, and the maximum Lyapunov number λ_1 scales as

$$\lambda_1 \propto Ra^{0.7}. \tag{4.173}$$

It becomes larger as the Rayleigh number becomes higher. The stronger the gradient, the larger the nonlinear decorrelation rate. This dependence is stronger than that of the linear growth rate $\gamma_n \propto Ra^{0.5}$. In a large Rayleigh number limit, the nonlinear decorrelation rate dominates the linear instability growth rate.

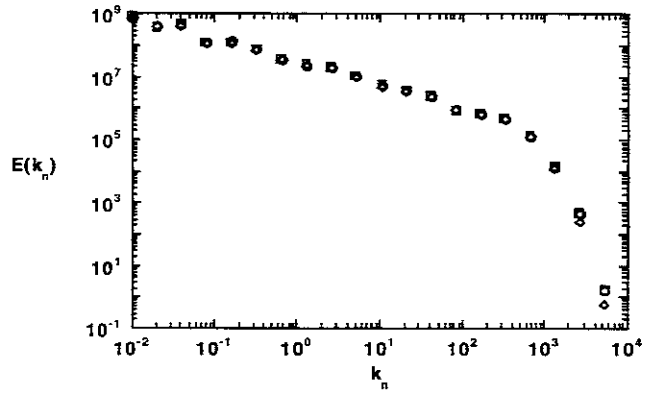

Figure 4.10. Time-average spectrum of the shell model (taken from [4.118]).

B2 Multiple-bin model In the presence of anisotropy, the shell model may be extended to a two-dimensional multiple-bin model. Figure 4.9(b) illustrates the division of segments in the absolute value of the wavenumber and the direction with respect to the global density gradient.

A system of Hasegawa–Mima (HM) equation (4.44), with a linearly unstable term

$$\left(1-\rho_{\mathrm{i}}^2\nabla_\perp^2\right)\frac{\partial}{\partial t}\phi+V_{\mathrm{de}}\frac{\partial}{\partial y}\phi+\frac{T}{eB}\left[\phi,\rho_{\mathrm{i}}^2\nabla_\perp^2\phi\right]=\gamma_{\mathrm{L}}\phi \tag{4.174}$$

added, has been analyzed by use of the multiple-bin model. The right hand side shows the additional linear instability term. According to Ref. [4.119], the numerical results for the fluctuation energy were compared under a properly chosen γ_{L} in [4.97]. Further reading about the derivation of the bin-averaged mode-coupling coefficients and the results is given in [4.97] and references therein.

C K–ε model The K–ε model has also been applied to plasma turbulence model. For an interchange mode, the fluctuation energy K and the dissipation rate ε obey [4.120]

$$\frac{\partial K}{\partial t}=C_p g_0\frac{K^2}{\varepsilon}-\varepsilon-C_J\frac{1}{\rho_{\mathrm{i}}^2}\frac{K^3}{\varepsilon}+\nabla\cdot\left(C_K\frac{K^2}{\varepsilon}\nabla K\right), \tag{4.175a}$$

$$\frac{\partial \varepsilon}{\partial t}=C_{\varepsilon 1}C_p g_0 K-C_{\varepsilon 2}\frac{\varepsilon^2}{K}-C_{\varepsilon J}C_J\frac{1}{\rho_{\mathrm{i}}^2}K^2+\nabla\cdot\left(C_\varepsilon\frac{K^2}{\varepsilon}\nabla\varepsilon\right), \tag{4.175b}$$

where the specific properties of plasma turbulence are included in the geometrical coefficients of the production terms (the first terms on the right-hand side), $g_0=(\nabla\tilde{p}\nabla\ln\tilde{B})\rho^{-1}$, and the Ohmic dissipation terms (the third terms). The dissipation in the vorticity equation and that in Ohm's law [e.g., Eq. (4.47b)] are treated independently and modelled in different forms. C_p, C_K, C_J, C_ε, $C_{\varepsilon 1}$, $C_{\varepsilon 2}$, and $C_{\varepsilon J}$ are numerical

constants [4.109]. The numerical solution of these transport equations is discussed in references [4.120].

When the transport terms in Eq. (4 175) are neglected, the stationary local solution is obtained as $K \propto g_0\rho_i^2$ and $\varepsilon \propto g_0^{1/2}K$. The diffusivity is given as $D = K^2/\varepsilon = C\sqrt{g_0}\rho_i^2$, where $C = (1-C_{\varepsilon 1})/C_J\sqrt{C_p}\sqrt{(C_{\varepsilon 1} - C_{\varepsilon J})(1 - C_{\varepsilon J})}$. This local result belongs to a family of gyro-reduced Bohm diffusion, and can be extended to include the transport effects of fluctuation energy and dissipation. Therefore D deviates from the local-balance value, which gives $D = C\sqrt{g_0}\rho_i^2$. It should be noticed that the local terms (i.e., the first–third terms on the right-hand side) are of order $(D\rho_i^{-2})K$ while the diffusion term (the fourth term) is of order $(DL^{-2})K$, where L is the characteristic scale length. When the inhomogeneity is weak, that is, $L^2 \gg \rho_i^2$, the turbulence level is determined by the local balance between the production and dissipation.

4.2.5. Mapping models Statistical property of the nonlinear dynamics has been investigated by use of the mapping models. The standard mapping is used for the study of the magnetic stochasticity and of the plasma heating problems, and so on. It is formulated as [4.51]

$$q_{n+1} = q_n + p_{n+1}, \tag{4.176a}$$

$$p_{n+1} = p_n + A\sin 2\pi q_n. \tag{4.176b}$$

If the nonlinear parameter (normalized amplitude) exceeds the threshold, $A > A_c = 0.1546\cdots$, stochasticity sets in. In the stochastic orbit, the diffusivity in the phase space is given as

$$D = \frac{A^2}{4}\frac{1 - 2J_1^2(2\pi A) - J_2^2(2\pi A) + 2J_3^2(2\pi A)}{[1 + J_2(2\pi A)]^2}, \tag{4.177}$$

where J_n is the n-th order Bessel function of the first kind. In the large A limit, one has $D = A^2/4$ [4.121]. From intermediate value of A, accelerator modes appear for some special values of A [4.122, 4.123]. The presence of accelerator modes suggests that the transport is not a purely diffusive process in the braided magnetic structure. The non-diffusive transport has been discussed in, e.g., [4.124]. The dispersion increases faster than time t, i.e., '*superdiffusion*' appears.

In addition to the standard map, Tokamap has been proposed to describe the magnetic-field lines in tokamak [4.125]. The selective interaction of particles with the toroidal Alfvén wave eigenmode (TAE mode) is taken in the TAE-mode mapping [4.126]. Below the threshold, $A < A_c$, the memory effect of orbits has been investigated statistically. A recent survey of the statistical theory of the standard map is given in [4.127].

This method is also applied to transport by the drift wave. In the vicinity of the magnetic surface with vanishing magnetic shear ($dq/dr = 0$), the standard non-twist map is applied [4.128]. The wave phase and radial position, (X, Y), are chosen as variables, and a set of mapping equations is given [4.129]:

$$X_{N+1} = X_N + \alpha_{\mathrm{SNM}} \left(1 - Y_{N+1}^2\right), \tag{4.178a}$$

$$Y_{N+1} = Y_N - \beta_{\mathrm{SNM}} \sin 2\pi X_N, \tag{4.178b}$$

where

$$\alpha_{\mathrm{SNM}} = v_{\parallel}(m - nq_*)/\omega_0 R q_*, \tag{4.179a}$$

$$\beta_{\mathrm{SNM}} = \frac{-2\pi m\tilde{\phi}}{a^2 B\omega_0} \left[\frac{2m(d^2q/dr^2)}{q_*(m - nq_*)}\right]^{1/2}, \tag{4.179b}$$

with m and n being the toroidal and poloidal mode numbers, respectively. Here, ω_0 is the wave frequency, q_* is the safety factor on the surface where $dq/dr = 0$, and $\tilde{\phi}$ is the static potential amplitude. This mapping model is used to study the transport near the surface where magnetic shear vanishes. Importance of such magnetic surface for turbulent transport is explained in §4.3.1E.

4.3. Inhomogeneity-Driven Turbulence

In inhomogeneous plasmas, the turbulent state is governed by the excitation and suppression mechanisms, which are functionals of gradient and turbulent decorrelation processes. The co-existence of various inhomogeneity and magnetic field induces a variety of plasma turbulence. By analyzing the nonlinear dispersion relation, Eq. (4.105), various turbulence have been analyzed. Some examples are illustrated in §4.3.1. Fluctuations on the scale length of the ion gyroradius [4.13-4.15], those on the scale length of the collisionless skin depth (or longer) [4.130-4.134] and those on the scale length of the electron cyclotron gyroradius [4.135] have been considered in conjunction with anomalous transport. The relationship of modes with length scales is given in Fig. 4.11. The flux which is driven by turbulence is surveyed in §4.3.2. Generation of fluid structure is discussed in §4.3.3. The influence of the inhomogeneous flow (electric field in plasmas) is discussed in §4.3.4.

4.3.1. Typical examples

A Dissipative interchange mode The instability in inhomogeneous plasmas in the presence of magnetic-field inhomogeneity, known as the interchange mode, has a fundamental role in the pressure-gradient-driven plasma turbulence. This is an analogue

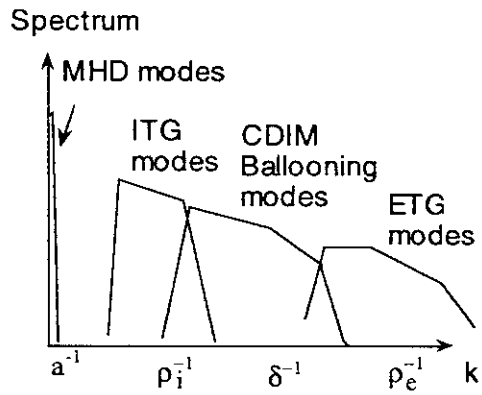

Figure 4.11. Characteristic length scales and various typical modes of plasma turbulence.

of the Rayleigh–Bénard instability in neutral-fluid dynamics. The free-energy source of the interchange mode is released when the electron free motion along the field line is impeded by a dissipative process (frozen-in condition is relaxed). The rate of growth is mainly determined by the competition between the energy release through the magnetic diffusion and the viscosity damping.

A1 Resistive interchange mode When the resistance in the Ohm's law is given by the electric resistivity, the renormalized dispersion equation (4.105) without noise-source term takes the form

$$\left(\frac{\partial}{\partial k_x}\frac{s^2k_y^2}{\eta_\parallel}\frac{\partial}{\partial k_x}+\frac{k_y^2G_0}{\chi k_\perp^2}-\mu k_\perp^4\right)\phi(k_x;k_y)=0, \tag{4.180}$$

where χ and μ are renormalized transport coefficients (sums of collisional and turbulent ones, i.e., $\chi=\chi_{\rm c}+\chi_{\rm N}$ and $\mu=\mu_{\rm c}+\mu_{\rm N}$), $\eta_\parallel$ is the resistivity, and G_0 is the driving source due to the inhomogeneity [4.136]. The critical condition (4.180) is rewritten as

$$\frac{G_0\eta_\parallel}{s^2\bar{\chi}}=C_{\rm r}\equiv\left\{\frac{\pi}{4\ln[2(G_0\bar{\mu}^{-1}\bar{\chi}^{-1}k_y^{-4})^{1/6}]}\right\}^2, \tag{4.181}$$

where $C_{\rm r}$ is a weakly varying function of G_0, and the coefficient $C_{\rm r}$ can be approximated as a constant.

From Eq. (4.181), the turbulent transport coefficient in a stationary state is derived as

$$\chi_{\rm N}=\frac{\eta_\parallel}{C_{\rm r}s^2}G_0 \tag{4.182}$$

in the limit of strongly turbulent transport, $\chi_{\rm N}\gg\chi_{\rm c}$. The turbulence decorrelation rate is given as

$$\tau_{\rm corr}\cong G_0^{-1}\tau_{\rm Ap}. \tag{4.183}$$

A2 Resistive ballooning mode In the case of toroidal geometry, in which the gradient of magnetic field changes its sign along the magnetic-field line, the resistive ballooning mode appears [4.137]. For this case, the condition on nonlinear marginal stability, Eq. (4.105), provides the relation

$$\chi_{\rm N} = 2\alpha\eta_{\parallel}, \tag{4.184}$$

where $\alpha = Rq^2 d\beta/dr$. The parameter α for the normalized pressure gradient includes the geometric effect of toroidal plasmas [4.28]. Comparing Eqs. (4.182) and (4.184), one sees the common role of resistive dissipation in combination with the pressure gradient. The turbulent transport coefficient is increased by the pressure gradient.

In addition to the resistive interchange/ballooning mode turbulence, a variety of resistive turbulence has been investigated; e.g., rippling modes [4.138], resistive drift waves [4.139] and others.

A3 Current diffusive interchange/ballooning mode (CDIM/CDBM) When the plasma temperature becomes high, the dissipation associated with the parallel current is controlled not by the electric resistivity but by the current diffusivity [4.130, 4.134, 4.140-4.149]. The current-diffusive interchange mode turbulence, which is a submarginal instability, has been analyzed by solving the nonlinear dispersion relation with the noise source. Subcritical excitation is discussed in §4.3.5. The Nonlinear decorrelation rate and coherence length are given as

$$\tau_{\rm corr}^{-1} = \lambda_1 \cong \frac{C_0}{2(1-C_0)} G_0^{1/2} \tau_{\rm Ap}^{-1}, \tag{4.185}$$

and

$$\ell_{\rm CDIM} \cong s^{-1} G_0^{1/2} \delta, \tag{4.186}$$

where $\delta = c/\omega_{\rm p}$ and the numerical constant C_0 originates from the contribution of random noise source, Eq. (4.148). The spectrum of fluctuation energy is given as

$$E_1(k_\perp) = \frac{2}{(1-C_0)} G_0 k_\perp^{-3}, \tag{4.187}$$

for $k_\perp > k_* \cong s G_0^{-1/2} \delta^{-1}$ [4.150, 4.151].

In toroidal geometry, one has current-diffusive ballooning mode (CDBM) turbulence, instead of interchange mode (CDIM) turbulence. For this case, the turbulence decorrelation time is given as

$$\tau_{\rm corr} \propto \alpha^{-1/2}. \tag{4.188}$$

The role of pressure gradient in determining the turbulence decorrelation time is seen in Eq. (4.185) or (4.188). Figure 4.12(a) illustrates the influence of gradient on the

decorrelation rate. It is noticed that the wavelength of an unstable current-diffusive ballooning mode could be much longer than the collisionless skin depth, as is shown in [4.145]. The coupling with the drift wave has been studied [4.152]. This coupling reduces the growth rate, but the strong nonlinear instability still remains.

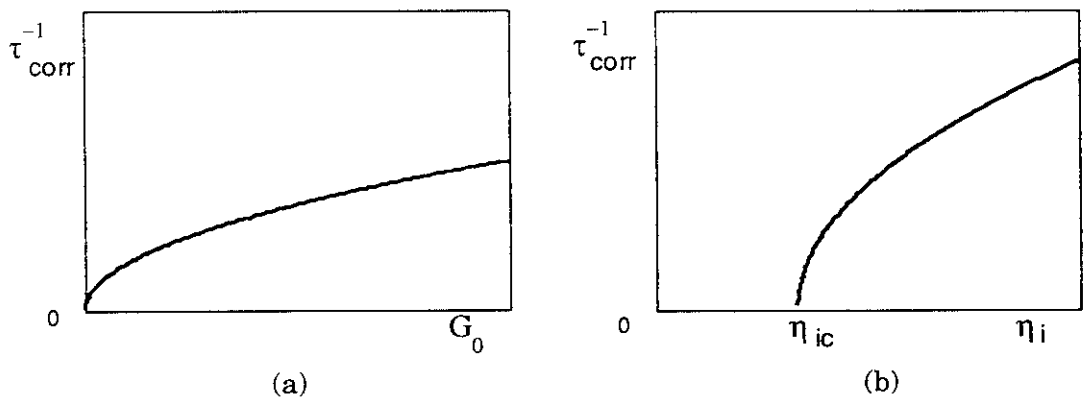

Figure 4.12. Turbulence decorrelation rate as a function of gradient. The case of current diffusive mode turbulence (a) and ion temperature gradient mode (b).

B Ion temperature gradient (ITG) mode The ion temperature gradient (ITG) mode becomes linearly unstable if the temperature gradient exceeds a threshold. Much work has been done [4.135, 4.153-4.155], and one estimate of the threshold is given as

$$\eta_{\mathrm{i}} \equiv \frac{L_n}{L_{T_{\mathrm{i}}}} > \eta_{\mathrm{ic}} = 0.5 + 2.5 \max\left[\frac{L_n}{R}, 0.2\right] \tag{4.189}$$

in toroidal plasmas [4.153]. Turbulence theories have been developed for the ITG mode.

The mode-coupling theory has provided a nonlinear dispersion relation [4.90] as

$$\omega\left\{\omega\frac{L_n}{c_{\mathrm{s}}} - \left[1 - k_{\perp}^2\rho_{\mathrm{s}}^2\left(1 + \frac{L_n}{L_T}\right) - 2\frac{L_n}{R}\right]\right\}\frac{L_n}{c_{\mathrm{s}}} + 2k_{\perp}^2\rho_{\mathrm{s}}^2\frac{L_n}{R}\left(1 + \frac{L_n}{L_T}\right)$$
$$- k_x^2\rho_{\mathrm{s}}^4\int_k^{\infty}\frac{dk'}{k'}(k' - k)(k'^2 + k^2)E(k') = 0. \tag{4.190}$$

The last term is the nonlinear interaction term and $E(k')$ is the fluctuation energy spectrum. The balance between the linear growth and nonlinear damping yields an evaluation of the stationary fluctuation level as

$$\left\langle\left(\frac{e\tilde{\phi}}{T_{\mathrm{e}}}\right)^2\right\rangle \cong \frac{1}{k_x^2 L_n^2}\frac{L_n}{R}\left(1 + \frac{L_n}{L_T}\right) \tag{4.191}$$

with

$$E(k) \propto k_{\perp}^{-3}. \tag{4.192}$$

For the range of $k_\perp \rho_s \sim 1$, the nonlinear decorrelation rate is estimated by $\Gamma_{corr} \cong \gamma_L$ with

$$\gamma_L \cong \frac{c_s}{\sqrt{RL_n}} \sqrt{\eta_i - \eta_{ic}}, \tag{4.193}$$

and is given as

$$\Gamma_{corr} \cong \frac{c_s}{\sqrt{RL_n}} \sqrt{\eta_i - \eta_{ic}}, \tag{4.194}$$

where $\eta_i = L_n/L_T$ [4.154]. Further elaboration of the mode-coupling theory is discussed in Ref. [4.17]. Figure 4.12(b) illustrates the decorrelation rate as a function of the temperature gradient.

It is noted that the linear eigen mode in toroidal geometry has a wavelength in the radial direction which is much longer than the ion gyroradius [4.156, 4.157]. However, this does not mean that the correlation length of the motion of a fluid element is much longer than the ion gyroradius.

C Electron temperature gradient (ETG) mode The origin of ITG mode instability is an effective negative compressibility owing to the ion temperature gradient as is shown by Eq. (4.16). The phase relation between density and pressure perturbations for ITG mode is given by the relation

$$\frac{\tilde{p}_i}{\bar{n}_i \bar{T}_i} \propto \left(1 - \frac{\omega_{*T_i}}{\omega}\right) \frac{\tilde{n}_i}{\bar{n}_i}. \tag{4.195}$$

A negative compressibility means that the pressure perturbation can be negative at a phase that the density perturbation is positive. A similar mechanism works for electrons in the presence of their temperature gradient. The mode in the range of

$$k_\perp \rho_e \sim 1 \tag{4.196}$$

becomes unstable if the electron temperature gradient exceeds a criterion. This instability is called the electron temperature gradient mode (ETG mode) [4.135]. Stability analyses have been made for slab plasmas [4.135, 4.158, 4.159] and in toroidal plasmas [4.160]. The stability boundary for the toroidal ETG mode is approximately given as

$$\eta_e \equiv \frac{L_n}{L_{T_e}} > \eta_{ec} = \frac{2}{3} + 2 \max\left[\frac{L_n}{R}, \frac{1}{3}\right] \tag{4.197}$$

from Fig. 1 of [4.160].

The mode-coupling theory has been developed for this mode. In a saturated state, the nonlinear mixing rate $\Gamma_\perp$ is considered to balance with the linear growth rate γ_L, and is estimated as

$$\Gamma_\perp \sim k_\perp \rho_e \sqrt{2\left(\eta_e - \frac{2}{3}\right)} \frac{v_{the}}{\sqrt{L_n R}}. \tag{4.198}$$

The fluctuation level is also evaluated as

$$\tilde{p}_{\mathrm{e}} = \frac{1}{|k_x|}\left|\frac{d\bar{p}_e}{dx}\right|. \tag{4.199}$$

D Kinetic instabilities A nonlinear dispersion relation has also been derived for kinetic instabilities, by employing the renormalized kinetic dielectric tensor. For instance, for an electrostatic perturbation with the wavelength which is longer than the Debye length, the dispersion relation is approximated by the charge-neutrality condition

$$\mathbf{k}\cdot\sum_{s=\mathrm{i.e}}\boldsymbol{\sigma}_{s,k\omega}\cdot\mathbf{k}=0, \tag{4.200}$$

where the conductivity tensor $\boldsymbol{\sigma}_{s,k\omega}$ is calculated by use of the renormalized propagator. One example is quoted from the work of [4.161].

In the presence of magnetic shear, the path integral along the field line which appears in, e.g., Eq. (4.9), takes the form

$$\begin{aligned}&\int_{-\infty}^{t} dt' \exp\left[i\mathbf{k}\cdot(\mathbf{x}'(t')-\mathbf{x})-i\omega(t'-t)\right]\\ &\qquad\cong\int_0^{\infty} d\tau \exp\left[i(\omega-k_{\parallel}v_{\parallel})\tau-\Gamma_{\perp}\tau-(\Gamma_{\mathrm{s}\parallel}\tau)^3\right],\end{aligned} \tag{4.201}$$

where $\Gamma_{\mathrm{s}\parallel}$ is the decorrelation rate which is enhanced by the diffusive motion in the sheared magnetic field,

$$\Gamma_{\mathrm{s}\parallel}=\left[(k'_{\parallel}v_{\parallel})^2 D_{\perp}/3\right]^{1/3} \tag{4.202}$$

and $\Gamma_{\perp}=D_{\perp}k_{\perp}^2$ is the conventional decorrelation rate ($k'_{\parallel}=dk_{\parallel}/dr$). For rapidly moving electrons, the decorrelation rate $\Gamma_{\mathrm{s}\parallel}$ is much larger than $\Gamma_{\perp}$. The argument of the plasma dispersion function is modified as

$$Z\left(\frac{\omega}{\sqrt{2}|k_{\parallel}v_{\mathrm{th}}|}\right)\rightarrow Z\left(\frac{\omega+i\Gamma_{\mathrm{s}\parallel}}{\sqrt{2}|k_{\parallel}v_{\mathrm{th}}|}\right), \tag{4.203}$$

and a nonlinear dispersion relation with the random noise source neglected, is given as

$$\begin{aligned}\left(\frac{d^2}{dx^2}-\left\{\frac{1}{d}\left[2-\frac{\Lambda_0(\omega-\omega_*)}{\omega}\right]-\mu^2x^2\right.\right.\\ \left.\left.-\frac{\alpha_s(\omega-\omega_*)}{\omega x}Z\left(\frac{\omega+i\Gamma_{\mathrm{s}\parallel}}{\sqrt{2}|k_{\parallel}v_{\mathrm{the}}|}\right)\right\}\right)\phi(x)=0,\end{aligned} \tag{4.204}$$

where

$$x=\frac{r-r_s}{\rho_{\mathrm{s}}}, \tag{4.205a}$$

$$\Lambda_n=I_n(b)\exp(-b), \tag{4.205b}$$

$$b = k_\theta^2 \rho_\mathrm{i}^2, \tag{4.205c}$$

$$\alpha_s = \left(\frac{m_\mathrm{e}}{2m_\mathrm{i}}\right)^{1/2} \frac{L_s}{L_n}. \tag{4.205d}$$

$$d = (\Lambda_0 - \Lambda_1)\left(\frac{\omega + \omega_*}{\omega}\right) - 3i\left(\frac{\omega - \omega_*}{\omega_*}\right)\frac{\alpha_s^2 \Gamma_{\mathrm{s}\|}}{\omega_*}, \tag{4.205e}$$

$$\mu = \frac{L_n}{L_s}\frac{\omega_*}{\omega}\left[\Lambda_0\left(\frac{\omega + \omega_*}{\omega}\right)d^{-1}\right]^{1/2} \quad \text{for the case of} \quad T_\mathrm{e} = T_\mathrm{i}. \tag{4.205f}$$

Here, r_s denotes the mode rational surface on which $k_\|$ vanishes, and L_S is the magnetic-shear length being defined as $L_s = Rr^{-1}q^2(dq/dr)^{-1} = qRs^{-1}$. This nonlinear dispersion relation provides the stationary state

$$D_\perp \sim 15\left(\frac{m_\mathrm{e}}{m_\mathrm{i}}\right)^{3/2}\left(\frac{L_s}{L_n}\right)^{7/2}\frac{c_\mathrm{s}\rho_\mathrm{s}^2}{L_n}. \tag{4.206}$$

E Influence of magnetic-field structure

E1 Drift due to the magnetic-field gradient As is illustrated in the previous subsections, the structure of the magnetic field is very influential on plasma turbulence. Particular emphasis has been imposed on the role of the magnetic shear. When the magnetic shear is strong, the fluctuations tend to be localized near the mode rational surface, so that the turbulence level is suppressed. When the magnetic shear changes its sign, the turbulence is affected as well.

Figure 4.13 illustrates the effect of the magnetic shear in toroidal plasmas. The drift orbit of trapped particles, which forms a banana orbit in the poloidal cross section, drifts in the toroidal direction. If the magnetic shear is positive:

$$\frac{dq}{dr} > 0, \tag{4.207}$$

the distance of toroidal motion is larger when the particles stay in the outer magnetic surface, i.e., the toroidal curvature drift increases. The toroidal drift direction coincides with the diamagnetic drift direction, so that the magnetic drift in the bad magnetic curvature increases. On the contrary, if the magnetic shear is negative:

$$\frac{dq}{dr} < 0, \tag{4.208}$$

the toroidal drift is reduced [4.87].

Another issue is the large toroidal shift. When the shift of inner magnetic surface becomes larger, owing to the higher plasma pressure, the magnetic-field line, in the bad magnetic curvature region, becomes shorter. The gradient-B drift in the destabilizing direction becomes smaller on average. See [1.35, 4.27].

Through these mechanisms of reduction of unfavourable toroidal drift, the turbulence level and turbulent transport coefficient reduce in the case of negative magnetic shear and large Shafranov shift.

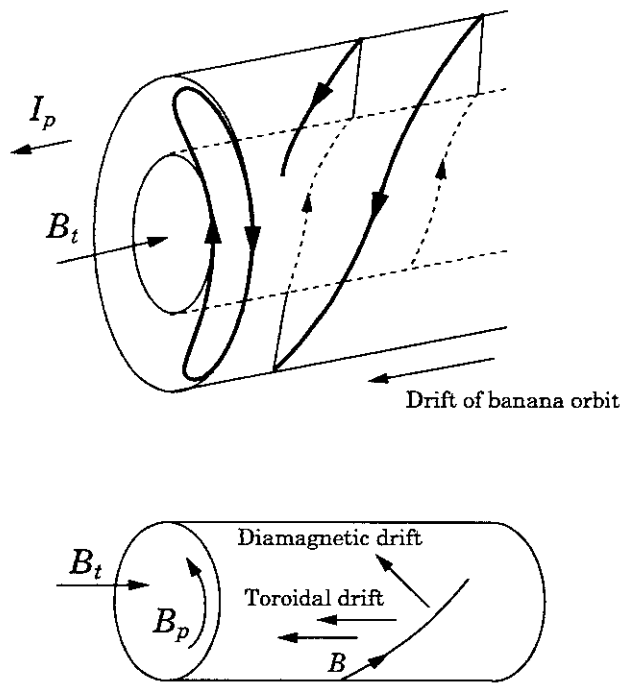

Figure 4.13. Trajectory of an ion in toroidal plasma. Orbit of banana particle is illustrated together with its projection on the poloidal cross section. When the magnetic-field shear is positive, the toroidal drift is in the same direction as the diamagnetic drift.

E2 Trapped particle instability The growth rate of the trapped ion instability is estimated as

$$\gamma_{\rm L} \cong \left(\frac{r}{R}\right)^{1/4} \sqrt{\omega_* \omega_{\rm M}}, \tag{4.209}$$

where $\omega_{\rm M} = k_\zeta V_{\rm D}$, k_ζ is the mode number in the toroidal direction, and $V_{\rm D}$ is the drift due to the gradient of magnetic field (see Fig. 4.13). As a result of the reduction of the gradient-B drift velocity $V_{\rm D}$, the growth rate is reduced in the case of negative magnetic shear. The control of cross-section shape leads to a similar result [4.162, 4.163].

E3 Toroidal ion-temperature-gradient (ITG) mode A simple analytic limit of the dispersion relation for the ion-temperature-gradient (ITG) mode in toroidal plasma is

given as

$$\frac{k_\parallel^2 v_{\rm thi}^2}{\omega^2} + k_\perp^2 \rho_{\rm i}^2 + \frac{\omega - \omega_{*\rm i}}{\omega - \omega_{*\rm i}(1 + L_n/L_T)} - \frac{\omega_{\rm M}}{\omega}(\cos\theta + s\theta \sin\theta) = 0, \quad (4.210)$$

where θ is the poloidal angle. The drift owing to the magnetic-field inhomogeneity is reduced when the magnetic-field shear is negative. This causes a reduction of $\omega_{\rm M}$, decreasing the growth rate [4.164-4.166]. The growth rate is illustrated in Fig. 4.14 [4.164]. The additional impact of weak magnetic shear has been pointed out. In weak magnetic shear, the distance between adjacent rational magnetic surfaces becomes longer. As a result of this, the perturbation extends on the magnetic surface. This effect further decreases the particle drift which is averaged over the eigenmode structure [4.167].

The influences of helical plasma shape on this instability has been studied, including the effect of helical ripples [4.168, 4.169].

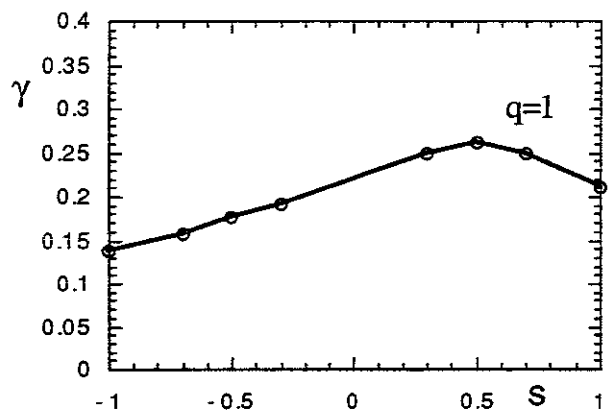

Figure 4.14. Growth rate of toroidal ion temperature gradient driven instability. In the negative shear region, growth rate becomes smaller. (Reproduced from [4.164].)

E4 Current diffusive ballooning mode (CDBM) turbulence This effect of negative magnetic shear is also effective to the MHD-like turbulence. The ideal MHD ballooning instability appears at high-pressure gradient. The critical pressure gradient for instability becomes higher when the magnetic shear becomes negative. It is often called the *second stability* regime [4.28-4.30]. This reduction of free energy for ballooning mode influences the turbulence. The current diffusive ballooning mode (CDBM) turbulence becomes weaker if the magnetic shear is negative [4.145, 4.170, 4.171].

4.3.2. Global flow driven by turbulence

A $E \times B$ transport and magnetic transport

A1 $E \times B$ transport The global flux of a certain quantity is calculated by use of a cross-correlation functions. In magnetized plasmas, the cross-field velocity is governed by the $E \times B$ drift velocity ($\mathbf{E} = -\nabla\phi$) in the simple case of electrostatic perturbations. The flux of a quantity X across the magnetic surface, F_X, is given as

$$F_X = \frac{1}{\bar{B}} \left\langle ik_y \tilde{X} \tilde{\phi}^* \right\rangle \tag{4.211}$$

in terms of the cross-correlation function between $\tilde{X}$ and $\tilde{\phi}$. By determining the cross-correlation functions, the global heat flux is derived. A goal of analysis is to express the flux in terms of global parameters:

$$F_X = -\mu_X \nabla \bar{X} + F_{\text{rest}}, \tag{4.212}$$

where F_{rest} does not include $\nabla \bar{X}$. It is often called a 'pinch' term [4.172]. The pinch flux which is induced by the gradient of magnetic field in toroidal plasmas [4.173] is discussed in Appendix A.

In a quasi-linear approximation, the flux is expressed in terms of a quadratic function of the fluctuation amplitude. The phase relation between two quantities is related to the imaginary part of the linear propagator, Eq. (4.60). For the particle flux in the presence of a density gradient, one has

$$\begin{aligned} \left\langle i\tilde{n}^*_{s,k,\omega} \tilde{\phi}_{k,\omega} \right\rangle = & -\Im \int \left[\frac{\omega - \omega_{*s}}{\omega - k_\parallel v_\parallel} J_0 \left(\frac{k'_\perp v_\perp}{\omega_{cs}} \right) \bar{f}_s \right] dv \\ & \times \frac{e_s}{T_s} \left\langle \tilde{\phi}^*_{k,\omega} \tilde{\phi}_{k,\omega} \right\rangle \qquad (s = \mathrm{e}, \mathrm{i}). \end{aligned} \tag{4.213}$$

This estimate is valid within a weak turbulence theory. That is, it holds only for the particular cases that satisfy Eq. (4.27). In usual circumstances, the nonlinear modification of the propagator is important. The evaluation of the global flux requires result from the nonlinear theory of plasma turbulence.

The simplest nonlinear argument is to consider the balance between the linear growth rate γ_{L} and the turbulent decorrelation rate $Dk_\perp^2$, Eq. (4.80). This balance gives an estimate

$$D \cong \frac{\gamma_{\mathrm{L}}}{k_\perp^2}. \tag{4.214}$$

This is a mixing length estimate explained in §3. A non-Markovian effect is discussed in [4.107], and the correction due to it is proposed as

$$D \cong \frac{\gamma_{\mathrm{L}}^2}{\omega_k^2 + \gamma_{\mathrm{L}}^2} \frac{\gamma_{\mathrm{L}}}{k_\perp^2}, \tag{4.215}$$

where ω_k is the real frequency of a linear mode.

The result Eq. (4.214) captures a certain aspect of unstable plasma. However, the characteristic rate of turbulence generation, which is the physical origin of the numerator of Eq. (4.214), could be different from the linear growth rate in strong turbulent plasmas. The use of the linear growth in the mixing-length estimate [Eq. (4.214)], which is called the Kadomtsev formula, might not be relevant in turbulent plasmas. Examples of nonlinear analysis are illustrated in this subsection.

A2 Magnetic braiding and transport When magnetic perturbations exist and Eq. (4.59) is satisfied, braiding of magnetic surfaces occurs, and the trajectory of magnetic-field line is subject to diffusion as

$$\langle [x(\ell) - x(0)]^2 \rangle = D_{\rm M} \ell, \tag{4.216}$$

where ℓ is the distance along the field line and $D_{\rm M}$ is called the magnetic-field diffusion coefficient. Magnetic-field fluctuations are characterized by two correlation lengths, the one in the direction of the unperturbed field line, $\ell_{c,\parallel}$, and the one across the magnetic-field line $\ell_{c,\perp}$ ($\ell_{c,\parallel}$: Euler view of correlation length). The correlation length along the *perturbed* magnetic-field line $L_{\rm ac}$, that determines $D_{\rm M}$ as $D_{\rm M} = (\tilde{B}_r/B)^2 L_{\rm ac}$, depends on the relative magnitude of perturbation $\tilde{B}_r/B$. In weak turbulence, one has $L_{\rm ac} = \ell_{c,\parallel}$. In the strong-turbulence case, the auto-correlation length $L_{\rm ac}$ is estimated by

$$L_{\rm ac} \cong \ell_{c,\perp} \left(\frac{\tilde{B}_r}{B} \right)^{-1}. \tag{4.217}$$

The diffusion coefficient of magnetic-field line is given as

$$D_{\rm M} = \begin{cases} \ell_{c,\parallel} (\tilde{B}_r/B)^2 & \text{for} \quad \tilde{B}_r/B < \ell_{c,\perp}/\ell_{c,\parallel}, \\ \ell_{c,\perp} (\tilde{B}_r/B) & \text{for} \quad \tilde{B}_r/B > \ell_{c,\perp}/\ell_{c,\parallel}. \end{cases} \tag{4.218}$$

The small-amplitude limit is the one in a quasi-linear formula, and the large amplitude limit is the strong turbulence case.

The response of plasma transport to stochastic magnetic fields has been discussed [4.4, 4.174-4.179]. The case of low collisionality is surveyed, i.e., $\nu^{-1} > \tau_{\rm t}$ and $\nu^{-1} \gg \tau_{\rm dec}$, where $\tau_{\rm t}$ is the transit time of particles, $\tau_{\rm t} = L_{\rm ac}/v_{\rm th}$, and $\tau_{\rm dec}$ is the decorrelation time of plasma due to the cross-field diffusion, which may be determined by various processes in addition to this magnetic braiding. In this simplified situation, the transport coefficient due to the magnetic stochasticity is given as [4.176]

$$\chi \cong \frac{\tau_{\rm dec}}{\tau_{\rm t}} (v_{\rm th} D_{\rm M}) \qquad \text{if} \quad \frac{\tau_{\rm dec}}{\tau_{\rm t}} \leq 1, \tag{4.219a}$$

$$\chi \cong v_{\rm th} D_{\rm M} \qquad \text{if} \quad \frac{\tau_{\rm dec}}{\tau_{\rm t}} > 1. \tag{4.219b}$$

For the given correlation lengths, $\ell_{c,\perp}$, $\ell_{c,\parallel}$, and $L_{\rm ac}$, and the amplitude of magnetic fluctuations, the diffusion coefficient for each species depends on the ratio $\tau_{\rm dec}/\tau_{\rm t}$ as well.

When the cross-field decorrelation time $\tau_{\rm dec}$ is determined by the magnetic perturbation (e.g., high temperature electrons in a braided magnetic region), the relation $\tau_{\rm dec} = \tau_{\rm t}$ holds. More complex formulae in general circumstances are summarized in [4.13] and [4.176, 4.177]. Super-diffusion can possibly occur due to the accelerator modes that is discussed by use of the mapping model (§4.2.5). In addition, a subdiffusive behaviour has also been found for stochastic magnetic fields [4.180].

The turbulence amplitude usually depends on the renormalized transport coefficients of the plasma. It is necessary to determine the correlation length and time, $L_{\rm ac}$ and $\tau_{\rm dec}$, and the amplitude $\tilde{B}_r/B$ simultaneously.

B Heat flux The energy flux is given by the formula in the electrostatic limit as

$$q_x = \frac{-1}{\bar{B}} \left\langle \tilde{p}^* \nabla_y \tilde{\phi} \right\rangle . \tag{4.220}$$

An application of the statistical approach in §4.2.3 is illustrated here. A decomposition of the fluctuating fields, e.g., Eq. (4.145), allows to relate the cross-correlation functions $\langle f_j' f_j^* \rangle$ and auto-correlation function $\langle f_1 f_1^* \rangle$. In the case of Eq. (4.145), there is a gradient of plasma pressure but no velocity gradient. In this case, one has

$$\bar{q}_x = - \left[\sum_k \frac{k_y^2}{\gamma_{\rm p} - \lambda_1} \left\langle f_{1.k}^{(1)*} f_{1.k}^{(1)} \right\rangle \right] \bar{p}' . \tag{4.221}$$

It is noted that the turbulence decorrelation rate λ_m and the eddy damping rate γ_j are given by the nonlinear balance. The cross-correlation functions are readily obtained, once the auto-correlation function $\langle f_1 f_1^* \rangle$ is given. One has an expression for the turbulent thermal conductivity, $\bar{q}_x = -\chi_{\rm turb} \bar{p}'$.

Three typical examples are shown; i.e., turbulence in the range of ion gyroradius [ion temperature gradient (ITG) mode], that in the range of collisionless skin depth [current diffusive interchange mode (CDIM)] and that in the electron gyroradius [electron temperature gradient (ETG) mode]. The inhomogeneities of pressure and magnetic-field strength are the primary origin of driving fluctuations. The influence of the shear of flow (i.e., inhomogeneous radial electric field) is discussed in §4.3.4.

Under many circumstances, the turbulent heat flux caused by pressure gradient dominates the dissipation $\sum_X F_X \nabla(\bar{X}^{-1})$ [e.g., the left hand side of Eq. (4.49)]. The 'pinch terms' in fluxes of other quantities could become noticeable without making the total dissipation negative. If one takes the example of drift waves, the flux of perpendicular electron energy is much larger than that of parallel electron energy [4.181], and an inward pinch of particle is deduced.

B1 ITG mode A case of ITG mode turbulence has been analyzed. As is illustrated in an argument of scale invariance theory, §4.2.2D, the transport coefficient has the

dimensional form of $\chi \cong c_s\rho_s^2/R$ (λ_I scales with c_s/R and ℓ_c is of order ρ_s.) It is given as

$$\chi_{ITG} = \frac{c_s\rho_s^2}{R} F\left(q, s, \frac{r}{R}, \frac{L_n}{L_T}, \frac{T_e}{T_i}, \cdots\right), \tag{4.222}$$

where the factor $F(q, s, r/R, L_n/L_T, T_e/T_i, \cdots)$ denotes a geometrical factor. One model has been proposed by taking this fact into account as [4.153]

$$\chi_{ITG} = 14\left(\frac{T_i}{T_e}\right)^{3/2} \sqrt{\frac{R(1-\eta_{ic}L_T/L_n)}{L_T}} \frac{c_s\rho_s^2}{R}. \tag{4.223}$$

Other models which have been proposed for the ITG-mode turbulence are listed in, e.g. [4.15]. The inward pinch of particles is discussed in relation to the ITG mode [4.182].

It is again noted that the characteristic step size of motion due to the ITG mode is not necessarily longer than the ion gyroradius, even though the radial wavelength is much longer than the gyroradius. The result in [4.156] and those in numerical simulations [4.165, 4.183] suggest that the radial wavelength is of the order of $\sqrt{a\rho_i}$. For the turbulence level of Eq. (4.40), the eddy turn-over time is estimated as $\sqrt{a/\rho_i}L_n c_s^{-1}$, which is much longer than the characteristic coherent time of turbulence, $L_n c_s^{-1}$. The Kubo number is given as

$$\mathcal{K} \sim \sqrt{\rho_i/a}, \tag{4.224}$$

and is much smaller than unity, if $\mathcal{K}$ is evaluated by use of the linear wavelength. In this case, the radial coherence length of random motion remains of the order of ion gyroradius, and the thermal conductivity has a scaling property like Eq. (4.223). The coherence length of the turbulent field in the Eulerian view is not always relevant for the step size of random motion. For the step size, one may choose the correlation length of the fluctuating motion (Lagrangian view), which can be different from the one-time coherence length.

B2 CDIM Fluctuations in the range of the collisionless skin depth are also important for plasma transport [4.130-4.134]. Fluctuations could be self-sustained even in the linearly stable situation. The mechanism for the nonlinear instability is discussed in §4.3.5. Such turbulence belongs to a family of electromagnetic turbulence, and its typical time scale is given by the poloidal Alfvén transit time τ_{Ap}. The CDIM leads to the characteristic coherence length and nonlinear decorrelation rate, Eqs. (4.186) and (4.185), and the turbulent transport coefficient is estimated as [1.35, 4.98]

$$\chi_{turb} \sim \frac{1}{(2-C_0)}\frac{1}{s^2} G_0^{3/2} \frac{\delta^2}{\tau_{Ap}}. \tag{4.225}$$

In the limit of small magnetic shear, $s \to 0$. Eq. (4.225) converges to a large but finite value as [4.184]

$$\chi \sim \left| \frac{q}{d^2q/dr^2} \right| G_0 \frac{\delta a}{\tau_{\rm Ap}}. \tag{4.226}$$

B3 ETG mode Among short wavelength fluctuations, the electron temperature gradient (ETG) mode could be important for energy transport [4.135]. The characteristic scale length and time rate are give by the electron gyroradius $\rho_{\rm e}$ and the electron transit time $R/v_{\rm the}$, respectively. The transport coefficient is given as

$$\chi_{\rm ETG} = \frac{v_{\rm the}\rho_{\rm e}^2}{R} F\left(q, s, \frac{r}{R}, \frac{L_n}{L_T}, \frac{T_{\rm e}}{T_{\rm i}}, \cdots\right). \tag{4.227}$$

Comparing Eqs. (4.223), and (4.227), one sees that a typical form for the ETG mode, $v_{\rm the}\rho_{\rm e}^2/R$, is about $\sqrt{m_{\rm e}/m_{\rm i}}$ times smaller than $\chi \cong c_{\rm s}\rho_{\rm s}^2/R$ for the ITG mode.

Several discussions have been given for possible higher transport coefficient. The linear growth rate is maximum in the range of Eq. (4.196). However, the estimate (4.214) is maximum in a longer wavelength region of collisionless skin depth. If one employs the collisionless skin depth as a decorrelation length, a possible high transport coefficient has been studied in [4.158-4.160]. For example, [4.160] gives

$$\chi_{\rm ETG} = \frac{c\rho_{\rm e}}{\omega_{\rm pe}} \frac{v_{\rm the}}{L_{T_{\rm e}}} \tag{4.228}$$

from random $E \times B$ motion, and

$$\chi_{\rm ETG} = \frac{r}{qR} \left(\frac{c}{\omega_{\rm pe}}\right)^2 v_{\rm the}, \tag{4.229}$$

owing to the stochastic motion induced by magnetic perturbations. The latter is independent of the gradient length of electron temperature, and has a similar dependence on the collisionless skin depth, as in the CDBM turbulence. This is because the collisionless skin depth is chosen as a relevant length.

In addition, the ETG mode induces a streamer [4.185], which is able to enhance the geometrical factor $F(q, s, r/R, L_n/L_T, T_{\rm e}/T_{\rm i}, \cdots)$ for the ETG mode. The direct numerical simulation provides [4.186]

$$\chi_{\rm ETG} \sim 60 \frac{v_{\rm the}\rho_{\rm e}^2}{L_n}, \tag{4.230}$$

which is not far away from Eq. (4.223) in magnitude.

B4 Low or negative magnetic shear Associated with the reduction of the free-energy source, the turbulent transport coefficient is also reduced in the low or negative magnetic shear region of a tokamak plasma,

$$\chi_{\rm CDBM} = F(\alpha, s)\alpha^{3/2} \frac{\delta^2}{\tau_{\rm Ap}}. \tag{4.231}$$

The contour of thermal conductivity is plotted on a plane of pressure gradient and magnetic shear (Fig. 4.15).

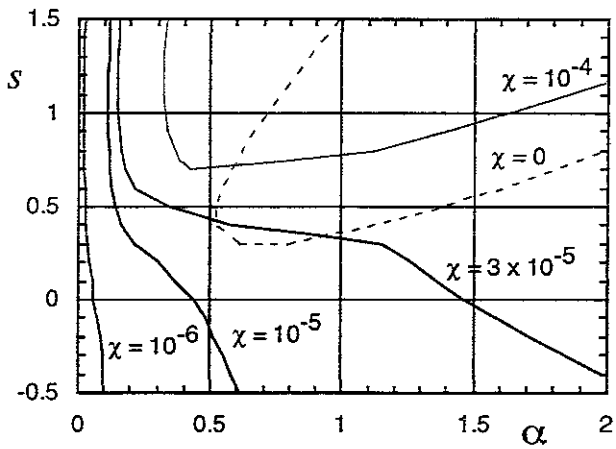

Figure 4.15. Contour of transport coefficient on the $s - \alpha$ plane, which is obtained from the numerical solution of nonlinear current diffusive ballooning mode. Normalized values for $\hat{\chi} = \tau_{\mathrm{Ap}} a^{-2} \chi$ are shown. For a fixed pressure gradient, the thermal diffusivity becomes smaller for the weaker magnetic shear. Dashed line indicates an instability boundary for linear ideal MHD ballooning modes [4.170].

It is pointed out that the connection length between the bad- and good-curvature regions for the resistive turbulence becomes shorter in the case of negative magnetic shear. This effect is favourable in reducing the turbulence level [4.187].

The influence of negative magnetic shear suggests that the current profile modifies the transport coefficients. If a magnetic shear is very weak (or negative), the geometrical factor to the turbulent conductivity becomes small. The influences of pressure profile and current profile are two keys for the structural formation in confined plasmas. Intensive analyses have been performed.

C Momentum flux and Reynolds stress The correlation between the momentum fluctuation and the radial velocity fluctuation determines the radial transport of momentum. The momentum flux induced by pressure-gradient driven turbulence could exist even in the limit of $\nabla \bar{V} \to 0$: the off-diagonal element of the transport matrix is important as well. The turbulent viscosity and spontaneous torque are discussed below. Then the convective cell formation through the parametric decay instability [4.188] is reviewed.

C1 Anomalous viscosity and spontaneous torque In the fluid picture of turbulence, all plasma particles are considered to respond in a similar way. In this case, the energy-

and momentum-transport coefficients are close to each other. That is, the turbulent Prandtl number is of order unity [4.189, 4.190]:

$$Pr^{\text{turb}} \cong 1. \tag{4.232}$$

This is in contrast to the case of kinetic instabilities, in which only selective particles that satisfy the resonance condition contribute to the turbulent fluxes. By employing a reduced set of equations, the flux of the perpendicular momentum in the radial direction, $\Pi^{\text{d}}_{\perp r}$, has been obtained. An example of CDBM turbulence has been expressed as [4.191]

$$\frac{\Pi^{\text{d}}_{\perp r}}{m_{\text{i}} n_{\text{i}}} = M_{11} \nabla \left(\frac{|\nabla \phi|}{B} \right) - M_{12} v_{\text{A}} \nabla \beta, \tag{4.233}$$

where M_{ij} is the (i, j) element of the transport matrix, and M_{11} is the shear viscosity $\mu_{\perp}$. The second term in the right-hand side is the off-diagonal transport. The off-diagonal element is driven by the asymmetry of propagation direction of perturbations. In this case, the rotation torque is induced by the pressure gradient. It is estimated as

$$\frac{M_{12}}{M_{11}} \sim \frac{1}{4q} \sqrt{\frac{m_{\text{i}}}{m_{\text{e}}}} \frac{c}{a \omega_{\text{p}}}. \tag{4.234}$$

The estimate of off-diagonal elements in Eq. (4.234) has also been given based on a $m = 1$ convection (m being the poloidal mode number) or loss of wave torque near the plasma periphery etc.

C2 Excitation of convective cell, zonal flow and streamer When turbulence is highly anisotropic, the coefficient μ_X in the flux–gradient relation

$$F_X = -\mu_X \nabla \bar{X} + F_{\text{rest}} \tag{4.235}$$

could be negative. That is, the turbulent-driven flux could enhance $\nabla \bar{X}$.

The generation of a convective cell by drift waves has been observed in numerical simulations [4.25, 4.192] and discussed by [4.24]. As has been shown by Eq. (4.13), there is a damped oscillation with $k_{\parallel} \cong 0$. The dispersion relation of drift waves, with finite-ion-gyroradius correction, is illustrated in Fig. 4.16. A decay instability [4.188] is possible for drift waves. Consider the case that there is a drift wave with wave number and frequency $(k_{\text{d.0}}, \omega_{\text{d.0}})$. This drift wave can decay into the convective cell with $(k_{\text{c}}, \omega_{\text{conv}})$ and the other drift wave with $(k_{\text{d.1}}, \omega_{\text{d.1}})$, if the conditions

$$\mathbf{k}_{\text{d,0}} = \mathbf{k}_{\text{c}} + \mathbf{k}_{\text{d.1}}, \tag{4.236a}$$

$$\omega_{\text{d.0}} = \omega_{\text{conv}} + \omega_{\text{d.1}} \tag{4.236b}$$

are satisfied (suffix d and c indicate drift wave and convective cell, respectively). As is seen from Fig. 4.16, the decay instability occurs in the vicinity of the peak of the dispersion curve of the drift wave.

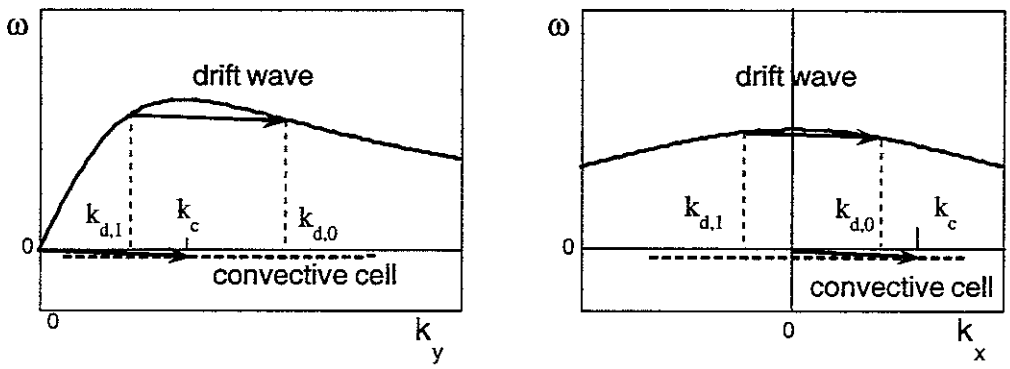

Figure 4.16. Decay process of the drift wave ($k_{\mathrm{d},0}$) into the convective cell (k_{c}) and drift wave ($k_{\mathrm{d},1}$). Dispersion relation for the drift wave (solid line) and that for the convective cell (dashed line) are illustrated. The case of streamer (left) and zonal flow (right).

The growth rate of the convective cell is expressed in terms of the amplitude of drift-wave fluctuations. Density and potential perturbations for drift and convective cell components are considered. They satisfy

$$\frac{\tilde{n}_{\mathrm{d}}}{\bar{n}} \cong \frac{e\tilde{\phi}_{\mathrm{d}}}{T_{\mathrm{e}}}, \tag{4.237a}$$

$$\frac{\tilde{n}_{\mathrm{c}}}{\bar{n}} \gg \frac{e\tilde{\phi}_{\mathrm{c}}}{T_{\mathrm{e}}}. \tag{4.237b}$$

The parametric decay instability is analyzed below. Quasi-linear equations are deduced; a bi-linear correction of convective cell is kept in the linear dispersion of the drift wave, and the quasi-linear excitation of a convective cell by drift waves is considered. A model set of equations is

$$\left[\left(1-\rho_{\mathrm{s}}^2\nabla_\perp^2\right)\frac{\partial}{\partial t}+V_{\mathrm{d}.e}\frac{\partial}{\partial y}\right]\tilde{n}_{\mathrm{d}} = -\frac{T_{\mathrm{e}}}{eB\bar{n}}\left[\tilde{n}_{\mathrm{d}},\tilde{n}_{\mathrm{c}}\right], \tag{4.238a}$$

$$\left(\frac{\partial}{\partial t}-\mu_{\mathrm{c}}\nabla_\perp^2\right)\tilde{n}_{\mathrm{c}} = \frac{T_{\mathrm{e}}}{eB\bar{n}}\left[\tilde{n}_{\mathrm{d}},\rho_{\mathrm{s}}^2\nabla_\perp^2\tilde{n}_{\mathrm{d}}\right]. \tag{4.238b}$$

The growth rate of the convective cell amplitude is given as [4.24]

$$\gamma_{\mathrm{conv}} = \gamma_{\mathrm{decay}} - \mu_{\mathrm{c}}k_{\perp,\mathrm{c}}^2 \tag{4.239}$$

with

$$\gamma_{\mathrm{decay}} = \gamma_{\mathrm{dec},s} \equiv \frac{T_{\mathrm{e}}}{eB}\left|\mathbf{k}_{\mathrm{d},0}\times\mathbf{k}_{\mathrm{d},1}\right|\sqrt{\frac{\left(k_{\mathrm{d},0}^2-k_{\mathrm{d},1}^2\right)}{k_{\mathrm{c}}^2}}\left|\frac{\tilde{n}_{\mathrm{d}.0}}{\bar{n}}\right| \tag{4.240}$$

for the case of the strong decay instability. If the decay instability is weak, one has

$$\gamma_{\rm decay} = \frac{\gamma_{\rm dec.s}^2}{\mu_\perp k_{\perp d2}^2}. \tag{4.241}$$

When the wave vector is directed in the radial direction, $\mathbf{k}_c \cong (k_r, 0, 0)$, one has a zonal flow. In the case of $\mathbf{k}_c \cong (0, k_\theta, 0)$, one has a streamer.

D Resistivity and current diffusivity Turbulent resistivity is an important element that dictates the plasma dynamics, in particular, for the evolution of magnetic field. If one takes the diffusion of magnetic flux and current into account, the Ohm's law takes the form

$$\bar{\mathbf{E}} + \bar{\mathbf{V}} \times \bar{\mathbf{B}} = (\eta_c + \eta_{\rm turb})\bar{\mathbf{J}} - (\lambda_c + \lambda_{\rm turb})\Delta_\perp \bar{\mathbf{J}}. \tag{4.242}$$

In the presence of $E \times B$ convective nonlinearlity, the anomalous resistivity $\eta_{\rm turb}$ and current diffusivity $\lambda_{\rm turb}$ are estimated as (see, e.g., [1.35, 4.130])

$$\eta_{\rm turb} \cong \mu_0 \chi_{\rm turb} \tag{4.243}$$

and

$$\lambda_{\rm turb} \cong \mu_0 \left(\frac{c}{\omega_p}\right)^2 \chi_{\rm turb}. \tag{4.244}$$

In the case of magnetic turbulence, one has

$$\lambda_{\rm turb} \cong \frac{\sqrt{\pi}}{2}\mu_0 \left(\frac{c}{\omega_p}\right)^2 v_{\rm the} D_M \sim \mu_0 \left(\frac{c}{\omega_p}\right)^2 \chi_{\rm turb,e}, \tag{4.245}$$

where D_M is given by Eq. (4.218) [4.193-4.197]. The resistivity is less affected by the magnetic perturbations and remains as

$$\eta_{\rm turb} \cong \mu_0 \chi_{E\times B}, \tag{4.246}$$

where $\chi_{E\times B}$ is a turbulent diffusivity due to the turbulent $E \times B$ motion [4.193]. An upper bound for the turbulent resistivity has been discussed for the reversed field pinch (RFP) plasmas. See Appendix D.

Off-diagonal elements in the transport matrix could also be important for the electromotive force. The global electromotive force that drives a global current is influenced by the pressure gradient, but the influence is found to be small in tokamaks [4.198]. The electromotive force which is caused by the velocity inhomogeneity has been investigated, with the name of γ or cross-helicity dynamo. The latter process is discussed in §3.4.

4.3.3. Generation of structure in flow In inhomogeneous plasmas, a spontaneous radial electric field is generated and induces transitions [4.199]. The transition involving the radial electric-field structure was found to be essential in the transport phenomena of plasmas. There are many processes that induce the radial electric field, and much work has been done on this processes, e.g.. [4.199-4.207].

A Break down of ambipolarity of turbulent flow It is often argued that the turbulence-driven particle flux is ambipolar in a steady state [4.13]; in other words, the turbulent transport does not continue to induce a radial electric field. This is not correct. The turbulence-driven flux does generate a radial electric field, causing a variety of nonlinear dynamics of plasma turbulence [1.35].

It is worth noting the momentum-conservation relation is associated with the perturbation-driven flux. One has the rate of change of the wave momentum as

$$\frac{\partial}{\partial t} P_{\text{wave},y} = -(\mathbf{J} \times \mathbf{B})_y. \tag{4.247}$$

This relation is derived with an assumption that there is no flux of wave momentum across a surface of the region over which an average is taken. Injection of torque by radio-frequency (rf) waves is discussed in [4.208-4.211]. In the stationary state, $\partial P_{\text{wave},y}/\partial t = 0$ holds, and the momentum-balance equation leads to an ambipolar condition

$$J_x = \sum_s e_s \Gamma_{s,x} = 0 \tag{4.248}$$

so long as an *average in a certain region* is treated. The basis and validity of ambipolarity is discussed in [4.212, 4.213].

It should be noted that the ambipolarity does not necessarily hold as the local balance. The flux is calculated as an *average within a small plasma volume*. In general, the wave can propagate in the direction of the gradient ($\hat{x}$-direction) and the local momentum balance does not hold in each region. Momentum exchange between the different magnetic surfaces can take place as is discussed in the following chapters. In such a case, local charge neutrality does not hold.

B Generation of zonal flow by drift-wave turbulence The perturbation amplitude of the convective cell (including the zonal flow and streamer) is constant along the field line. If one calculates the average of density (or potential) over some flux tube, the contribution from drift waves (and other waves) is averaged out, but that from a convective cell remains finite. The excitation of convective cell, zonal flow and streamer, is interpreted as the occurrence of a structure with meso-scale. *Meso-scale* [4.214] means that the characteristic scale length is longer than fluctuating turbulence, but is shorter than the system size. The mechanism of flow generation has an analogy to the magnetic dynamo. The generation of a small-scale DC radial electric field, i.e., a convective cell,

has been confirmed by numerical simulations [4.192]. A DC radial electric field could be generated in a global scale, and this process has also been confirmed by numerical simulations [4.215-4.220]. See also discussions in [4.221, 4.222].

The generation of the flow by electrostatic turbulence is briefly discussed here. The generation through MHD turbulence, in which the global gradient of the current is the source of torque, is explained in §3.4.

One can extend the analysis of Eq. (4.238) to the nonlinear evolution equation with respect to the amplitude of a convective cell [4.223]. Note that Eq. (4.238) is linear in the amplitude of the convective cell. If one employs a simple assumption that the drift-wave fluctuations are in a stationary state, the action

$$N_k \equiv \frac{\mathcal{E}_k}{\omega_k} \propto (1+k_\perp^2)^2 |\tilde{\phi}_k|^2 \tag{4.249}$$

is conserved. For a conserved quantity the ray-tracing equation holds. A detailed description of the ray-tracing equation is given in , e.g., [4.224]. It is applied to dift waves as

$$\frac{\partial}{\partial t} N_k + \frac{\partial \omega_k}{\partial \mathbf{k}} \frac{\partial}{\partial \mathbf{x}} N_k - \frac{\partial \omega_k}{\partial \mathbf{x}} \frac{\partial}{\partial \mathbf{k}} N_k = 0 \tag{4.250}$$

(see also [4.225]). In the case of zonal flow generation, $\mathbf{k_c} \cong (k_r, 0, 0)$, one has

$$\frac{\partial}{\partial t} V_c - u \frac{\partial}{\partial r} V_c - b \frac{\partial}{\partial r} V_c^2 - \gamma_{\rm conv} V_c = 0, \tag{4.251}$$

where the coefficients for the convective term and the nonlinear term are given as

$$u = \frac{1}{B^2} \int d^2k \frac{k_\theta^2 k_r}{(1+k_\perp^2)^2} \left(\frac{\partial \omega_k}{\partial k} \right)^{-1} \frac{\partial N_k}{\partial k_r}, \tag{4.252}$$

$$b = \frac{1}{2B^2} \int d^2k \frac{k_\theta^3 k_r}{(1+k_\perp^2)^2} \left(\frac{\partial \omega_k}{\partial k} \right)^{-1} \frac{\partial}{\partial k_r} \left[\left(\frac{\partial \omega_k}{\partial k} \right)^{-1} \frac{\partial N_k}{\partial k_r} \right]. \tag{4.253}$$

C Generation of poloidal flow by collisional processes The collisional process can also induce the poloidal rotation. The neoclassical transport theory, which is based on the small-gyroradius expansion with respect to the scale length, ρ_i/L_n, has shown that the particle flux remains to be almost ambipolar. The ambipolarity mechanism breaks down in neoclassical transport theory at the order of ρ_i^2/L_n^2 [4.44]. In the presence of steep radial gradients, which are relevant to the improved confinement phenomena in toroidal plasmas, the collisional process may drive the radial electric field and plasma rotation [4.199- 4.202, 4.206]. See reviews [1.22-1.35]. The spontaneous onset of poloidal rotation of a tokamak plasma in the framework of neoclassical theory is given in, e.g., [4.226] and related work is also found in [4.227, 4.228].

The source due to the collisional process is added to Eq. (4.251)

$$\frac{\partial}{\partial t}V_c - u\frac{\partial}{\partial r}V_c - b\frac{\partial}{\partial r}V_c^2 - \gamma_{conv}V_c = S_c. \tag{4.254}$$

The source term S_c could be a nonlinear function of the radial electric field (i.e., the flow velocity V_c). Even in the limit of $n_d/\bar{n} \to 0$, i.e., without the drive by drift waves, Eq. (4.254) can show a bifurcation. The important roles of ion orbit loss, neutral particles, the ion transit time magnetic pumping, etc., have been investigated. In plasmas without toroidal symmetry like stellarators or helical systems, the neoclassical transport drives a strong radial electric field, inducing transitions [4.229, 4.230]. The interface of radial electric-field domain is also generated by the nonlinearlity in S_c. The electric domain interface is demonstrated in [4.231] and following work (see, e.g., [4.232]). Details are discussed in later subsections.

D Electric-field domain interface Equations (4.251) and (4.254) allow solitary structures of radial electric field and flow velocity. A soliton-like structure and a kink-soliton-like structure are obtained. A kink-soliton-like solution with the boundary conditions $V_c \to V_1$ at $r \to -\infty$ and $V_c \to V_2$ at $r \to \infty$ is given as

$$V_c = \frac{V_2 + V_1}{2} + \frac{V_1 - V_2}{2}\tanh\left[\ell_{zf}^{-1}(r - r_c)\right], \tag{4.255}$$

where $\ell_{zf} = b(V_1 - V_2)/(2\gamma_{conv})$ and r_c is the location of the knee of the kink [4.233]. The radial propagation velocity is of the order of drift velocity, $u \cong V_d = T_e/(eBL_n)$. Another example of a soliton-like solution which is induced by an external bias current is illustrated in Fig. 4.17 [4.234]. Generation of the plasma rotation by the torque of rf waves is discussed in [4.208-4.211].

A poloidal shock can occur [4.235-4.238]. In the case of a weak radial gradient limit, the poloidal flow (V_θ) is governed by the source rotating the plasma and by poloidal derivatives. An example of the V_θ equation is [4.238]

$$\frac{\partial}{\partial t}V_\theta + V_\theta\frac{1}{r}\frac{\partial}{\partial\theta}V_\theta - \frac{\mu}{2}\frac{1}{r^2}\frac{\partial^2}{\partial\theta^2}V_\theta = -\frac{F_\theta}{2}\sin\theta, \tag{4.256}$$

where $S_c = -(F_\theta/2)\sin\theta$ models the drive by an $m = 1$ component. The formation of poloidal shock has been obtained if the poloidal Mach number is close to unity.

E Streamer formation When a streamer is excited by drift wave fluctuations, $\mathbf{k}_c \cong (0, k_\theta, 0)$, it induces a modification of the density profile, which is estimated from the balance

$$D\nabla_\perp^2 N_{streamer} \cong V_{streamer}\nabla_\perp \bar{N}. \tag{4.257}$$

The deformed density contour is illustrated in Fig. 4.18. Figures 4.18(a) and (b) show schematically the potential perturbation and deformed density contour in toroidal plasmas. Detailed profile of the density deformation is given in Fig. 4.18(c).

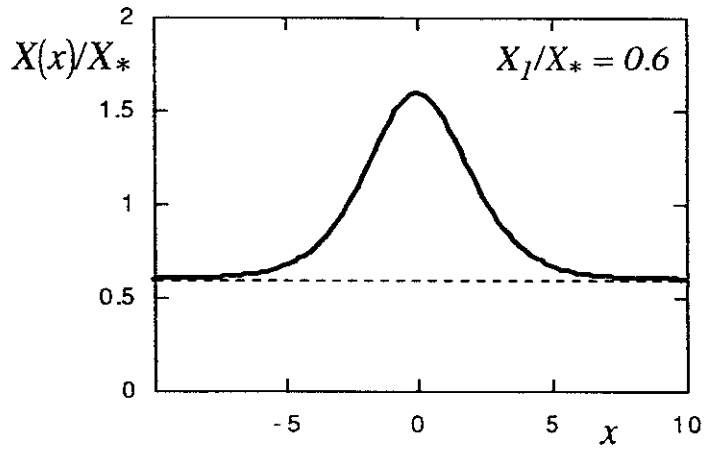

Figure 4.17. Solitary structure of radial electric field (electric field as a function of the normalized radius. Electric field is constant on the magnetic surface, and radial structure is illustrated. See [4.234] for the details.

The assumption of the conservation of drift-wave fluctuations [Eq. (4.192)] is an idealized simplification. The back-interaction for the drift wave allows nonlinear instabilities. This process is discussed in §4.3.5.

4.3.4. Flow-shear suppression A flow shear itself is a source of turbulence. However, if the flow shear exists together with a pressure gradient, being another source of turbulence, it may suppress the turbulence. A competition between the pressure gradient and flow shear is surveyed in a framework of linear stability. Then the suppression of turbulent quantities by the flow shear is discussed.

The influence of flow shear on the pressure-gradient-driven turbulence has attracted attention in the context of the improved confinement of plasmas [1.22-1.35].

A Linear stability in fluid dynamics Effects of shear and gravity on flow instability have been studied in fluid dynamics [4.239-4.241]. Gravity in the presence of a heat source can cause the Rayleigh–Bénard instability (Fig. 4.19a), and flow shear (Fig. 4.19b) may drive the Kelvin–Helmholtz (KH) instability. Their stability diagrams are shown in Fig. 4.20 [4.241]. The regions of Rayleigh–Bénard instability and Tollmein–Schlichting instability are dictated by the Richardson number

$$Ri \equiv \frac{Ra}{64Re^2Pr}, \tag{4.258}$$

where Ra is the Rayleigh number defined by Eq. (4.165). The transition from roll to wave structures occurs at $Ri = Ri_* \cong 10^{-5}$. When the velocity shear is weak and Reynolds number is small, the stability boundary for the Rayleigh–Bénard instability,

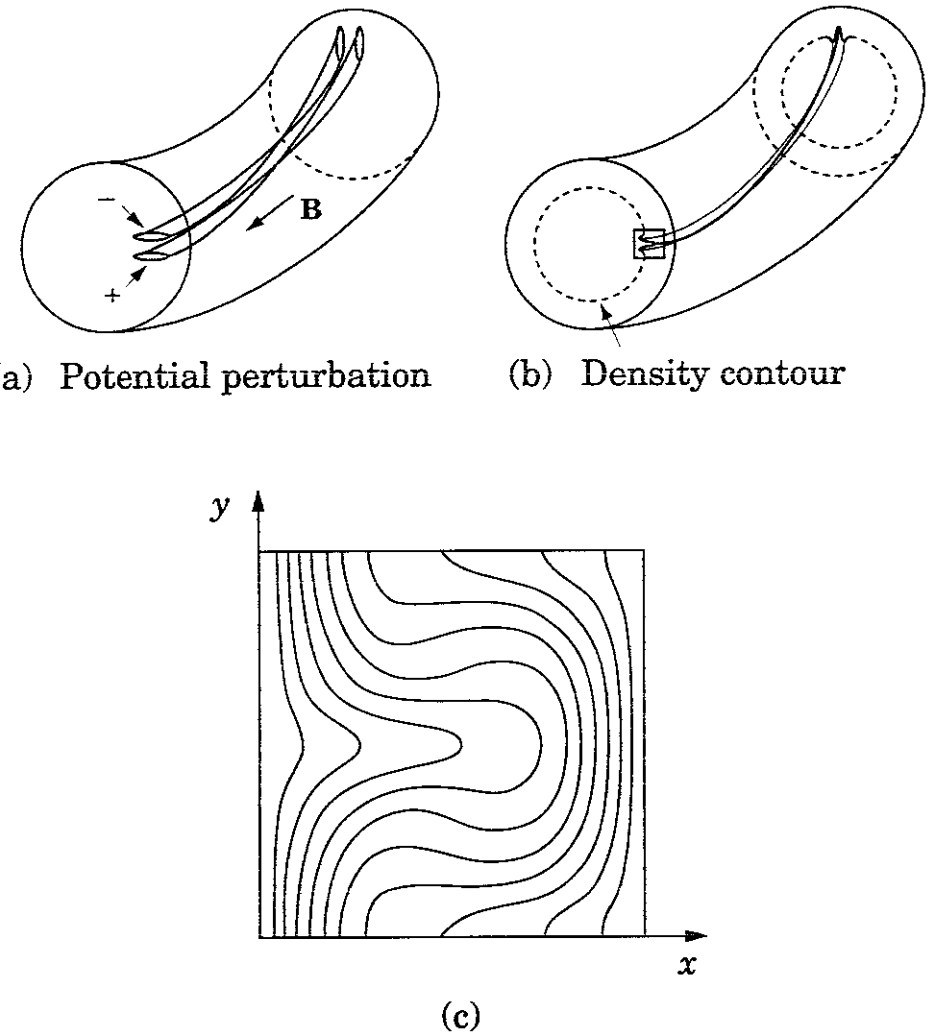

Figure 4.18. Illustration of density contour in the presence of streamer. The potential perturbation and deformed density contour in toroidal plasmas are shown in (a) and (b). Detailed profile of the density deformation [expand view of the region of thick square in (b)] is given in (c). Detailed illustration (c) is based on [1.31].

Ra_c, becomes higher due to the effect of shear flow as

$$Ra_c = Ra_{c,0}(1 + c_1 Re^2 + \cdots) \tag{4.259}$$

in the small-Re limit, where $c_1 \sim 10^{-1}$ for the case of Fig. 4.20. If the flow shear becomes too strong, the KH-type instability takes place.

B Linear stability in plasma dynamics Some mechanisms of linear stability, i.e., fluid-like response, Landau resonance, and drift reversal, are shown here as examples.

A flute mode is a typical example of plasma instability. In the presence of pressure gradient ∇p parallel to a 'gravity' g (either the real gravity or the centrifugal force due

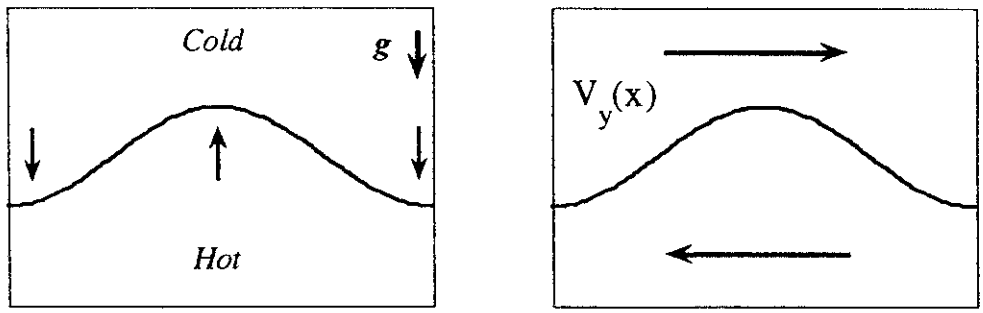

Figure 4.19. Rayleigh–Bénard instability in the gravity (a) and the Kelvin–Helmholtz (KH) instability in the sheared flow (b).

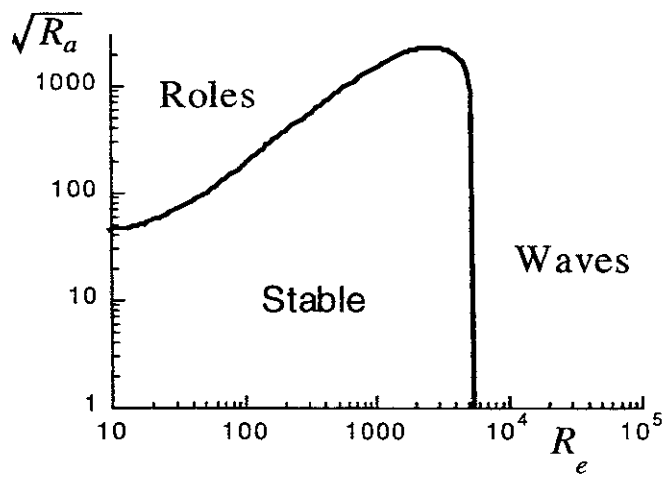

Figure 4.20. Stability diagram in the Poiseulle flow. in the presence of the heat source from the bottom. is given in the Rayleigh number - Reynolds number plane (Ra, Re). A case that the wave vector is in the direction of shear flow is reproduced from [4.241].

to the magnetic curvature) a fluid-like instability, the flute mode, can occur with its linear growth rate $\gamma_L \sim \sqrt{g/L_p}$ ($L_p = -n/n'$ for $\nabla T = 0$). When the electric field is radially inhomogeneous, the flow velocity is inhomogeneous and the growth rate is reduced [4.242]. An off-resonant type of stabilization is possible if the condition

$$|V'_{E\times B}| \sim \gamma_{L0} \tag{4.260}$$

is satisfied, where γ_{L0} is the linear growth rate in the limit of $V'_{E\times B} = 0$ [4.243-4.245]. This order-of-magnitude estimate is widely applicable for the *linear-stability* analysis.

Another type of stabilization mechanism is seen in a wave-particle resonance. Landau damping is one of the main mechanisms for instabilities, and can also be important as a nonlinear mechanism. The ion orbit is modified by the inhomogeneous

electric field, and Landau damping is expected to occur. A strong ion Landau damping takes place if the inhomogeneity is strong enough [4.246]:

$$\frac{L_{n2}\rho_{\rm i}eE_r'}{T_{\rm i}} \cong \frac{\omega}{k_\theta v_{\rm thi}}, \tag{4.261}$$

even for a flute mode with $k_\parallel \cong 0$.

The drift reversal of trapped particles due to an inhomogeneous electric field is also influential on a stability. The toroidal drift velocity of trapped ions is modified by a factor $(1+2u_g)$ where $u_g = \rho_p v_{\rm thi}^{-1} B_p^{-1}(dE_r/dr)$. If the condition $u_g < -1/2$ is satisfied, trapped particles drift as if a magnetic curvature were favourable. Owing to this modification, the growth rate turns to be

$$\Im(\omega) \cong (2\varepsilon)^{1/4}\sqrt{(1+u_g)\omega_{\rm Me}\omega_*}. \tag{4.262}$$

The trapped-ion mode is stabilized by a drift reversal in the range of

$$u_g < -1. \tag{4.263}$$

This stabilization mechanism has an asymmetry with respect to the sign of E_r' [4.247].

An inhomogeneity of the toroidal flow is also known to stabilize plasma instabilities. Effects of toroidal flow on various instabilities are seen in [4.248-4.251].

When the flow shear becomes too large, the KH-type instability may occur in the plasma. The competition between the flute instability and KH instability is illustrated in Fig. 4.21 [4.252]. In this model, an inhomogeneous $E \times B$ flow of the form $V_{E\times B} = V_0 \tanh(x/L_E)$ in the poloidal direction is imposed on the plasma. The influence of the shear flow on the linear growth rate is plotted on Fig. 4.21 for a given value of Δ_x/L_E (Δ_x and $\gamma_{\rm g}$ are the radial width and growth rate, respectively, of the resistive interchange mode in the absence of an inhomogeneous radial electric field). For a fixed pressure gradient, the flow shear first stabilizes the mode. In a strong flow-shear limit, the KH instability dominates, and a strong instability may appear.

C Suppression of turbulence

C1 Decorrelation rate As is explained by the model equation for a passive scalar quantity in the background fluctuations, the rapidly changing effects are included in the turublent transport coefficient in Eq. (4.93), as

$$\frac{\partial}{\partial t}\tilde{X} + \bar{V}_y(x)\frac{\partial}{\partial y}\tilde{X} - D\nabla^2\tilde{X} = \tilde{S}^{\rm ext}. \tag{4.264}$$

Owing to the inhomogeneous static flow, the stretching of test perturbations takes place, and statistical property is influenced. The turbulence level is suppressed by $\partial\bar{V}_y/\partial x$ (i.e., E_r' in magnetized plasmas), and is discussed in this subsection.

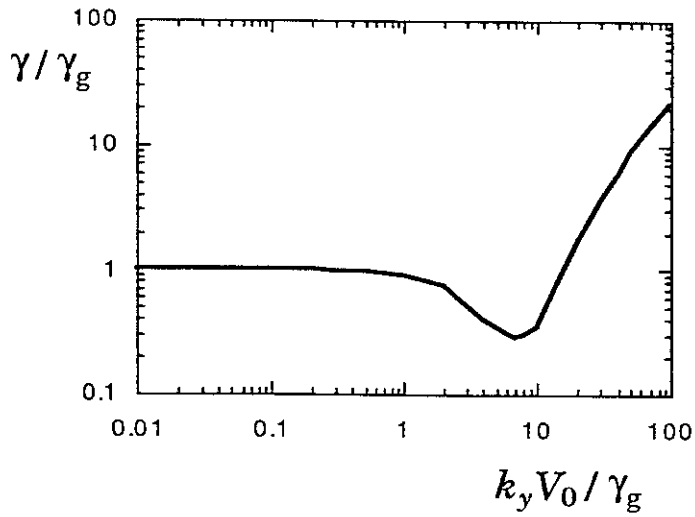

Figure 4.21. Linear growth rate of pressure-gradient-driven instability as a function of the flow shear for the case of $\Delta_x/L_E = 0.5$. (Quoted from [4.252].)

Figure 4.22 illustrates a sheared flow and the stretching of a fluid element. Its mean velocity in the y-direction (poloidal direction), which has a shear in the x-direction (radial direction), is expressed as

$$\bar{V}_y = S_v x \tag{4.265}$$

in local coordinates. The flow velocity shear is interpreted as

$$S_v = r\frac{d}{dr}\left(\frac{E_r}{Br}\right) \tag{4.266}$$

in a cylindrical geometry. Consider a deformation of an element which is circular at $t = 0$. After a time t, a circular element is stretched to an ellipse, in which the major axis has a length $L_l \cong \sqrt{L^2 + (LS_v t)^2}$. Since an area is preserved by this stretching, a length of minor axis is given as

$$L_\perp = \frac{L}{\sqrt{1 + S_v^2 t^2}}. \tag{4.267}$$

This result shows that the perpendicular wavelength, $k_\perp^{-1}$, of any mode is compressed due to the shear flow. The characteristic perpendicular wavenumber for the test field $\tilde{X}$ is effectively enhanced by a factor $(1 + S_v^2 t^2)$ [4.200, 4.253-4.255], $\ell_{\perp\mathrm{eff}}^{-2} = \ell_c^{-2}(1 + S_v^2 t^2)$. As a consequence, a decorrelation rate, τ_D^{-1}, which is defined by the relation

$$1/\tau_D \cong D\ell_{\perp\mathrm{eff}}^{-2}, \tag{4.268}$$

becomes larger for a given value of D by this increment of perpendicular wavenumber.

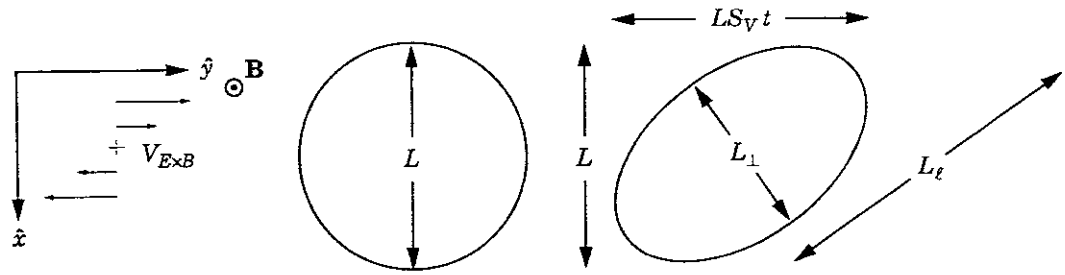

Figure 4.22. Flow in the y-direction, which is inhomogeneous in the x-direction, and the stretching of a fluid element.

The stretching of turbulent vortex, whose decorrelation time is τ_D, continues until the elapse time reaches τ_D. Substituting the relation $t = \tau_D$ into Eq. (4.267), an effective mode number $k_{\perp \text{eff}}$ (i.e., an inverse of decorrelation length) is estimated as

$$\ell_{\perp \text{eff}}^{-2} = \ell_c^{-2}(1 + S_v^2 \tau_D^2). \tag{4.269}$$

Substituting it into Eq. (4.268), we have the equation that determines a consistent decorrelation rate $1/\tau_D$ as

$$\frac{1}{\tau_D} = D\ell_c^{-2}(1 + S_v^2 \tau_D^2). \tag{4.270}$$

Depending on the magnitude of the flow shear, $|S_v|$, two limiting cases are derived from Eq. (4.270) as

$$\frac{1}{\tau_D} = \begin{cases} D\ell_c^{-2} + S_v^2 D^{-1} \ell_c^2 + \cdots & (|S_v| \ll D\ell_c^{-2}), \\ (D\ell_c^{-2})^{1/3} S_v^{2/3} & (|S_v| \gg D\ell_c^{-2}). \end{cases} \tag{4.271}$$

The limiting form of $\tau_D \sim (D\ell_c^{-2})^{-1/3} S_v^{-2/3}$ is similar to the one which was derived from the renormalization of the turbulent electron parallel motion in a sheared magnetic field [4.161]. This result [Eq. (4.271)] shows that a decorrelation due to the shear flow is effective if the flow shear rate S_v reaches a level $Dk_{\perp 0}^2$. If the diffusion coefficient D is constant, the relation $S_v \cong Dk_{\perp 0}^2$ is satisfied for the long-wavelength mode even when S_v is small. That is, the stabilization by shear flow is more effective for longer wavelength modes.

The reduction of the correlation length leads to the suppression of the fluctuation amplitude of the test field $\tilde{X}$. According to the statistical average in §4.2.2B1, $\mathcal{I} \sim \tau_D \lim_{\ell \to 0} \mathcal{S}^{\text{ext}}(\ell)$, the fluctuation intensity is

$$\frac{\langle \tilde{X}^2 \rangle}{\langle \tilde{X}^2 \rangle_{\text{ref}}} \cong \frac{1}{1 + S_v^2 \tau_D^2} \tag{4.272}$$

assuming that the magnitude of the source term $\lim_{\ell \to 0} \mathcal{S}^{\text{ext}}(\ell)$ is unaffected, where the suffix 'ref' indicates the reference case where $S_v = 0$. The Lorentzian correction

appears [4.200, 4.254, 4.255] In the large-shear limit, $\tau_{\rm cor} \sim (Dk_{\perp 0}^2)^{-1/3} S_v^{-2/3}$, reduced fluctuations were discussed. If one employs the mixing-length estimate, a similar reduction factor is expected for the diffusivity. A stochastic Doppler shift is also effective in reducing the turbulence level, as is shown in Eq. (4.89). This process has also attracted attention recently [4.74, 4.256].

C2 Turbulence level and turbulent transport These arguments on fluctuation level and transport, however, should not be taken as a conclusion. As was carefully discussed in [4.200], these analyses have been developed assuming that the basic properties of fluctuations (such as the wavenumber $k_{\perp 0}$ of a relevant mode and so on) are unchanged. These terms can also be functions of E_r and dE_r/dr. Effects of E_r and dE_r/dr, as a whole, can be simultaneously determined once the turbulence structure is properly solved. Numerical simulations have also revealed a subtle balance between various nonlinear interactions [1.28, 4.219].

Analyses have been performed for ITG modes, e.g., [4.17, 4.257-4.259]. An analytic formula has been used for the ion temperature gradient driven turbulence. For instance, a formula for the turbulent transport coefficient due to the ITG-mode turbulence has been proposed as [4.259]

$$\chi_{\rm turb} \cong \frac{(\gamma_{\rm L} - \omega_{E1} - \gamma_{*1})^{1/2} \gamma_{\rm d}^{1/2}}{k_y^2}, \tag{4.273}$$

where $\gamma_{\rm L}$ is the linear growth rate in the absence of flow shear, ω_{E1} is the $E \times B$ flow shear [4.260]

$$\omega_{E1} = \frac{r}{q} \frac{d}{dr} \left(\frac{qE_r}{rB} \right). \tag{4.274}$$

γ_{*1} is the shear of diamagnetic flow, $\gamma_{\rm d}$ is a damping rate of a representative beat mode, being approximated as

$$\gamma_{\rm d} \cong 0.3 (T_{\rm i}/T_{\rm e}) \omega_{\rm M} \tag{4.275}$$

($\omega_{\rm M}$: toroidal gradient-B drift frequency), and k_y is taken from the most unstable mode. The dependence of $\chi_{\rm turb}$ on ω_{E1} is adjusted to the observation of nonlinear simulation.

For the case of self-sustaining turbulence, thermal diffusivity has been derived for CDIM turbulence as [4.261]

$$\chi \sim \frac{1}{1 + 0.5 G_0^{-1} \omega_{E1}^2} \frac{G_0^{3/2}}{s^2} \left(\frac{c}{\omega_{\rm p}} \right)^2 \frac{v_{\rm Ap}}{a}, \tag{4.276}$$

where $\omega_{E1} = k_\theta \tau_{\rm Ap} E_r'/B$ and

$$\langle k_\perp^2 \rangle \propto (1 + 0.5 G_0^{-1} \omega_{E1}^2) G_0^{-1}. \tag{4.277}$$

As the gradient of the radial electric field becomes larger, the correlation length becomes shorter and the decorrelation rate becomes higher. In toroidal geometry (i.e., current-diffusive ballooning mode turbulence), the normalized parameter

$$\omega_{E1} = \tau_{\mathrm{Ap}} \frac{1}{srB} \frac{dE_r}{dr} \tag{4.278}$$

controls the turbulence level and turbulent transport [4.255]. The $E \times B$ flow-shear effect is more effective for the lower-magnetic shear case. This shear dependence is also found for ITG modes [4.17].

The electron-temperature-gradient (ETG) mode has a larger linear growth rate and shorter characteristic wavelength. This fact suggests that the $E \times B$ flow shear has a weaker effect in comparison with the ITG mode or the CDBM turbulence. It must be noted, however, that the streamer formation plays an important role for the transport by ETG modes. Streamers could be affected by the $E \times B$ shear and so the transport by ETG modes. This suggests that a further study is required for the transport due to shorter wavelength turbulence.

In addition to the inhomogeneity of flow across the magnetic surfaces, the inhomogeneity within the magnetic surface is also effective in suppression of turbulence. The toroidal flow in tokamaks varies in the poloidal direction if a hot-ion component exists. This poloidal dependence of toroidal flow suppresses nonlinear turbulence [4.262].

Some discussion has occurred on the dependence of χ_{turb} on ω_{E1}. The expression

$$\chi \propto \frac{1}{1 + (\omega_{E1}/\gamma)^h} \tag{4.279}$$

has been derived analytically with index h (γ: decorrelation rate or instability growth rate in the absence of $E \times B$ shear). The index was given as $h = 2$ in the models [4.200, 4.254, 4.255, 4.261] and $h = 2/3$ in the model [4.253]. These are analytic estimate: in toroidal plasma configuration, a nonlinear simulation has suggested a dependence such as Eq. (4.273) for ITG mode turbulence. A further elaboration of theory might be required to derive a formula which is relevant in a wide parameter region. The comparison of the index h with experimental observations has been reported [4.263] for the condition that the electric bifurcation is controlled by an external bias current [4.264]. Other examples are summarized in review article of [1.32].

4.3.5. Subcritical excitation Inhomogeneity-driven turbulence has larger amplitude at higher gradient. Turbulence can grow as an evolution of linear instabilities. On the other hand, there are many cases where turbulence is sustained under the condition for which a linear theory predicts the stability. Figure 4.23 illustrates a schematic relation between the fluctuation amplitude and driving parameter that represents the gradient of a system. This type of turbulence is called the submarginal turbulence or the subcritical excitation. Nonlinear theory has been developed for the study of such turbulence.

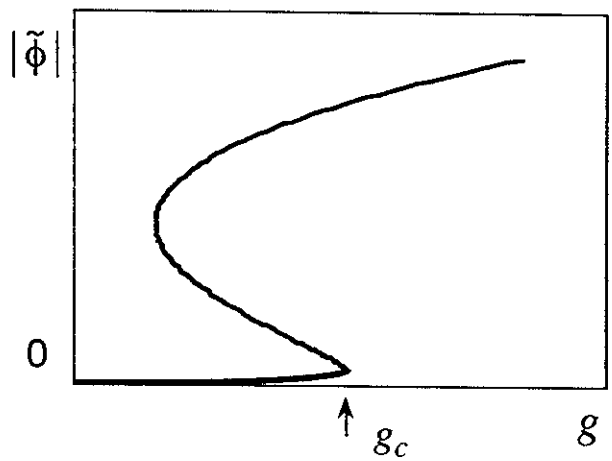

Figure 4.23. Excitation of submarginal turbulence. Steady-state amplitude of turbulence is illustrated as a function of the driving parameter g (e.g., pressure gradient, Reynolds number, etc.). g_c denotes the linear stability boundary. The lower branch is excited by thermodynamical excitations.

If a dynamical equation is expanded in a series of a perturbation amplitude $\tilde{A}$, the time evolution of $\tilde{A}$ may be written as

$$\frac{\partial}{\partial t}\tilde{A} = \gamma_{\rm L}\tilde{A} + N_1\tilde{A}^3 + N_2\tilde{A}^5 + \cdots. \tag{4.280}$$

From a symmetry consideration, one sees that only odd-order terms remain for symmetry-breaking perturbations. In the case of supercritical excitation, the mode is excited by the linear growth rate, $\gamma_{\rm L}$, and is suppressed by the low-order nonlinear effects $N_1\tilde{A}^3$ with $N_1 < 0$. However, in the case of subcritical excitation, nonlinear terms have a destabilizing influence (e.g., $N_1 > 0$, or $N_2 > 0$), so that a finite-amplitude solution may exist even in the regime of $\gamma_{\rm L} < 0$.

A Subcritical excitation in neutral fluid There are several examples of submarginal turbulence in fluids. First example is a plane Couette flow. Other famous examples are a plane Poiseuille flow and a pipe flow. The linear stability analysis has shown that a pipe flow is linearly stable. However, in reality, turbulence develops in a pipe flow if $Re > 2200$ holds. Nonlinear analysis is inevitable.

A1 Nonlinear marginal stability condition Analysis has been performed for a plane Poiseuille flow, by truncating the series of Eq. (4.280) at a certain order [4.265]. Figure 4.24 shows an example of the analysis in which the series of Eq. (4.280) is truncated. The nonlinear marginal stability boundary is illustrated in the space of the Reynolds number Re and perturbation amplitude $\tilde{A}$. A backward bifurcation is demonstrated. The growth rate of fluctuation becomes positive if the amplitude exceeds

the nonlinear marginal condition. It is possible that subcritical turbulence is sustained in a region where the linear stability is predicted. In addition, one must notice that the truncation at a finite order of $\tilde{A}$ is not a relevant approach. When the higher-order terms are retained in Eq. (4.280), one by one, the nonlinear marginal stability condition does not converge to an asymptotic limit, but oscillates considerably on the $(Re, \tilde{A})$ plane.

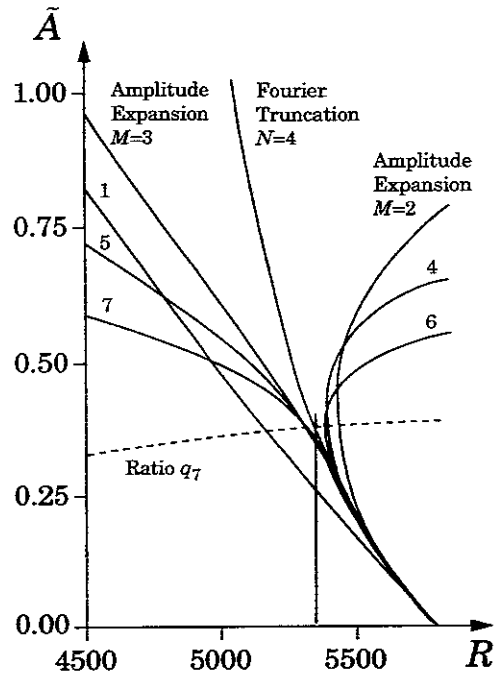

Figure 4.24. Nonlinear stability boundary for Poiseuille flow on $(Re, \tilde{A})$ plane. Reproduced from [4.265].

A2 Self-sustaining mechanism Subcritical turbulence has been studied by taking into account secondary-flow (roll) generation. When a planar flow is slightly deformed by the roll, the deformed two-dimensional flow has been known to be unstable for three-dimensional perturbations [4.266]. If the roll is driven by a three-dimensional perturbation, the self-sustaining instability is possible to occur. The idea of subcritical turbulence has been proposed by taking into account of secondary-flow generation.

Waleffe's model was proposed to study self-sustaining turbulence in shear flows ([4.267] and references therein). Consider a plane shear flow

$$\mathbf{V}_0 = [0, 0, U(x)]. \tag{4.281}$$

The x-axis is in the direction of inhomogeneity (the 'radial' direction), the y-axis is in the spanwise direction (the 'poloidal' direction), and the z-axis is in the direction of

flow. Note that coordinates are re-oriented for the convention of the plasma physics. Basic idea is to study effects of streaks, which is induced by the role-type instability. When the roll-type flow

$$\mathbf{V}_{\rm roll} = [V(x,y), W(x,y), 0] \tag{4.282}$$

(an analogue of a convective cell in plasma physics) exists, the streak,

$$\mathbf{V}_{\rm streak} = [0, 0, \delta U(x,y)]. \tag{4.283}$$

is induced by the convection. The simple shear flow $\mathbf{V}_0$ is linearly stable. However, the deformed shear flow, $\mathbf{V}_{\rm s} = [0, 0, U(x) + \delta U(x,y)]$ can be unstable against waves of the form

$$\tilde{\mathbf{V}} = [v(x) \sin k_y y, w(x) \cos k_y y, 0] \exp(ik_z z). \tag{4.284}$$

if the amplitude of the streak is large enough. By nonlinear interactions, the roll-type flow is induced by the wave-like perturbations.

This nonlinear chain is summarized in Fig. 4.25. The self-sustaining mechanism consists of three processes:

(i) advection of mean-flow shear by rolls (vortices) inducing a streak-like structure;

(ii) a linear instability occurs if the streak is strong enough; and

(iii) this instability enhances the roll, closing a nonlinear chain.

This model has a similarity to one of the mechanisms that has been proposed for submarginal plasma turbulence. In [4.267], a Lorenz-model-like equations with eoght variables are proposed, and a model with four variables is also discussed. The similarity of this nonlinear instability mechanism to those in plasma turbulence has been discussed in [1.31].

B Subcritical excitation in plasma turbulence The nonlinear excitation of instabilities is important in understanding dynamic events in plasmas. There are abundant observations on the abrupt excitation of strong perturbations in plasmas, which may not be explained by the growth of linear instabilities. See, for review, [4.268]. Self-sustained fluctuations and perturbations, in the parameter regime of linear stability, have been obtained by theories and numerical simulations [4.134, 4.144, 4.161, 4.269-4.286].

In plasmas, dissipation can induce varieties of instabilities as has been shown for MHD instabilities and drift instabilities. This might be in contrast compared to neutral fluids, where the dissipation-like viscosity and thermal conductivity usually stabilize the system. When the electron motion is impeded by a dissipation mechanism, the electron response deviates from the Boltzmann response ($\tilde{n}_{\rm e}/\bar{n} = e\tilde{\phi}/T_{\rm e}$), and the perturbed

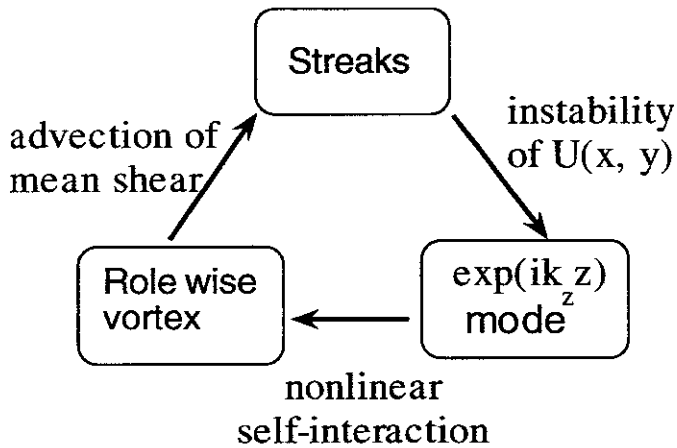

Figure 4.25. Subcritical excitation mechanism for shear-flow turbulence (based on [4.267]).

electric field appears on the magnetic surface. This mechanism drives instabilities. The stability property could be different in the presence of background turbulence, because the electron response is easily modified by turbulence. Subcritical excitation in the presence of dissipation is an important process for plasma turbulence. Examples include interchange-mode turbulence, drift-wave turbulence, tearing-mode excitation, and MHD turbulence.

B1 Current diffusive interchange mode (CDIM) turbulence The interchange mode is stabilized when it has a finite mode number along the magnetic-field line, $k_\parallel$. This is because the free electron motion along the magnetic-field line tends to neutralize the charge separation which is the origin of the instability. If this electron motion is impeded, the neutralization of charge separation is not perfect so that the instability occurs. The marginal stability condition, which is determined by the balance between excitation by the current diffusivity (i.e., electron viscosity μ_e) and damping by the viscosity μ and thermal conductivity χ was derived as [4.282]

$$\mathcal{I}_t \equiv \frac{G_0}{s^{4/3}} \left(\frac{\delta}{a}\right)^{4/3} \frac{(\mu_{e,N} + \mu_{e,c})^{2/3}}{(\chi_N + \chi_c)(\mu_N + \mu_c)^{1/3}} = \mathcal{I}_c, \tag{4.285}$$

where $\mathcal{I}_c$ is the critical Itoh number which is of the order of unity. Suffices N and c indicate the turbulent and collisional contribution, respectively.

As has been explained in §4.2.4C, turbulence could enhance all the transport coefficient $\mu_{e,N}$, χ_N, and μ_N. Equation (4.285) shows that the turbulent electron viscosity destabilizes the mode. In the small-amplitude limit of fluctuations, the destabilizing effect through the enhanced electron viscosity dominates the other nonlinear damping processes, leading to the nonlinear instability. The turbulent viscosity and thermal

conductivity suppress the turbulence. The nonlinear chain is illustrated in Fig. 4.26(a). There are both a similarity and a dissimilarity to the neutral fluid. The Rayleigh–Bénard convection is excited if the Rayleigh number [Eq. (4.165)] exceeds a critical value. Both the quantities $\mathcal{I}_t$ and Ra increase with the gradient of pressure or temperature, and decrease with increase of the viscosity and thermal-conductivity enhancement. In the case of this plasma turbulence, the increment of electron viscosity makes $\mathcal{I}_t$ larger and destabilizes the mode.

By expanding Eq. (4.285) near $G_0 \cong G_c$, which is the linear stability boundary, the amplitude $\tilde{\phi}$ near the marginal condition is given as

$$\tilde{\phi}^2 \cong -\frac{3\mu_{e,c}^2}{2}\left(\frac{G_0}{G_c} - 1\right). \tag{4.286}$$

where $\mu_{e,c}$ is the collisional electron viscosity. This result shows the existence of a backward bifurcation near the linear-stability limit. The fluctuation level as a function of the gradient is illustrated in Fig. 4.26(b).

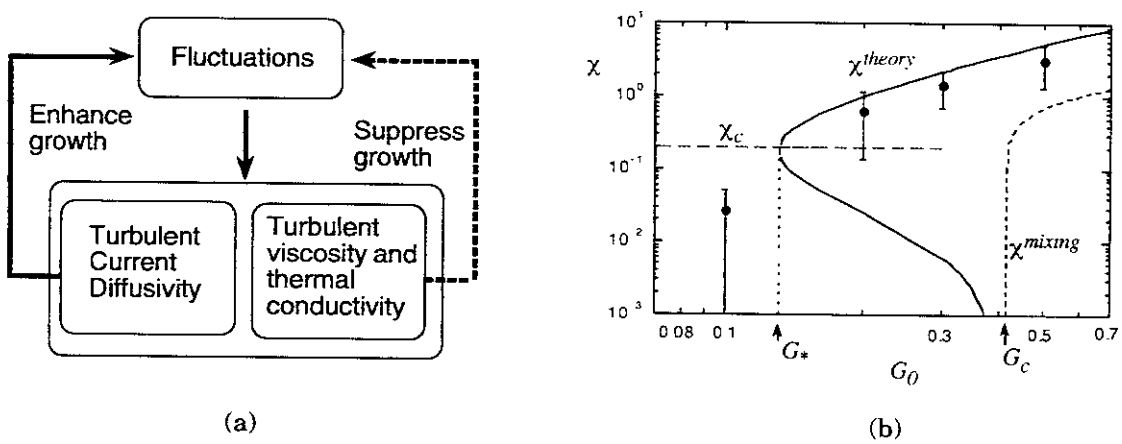

Figure 4.26. Mechanism of nonlinear instability for the CDIM turbulence (a). Turbulence fluctuation level as a function of the pressure gradient is shown in (b). Analytic theory (solid line) predicts the subcritical excitation, and the direct nonlinear simulation (dots) demonstrates the self-sustained turbulent state below the critical pressure gradient for linear instability [4.285].

B2 Nonlinear drift instabilities Drift waves are subject to nonlinear instabilities as well. Linear theories of drift waves in a slab geometry show that the various linear stabilizing and destabilizing mechanisms are nearly in balance, and the drift wave in a sheared magnetic field is stable (marginal at most) [4.287-4.291].

The nonlinear theory of drift wave in a sheared magnetic field has shown that the drift wave in a sheared magnetic field is unstable if the fluctuation amplitude is high

enough. The analysis based on Eq. (4.204) indicates that the mode is stable if $\Gamma_{s\|} = 0$ (linear theory), but that it is unstable if $\Gamma_{s\|}$ is large enough. The electron motion is impeded by the scattering by turbulence.

Another mechanism for the nonlinear excitation of drift wave has been recently proposed [4.281]. This is a nonlinear linkage that includes the excitation of a streamer by drift-wave turbulence, which is discussed in §4.3.3E. The nonlinear chain consists of:

(i) streamers ($k_\| \cong 0$, being a kind of convective cell) are induced by the drift waves ($k_\| \neq 0$), being associated with the strongly sheared radial flow (Fig. 4.18);

(ii) this system with a radial drift flow is unstable for the drift waves ($k_\| \neq 0$); and

(iii) the unstable drift waves regenerates streamers, closing the nonlinear link.

The mechanism is illustrated in Fig. 4.27.

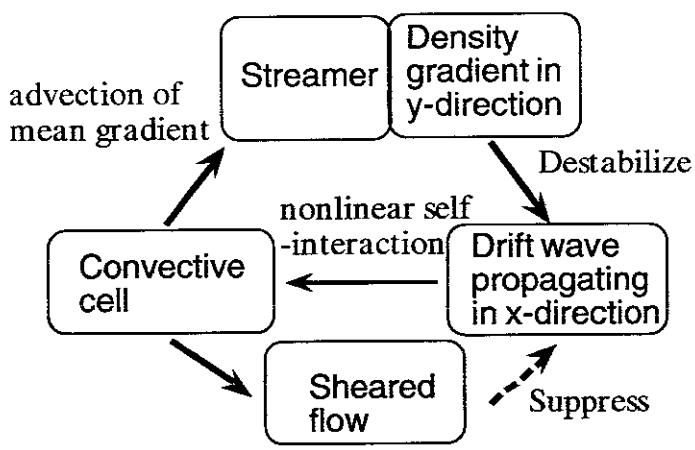

Figure 4.27. Nonlinear self-sustaining mechanism for the streamer and drift wave. A loop of solid lines is compared with Fig. 4.25.

A set of equations for the streamer and drift wave has been proposed [4.281]. A potential perturbation of the form

$$\tilde{\phi} = \phi_c \cos \pi y + (\phi_{d1} \cos \pi y + \phi_{d2} \sin 2\pi y) \sin k_z z \exp(ik_x x) \tag{4.287}$$

is considered, where ϕ_c is the streamer amplitude, ϕ_{d1} is the least stable drift wave, and ϕ_{d2} denotes the damped drift wave. The original density gradient is in the x-direction, but the density gradient appears in the y-direction, owing to the streamer formation. The drift wave in Eq. (4.287) is propagating in the x-direction, owing to the density gradient of streamer in the y-direction. The potential and density evolution equations for the streamer are

$$\frac{\partial}{\partial t}\phi_c = A_0 |\phi_{d1}|^2 \phi_c \tag{4.288}$$

and

$$\frac{\partial}{\partial t}\left(\frac{\partial \bar{n}}{\partial y}\right) = 2\pi o_{\rm c}. \tag{4.289}$$

where A_0 is the coefficient in the growth rate of convective cells in the limit of weak dissipative growth, Eq. (4.241). The complex growth rate of the drift wave is calculated by taking the lowest-order correction from the streamer as

$$\gamma\left(1 + k_\perp^2\rho_{\rm s}^2 + \frac{k_{i1}^2}{k_z^2}\gamma\right) = -\imath k_x \frac{\partial \bar{n}}{\partial y}. \tag{4.290}$$

From this set of equations, one sees the nonlinear linkage of self-sustainment: the drift wave causes the convective cell formation, the cell leads to the density streamer, the density gradient in the y-direction destabilizes the drift wave. Note that the normalizations in this model are $L_s = qR/s$ as the parallel scale length, the resistive scale length $L_\perp = [\nu_{\rm e}L_s^2\rho_{\rm s}^2/(\omega_{\rm ce}L_n)]^{1/3}$ as the perpendicular scale length, and $L_nL_\perp/(c_{\rm s}\rho_{\rm s})$ as the time scale.

The second-order correction from the streamer is the stabilizing influence of a sheared flow. The quasi-stationary state is considered, in which a balance holds between the destabilizing effect ($\partial\bar{n}/\partial y$ term) and the stabilizing effect ($\phi_{\rm c}^2$ terms) of the streamer on drift waves. This requires

$$\phi_{\rm c}^4 = \gamma_1 \frac{\partial \bar{n}}{\partial y}, \tag{4.291}$$

where the coefficient γ_1 is given by the nonlinear interaction terms, and its explicit formula is given in [4.281]. Combining Eqs. (4.289) and (4.291), one has an algebraic growth of the streamer amplitude as

$$\frac{\partial \bar{n}}{\partial y} \sim t^{4/3}. \tag{4.292}$$

This result shows that the submarginal drift-wave turbulence self-sustains in the presence of density gradient.

B3 Tearing mode at high pressure gradient Nonlinear destabilization is possible for large-scale instabilities in magnetized plasmas. When symmetry breaking current perturbation $\tilde{\mathbf{J}}_\parallel \propto \exp(im\theta - in\zeta)$ exists on a mode rational surface, $q = m/n$, the topology of the magnetic surface changes and magnetic islands appear at the location of the rational surface. Helical magnetic islands have a self-sustaining mechanism, and the subcritical excitation of them is possible.

The dynamics of the helical magnetic island is conveniently described by introducing a helical flux function $A_{\rm h} = A_\zeta + (nr^2/2Rm)\bar{B}_\zeta$, where the suffix h denotes the helical coordinate, $\ell = \zeta/q - \theta$. Magnetic perturbations are given as $\tilde{\mathbf{B}}_\perp = \hat{\mathbf{b}} \times \nabla\tilde{A}_\zeta$, and the

width of an island, w, is given as $w = \sqrt{(R/r)(q^2/q')\bar{B}^{-1}\tilde{A}_{\rm h}(r_s)}$, where r_s is the mode rational surface. The induction equation

$$\frac{\partial}{\partial t}\tilde{A}_{\rm h} = \eta_{\parallel}\tilde{J}_{\rm h} \tag{4.293}$$

governs the evolution of the perturbed fields. Once the relation between the perturbed current and the flux function is given as

$$\tilde{J}_{\rm h}(r_s) = F_J\left[\tilde{A}_{\rm h}(r_s)\right], \tag{4.294}$$

Eqs. (4.293) and (4.294) close the dynamical evolution.

In the presence of the current gradient $d\bar{J}_\zeta/dr$, an explicit relation of Eq. (4.294) is deduced [4.292]. Away from the mode rational surface, the perturbation approximately satisfies the MHD equilibrium equation, $\mathbf{J}\times\mathbf{B} = 0$, because the time evolution is much slower than the Alfvén time. That is, one has

$$\bar{B}_{\rm h}\Delta_\perp\tilde{A}_{\rm h} + \left(\frac{-d\bar{J}_\zeta}{dr}\right)\tilde{A}_{\rm h} = 0, \tag{4.295}$$

where $\bar{B}_{\rm h} = \bar{B}_\theta - \bar{B}_\zeta rn/(mR)$. The logarithmic derivative of this perturbation across the magnetic island

$$\Delta'(w) = \left[\frac{d}{dr}\ln(\tilde{A}_{\rm h})\right]_{r_s+w} - \left[\frac{d}{dr}\ln(\tilde{A}_{\rm h})\right]_{r_s-w} \tag{4.296}$$

is related to the perturbed current averaged on the magnetic island as (see, e.g., [4.4])

$$\tilde{J}_{\rm h}(r_s) \cong \frac{1}{\mu_0}\frac{\Delta'}{w}\tilde{A}_{\rm h}(r_s). \tag{4.297}$$

This relation is one of the explicit forms of Eq. (4.294). The combination of Eqs. (4.293) and (4.296) together with the relation $w \propto \sqrt{\tilde{A}_{\rm h}(r_s)}$ provides the temporal evolution equation as

$$\frac{\partial}{\partial t}\frac{w}{a} = \gamma_{\rm R}\cdot\Delta' a, \tag{4.298}$$

where the resistive diffusion rate $\gamma_{\rm R} = \eta_{\parallel}\mu_0^{-1}r_s^{-2}$ is characterized by the electric resistivity [4.292]. Δ' vanishes if the island width reaches the equilibrium value $w = w_{\rm eq}$. The growth of magnetic island is slow, if it is regulated by Eq. (4.298). Acceleration mechanism of the growth is discussed later in §4.3.5C. Note that the parameter Δ' at the zero island width, $\Delta'(0)$, dictates the linear stability:

$$\Delta'(0) > 0 \tag{4.299}$$

is the condition for the destabilization of linear tearing modes.

If there is an additional mechanism that the magnetic island induces the perturbed current $\tilde{J}_{\rm h}$, there could happen a nonlinear instability. Reference [4.270] has suggested

that local plasma heating or radiation loss drives a perturbation current as $\tilde{J}_{\rm h} \propto w^3$, giving the relation

$$\tilde{J}_{\rm h}(r_s) \cong \frac{1}{\mu_0}\frac{\Delta'}{w}\tilde{A}_{\rm h}(r_s) + N_{\rm rad} w^3, \tag{4.300}$$

where $N_{\rm rad}$ is a certain positive coefficient. The right-hand side can become positive if w becomes large enough even if $\Delta' < 0$. This result allows a self-sustained magnetic island even if the system is linearly stable, $\Delta'(0) < 0$.

Another origin for perturbed current is the Bootstrap current. The collisional diffusion process associated with the radial pressure gradient induces the toroidal current, which is known as Bootstrap current. When the magnetic island appears, the pressure gradient vanishes on it, causing the loss of Bootstrap current on the magnetic island [4.293, 4.294]. The perturbed current associated with this process has the form

$$\tilde{J}_{\rm h} \propto \frac{w^2}{w_0^2 + w^2}\beta_p', \tag{4.301}$$

where β_p' is the pressure gradient being normalized using the poloidal magnetic-field pressure. A finite width w_0 is introduced because the pressure flattening is not expected for $w < w_0$, because perpendicular diffusion tends to keep a finite pressure gradient [4.295]. This process may also induce a self-sustained magnetic island. The equilibrium island width is determined by the relation

$$\Delta'(w_{\rm eq}) - N_{\rm c,NC}\frac{w_{\rm eq}}{w_0^2 + w_{\rm eq}^2}\beta_p' = 0. \tag{4.302}$$

Detailed explanations including the coefficient $N_{\rm c,NC}$ is given in literature [4.293-4.300]. This mechanism is called the neoclassical tearing mode. Detailed analyses have been performed, including the effect of the polarization drift current. Figure 4.28 shows the saturated island width as a function of the driving parameter. Below the linear stability boundary, a self-sustained perturbation is possible for the case of a finite pressure gradient. Applications to tokamak plasmas are discussed in [4.301-4.304].

B4 Turbulence-turbulence transition (M-mode transition) Subcritical excitation of turbulence associated with magnetic braiding is also predicted. As is discussed in §4.2.4A2, the transport due to the magnetic braiding is more influential on electrons than ions. Hence, the electron viscosity is more pronouncedly enhanced than the ion viscosity once threshold condition, Eq. (4.59), is satisfied. The electron viscosity is selectively enhanced in Eq. (4.219a) so that the new nonlinear instability occurs.

First example is the onset of global stochasticity associated with $m = 1$ magnetic island. When the amplitude of an $m = 1$ magnetic island exceeds a critical size in toroidal plasmas, global stochasticity sets in. This is because that, when a helical perturbation is imposed on toroidal plasma, the system loses symmetry. If the symmetry

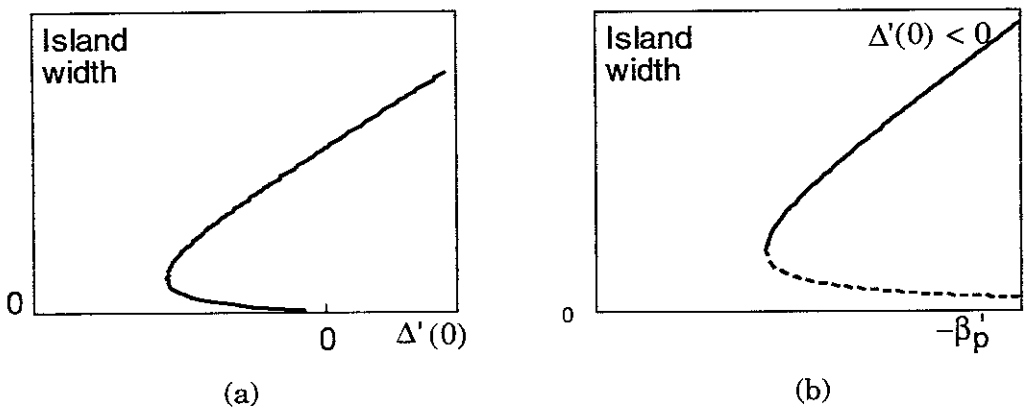

Figure 4.28. Saturation level of tearing mode perturbation, as a function of the MHD driving parameter $\Delta'(0)$ for fixed pressure gradient (a) and as a function of the pressure gradient for fixed value of $\Delta'(0)$ (b). Tearing mode is linearly stable if $\Delta'(0) < 0$. In the linearly stable case ($\Delta'(0) < 0$), a finite amplitude island is self-sustained if the pressure gradient becomes large enough. In (b), unstable branch of nonlinear marginal condition is denoted by dotted line, which is a threshold for subcritical excitation.

breaking is strong, the stochastization of the magnetic field may occur. This criterion is given as [4.305, 4.306]

$$\sqrt{2\left[\frac{1}{q(0)}-1\right]\frac{R\tilde{B}_r}{r\bar{B}}} > \frac{1}{7}. \tag{4.303}$$

When the magnetic perturbation grows and the criterion (4.303) is satisfied, the magnetic braiding and its associated enhancement of the electron viscosity switch on. By this onset of electron viscosity, nonlinear instability sets in. Dynamics of this instability is discussed in [4.144, 4.277].

The transition from electrostatic perturbation to turbulence with magnetic braiding occurs for the case of micro instabilities [4.307]. The case of the current-diffusive ballooning mode (CDBM) turbulence has been studied. It has been shown that, for the self-sustained current-diffusive turbulence in the low pressure gradient limit, the associated magnetic island width w_{is} scales as $w_{is} \propto \alpha^{3/2}$, while the island separation d_{is} scales as $d_{is} \propto \alpha^{1/2}$. Here, α is the normalized pressure gradient ($\alpha = -q^2 R d\beta/dr$). The Chirikov parameter, w_{is}/d_{is}, has a dependence on the pressure gradient as $w_{is}/d_{is} \propto \alpha^{1/2}$. When the pressure gradient becomes high and exceeds a criterion $\alpha > \alpha_c$ so that $w_{is}/d_{is} > 1$ holds, the magnetic stochasticity sets in. As a result, an enhancement of turbulence takes place, which induces a magnetic braiding. The turbulent transport coefficients for the case of CDBM are estimated as

$$\chi_i^M \cong \sqrt{\frac{m_i}{m_e}}\beta_i \alpha F(\alpha, s)\alpha^{3/2}\left(\frac{\delta^2}{\tau_{Ap}}\right), \tag{4.304a}$$

$$\chi_e^{\mathrm{M}} \cong \frac{m_i}{m_e}\beta_i \alpha F(\alpha, s)\alpha^{3/2}\left(\frac{\delta^2}{\tau_{\mathrm{Ap}}}\right), \tag{4.304b}$$

which are larger than Eq. (4.231). Superscript M stands for the magnetic braiding. This state is called the M-mode, and s is the magnetic shear parameter ($s = rq^{-1}dq/dr$). The condition for the onset of the M-mode is illustrated in Fig. 4.29.

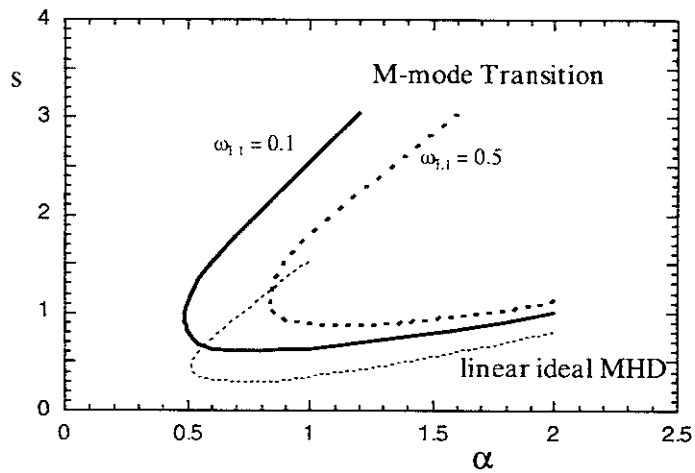

Figure 4.29. Region of M-mode turbulence in tokamak plasmas [4.307].

C Abrupt transition

C1 Microscopic turbulence and transport coefficient The time scale for the onset of H- to M-mode bifurcation, τ_{gr}, is of the order of the poloidal Alfvén time. During the transition, the magnetic-island overlap is associated with the nonlinear growth of turbulence. The time scale τ_{gr} is given by the inverse of the nonlinear growth rate, $\tau_{\mathrm{gr}} = \gamma_{\mathrm{NL}}^{-1}$, which was calculated as [4.307]

$$\gamma_{\mathrm{NL}}\tau_{\mathrm{Ap}} \sim s^{-1/3}F(s,\alpha)^{-1/6}\left[1 + s^2F(s,\alpha)\right]^{1/3}\alpha^{1/2} \tag{4.305}$$

for the M-mode transition in a strong-shear limit. This indicates that the typical time scale for the mode growth is given by $\tau_{\mathrm{Ap}}/\sqrt{\alpha}$. The change of turbulent transport coefficient at the critical condition for the turbulence-turbulence transition is a rapid process in comparison with the transport time. An abrupt growth of turbulence is predicted for a steep gradient [4.308]. These subcritical excitations for plasma turbulence are essential for understanding the dynamics of global structures.

C2 MHD modes Equation (4.298) predicts a slow growth of the resistive diffusion time. The acceleration of the MHD growth rate is possible in the presence of the scattering of electrons by turbulence [4.309]. Much faster growth, i.e., an explosive growth, is possible to occur. The nonlinear destabilization of global MHD modes, for which the growth rate is increased by a finite amplitude, shows an abrupt growth. The explicit dependence of the growth rate on the amplitude leads to the explosive growth of the mode, which is more violent than the exponential growth. If the growth rate is expressed in an asymptotic form as

$$\gamma \propto |\tilde{B}|^{\nu}, \tag{4.306}$$

then the mode amplitude shows the time evolution

$$|\tilde{B}| \propto \frac{1}{(t_0 - t)^{1/\nu}}. \tag{4.307}$$

An explosive growth occurs.

Typical examples are given for various cases. For instance, the interactions of the $m/n = 2/1$, $m/n = 3/2$, and $m/n = 5/3$ modes have been studied [4.310-4.315]. When the $m/n = 2/1$ and $m/n = 3/2$ islands overlap, then there appears a stochastic region near the rational surface $q(r_s) \cong 5/3$. The $m/n = 5/3$ mode is subject to tearing destabilization, whose growth rate is increased by the enhanced anomalous resistivity [$\nu = 3/4$ in Eq. (4.306)]. Nonlinear destabilization through the magnetic braiding is also obtained. After slow growth, the fast increment of the growth rate is recovered by the simulation. The change of the growth rate from the classical tearing mode to the nonlinear destabilization takes place in the event. For the case of current-diffusive MHD mode, one has $\nu = 2/5$ in Eqs. (4.306) and (4.307).

D Bubble formation and suppression by shear flow One of the typical phenomena of a subcritical excitation is a bubble formation. Flow shear is also influential on the transition phenomena like the bubble formation, which was analyzed in the neutral-fluid dynamics [4.316].

The bubble formation is strongly influenced by a shear flow. Two forces work on a bubble in a sheared flow: A shearing force $\bar{\mu} S_v$ tends to stretch a bubble ($\bar{\mu}$ being a coefficient of fluid viscosity). A surface tension $\bar{\sigma}/L$ acts to restore a spherical shape ($\bar{\sigma}$: a coefficient for surface tension, L: a size of bubble). See Fig. 4.30(a). If the shearing force is greater than the surface tension, $\bar{\mu} S_v > \bar{\sigma}/L$, the bubble is destroyed. A critical size above which a bubble collapses,

$$L_{\mathrm{cr}} = \frac{\bar{\sigma}}{\bar{\mu} S_v}, \tag{4.308}$$

can be found.

On the one hand, there is a critical (minimum) size for nucleation, $L_{\rm min}$, because the bubble formation is a subcritical phenomenon [4.317]. Below this size, a bubble does not grow and disappears with a finite life time even in the absence of sheared flow. The latter size is determined by a balance between the surface tension and the difference in the free energy inside of the bubble and the outer fluid. The free energy associated with the bubble formation is illustrated in Fig. 4.30(b). If the velocity shear is strong enough so that a condition

$$L_{\rm cr} < L_{\rm min} \tag{4.309}$$

is satisfied, then nucleation of the bubble is strongly suppressed. The condition $L_{\rm cr} < L_{\rm min}$ is rewritten as

$$S_v > \frac{\bar{\sigma}}{\bar{\mu} L_{\rm min}}. \tag{4.310}$$

As the critical size for the onset of nucleation, $L_{\rm min}$, becomes larger, the suppression by shear flow appears at the lower level of the flow shear rate.

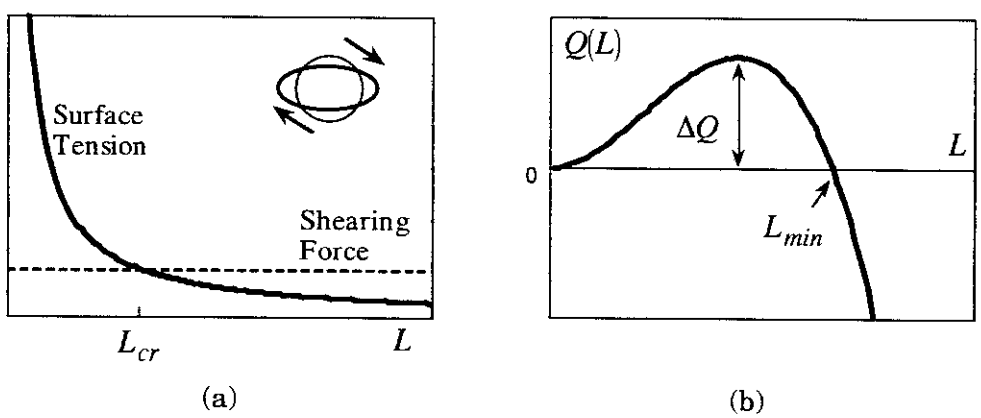

Figure 4.30. Shearing force and surface tension (per unit volume) vs bubble size (a). Free energy of bubble formation as a function of bubble size (b). Activation energy ΔQ and minimum size $L_{\rm min}$ for nucleation are shown.

4.4. Bifurcation

As is reviewed in previous subsections, one comes to the following view about turbulence in inhomogeneous plasma:

(i) Fluctuations do not follow the equi-partition law;

(ii) Various turbulent states exist;

(iii) The differences between turbulent states are seen:

(iii-1) not only from quantities such as the average spectrum and the dependencies on the global driving parameters and local plasma parameters,

(iii-2) but also by the difference in the associated dynamical and spatial structures, e.g., shape of global profile, meso-scale structure (interface), zonal flow or streamer, etc.

(iv) The change between turbulence happens in the short time of the nonlinear decorrelation rate, often being triggered by subcritical excitation.

These features suggest that the dynamical change of turbulence should be understood within the concept of bifurcation.

At the same time, the physics of *phase transition* may be extended for inhomogeneous plasmas which are away from thermodynamical equilibrium state. One way to extend physics of critical phenomena to turbulent systems is using the concept of structural transition. That is, the changes of global structure (gradient, symmetry, shape) are described simultaneously together with the turbulence spectra. The view of (iii) fits to this way of thinking, and the physics of turbulent plasma transition has been developed along this line of thought. The driving motivation has been the observation of the transition between the L-mode and H-mode [1.14].

The change of turbulence levels across a certain boundary in parameter space has been discussed. Self-organized dynamical oscillations have also been investigated. As is illustrated in Fig. 4.31, a transition between states A and B takes place. A case of subcritical excitation is shown as an example. The statistical properties of the turbulence are different from those for the thermodynamical equilibrium, so that the transition probability between different turbulent states is modified. An overview of various properties of bifurcations and transitions is given in the following. In this subsection, research in this direction is surveyed, with elucidating the non-equilibrium property of plasma turbulence.

4.4.1. System with hysteresis Under given inhomogeneities of global plasma parameters, turbulence and meso-scale structures develop according to the nonlinear self-regulating mechanisms. Figure 4.32 illustrates a typical concept: Figure 4.32(a) shows various structures in k space, and Fig. 4.32(b) demonstrates their mutual interaction processes. Micro-turbulence drives turbulent transports, possibly owing to nonlinear instabilities, and at the same time induces meso-scale structures such as the electric domain interface, zonal flow, solitary radial electric field, streamer, and so on. Some of them (like electric domain interface) tend to suppress turbulence, but others (like streamer) drive nonlinear destabilization of turbulence. According to the turbulent transport, the plasma profiles evolve, being controlled by external source and boundary conditions. Micro-scale fluctuations with a large number of positive Lyapunov exponents

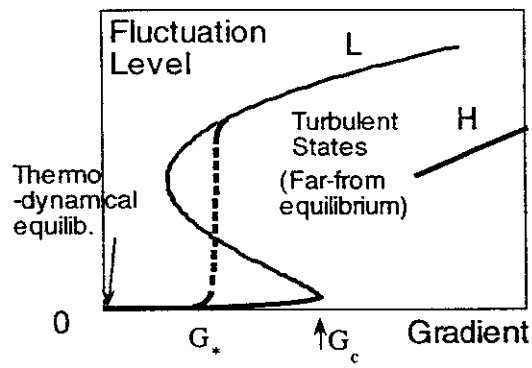

Figure 4.31. Bifurcation of turbulent state and transition between them. Two turbulent states ('H' and 'L') and thermodynamical equilibrium fluctuation are schematically shown.

exist in the turbulent state. meso-scale structures might be described by a system of a small degree of freedom. Combined dynamics of turbulence and chaos are expected to occur in inhomogeneous plasmas.

Another example is the mutual interaction of the plasma gradient and turbulent transport. In many circumstances. the pressure gradient is the origin of turbulent transport (e.g., Fig. 4.12), which has a feedback effect on the pressure gradient under the fixed flux condition [Fig. 4.33(a)]. However, if the pressure gradient becomes high enough, as is discussed in §4.3.1E, it suppresses turbulent transport through the reduction of magnetic shear. In this case, there arises a nonlinear linkage that enhances the plasma pressure gradient [Fig. 4.33(b)].

A Dynamical equations for structural transition In order to describe these nonlinearly interacting systems, one employs a set of model equations, which describes the dynamics of global plasma parameters, e.g., plasma pressure, as

$$\frac{\partial \bar{p}}{\partial t} = \nabla \cdot \left(\chi_{\rm turb} \left[\tilde{\phi}; \nabla \bar{p}; \nabla \bar{E}_r \cdots \right] \nabla \bar{p} \right) + P_{\rm heat}, \tag{4.311}$$

and the electromagnetic field [e.g., radial electric field (including zonal flow and electric-field interface) and poloidal magnetic field] as

$$\frac{\partial \bar{E}_r}{\partial t} = \nabla \cdot \left(\mu_{\rm turb} \left[\tilde{\phi}; \nabla \bar{p}; \nabla \bar{E}_r \cdots \right] \nabla \bar{E}_r \right) + N \left[\bar{E}_r; \nabla \bar{p}; \cdots \right], \tag{4.312}$$

$$\frac{\partial \bar{B}_\theta}{\partial t} = \nabla \cdot \left(\eta_\parallel \nabla \bar{B}_\theta \right) + N_{\rm B} \left[\bar{B}_\theta; \nabla \bar{p}; \cdots \right], \tag{4.313}$$

and fluctuating quantities $\tilde{\mathbf{f}}$

$$\frac{\partial}{\partial t} \tilde{\mathbf{f}} + \mathcal{L} \tilde{\mathbf{f}} = \tilde{\mathbf{S}} + \tilde{\mathbf{S}}_{\rm th}. \tag{4.314}$$

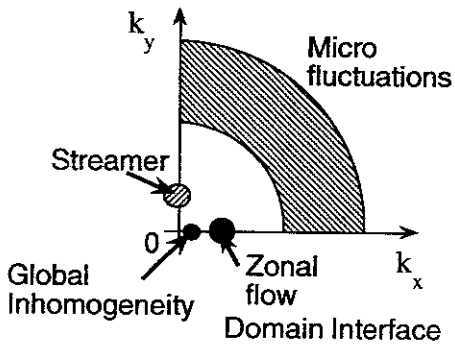

(a)

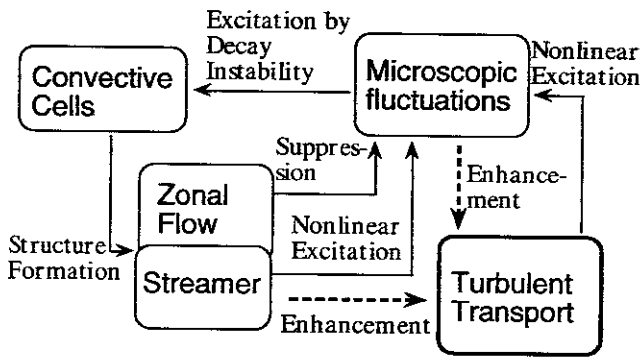

(b)

Figure 4.32. Schematic drawing of the self-regulating mechanisms in plasma turbulence and structural formation.

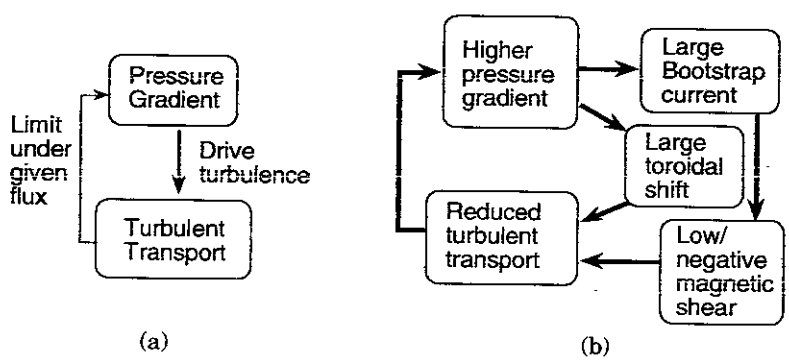

(a) (b)

Figure 4.33. Other nonlinear chain for structural formation through the modification of the current profile.

The explicit formulae for transport coefficients $\mu_{\rm turb}[\tilde{\phi}; \nabla\bar{p}; \nabla\bar{E}_r \cdots]$, the nonlinear source term $N[\bar{E}_r; \nabla\bar{p}; \cdots]$, and the renormalized operator $\mathcal{L}$ have been discussed for several examples of turbulence modelling. The term $N_{\rm B}[\bar{B}_\theta; \nabla\bar{p}; \cdots]$ represents the driving source like the Bootstrap current. The last equation, Eq. (4.314), could be subject to a bifurcation, which is surveyed in §4.3.5.

B Nonlinearity in flux-gradient relation To analyze the bifurcation and transition phenomena, a time-scale separation is introduced first. We consider the case that the evolution time of the turbulence level, $\tau_{\rm fluc}$ is shorter than the evolution time of plasma inhomogeneities, $\tau_{\rm global}$,

$$\tau_{\rm fluc} \ll \tau_{\rm global}. \tag{4.315}$$

Then the fluctuation level and the turbulence transport coefficient are evaluated by the counterparts of the stationary state when the evolution within the time scale $\tau_{\rm global}$ is solved. The fluctuation level is no longer an independent variable in the evolution equation for the global plasma structure. Taking two global-parameter variables (pressure gradient and radial electric field, i.e., plasma flow velocity), we have a system of plasma transport equations as

$$\frac{\partial\bar{p}}{\partial t} = \nabla\cdot(\chi_{\rm turb}\nabla\bar{p}) + P_{\rm heat}, \tag{4.316}$$

$$\frac{\partial\bar{E}_r}{\partial t} = \nabla\cdot\left(\mu_{\rm turb}\nabla\bar{E}_r\right) + N\left[\bar{E}_r\right], \tag{4.317}$$

where $P_{\rm heat}$ is the heating power, $N[\bar{E}_r]$ is the nonlinear source that generates a radial electric field. Examples are discussed in §4.3.3C as Eq. (4.254). Here, $\chi_{\rm turb}$ and $\mu_{\rm turb}$ are functional of the pressure gradient and electric-field structure, $\chi[\nabla p, \nabla\bar{E}_r](r)$ and $\mu_{\rm turb}[\nabla\bar{p}, \nabla\bar{E}_r](r)$. Simplified relation $\mu_{\rm turb} \cong \chi_{\rm turb}$ is sometimes employed [see discussions for Eq. (4.232)]. This system is known to have a hysteresis [1.32, 1.35, 4.318, 4.319].

When one further introduces the time-scale separation that Eq. (4.317) has a faster time scale than Eq. (4.316), then a stationary solution of Eq. (4.317), $E_r(r) = E_r[\nabla\bar{p}, \cdots]$, is obtained in a fast time scale, and is substituted into Eq. (4.316). On this slow time scale, Eq. (4.316) is solved with the thermal transport coefficient which is expressed in terms of global plasma parameters. Figure 4.34 illustrates the energy transport coefficient as a function of the pressure gradient and other plasma parameters, with an example of the case of electric-field bifurcation model. It is possible for a cusp type catastrophe to occur. The thermal conductivity is subject to change at critical pressure gradients. In association with the change of transport coefficient between the upper and lower branches of Fig. 4.34, the flow pattern is different, as is illustrated in

Figs. 4.35(a) and (b). In the state of Fig. 4.35(b), the electric field is weak: damping of the poloidal flow due to the transit time magnetic pumping is large. The plasma rotates in the toroidal direction. When the electric field becomes strong enough, it is possible for the plasma to rotate in the poloidal direction. See §19 of [1.35].

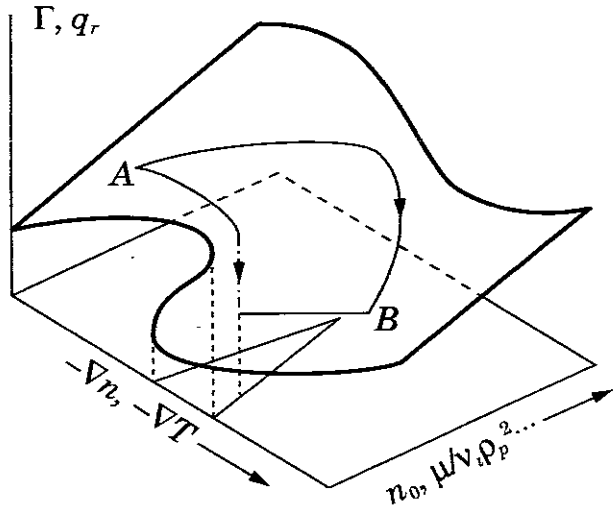

Figure 4.34. Cusp type catastrophe [1.35]

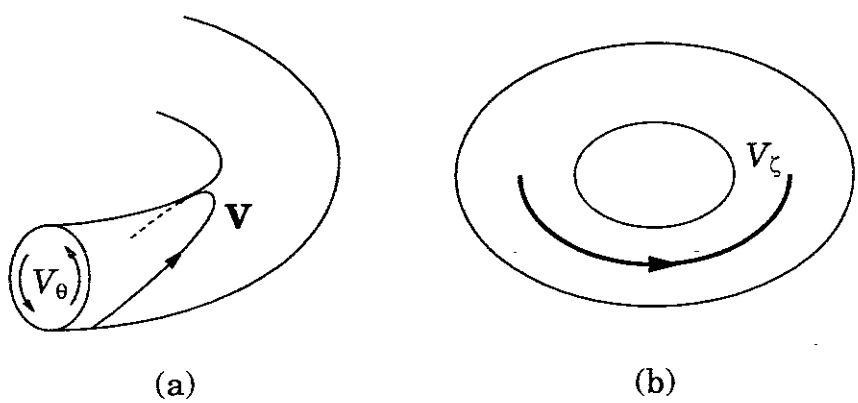

Figure 4.35. Bifurcation in flow pattern. The flow pattern in an reduced transport state (a) and that in an ordinary turbulent state (b) [1.35].

Another model of the transition is based on the theory of instabilities in the range of drift waves [4.320-4.327]. The temperature gradient induces drift-wave turbulence, which can be suppressed by the density gradient. According to the balance between them, a phase diagram of drift-wave turbulence has been proposed [4.320]. Figure 4.36 illustrates a diagram for the tokamak edge turbulence, for fixed value of η_i, $\eta_i = 2.5$, on

the $(\varepsilon_n, \alpha_d)$ plane, where

$$\varepsilon_n = \frac{2L_n}{R}, \tag{4.318}$$

and

$$\alpha_d = \frac{\rho_s}{(1+T_e/T_e)L_\perp}\sqrt{\frac{R}{L_n}}, \tag{4.319}$$

where $L_\perp = [\nu_e L_s^2 \rho_s^2/(\omega_{ce} L_n)]^{1/3}$. The parameter ε_n controls the effective compressibility, and α_d measures the strength of the diamagnetic drifts in the plasma edge.

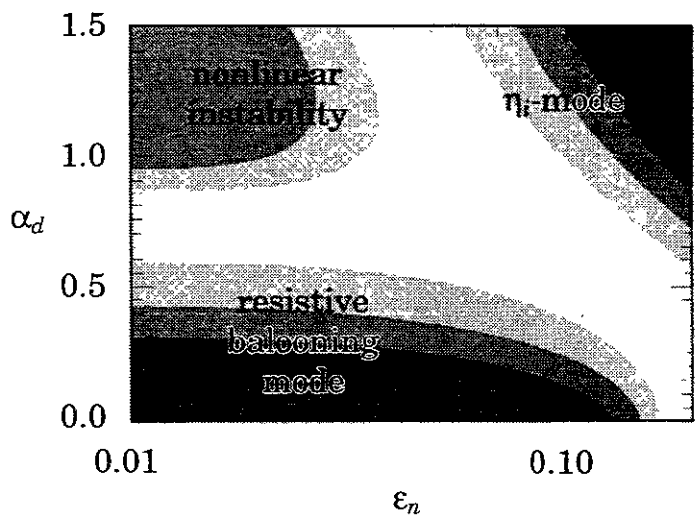

Figure 4.36. Phase diagram of drift wave turbulence. Reproduced from [4.320].

A much simplified model of the bifurcation in energy transport has been proposed, corresponding to one section of Fig. 4.34, as

$$\chi = \frac{\chi_1}{1 + c_1(a/L_T)^2 + c_2(a/L_T)^4} + \chi_2, \tag{4.320}$$

where c_1 and c_2 are numerical coefficients, and L_T is the temperature-gradient scale length. Here, χ_1 and χ_2 represent two different mechanisms that induce the cross-field transport of energy [4.328, 4.329]. This model also predicts a bifurcation of pressure gradient in certain conditions. In some models, the curvature of temperature, $d^2T_{e,i}/dr^2$, is included in the denominator of Eq. (4.320). In this case, the temperature profile is not necessarily determined uniquely even if boundary conditions are imposed [4.330].

Various turbulence models, which include the turbulence-suppression mechanisms, can be combined with the transport picture of Eqs. (4.316) and (4.317). Applications have been made to analyze the transitions in plasma confinement and the establishment of steep gradients in plasmas [4.319, 4.331-4.343]. Objective of these research is to

examine whether the transport models based on turbulence theories can reproduce the anomalous loss in L-mode plasmas as well as the transition phenomena to improved confinement states [1.14-1.21]. At least the qualitative understanding has been given on the plasma loss which increases as the heating power increases, and on the formation of transport barriers. Exhaustive references are found in [4.344].

C Simultaneous evolution of fluctuation, flow and gradient When the system size becomes smaller, the characteristic time for the change of the average profile and that for the change of turbulence level becomes closer to each other:

$$\tau_{\rm fluc} \sim \tau_{\rm global}. \tag{4.321}$$

Under such circumstance, the evolution of the fluctuation level must be simultaneously solved together with plasma gradients and flows. As is illustrated in Fig. 4.32, meso-scale structures and turbulence are then nonlinearly regulating each other. When the time-scale separation is not allowed under the circumstance of Eq. (4.321), a complicated spatio-temporal evolution is expected to occur, including the plume ([4.207, 4.318]).

With the ordering of Eq. (4.321), a soft-type bifurcation has also been examined in a dynamical model with a local approximation. An example is presented below, e.g., in the form of a set of equations for the plasma pressure, the electric-field inhomogeneity, and the fluctuation level [4.207]. In this model, a set of coupled equations is proposed as

$$\dot{A} = \gamma_0 A - \alpha_1 A^2 - \alpha_2 U A, \tag{4.322a}$$

$$\dot{U} = -\mu U + \alpha_3 A U, \tag{4.322b}$$

$$\dot{G} = -\alpha_5 G - \alpha_4 G A + P, \tag{4.322c}$$

where A is the fluctuation level, $A \sim \tilde{n}/n$, U is the flow shear, G is the pressure gradient, and P is the heating power. This particular form is derived by dimensional arguments, and is not necessarily unique. Its extension is given in [4.345, 4.346]. Similar, but not identical, dynamical models are given by other groups [4.114, 4.205, 4.347-4.349]. The set of equations (4.322a)-(4.322c) is a representative one of this kind. This type of dynamical models has two types of steady states, i.e.,

$$A = \frac{\gamma_0}{\alpha_1},\ U = 0, \tag{4.323a}$$

and

$$A = \frac{\mu}{\alpha_3},\ U = \left(\gamma_0 - \frac{\alpha_1 \mu}{\alpha_3}\right)\frac{1}{\alpha_2}. \tag{4.323b}$$

These two branches merge smoothly at the condition $\gamma_0 \alpha_3 = \mu \alpha_1$. Only a soft transition (pitch-fork bifurcation) is predicted. These types of models would be useful in analyzing phenomena of a soft transition.

Before closing this subsection, one example is quoted from a numerical simulation. The evolution of the fluctuation energy in the regimes of meso-scale and microscale is plotted in Fig. 4.37. Complex dynamics among fluctuations of different scale lengths is observed [4.350]. A survey of plasma turbulence is made in [4.351] from a complementary viewpoint. The complicated behaviour in confined plasmas are summarized from other approach of variable reduction.

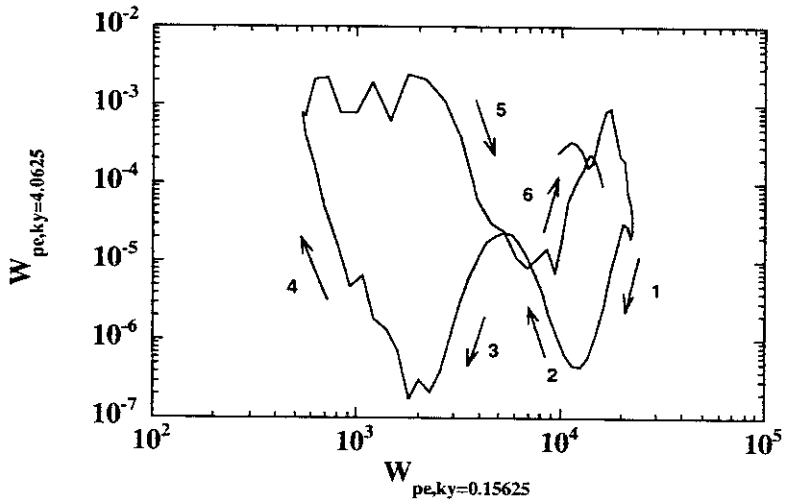

Figure 4.37. Energy in the long-wavelength region (meso scale) - horizontal axis - and that in microscale fluctuations - vertical axis - show complicated dynamics. Quoted from [4.350].

4.4.2. Self-organized dynamics In inhomogeneous plasmas, nonlinearity drives self-organized dynamics. One example is the sequences of repetitive destabilization and stabilization. Systems with a few degrees of freedom, like the Lorenz model or the Volterra–Lotka model, allow a limit-cycle oscillation under fixed external parameters. The amplitude of one distinct mode repeats growth and damping periodically. As is discussed in §4.4.1, structural transitions occur in inhomogeneous plasmas. The structural transition can occur periodically as well. Examples of the self-organized dynamics which is related to the edge localized modes (ELMs) [1.15, 1.18] are surveyed below.

A Dithering ELMs The hysteresis in the gradient–flux relation gives rise to self-organized dynamics under a constant supply. A cross section of Fig. 4.34 has a hysteresis. An example is illustrated in Fig. 4.38. There could appear a linkage in Fig. 4.38(a). In a state of small transport coefficient, the density increases (path A); the critical condition is reached, and the transport changes abruptly (jump B); on the branch of

larger transport, the density decreases (path C); other critical condition is satisfied, and the transition takes place (jump D), closing a cycle. A set of equations like Eqs. (4.316) and (4.317) are solved, and a repetitive burst of plasma flux is obtained. Associated with this repetitive change of plasma flux, the turbulence level as well as the global plasma gradient periodically change [4.214, 4.352-4.354]. This self-organized dynamics is one typical model of dithering ELMs that has been observed. Compound dithers have also been theoretically predicted [4.355].

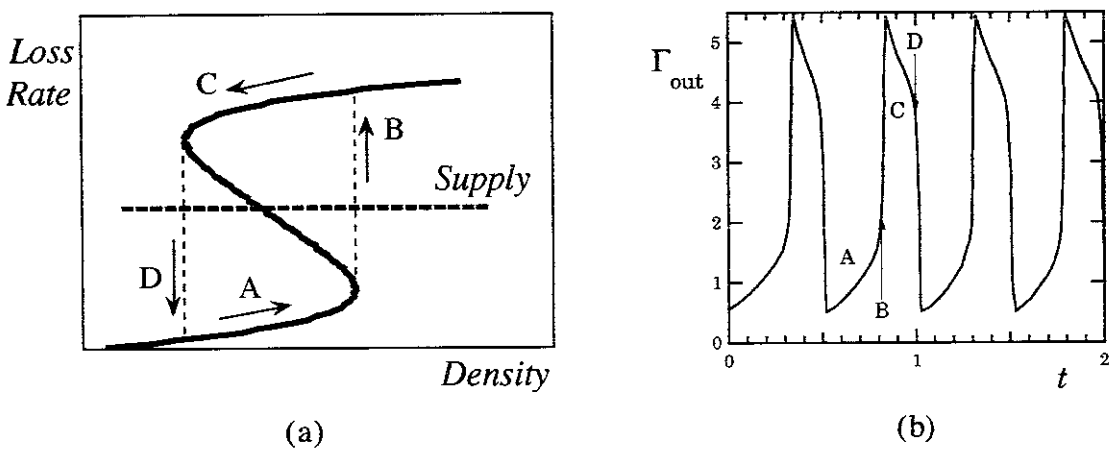

Figure 4.38. Example of the self-organized dynamics in structural transition. Hysteresis in the plasma parameter - loss space is shown in (a), and temporal evolution of the plasma outflux across the surface is shown in (b).

Soft transition models also predict self-organized dynamics under a constant supply of plasma [4.113, 4.114, 4.207, 4.356, 4.357]. A variety of limit-cycle oscillation is possible in plasmas with hysteresis in the transport property.

B Giant ELMs Self-organized dynamics in §4.4.2A is expected to occur in a particular region of the parameter space (e.g., near the critical condition that predicts the L–H transition). If the parameters are chosen so that the steep pressure gradient is established, the dithering cycle does not occur. In this case another type of repetitive structural transition may take place.

A pair of instabilities are proposed to cause repetitive bursts [4.358-4.360] (see Fig. 4.39). The ballooning instability is excited by the pressure gradient, while the surface kink instability [4.361, 4.362] is driven by the current density near the plasma surface. The instability region is illustrated in Fig. 4.39. In the stable region, the pressure gradient increases due to the high heat flux (path A). Once the ballooning-instability criterion is reached, the pressure gradient might stop increasing at the critical value even though the heating continues. The characteristic diffusion time of the

magnetic flux and current is slower than that of energy, so that the current density near surface increases (path B). When the criterion for the kink instability is reached, then the pressure gradient and the current density decay (path C) so as to close the loop.

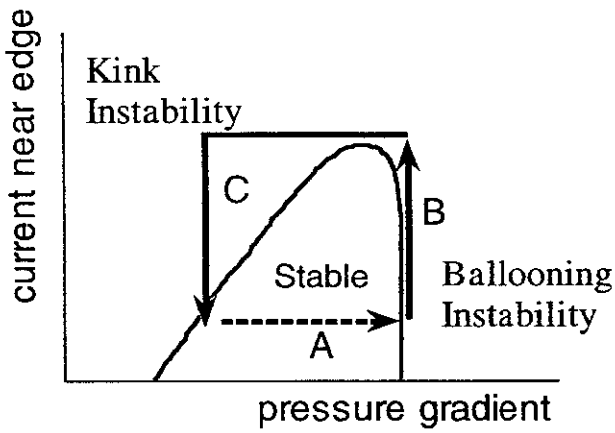

Figure 4.39. A pair of instabilities, under constant heating condition, causes the repetitive rise and decay of pressure gradient. After Ref. [4.360].

The transition in turbulence and turbulent transport owing to the onset of magnetic stochasticity is discussed in §4.3.5.B4 [4.307]. Based on this transition, a sequence for the structural transitions has been predicted [4.363, 4.364]. This mechanism causes the periodic collapse of transport barriers and the burst of plasma loss. Figure 4.40 illustrates the transition of turbulent transport coefficient as a function of the plasma pressure gradient $\alpha = (q^2 R/a) d\beta/dr$. The critical pressure gradient for the transition to turbulence with magnetic braiding, α_c, is illustrated in Fig. 4.29. The plasma pressure increases at the H-branch due to the strong heating power. The critical pressure gradient α_c is reached, at which the transition to the strongly turbulent state takes place. The enhanced transport coefficient causes the collapse of pressure gradient. When the pressure gradient becomes low, the back-transition to the lower turbulent transport coefficient occurs at $\alpha = \alpha_1$. The pressure gradient starts increasing again, closing the loop.

Reference [1.32] provides a very detailed survey of the theoretical work on L–H transitions, and comparisons with experimental observations are extended. It contains exhaustive references on this subject.

4.4.3. Transition probability Multiple states with different turbulence characteristics are allowed in plasmas. The transition between two different states has been studied by use of dynamical equations like Eqs. (4.316) and (4.317) or Eq. (4.320). These model

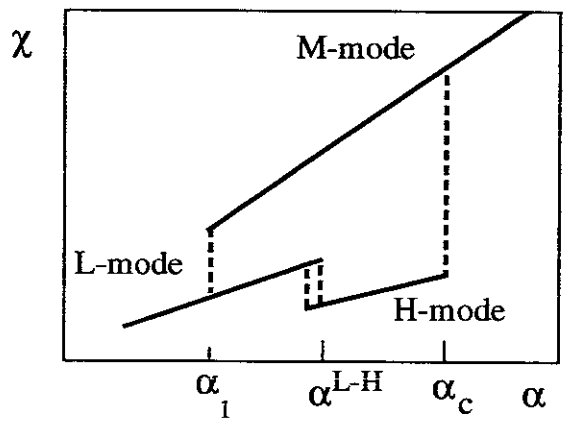

Figure 4.40. Transport coefficient as a function of the pressure gradient. Transition between the turbulent states is predicted.

equations are formulated as deterministic equations. However, as is explained in the statistical theory of plasma turbulence in §4.2.3, the random source is also induced by the turbulence interactions. If one accounts for the statistical noise source in the dynamics of turbulence, one may see that the transition from one turbulent state to the other turbulent state takes place as a statistical process. The transition occurs with a finite probability when the controlling parameter approaches the critical value that is obtained by the deterministic model [4.365, 4.366].

In systems at thermodynamical equilibrium, deviations from equilibrium occur as the thermal fluctuations, and the transition probability follows the Arrhenius law [4.367]. In turbulent plasmas, the probability density function deviates from the Boltzmann distribution; therefore the transition probability is different from the Arrhenius law.

A Fokker–Planck equation for macro variable (coarse-grained quantity) The Langevin equations for each k-component, Eq. (4.100), are reduced to one for a macro variable. The total fluctuating energy, which is the quantity integrated over some finite-size volume (L^2 in the perpendicular cross section),

$$\mathcal{E} \equiv (1/2) \sum_k k_\perp^2 \phi_k^2, \tag{4.324}$$

is introduced. The Fokker–Planck equation for the probability distribution function of the coarse-grained quantity, $P(\mathcal{E})$, is described as

$$\frac{\partial}{\partial t} P(\mathcal{E}) = \frac{\partial}{\partial \mathcal{E}} \left(2\Lambda \mathcal{E} + \frac{1}{2} \mathcal{G} \frac{\partial}{\partial \mathcal{E}} \mathcal{G} \right) P(\mathcal{E}) \tag{4.325}$$

(see also refs. [4.101, 4.102] for the basis for the reduction to the Fokker–Planck equation). In the Langevin equation for the average energy $\mathcal{E}$, the damping rate is

given as

$$\Lambda \equiv \mathcal{E}^{-1} \sum_k 2\lambda_{1,k} k_\perp^2 \phi_k^2 \tag{4.326}$$

($\lambda_{1,k}$ being the nonlinear decorrelation rate of the k-mode), and the magnitude of the statistical source term is written as

$$\mathcal{G}^2 = 4\hat{T}\gamma_{\rm m}\mathcal{E} + \sum_k (\sum_{j=1}^{3} A_{1j}\mathcal{G}_{j,k})^2 k_\perp^4 \phi_k^2. \tag{4.327}$$

It is also useful to introduce the mean classical decorrelation rate

$$\gamma_{\rm m} \equiv \mathcal{E}^{-1} \sum_k \gamma_{\nu c}\mathcal{E}_k \tag{4.328}$$

($\gamma_{\nu c} = \mu_{\nu c} k_\perp^2$). When the fluctuation level changes, the decorrelation coefficient deviates from the value in the thermodynamical-equilibrium limit.

B Transition probability

B1 Equilibrium probability density function The equilibrium probability distribution, being the solution of Eq. (4.325), is governed by the effective potential

$$S(\mathcal{E}) = \int^{\mathcal{E}} \frac{4\Lambda\mathcal{E}}{\mathcal{G}^2} d\mathcal{E}. \tag{4.329}$$

The equilibrium probability density function (PDF) is given as

$$P_{\rm eq}(\mathcal{E}) = \bar{P}\frac{1}{\mathcal{G}} \exp[-S(\mathcal{E})]. \tag{4.330}$$

Therefore, the minimum of the effective potential $S(\mathcal{E})$ (e.g., states A and B in Fig. 4.41) predicts the probable state of plasma turbulence.

The analysis in the large-amplitude limit has shown the existence of a tail component as

$$P_{\rm eq}(\mathcal{E}) \propto \left(\frac{\mathcal{E}}{\mathcal{E}_{\rm eq}}\right)^{-\eta} \tag{4.331}$$

with the power index as

$$\eta = \frac{5}{4} + \frac{3}{2C_0}\frac{\overline{\overline{\Lambda}}}{\gamma_{k,\rm eq}} s \left(\frac{L}{\delta}\right)^2 G_0^{-1}, \tag{4.332}$$

where $\mathcal{E}_{\rm eq}$ is the mean of the fluctuation energy, the coefficient $\overline{\overline{\Lambda}}$ is the asymptotic coefficient of nonlinear damping rate $\overline{\overline{\Lambda}} = \lim_{\mathcal{E}\to\infty} \Lambda(\mathcal{E}/\mathcal{E}_{\rm eq})^{-1/2}$, and $\gamma_{k,\rm eq}$ is the nonlinear eddy damping rate at $\mathcal{E} = \mathcal{E}_{\rm eq}$. For a fixed averaging-size L, the power index depends on the inhomogeneity as

$$(\eta - 5/4) \propto G_0^{-1}. \tag{4.333}$$

As the gradient increases, the tail component becomes larger.

B2 Transition probability The flux of probability from the A state to the B state in Fig. 4.41 is obtained. The saddle point is denoted by the suffix C. The function $\Lambda(\mathcal{E})$ is Taylor expanded in the vicinity of $\mathcal{E}_C$ as

$$\Lambda(v) = \Lambda(v_{*1}) - \Lambda_0'(v - v_{*1}) + \cdots \tag{4.334}$$

($v = \sqrt{\mathcal{E}}$, $v_{*1} = \sqrt{\mathcal{E}_C}$), and the transition rate is given as [4.366]

$$r_{A\to B} = \frac{\sqrt{\lambda_0}}{2\sqrt{\pi}} \frac{1}{\Delta\mathcal{E}_A} g(\mathcal{E}_A) \exp[S(\mathcal{E}_A) - S(\mathcal{E}_C)], \tag{4.335}$$

where $\lambda_0 = \Lambda_0' v_{*1}$ and $\Delta\mathcal{E}_A$ is the width of the PDF at the state A. The transition probability from B to A is calculated in a similar manner.

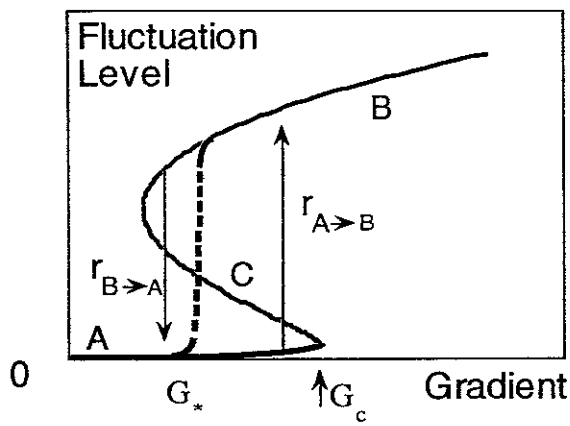

Figure 4.41. Transition probability between two states is calculated.

In the thermodynamical limit, where the fluctuation spectrum is given by the thermal-fluctuation counterpart, Eq. (4.335) reduces to

$$r_{A\to B} = \pi^{-1/2}\gamma_m \exp(-\mathcal{E}_C/\hat{T}). \tag{4.336}$$

One recovers the relation $\ln(r_{A\to B}) \propto -1/T$ which is the Arrhenius law.

Away form the thermodynamical equilibrium, the transition probability obeys a power law. In the vicinity of the critical linear stability boundary G_C in Fig. 4.41, the transition probability is given as a function of the distance from the critical pressure gradient, $G_C - G_0$, as

$$r_{A\to B} \sim \frac{\gamma_m}{\sqrt{\pi}} \left(\frac{\mu_{ec}}{2}\right)^{-2b_1} k_0^{-4b_1/3} \left(\hat{T}\gamma_m \frac{3}{16C_0}\right)^{2b_1/3} \left(1 - \frac{G_0}{G_C}\right)^{-b_1}, \tag{4.337}$$

where

$$b_1 \cong (1/3)[3/(16C_0)]^{2/3}\hat{T}^{-1/3}(L/a)^2, \tag{4.338}$$

$$d^3 = \hat{T}\gamma_m[3/(16C_0)]k_0(L/a)^3, \tag{4.339}$$

and L is the size of a small region over which the fluctuation energy $\mathcal{E}$ is integrated [4.366].

Comparing Eq. (4.337) with Eq. (4.336), the characteristic features of the turbulent transition are seen. First, the transition probability is explicitly expressed in terms of the plasma-inhomogeneity parameter. Second, it is greatly enhanced owing to a large statistical variance. Third, it has a power-law dependence on the plasma-inhomogeneity parameter. Namely, the transition probability increases as

$$\tau_{A\to B} \propto (G_C - G_0)^{-b_1} \tag{4.340}$$

when the gradient parameter G_0 approaches to G_C. These results, combined with the dynamical and spatial structural formations, are the distinct features of the transition of turbulence away from the thermodynamical equilibrium.

The '*phase boundary*' between states A and B in parameter space is defined by the relation that the transition probability from A to B is equal to the back-transition probability, i.e.,

$$\tau_{A\to B} = \tau_{B\to A}. \tag{4.341}$$

In Eq. (4.335), an exponential dependence on the difference of effective potential $S(\mathcal{E}_A) - S(\mathcal{E}_C)$ dominates the transition probability. Therefore the balance equation is approximated by the relation

$$S(\mathcal{E}_A) = S(\mathcal{E}_C) \tag{4.342}$$

with a logarithmic correction. This result is a generalization of the '*Maxwell's construction rule*' for the phase boundary in thermodynamics.

4.4.4. Probabilistic transition In a system with hysteresis like inhomogeneous plasmas, a self-generated oscillation is possible to occur under the condition of constant supply of energy and particle. The discussions in §4.4.2 is based on a deterministic picture, in which a transition takes place when a certain critical condition is reached. In other words, the transition at critical condition is formulated based upon the deterministic view. As is reviewed in §4.2.3, the turbulent state is associated with the random excitations which are much stronger than the thermodynamical fluctuations. As a result, the transition occurs according to the probabilistic law, as is discussed in §4.4.3. The probabilistic excitation of transitions introduces the concept of a life time during which the plasma is in a certain state of turbulence [4.368].

This process has been analyzed by including the noise term in model equations that describe the transitions. For instance, the model equations for the dithering ELMs are given as

$$\frac{\partial}{\partial t}\alpha = S - \gamma\alpha, \tag{4.343a}$$

$$\zeta \frac{\partial}{\partial t}\gamma = \alpha - 1 + a(\gamma - 1) - b(\gamma - 1)^3, \tag{4.343b}$$

where the variables α and γ represent the global plasma parameter (density, temperature, or their gradients) and the level of turbulence (turbulent transport), respectively. This set of equations is a simplified model of Eqs. (4.316) and (4.317). The notation is as follows: S is the energy influx into the layer, ζ is the possible difference of dynamical time between α and γ; the cubic equation $a(\gamma - 1) - b(\gamma - 1)^3$ describes the shape of the hysteresis in the gradient–flux relation. This Ginzburg–Landau model describes the dithering ELMs under a given source of magnitude S. In turbulent plasmas, the turbulent state itself fluctuates in time, so that the coefficient a that determines the turbulence level is fluctuating as well. Based on this, the coefficient a is modelled to include the fluctuating part as

$$a = a_0 + \varepsilon_a. \tag{4.344}$$

A power-law noise is assumed, and the probability distribution function of ε_a is taken as

$$P(\varepsilon_a) \propto \varepsilon_a^{-k}. \tag{4.345}$$

Equations (4.343), (4.344) and (4.345) are solved, and the self-regulated oscillation and transition probability are calculated. The probability for the transition to occur at $\alpha_c^{\rm obs}$is found to follow

$$P(\alpha_c^{\rm obs}) \propto (\alpha_{c0} - \alpha_c^{\rm obs})^{-k}, \tag{4.346}$$

where α_{c0} is the critical value of the deterministic picture, which is given in the absence of the statistical noise [4.369].

4.5. Transient response and transport

In the discussion of turbulent transport, it is often assumed that a temporal and spatial scale separation holds between the global transport and the microscopic fluctuations. This leads to the picture that the change of global profile propagates in space with the diffusion time scale. The characteristic diffusion time is estimated by the global scale length and the turbulent diffusion coefficient. This scale separation is not always satisfied in plasma turbulence. If it is not satisfied, the transient response of inhomogeneous plasma could be different from those described by a diffusion process. See review of [1.13, 4.172, 4.370] for the phenomena of transient response.

4.5.1. Long scale length of fluctuations It is possible that fluctuations have long radial correlation length (Fig. 4.42). If the correlation length includes a meso-scale or is comparable to the global gradient scale length, the change of transport properties

propagates rapidly, at the level of group velocity of waves [4.371, 4.372]. In the case of long correlation length, the gradient–flux relation usually becomes an integro-differential equation. [In some cases, however, the Fick's law (i.e., the local equation) is valid for the particle flux in a long mean-free-path regime [4.373].]

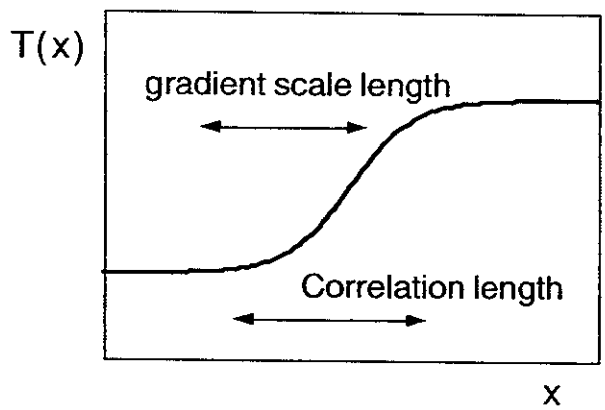

Figure 4.42. Schematic illustration of correlation length which is comparable to the scale length of inhomogeneity.

In addition, the amplitude of fluctuations with long correlation length is not determined by the local plasma parameter. The long-wavelength modes can be excited by micro-fluctuations within its coherence length. Based on this process, the electron heat flux q_e is modelled as a sum of the local diffusion and non-local flux as [4.374]

$$q_e(r,t) = -\int_0^a n_e(r',t)\chi_e(r',t)K_l(r,r') \times [\lambda\nabla T_e(r,t) + (1-\lambda)\nabla' T_e(r',t)]\,dr', \tag{4.347}$$

where

$$K_l(r,r') \equiv \frac{r}{r'}\left\{C_{\text{local}}\delta(r-r') + C_{\text{global}}\frac{1}{\sqrt{\pi}l}\exp\left[-\left(\frac{r-r'}{l}\right)^2\right]\right\}. \tag{4.348}$$

Here l is the half width of non-local interactions, $\delta(r-r')$ is the delta function, and $\lambda(0 \le \lambda \le 1)$, C_{local} and C_{global} $(C_{\text{local}} + C_{\text{global}} = 1)$ are numerical constants. The parameter λ represents the ratio of the role of the local temperature gradient in the non-local transport process. The length l is based on the correlation length of the long-wavelength fluctuations that bear the additional non-local transport.

According to this process, the heat flux at one location is influenced by the plasma inhomogeneity at another location. The gradient–flux relation is no longer a unique line, but constitutes a hysteresis loop, depending on the rapidness of the temporal change. A schematic diagram is given in Fig. 4.43. The transient response is different from

the static response [4.375]. It is noted that the change of flux *precedes* the change of gradient.

Other models, in which the global term is switched on/off, have also been applied to the study of transient response [4.376. 4.377].

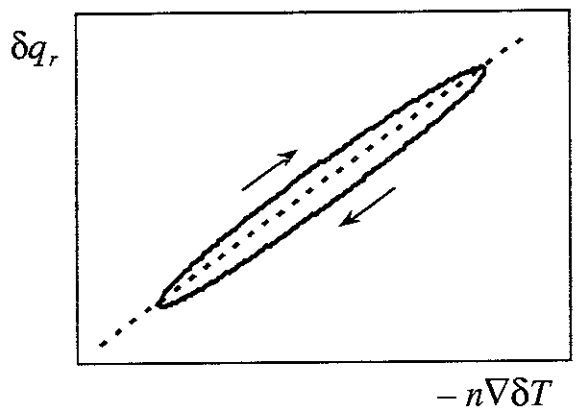

Figure 4.43. Perturbed heat flux and perturbed gradient on one magnetic surface (near half radius, $r \sim a/2$) against a periodic modulation of the heat source at the center. (Schematic)

4.5.2. Memory effects The non-Markovian effect also affects the transient response. According to the arguments of §4.2.3F, the memory effect makes the transport equation into an integro-differential equation. Given the long-time assumption, a transport equation is obtained as [4.104]

$$\frac{\partial}{\partial t}n(x,t) = \int_0^t dt' C_{\mathrm{L}}(t')\nabla^2 n(x,t-t'). \tag{4.349}$$

The contribution of the tail to the correlation function is separated, and an approximate form is given as

$$\frac{\partial}{\partial t}n(x,t) = D_0\nabla^2 n(x,t) - H_0\int_{t_{\min}}^t (t')^{\alpha_{\mathrm{tail}}-2}\nabla^2 n(x,t-t')dt', \tag{4.350}$$

where $\alpha_{\mathrm{tail}} = 0.58$, D_0 is the conventional diffusion component, and the coefficient of the tail, H_0, is discussed in [4.104, 4.105]. This transport equation provides a subdiffusive transport, as is discussed in Eq. (4.161). The dispersion evolves in time as [4.105]

$$\left\langle [x(t)-x(0)]^2 \right\rangle \propto t^{\alpha_{\mathrm{tail}}}. \tag{4.351}$$

The relation $\alpha_{\mathrm{tail}} < 1$ holds, and the response is different from a Gaussian packet. The central peak decays much slower than a Gaussian packet (i.e., subdiffusion), but the tail of the packet propagates *much faster*. The long-time tail in the Lagrangian correlation modifies the transient response from a simple diffusive process.

4.5.3. Fast propagation of bump In many cases, multiple scale lengths are necessary to describe global plasma profile. For instance, bumps are imposed on a smooth inhomogeneous profile. The temporal evolution of bumps may be different from the energy flow associated with the smooth gradient.

Fast (ballistic) propagation of a bump is possible if the plasma state is close to the critical condition for the onset of instability. The change of heat flux, δq_r, associated with a bump of pressure, δp, is modelled as [4.378]

$$\delta q_r = \frac{\Lambda}{2}\delta p^2 + C_2\left(\frac{d}{dr}\delta p\right)^2 + \cdots. \tag{4.352}$$

As a simple model, the case of $\delta q_r = (\Lambda/2)\delta p^2$ was discussed. The temporal evolution of the perturbed profile is described by the energy balance equation

$$\frac{\partial}{\partial t}\delta p + \frac{\partial}{\partial x}\left(\frac{\Lambda}{2}\delta p^2\right) - D_0\frac{\partial^2}{\partial x^2}\delta p = \tilde{S}, \tag{4.353}$$

where D_0 is the diffusivity in the unperturbed state, and $\tilde{S}$ represents a source. Equation (4.353) in a slab geometry is expressed as a form of Burger's equation, and represents the ballistic propagation of the bump at the speed of

$$V_r = \Lambda\delta p_0, \tag{4.354}$$

where δp_0 is the height of the bump. The higher the bump, the faster the propagation speed. It is shown that the transient perturbation may propagate much faster than the diffusive propagation. See also [4.379] for some remarks on [4.378].

4.5.4. Plume, avalanche, and self-organized criticality Considerations in §4.5 leads to the view that a meso-scale structure appears, time to time, in inhomogeneous plasmas. A meso-scale structure may give rise to the rapid propagation of energy through long auto-correlations or the propagation of large bumps. The localized structure of a radial electric field, on the other hand, may suppress turbulence (e.g., suppression by sheared flow). The dynamic evolution of the meso-scale structure is an essential element in plasma turbulence. Therefore the damping rate of the meso-scale structure, a simple form of which is given in Eq. (4.239), has an important role for the level of turbulence that drives turbulent transport [4.380, 4.381]. Such an influence of damping rate of meso-scale structure has been confirmed in direct nonlinear simulations.

Recent progress in nonlinear simulations also demonstrates the importance of an intermittent appearance of a strong flow. A strong global modification of the profile appears in a short time (Fig. 4.44). In other words, an 'avalanche' is observed [4.382-4.386]. An alternative type of nonlinear simulation has been performed by taking into account the meso-scale structure in a tokamak plasma [4.387, 4.388]. It has been shown that symmetry breaking structures with intermediate mode numbers have substantial

effects on the evolution of plasma profiles. A hierarchical approach including the meso-scale structure and micro turbulence has been proposed [4.389, 4.390].

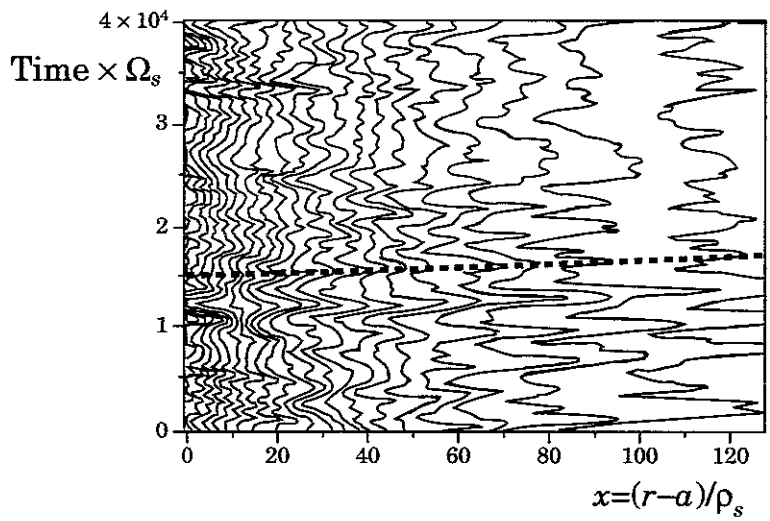

Figure 4.44. Nonlinear simulation with fixed flux source. Iso-density contours, $\overline{n(x,t)}_y$ averaged over y-direction, are shown. Strong global modification of the profile appears in a short time, being observed as an 'avalanche'. Reproduced from [4.386].

An avalanche has also been predicted as a consequence of successive M-mode transitions. Consider a case that a transition from L-mode to M-mode (Fig. 4.40) occurs at a certain magnetic surface. As a consequence of this, a large amount of energy is transported from this transition region to the neighbouring regions. It causes pressure steepening in the neighbouring regions, so as to reach the critical condition for the M-mode transition there. A successive M-mode transition occurs, and the location of the transition propagates in the radial direction. It was shown that the successive transitions propagate in space as an avalanche, not as diffusion [4.391, 4.392].

The theoretical study of plasma bifurcation presents the view that there are bifurcation boundaries in the parameter space and a plasma profile is rapidly modified when the parameter reaches the boundary. The modification of the profile propagates rapidly in space. Extending this way of thinking, analyses have been performed [4.378, 4.393, 4.394] based on the sand-pile model which gives rise to self-organized criticality (SOC) [4.395]. This model introduces discrete automata which have number-conserving topping rules with a nonlinear threshold, and exhibits avalanches at all scales.

The long-time correlation of perturbations, which has a power law, is deduced from this model. Examination of the experimental data has been performed, and the long-time tail has been observed. Based on the experimental observations, the importance of the SOC model of plasma transport has also been stressed [4.396, 4.397]. As is

discussed in examples [4.378, 4.391, 4 392], the SOC model provides a basis of deduction for some cases. The model might have relevance in much wider circumstances: This is because there are a lot of subcritical instabilities in plasmas and they have non-zero correlation length and a nonlinear threshold for excitation as is surveyed in §4.3.5. At the same time, however, some care is necessary for widening the applicability using the observed probability density function (PDF) [4.398]. Nonlinear theories, even in the framework of the local model, did predict a power-law distribution. For instance, algebraic evolution is predicted for nonlinear drift-wave turbulence as Eq. (4.292), and strong plasma turbulence exhibits a power law in the PDF and associated transition probability function, as in Eqs. (4.331) and (4.337).

It is thus stressed that the transport properties of inhomogeneous plasma may be different depending on whether the global gradient is a fixed constant or the source is a fixed constant. This difference is one of the characteristic features of far-non-equilibrium turbulent plasmas. Contrary to this fact, the materials in thermal equilibrium show the common transport property that is independent of the constraints of either a fixed gradient or a fixed flux.

References

[4.1] Kadomtsev B B 1965 *Plasma Turbulence* (New York, Academic Press)

[4.2] Yoshikawa S and Iiyoshi A 1972 *Introduction to Controlled Thermonuclear Reaction* (Tokyo: Kyoritu) (in Japanese)

[4.3] Ichimaru S 1973 *Basic Principles of Plasma Physics* (Reading: Benjamin)

[4.4] Kadomtsev B B 1992 *Tokamak Plasma: A Complex Physical System* (Bristol: IOP Publishing)

[4.5] Krall N A and Trivelpiece A W 1973 *Principles of Plasma Physics* (New York: McGraw–Hill)

[4.6] Stix T H 1962 *Theory of Plasma Waves* (New York: McGraw–Hill)

[4.7] Nishikawa K and Fukuyama A 2001 *Plasma Kinetic Theory* (Tokyo: Baifukan) (in Japanese).

[4.8] Mikailowski A B 1974 *Theory of Plasma Instabilities* (transl. Barbour J B, Consultants Bureau, New York)

[4.9] Mikailowski A B 1992 *Electromagnetic Instabilities in an Inhomogeneous Plasma* (Bristol: IOP Publishing)

[4.10] White R 1989 *Theory of Tokamak Plasmas* (New York: North Holland)

[4.11] Hasegawa A 1975 *Plasma Instabilities and Nonlinear Effects* (Berlin: Springer)

[4.12] Tang W M 1978 Nucl. Fusion **18** 1089

[4.13] Horton C W 1984 in *Basic Plasma Physics II* (ed. Galeev A A and Sudan R N, North Holland, Amsterdam) chap 6.4

[4.14] Kadomtsev B B and Pogutse O P 1971 Nucl. Fusion **11** 67

[4.15] Connor J W et al. 1993 Plasma Phys. Contr. Fusion **35** 319

[4.16] Connor J W and Wilson H R 1994 Plasma Phys. Contr. Fusion **36** 719

[4.17] Horton C W 1999 Rev. Mod. Phys. **71** 735

[4.18] Weiland J 2000 *Collective Modes in Inhomogeneous Plasma* (IOP, England)

[4.19] Hammett G W and Perkins F cW 1990 Phys. Rev. Lett. **64** 3019

[4.20] Chang Z and Callen J D 1992 Phys. Fluids B **4** 1167
[4.21] Beer M A and Hammett G W 1996 Phys. Plasmas **3** 4018
[4.22] Snyder P B, Hammett G W and Dorland W 1997 Phys. Plasmas 4 2687
[4.23] Mattor N 1998 Phys. Plasmas **5** 1822
[4.24] Sagdeev R Z, Shapiro V D and Shevchenko V I 1978 Sov. J. Plasma Phys. **4** 306 [Fiz. Plasmy 4 551 (1978)]
[4.25] Okuda H and Dawson J M 1973 Phys. Fluids **16** 408
[4.26] Sagdeev R Z, Shapiro V D and Shevchenko V I 1978 JETP Lett. **27** [Pis'ma Zh. Eksp. Teor. Fiz. **27** (1978)]
[4.27] Wesson J A 1987 *Tokamaks* (Oxford: Oxford University Press)
[4.28] Connor J W, Hastie R J and Taylor J B 1979 Proc. R. Soc. A **365** 1
[4.29] Lortz D and Nuhrenberg J 1978 Phys. Lett. **68**A 49
[4.30] Coppi B et al. 1979 Comments Plasma Phys. Contr. Fusion **5** 1
[4.31] Sagdeev R Z and Galeev A A 1969 *Nonlinear Plasma Theory* (ed. O'Neil T M, Book D L, Benjamin, New York).
[4.32] Elsässer K and Gräff P 1971 Annals of Physics (NY) **68** 305
[4.33] Sagdeev R Z 1979 Rev. Mod. Phys. **51** 1
[4.34] Berk H and Breizman B N 1995 Phys. Fluids B **2** 2226, 2235, 2246
[4.35] Breizman B N 1978 Sov. Phys. JETP **45** 271 [Zh. Eksp. Teor. Fiz. **72** (1977) 518]
[4.36] Itoh K and Itoh S-I 1985 J. Phys. Soc. Jpn. **54** 1228
[4.37] Hazeltine R D, Mahajan S M and Hitchcock D A 1981 Phys. Fluids **24** 1164
[4.38] Shaing K C 1988 Phys. Fluids **31** 2249
[4.39] Itoh S-I 1992 Phys. Fluids B **4** 796
[4.40] Sugama H and Horton W 1995 Phys. Plasmas **2** 2989
[4.41] See also: Balescu R 1991 Phys. Fluids B **3** 564
[4.42] Galeev A A and Sagdeev R Z 1973 in Review of Plasma Physics (ed. M. A. Leontovich, Consultants Bureau, New York) vol 7 p 257
[4.43] Rosenbluth M N, Hinton F L and Hazeltine R D 1972 Phys. Fluids **15** 116
[4.44] Balescu R 1988 *Transport Processes in Plasmas 2. Neoclassical transport theory* (Amsterdam: North-Holland)
[4.45] Terry P W and Diampond P H 1985 Phys. Fluids **28** 1419
[4.46] Taylor J B 1997 Plasma Phys. Contr. Fusion **39** A1
[4.47] Hasegawa A 1985 Adv. Phys. **34** 1
[4.48] Onsager L 1949 Nuovo Cimento Suppl. **6** 279
[4.49] Batchelor G K 1959 *Theory of Homogeneous Turbulence* (Cambridge: Cambridge University Press)
[4.50] Sugama H 2000 Phys. Plasmas **7** 466
[4.51] Chirikov B V 1979 Phys. Reports **52** 263
[4.52] Lichtenberg A J and Liebermann M A 1984 *Regular and Stochastic Motion* (New York: Springer)
[4.53] Barescu R 1975 *Equilibrium and Nonequilibrium Statistical Mechanics* (New York: Wiley)
[4.54] Rosenbluth M N, Sagdeev R Z, Taylor J B and Zaslavsky G M 1966 Nucl. Fusion **6** 297
[4.55] Filonenko N N, Sagdeev R Z and Zaslavsky G M 1967 Nucl. Fusion **7** 253
[4.56] Fukuyama A, Momotoa H and Itatani R 1977 Phys. Rev. Lett. **38** 701
[4.57] Dupree T H 1970 Phys. Rev. Lett. **25** 789

[4.58] Kadomtsev B B and Pogutse O P 1970 Phys. Rev. Lett. bf 25 1155
[4.59] Horton C W and Choi D 1979 Phys. Reports **49** 273
[4.60] Krommes J A 1984 in *Basic Plasma Physics II* (ed. A. A. Galeev and R. N. Sudan, Amsterdam: North Holland) chap 5.5
[4.61] Cook I and Taylor J B 1973 J. Plasma Phys. **9** 131
[4.62] Dupree T H 1966 Phys. Fluids **9** 1773
[4.63] Kono M, Sanuki H and Todoroki J 1995 Phys. Lett. **51** A 247
[4.64] Dupree T H 1967 Phys. Fluids **10** 1049
[4.65] Corrsin S 1959 in *Atmospheric Diffusion and Air Pollution* (ed. F. N. Frenkiel and P. A. Sheppard, New York: Academic)
[4.66] Kubo R 1962 J. Phys. Soc. Jpn. **17** 1100
[4.67] Krommes J A and Smith R A 1987 Phys. Rev. E **53** 7359
[4.68] Vlad M, Spineanu F, Misguich J H and Balescu R 1998 Phys. Rev. E **53** 7359
[4.69] Isichenko M B 1992 Rev. Mod. Phys. **64** 961.
[4.70] Kleva R G and Drake J F 1984 Phys. Fluids **27** 1686.
[4.71] Chernikov A A, Neishtadt A I, Rogalsky A V and Yakhnin V Z 1991 Chaos **1** 206
[4.72] Isichenko M B, Horton W, Kim D E, Heo E G and Choi D-I 1992 Phys. Fluids B **4** 3973
[4.73] Ottaviani M 1992 Euro. Phys. Lett. bf 20 111
[4.74] Krommes J A 2000 Phys. Plasmas **7** 1148
[4.75] Krommes J A 1997 Phys. Plasmas **4** 655
[4.76] Kraichnan R H 1994 Phys. Rev. Lett. **72** 1016
[4.77] See, e.g., Kubo R, Toda M and Hashitsume N 1985 *Statistical Physics II* (Berlin: Springer)
[4.78] Howard L N 1963 J. Fluid Mech. **17** 405
[4.79] Connor J W 1988 Plasma Phys. Contr. Fusion **30** 619
[4.80] Lamb H 1932 *Hydrodynamics* Sixth edition (Cambridge: Cambridge University Press)
[4.81] Landau L D and Lifshits E M 1959 *Fluid Mechanics* (Oxford: Pergamon Press)
[4.82] Kolmogorov A N 1941 Dokl. Akad. Nauk SSSR [Sov. Phys. Dokl.] **30** 299
[4.83] Yoshikawa S 1970 Phys. Rev. Lett. **25** 353
[4.84] Düchs D F, Post D E and Rutherford P H 1977 Nucl. Fusion **17** 565
[4.85] Waltz R E, Dominguez R R, Wong S K, Diamond P H, Lee G S, Hahm T S and Mattor N 1986 in *Plasma Phyics and Controlled Nuclear Fusion Research* (Proc. 11th Conf. Kyoto 1986, Vienna: IAEA) vol 1 p 345
[4.86] Romaneli F, Tang W M and White R B 1986 Nucl. Fusion **26** 1515
[4.87] Kadomtsev B B and Pogutse O P 1970 in *Review of Plasma Physics* (ed. M. A. Leontovich, New York: Consultants Bureau) vol 5 p 249
[4.88] Similon P L and Diamond P H 1984 Phys. Fluids **28** 1419
[4.89] Chen L, Berger R L, Lominadze J G, Rosenbluth M N and Rutherford P H 1977 Phys. Rev. Lett. **39** 754
[4.90] Horton W, Choi D-I and Tang W M 1981 Phys. Fluids **24** 1077
[4.91] Lee G S and Diamond P H 1986 Phys. Fluids **29** 3291
[4.92] Connor J W 1993 Plasma Phys. Contr. Fusion **35** 757
[4.93] Yagi M, Wakatani M and Shaing K C 1998 J. Phys. Soc. Jpn. **57** 117
[4.94] Yagi M 1995 J. Plasma and Fusion Research **71** 1123
[4.95] Krommes J A 1996 Phys. Rev. E **53** 4865

[4.96] Bowman J C, Krommes J A and Ottaviani M 1993 Phys. Fluids B **5** 3558
[4.97] Bowman J C and Krommes J A 1997 Phys. Plasmas **4** 3895
[4.98] Itoh S-I and Itoh K 1999 J. Phys. Soc. Jpn. **68** 1891
[4.99] Itoh S-I and Itoh K 1999 J. Phys. Soc. Jpn. **68** 2611
[4.100] Itoh S-I and Itoh K 2000 J. Phys. Soc. Jpn. **69** 3253
[4.101] Kubo R 1963 J. Math. Phys. **4** 174
[4.102] Kitahara K and Yoshikawa K 1994 *Science of Non-Equilibrium Systems I* (Tokyo: Kodansha Scientific) §3.2 (in Japanese)
[4.103] Ueshima Y, Nishihara K, Barnett D M, Tajima T and Furukawa H 1997 Phys. Rev. E **55** 3439
[4.104] Balescu R 2000 Plasma Phys. Contr. Fusion **42** B1
[4.105] Balescu R 1995 Phys. Rev. E **51** 4807
[4.106] Balescu R 1997 *Statistical Dynamics: Matter out of Equilibrium* (London: Imperial College Press)
[4.107] Zagorodny A and Weiland J 1999 Phys. Plasmas **6** 2359
[4.108] Lorenz E N 1993 *The Essence of Chaos* (Reattle: University Washington Press) chap 4
[4.109] Bradshaw P, Cebeci, T, Whitelaw, J H 1981 *Engineering Calculation Method for Turbulent Flow* (London: Academic Press) p 37
[4.110] Moore D R, Toomre J, Knobroch E and Weiss N O 1983 Nature **303** 663
[4.111] Cross M C 1986 Phys. Letters A **119** 21
[4.112] Bazdenkov S V and Pogutse O P 1990 JETP Letters **57** 410
[4.113] Pogutse O P, Kerner W, Gribkov V, Dazdenkov S and Osipenko M V 1994 Plasma Phys. Contr. Fusion **36** 1963
[4.114] Sugama H and Horton W 1995 Plasma Phys. Contr. Fusion **37** 345
[4.115] Aoyagi T, Yagi M and Itoh S-I 1997 J. Phys. Soc. Jpn. **66** 2689
[4.116] Thyagaraya A, Haas F A and Harvey D J 1999 Phys. Plasmas **6** 2380
[4.117] Jensen M H, Paladin G and Vulpiani A 1992 Phys. Rev. A **45** 7214
[4.118] Yagi M, Itoh S-I, Itoh K and Fukuyama A 1999 Chaos **9** 393
[4.119] Waltz R E 1983 Phys. Fluids **26** 169
[4.120] Sugama H, Okamoto M and Wakatani M 1992 in *Plasma Physics and Controlled Nuclear Fusion Research* (Proc. 14th Conf. Würzburg 1992, Vienna: IAEA) vol 2 p 353
[4.121] Meiss J D, Cary J R, Grebogi C, Crawfield J D and Abarbanel H D I 1983 Physica D **6** 375
[4.122] Karney C F F 1983 Physica D **8** 360
[4.123] Ichikawa Y H, Kamimura T and Hatori T 1987 Physica D **29** 247
[4.124] Zaslavsky G M, Stevens D and Weitzner H 1993 Phys. Rev. E **48** 1683
[4.125] Balescu R, Vlad M and Spineau F 1998 Phys. Rev. E **58** 951
[4.126] Berk H L, Breizman B N, Ye H C 1993 Phys. Fluids B **5** 1506
[4.127] Balescu R 2000 J. Statistical Physics **98** 1169
[4.128] del-Castillo-Negrete D and Morrison P J 1993 Phys. Fluids A **5** 948
[4.129] Horton W, Park H-B, Kwon J-M, Strozzi D, Morrison P J and Choi D-I 1998 Phys. Plasmas **5** 3910
[4.130] Schmidt J and Yoshikawa S 1971 Phys. Rev. Lett. **26** 753
[4.131] Ohkawa T 1978 Phys. Lett. **67** A 35
[4.132] Parail V V and Pogutse O P 1980 JETP Letters **32** 384
[4.133] Kadomtsev B B and Pogutse O P 1985 in *Plasma Physics and Controlled Nuclear Fusion*

Research (Proc. 10th Conf. London 1984, Vienna: IAEA) vol 2 p 69
[4.134] Itoh K, Itoh S-I, Fukuyama A 1992 Phys. Rev. Lett. **69** 1050
[4.135] Kadomtsev B B and Pogutse O P 1970 in *Review of Plasma Physics* (ed. M. A. Leontovich, New York: Consultants Bureau) vol 5 p 312
[4.136] Carreras B A et al. 1983 Phys. Rev. Lett. **50** 503
[4.137] Guzdar P N, Drake J F, McCarthy D, Hassma A B and Liu C S 1993 Phys. Fluids B **5** 3712
[4.138] Terry P W, Diamond P H, Shaing K C, Garcia L, Carreras B A 1986 Phys. Fluids **29** 2501
[4.139] Wakatani M and Hasegawa A 1984 Phys. Fluids **27** 611
[4.140] Speiser T W 1970 Planet. Space. Sci. **18** 613
[4.141] Kaw P J, Valeo E J, Rutherford P H 1979 Phys. Rev. Lett. **43** 1398
[4.142] Aydemir A Y 1990 Phys. Fluids B **2** 2135
[4.143] Wesson J A 1991 in *Plasma Physics and Controlled Nuclear Fusion Research* (Proc. 13th Conf. Washington DC 1990, Vienna: IAEA) vol 2 p 79
[4.144] Lichtenberg A J, Itoh K, Itoh S-I and Fukuyama A 1992 Nucl. Fusion **32** 495
[4.145] Yagi M,Itoh K, Itoh S-I, Fukuyama A and Azumi M 1993 Phys. Fluids B **5** 3702
[4.146] Biskamp D, Drake J F 1994 Phys. Rev. Lett. **73** 971
[4.147] Ottaviani M and Polcelli F 1993 Phys. Rev. Lett. **71** 3802
[4.148] Naitou H, Kobayashi T and Tokuda S 1999 J. Plasma Phys. **61** 543
[4.149] Naitou H, Kuramoto T, Kobayashi T, Yagi M, Tokuda S and Matsumoto T 2000 J. Plasma Fusion Res. **76** 778
[4.150] Itoh S-I and Itoh K 1996 Plasma Phys. Control. Fusion **40** 1729
[4.151] Itoh S-I and Itoh K 1997 J. Phys. Soc. Jpn. **66** 1571
[4.152] Uchida M, Fukuyama A, Itoh K, Itoh S-I and Yagi M 1999 J. Plasma Fusion Res. series **2** p 117
[4.153] Romanelli F 1989 Phys. Fluids B **1** 1018
[4.154] Hong B-G and Horton W 1990 Phys. Fluids B **2** 978
[4.155] Hong B-G, Choi D-I and Horton W 1986 Phys. Fluids **29** 1872
[4.156] Connor J W, Taylor J B and Wilson H R 1993 Phys. Rev. Lett. **70** 1803
[4.157] Kim J Y and Wakatani M 1994 Phys. Rev. Lett. **73** 2200
[4.158] Rozhanskii V A 1981 JETP Lett. **34** 56 [Pis'ma Zh. Eksp. Teor. Fiz. **34** (1981) 60]
[4.159] Lee Y C, Dong J Q, Guzdar P N and Liu C S 1987 Phys. Fluids **30** 1331
[4.160] Horton W, Hong B G and Tang W M 1988 Phys. Fluids **31** 2971
[4.161] Hirshman S P and Molvig K 1979 Phys. Rev. Lett. **42** 648
[4.162] Glasser A, Frieman E A and Yoshikawa S 1974 Phys. Fluids **17** 181
[4.163] Roach C M et al. 1995 Plasma Phys. Contr. Fusion **37** 679
[4.164] Kim J and Wakatani M 1995 Phys. Plasmas **2** 1012
[4.165] Kishimoto Y et al. 1996 in *Proc. 16th International IAEA Fusion Energy Conference* (Montreal 1996) vol 2 p 581
[4.166] Romaneri F 1993 in *AIP Conference Proceedings 284* (New York: AIP) p 391
[4.167] Kishimoto Y, Kim Y-J, Horton W, Tajima T, LeBrun M J and Shirai H 1999 Plasma Phys. Contr. Fusion **41** A663
[4.168] Lewandowski J L V 1998 Plasma Phys. Contr. Fusion **40** 283
[4.169] Kuroda T, Sugama H, Kanno R and Okamoto M 2000 J. Phys. Soc. Jpn. **69** 2485
[4.170] Yagi M et al. 1994 J. Phys. Soc. Jpn. **63** 10
[4.171] Fukuyama A et al. 1994 Plasma Phys. Contr. Fusion **36** 1385

[4.172] Loses-Cardozo N 1995 Plasma Phys. Contr. Fusion **37** 799
[4.173] Smolyakov A I, Callen J D and Hirose A 1993 in *Local Transport Studies in Fusion Plasmas* (ed. J. D. Callen, G. Gorini and E. Sindoni, Bologna: SIF) p 87
[4.174] Rechester A B and Rosenbluth M N 1978 Phys. Rev. Lett. **40** 38
[4.175] Galeev A A and Zelenyi L M 1979 JETP Lett. **29** 614 [Pis'ma Zh. Eksp. Teor. Fiz. **29** (1979) 669]
[4.176] Krommes J A et al. 1983 J. Plasma Phys. **30** 11
[4.177] Galeev A A 1984 in *Basic Plasma Physics II* (ed. A. A. Galeev and R. N. Sudan, Amsterdam: North Holland) chap 6.2
[4.178] Mel'nikov Yu P 1996 JETP **82** 860 [Zh. Eksp. Teor. Fiz. **109** (1996) 1599]
[4.179] Eijnden E V and Balescu R 1997 Phys. Plasmas **4** 270
[4.180] Balescu R, Wang H-D and Misguich J H 1994 Phys. Plasmas **1** 3826
[4.181] Tange T, Inoue S, Itoh K and Nishikawa K 1979 J. Phys. Soc. Jpn. **46** 266
[4.182] Coppi B and Spight C 1978 Phys. Rev. Lett. **41** 551
[4.183] Waltz R E, Kerbel G D and Milovich J 1994 Phys. Plasmas 1 2229
[4.184] Itoh K, Yagi M, Itoh S-I and Fukuyama A 1997 Plasma Phys. Control. Fusion **39** 1561
[4.185] Drake J F, Guzdar P N and Hassam A B 1988 Phys. Rev. Lett. **61** 2205
[4.186] Jenko F, Dorland W, Kotschenreuther M and Rogers B N 2000 Phys. Plasmas **7** 1904
[4.187] Antonsen T et al. 1996 Phys. Plasmas **3** 2221
[4.188] Mima K and Nishikawa K 1984 in *Basic Plasma Physics II* (ed. A. A. Galeev and R. N. Sudan, Amsterdam: North Holland) chap 6.5
[4.189] Itoh S-I et al. 1994 Phys. Plasmas **1** 1154
[4.190] Itoh K, Itoh S-I, Fukuyama A, Yagi M and Azumi M 1993 J. Phys. Soc. Jpn. **62** 4269
[4.191] Itoh K, Itoh S-I, Fukuyama A and Yagi M 1996 J. Phys. Soc. Jpn. **65** 760
[4.192] Cheng C Z and Okuda H 1977 Phys. Rev. Lett. **38** 708
[4.193] Diamond P H et al. 1984 Phys. Fluids **27** 1449
[4.194] Strauss H R 1986 Phys. Fluids **29** 3668
[4.195] Bahattacharjee A and Hameiri E 1986 Phys. Rev. Lett. **57** 206
[4.196] Boozer A A 1986 J. Plasma Phys. **35** 133
[4.197] Yagi M, Itoh S-I, Itoh K and Fukuyama A 1997 J. Korean Phys. Soc. (Proc. Suppl.) **31** S189
[4.198] Itoh S-I and Itoh K 1988 Phys. Lett. A **127** 267
[4.199] Itoh S-I and Itoh K 1988 Phys. Rev. Lett. **60** 2276
[4.200] Shaing K C et al. 1989 in *Plasma Physics and Controlled Nuclear Fusion Research* (Proc. 12th Conf. Nice 1988, Vienna: IAEA) vol 2 p 13
[4.201] Itoh S-I and Itoh K 1989 Nucl. Fusion **29** 1031
[4.202] Shaing K C and Crume E Jr. 1989 Phys. Rev. Lett. **63** 2369
[4.203] Yoshizawa A 1991 Phys. Fluids B **3** 2723
[4.204] Drake J F et al. 1992 Phys. Fluids B **4** 488
[4.205] Rozhanskii V and Tendler M 1992 Phys. Fluids B **4** 1877
[4.206] Stringer T E 1993 Nucl. Fusion **33** 1249
[4.207] Diamond P H, Liang Y-M, Carreras B A and Terry P W 1994 Phys. Rev. Lett. **72** 2565
[4.208] Inoue S and Itoh K 1981 in *Plasma Physics and Controlled Nuclear Fusion Research* (Proc. 8th Conf. Brussel 1980, Vienna: IAEA) vol 2 p 649
[4.209] Craddock G G and Diamond P H 1991 Phys. Rev. Lett. **67** 1535

[4.210] Qiu X M, Bai L and Ran L B 1993 in *Plasma Physics and Controlled Nuclear Fusion Research* (Proc 14th Conf. Würzburg 1992, Vienna: IAEA) vol 2 p 269
[4.211] Ono M 1993 Phys. Fluids B **5** 241
[4.212] Inoue S et al. 1979 Nucl. Fusion **19** 1252
[4.213] Waltz R E 1982 Phys. Fluids **25** 1269
[4.214] Itoh S-I, Itoh K, Fukuyama A and Miura Y 1991 Phys. Rev. Lett. **67** 2485
[4.215] Hasegawa A and Wakatani M 1987 Phys. Rev. Lett. **59** 1581
[4.216] Carreras B A, Lynch V E and Garcia L 1991 Phys. Fluids B **3** 1438
[4.217] Wakatani M, Watanabe K, Sugama H and Hasegawa A 1992 Phys. Fluids B **4** 1754
[4.218] Drake J F, Antonsen T M, Finn J M et al. 1993 in *Plasma Physics and Controlled Nuclear Fusion Research* (Proc. 14th Conf. Würzburg 1992, Vienna: IAEA) vol 2 p 115
[4.219] Carreras B A et al. 1993 Phys. Fluids B **5** 1491
[4.220] Hallatscheck K 2000 Phys. Rev. Lett. **84** 5145
[4.221] Diamond P H and Kim Y B 1991 Phys. Fluids B **3** 1626
[4.222] Takayama A, Wakatani M and Sugama H 1996 Phys. Plasmas **3** 3
[4.223] Smolyakov A I and Diamond P H 1999 Phys. Plasmas **6** 4410
[4.224] Bernsteain A I and Diamond P H 1983 in *Basic Plasma Physics I* (ed. A. A. Galeev and R. N. Sudan, Amsterdam: North Holland) chap 2.5
[4.225] Krommes J A and Kim C-B 2000 Phys. Rev. E **62** 8508
[4.226] Galeev A A, Sagdeev R Z, Liu C S and Novakovskii V 1996 JETP **82** 875 [Zh. Eksp. Teor. Fiz. **109** (1996) 1626]
[4.227] Taguchi M 1991 Plasma Phys. Contr. Fusion **33** 859
[4.228] Hsu C T, Shaing K C and Gormly R 1994 Phys. Plasmas 1 132
[4.229] Kovrizhnykh L M 1984 Nucl. Fusion **24** 851
[4.230] Hastings D E and Kamimura T 1985 J. Comp. Phys. **61** 286
[4.231] Hastings D E, Hazeltine R D and Morrison P J 1986 Phys. Fluids **29** 69
[4.232] Yahagi E, Itoh K and Wakatani M 1988 Plasma Phys. Contr. Fusion **30** 1009
[4.233] Diamond P H, Lebedev V B, Newmann D E et al. 1995 Phys. Plasmas **2** 3685
——1997 Phys. Rev. Lett. **78** 1472
[4.234] Itoh K, Itoh S-I, Yagi M and Fukuyama A 1998 Phys. Plasmas **5** 4121
[4.235] Hazeltine R D, Lee E P and Rosenbluth M N 1971 Phys. Fluids **14** 361
[4.236] Greene J M, Johnson J L, Weimer K E and Winsor N K 1971 Phys. Fluids **14** 1258
[4.237] Shaing K C, Hazeltine R D and Sanuki H 1992 Phys. Fluids B **4** 404
[4.238] Taniuti T, Moriguchi H, Ishii Y, Watanabe K and Wakatani M 1992 J. Phys. Soc. Jpn. **61** 568
[4.239] Kuo H L 1963 Phys. Fluids **6** 195
[4.240] Deardorff J W 1965 Phys. Fluids **8** 1027
[4.241] Gage K S and Reid W H 1968 J. Fluid Mech. **33** 21
[4.242] See, e.g., Lehnert B 1966 Phys. Fluids **9** 1367
[4.243] Shaing K C 1991 Comments Plasma Phys. Contr. Fusion **14** 41
[4.244] Hassam A B 1991 Comments Plasma Phys. Contr. Fusion **14** 275
[4.245] Waltz R E, Kerbel G D, Milovich J and Hammett G W 1994 Phys. Plasmas **1** 2229
——1995 Phys. Plasmas **2** 2408
[4.246] Sanuki H 1984 Phys. Fluids **27** 2500
[4.247] Itoh S-I, Itoh K, Ohkawa T and Ueda N 1989 in *Plasma Physics and Controlled Nuclear Fusion*

Research (Proc. 12th Conf. Nice 1988, Vienna: IAEA) vol 2 p 23
[4.248] Inoue S, Itoh K and Yoshikawa S 1980 J. Phys. Soc. Jpn. **49** 367
[4.249] Waelbroeck F L et al. 1992 Phys. Fluids B **4** 1441
[4.250] Chu M S et al. 1995 Phys. Plasmas **2** 2236
[4.251] Bai L, Fukuyama A and Uchida M 1998 Plasma Phys. Contr. Fusion **40** 785
[4.252] Sugama H and Wakatani M 1991 Phys. Fluids B **3** 1110
[4.253] Biglari H, Diamond P H and Terry P W 1990 Phys. Fluids B **2** 1
[4.254] Zhang Y Z and Mahajan S M 1992 Phys. Fluids B **4** 1385
[4.255] Itoh S-I, Itoh K, Fukuyama A and Yagi M 1994 Phys. Rev. Lett. **72** 1200
[4.256] Hahm T S, Burrell K H, Lin Z, Nazikian R and Synakowski E J 2000 Plasma Phys. Contr. Fusion **42** A205
[4.257] Hamaguchi S and Horton W 1992 Phys. Fluids B **4** 319
[4.258] Kim Y-J, Kishimoto Y, Wakatani M and Tajima T 1996 Phys. Plasmas **3** 3689
[4.259] Waltz R E, Staebler G M, Dorland W, Hammett G W, Kotschenreuther M and Konings J A 1997 Phys. Plasmas **4** 2482
[4.260] Hahm T S and Burrell K H 1995 Phys. Plasmas **2** 1648
[4.261] Itoh K, Itoh S-I, Fukuyama A, Sanuki H and Yagi M 1994 Plasma Phys. Contr. Fusion **36** 123
[4.262] Itoh K, Ohkawa T, Itoh S-I, Yagi M and Fukuyama A 1998 Plasma Phys. Contr. Fusion **40** 661
[4.263] Weynants R R, Jachmich S and Van Oost G 1998 Plasma Phys. Contr. Fusion **40** 635
[4.264] Cornelis J, Sporken R, Van Oost G and Weynants R R 1994 Nucl. Fusion **34** 171
[4.265] Herbert T 1980 AIAA J. **18** 243
[4.266] Montgomery D 1989 in *Nagoya Lectures in Plasma Physics and Controlled Fusion* (ed. Y. H. Ichikawa and T. Kimimura, Tokyo: Tokai University Press) p 207
[4.267] Waleffe F 1997 Phys. Fluids **9** 883
[4.268] Itoh S-I, Itoh K, Zushi H and Fukuyama A 1998 Plasma Phys. Contr. Fusion **40** 879
[4.269] Berman R H, Tetreault D J and Dupree T H 1983 Phys. Fluids **26** 2437
[4.270] Rebut P H and Hugon M 1985 in *Plasma Physics and Controlled Nuclear Fusion Research* (Proc. 10th Conf. London 1984, Vienna: IAEA) vol 2 p 197
[4.271] Waltz R E 1985 Phys. Rev. Lett. **55** 1098
[4.272] Biskamp D and Walter M 1985 Phys. Lett. **109** A 34
[4.273] Sydora R D et al. 1985 Phys. Fluids **28** 528
[4.274] Scott B D 1990 Phys. Rev. Lett. **65** 3289
[4.275] Scott B D 1992 Phys. Fluids B **4** 2468
[4.276] Carreras B A, Sidikman K, Diamond P H, Terry P W and Garcia L 1992 Phys. Fluids B **4** 3115
[4.277] Fukuyama A et al. 1993 in *Plasma Physics and Controlled Nuclear Fusion Research* (Proc. 14th Conf. Würzburg 1992, Vienna: IAEA) vol 2 p 363
[4.278] Nordman H, Pavlenko V P and Weiland J 1993 Phys. Plasmas B **5** 402
[4.279] Itoh K, Itoh S-I, Fukuyama A, Yagi M and Azumi M 1994 Plasma Phys. Cont. Fusion **36** 279
[4.280] Biskamp D and Zeiler A 1995 Phys. Rev. Lett. **74** 706
[4.281] Drake J F, Zeiler A and Biskamp D 1995 Phys. Rev. Lett. **75** 4222
[4.282] Itoh K et al. 1996 J. Phys. Soc. Jpn. **65** 2749
[4.283] Knobloch E and Weiss N O J 1983 Physica D **9** 379
[4.284] Bekki N and Karakisawa T 1995 Phys. Plasmas **2** 2945
[4.285] Yagi M, Itoh S-I, Itoh K, Fukuyama A and Azumi M 1995 Phys. Plasmas **2** 4140

[4.286] Pfirsch D 1993 Phys. Rev. E **48** 1428
[4.287] Pearlstein L D and Berk H L 1969 Phys. Rev. Lett. **23** 220
[4.288] Ross D W and Mahajan S M 1978 Phys. Rev. Lett. **40** 324
[4.289] Tsang K T, Catto P J, Whitson J C and Smith J 1978 Phys. Rev. Lett. **40** 327
[4.290] Guzdar P N, Chen L, Kaw P K and Oberman C 1978 Phys. Rev. Lett. **40** 1566
[4.291] Cordey J G, Jones E M and Start D F H 1979 Plasma Phys. **21** 725
[4.292] Rutherford P H 1973 Phys. Fluids **6** 1903
[4.293] Callen J D, Qu W X, Siebert K D, Carreras B A, Shaing K C and Spong D 1986 in *Plasma Physics and Controlled Nuclear Fusion Research* (Proc. 11th Conf. Kyoto 1986, Vienna: IAEA) vol 2 p 157
[4.294] Carrera R, Hazeltine R D and Kotschenreuther M 1986 Phys. Fluids **29** 899
[4.295] Waelbroeck F L and Fitzpatrick R 1997 Phys. Rev. Lett. **78** 1703
[4.296] Smolyakov A I 1993 Plasma Phys. Contr. Fusion **35** 657
[4.297] Zabiego M and Garbet X 1994 Phys. Plasmas **1** 1890
[4.298] Wilson H R, Connor J W, Hastie R J and Hegna C C 1996 Phys. Plasmas **3** 248
[4.299] Mikhailovskii A B, Pustovitov V D, Tsypin V S and Smolyakov A I 2000 Phys. Plasmas **7** 1204
[4.300] Mikhailovskii A B, Pustovitov V D, Smolyakov A I and Tsypin V S 2000 Phys. Plasmas **7** 1214
[4.301] Chang Z, Callen J D, Fredrickson E D et al. 1995 Phys. Rev. Lett. **74** 4663
[4.302] Zohm H, Gates D A, Wilson H R et al. 1997 Plasma Phys. Contr. Fusion **39** B237
[4.303] Sauter O, Lahaye R J, Chang Z et al. 1997 Phys. Plasmas 4 1654
[4.304] See also *ITER Physics Basis* 1999 Nucl. Fusion **39** chap 3, sec 2.3
[4.305] Mercier C 1983 Sov. J. Plasma Phys. **9** 82 [Fiz. Plasmy **9** (1983) 132]
[4.306] Lichtenberg A J 1984 Nucl. Fusion **24** 1277
[4.307] Itoh S-I, Itoh K, Fukuyama A and Yagi M 1996 Phys. Rev. Lett. **76** 920
[4.308] Fukuyama A, Itoh K, Itoh S-I and Yagi M 2000 Nucl. Fusion **40** 685
[4.309] Furuya A, Itoh S-I and Yagi M 2000 Contrib. Plasma Phys. **40** 375
[4.310] Waddel B V, Carreras B, Hicks H R, Holmes J A and Lee D K 1978 Phys. Rev. Lett. **41** 1386
[4.311] Carreras B A et al. 1981 Phys. Fluids **24** 66
[4.312] Biskamp D and Welter H 1983 in *Plasma Physics and Controlled Nuclear Fusion Research* (Proc. 9th Conf. Baltimore 1982, Vienna: IAEA) vol 3 p 373
[4.313] Izzo R et al. 1983 Phys. Fluids **26** 2240
[4.314] Kurita G et al. 1986 Nucl. Fusion **26** 449
[4.315] Bondeson A 1986 Nucl. Fusion **26** 929
[4.316] Taylor G I 1934 Proc. R. Soc. London A **146** 501
[4.317] For recent review, see, e.g., Mel'nikov V I 1991 Phys. Rep. **209** 1
[4.318] Itoh S-I and Itoh K 1990 J. Phys. Soc. Jpn. **59** 3815
[4.319] Fukuyama A, Itoh K, Itoh S-I, Yagi M, Azumi M 1995 Plasma Phys. Contr. Fusion **37** 611
[4.320] Zeiler A, Biskamp D, Drake J F and Rogers B N 1998 Phys. Fluids **5** 2654
[4.321] Rogister A L 1994 Plasma Phys. Contr. Fusion **36** A219
[4.322] Cohen R H and Xu X 1995 Phys. Plasmas **2** 3374
[4.323] Guzdar P and Hassma A B 1996 Phys. Plasmas **3** 3701
[4.324] Rogers B N and Drake J F 1997 Phys. Rev. Lett. **79** 229
[4.325] Scott B D 1998 Plasma Phys. Contr. Fusion **40** 823
[4.326] Chankin A V and Matthews G F 1998 Contrib. Plasma Phys. **38** 177

[4.327] Kerner W, Igitkhanov Yu, Janeschitz G and Pogutse O 1998 Contrib. Plasma Phys. **38** 118
[4.328] Hinton F L 1991 Phys. Fluids B **3** 696
[4.329] Hinton F L and Staebler G M 1993 Phys. Fluids B **5** 1281
[4.330] Taylor J B, Connor J W and Helander P 1998 Phys. Plasmas **5** 3065
[4.331] Hinton F L, Staebler G M and Kim Y-B 1994 Plasma Phys. Contr. Fusion **36** A237
[4.332] Fukuyama A, Itoh S-I, Yagi M and Itoh K 1995 Nucl. Fusion **35** 1669
[4.333] Kotschenreuther M, Dorland W, Beer M A and Hammett G W 1995 Phys. Plasmas **2** 2381
[4.334] Fukuyama A et al. 1996 Plasma Phys. Contr. Fusion **38** 1319
[4.335] Staebler G M, Hinton F L and Wiley J C 1996 Plasma Phys. Contr. Fusion **38** 1461
[4.336] Connor J W et al. 1996 in *Proc. Int. Conf. on Fusion Energy* (Montreal. 1996) vol 2 p 935
[4.337] Kinsey J, Bateman G, Kritz A and Redd A 1996 Phys. Plasmas **3** 561
[4.338] Cherubini A, Erba M, Parail V, Springmann E and Taroni A 1996 Plasma Phys. Contr. Fusion **38** 1421
[4.339] Nordoman H, Strand P, Weiland J and Christiansen J P 1997 Nucl. Fusiobn **37** 413
[4.340] Zonca P, Frigione D, Marinucci M, Zanza V and Romaneli F 1997 in *Theory of Fusion Plasmas* (ed. J. W. Connor, E. Sindoni and J. Vaclavik, Bologna: Editrice Compositori) p 399
[4.341] Tendler M 1997 Plasma Phys. Contr. Fusion **39** B371
[4.342] Fukuyama A et al. 1998 Plasma Phys. Contr. Fusion **40** 653
[4.343] Rosenbluth M N 1999 Plasma Phys. Contr. Fusion **41** A99
[4.344] *ITER Physics Basis* 1999 Nucl. Fusion **39** 2175 sec 8
[4.345] Carreras B A, Newmann D E, Diamond P H and Liang Y-M 1994 Phys. Plasmas **1** 4014
[4.346] Carreras B A, Diamond P H and Vetoulix G 1996 Phys. Plasmas **3** 4016
[4.347] Dnestrovskij A Yu, Parail V V and Vojtsenkhhovich I A 1993 in *Plasma Physics and Controlled Nuclear Fusion Research* (Proc. 14th Conf. Würzburg 1992, Vienna: IAEA) vol 2 p 371
[4.348] Horton W, Hu G and Laval G 1996 Phys. Plasmas **3** 2912
[4.349] Osipenko M V 1997 Plasma Phys. Report **23** 837
[4.350] Yagi M, Itoh S-I, Itoh K and Fukuyama A 1997 Plasma Phys. Contr. Fusion **39** 1887
[4.351] Spatschek K H 1999 Plasma Phys. Contr. Fusion **41** A115
[4.352] Itoh S-I, Itoh K and Fukuyama A 1993 Nucl. Fusion **33** 1445
[4.353] Zohm H 1994 Phys. Rev. Lett. **72** 222
[4.354] Vojtsekhovich L A, Dnestrovskij A Yu and Parail V V 1995 Nucl. Fusion **35** 631
[4.355] Toda S et al. 1996 Plasma Phys. Contr. Fusion **38** 1337
[4.356] Lebedev V B, Diamond P H, Gruzinova I and Carreras B A 1995 Phys. Plasmas **2** 3345
[4.357] Takayama A and Wakatani M 1996 Plasma Phys. Contr. Fusion **38** 1411
[4.358] Hegna C, Connor J W, Hastie R J and Wilson H R 1996 Phys. Plasmas **3** 248
[4.359] Connor J W and Wilson H R 1997 in *Theory of Fusion Plasmas* (ed. J. W. Connor, E. Sindoni and J. Vaclavik, Bologna: Editrice Compositori) p 441
[4.360] Connor J W, Hastie R J, Wilson H R and Miller R L 1998 Phys. Plasmas **5** 2687
[4.361] Manickam J 1992 Phys. Fluids B **4** 1901
[4.362] Huysmans G T A, de Blanck H J, Kerner W, Goedbread J P and Nave M F F 1992 (Proc. 19th EPS Conf. on Controlled Fusion and Plasma Physics Innsbruck 1992) (ed. W Freysinger et al., Geneva: European Physical Society) part I p 247
[4.363] Itoh S-I, Itoh K, Fukuyama A and Yagi M 1996 Plasma Phys. Contr. Fusion **38** 527
[4.364] Itoh S-I, Itoh K, Fukuyama A and Yagi M 1996 Plasma Phys. Contr. Fusion **38** 1367

[4.365] Itoh S-I and Itoh K 2000 J Phys. Soc. Jpn. **69** 408
[4.366] Itoh S-I and Itoh K 2000 J. Phys. Soc. Jpn. **69** 427
[4.367] Fowler R H 1936 *Statistical Mechanics* Second edition (Cambridge: Cambridge University Press) chap 18
[4.368] Itoh S-I, Toda S, Yagi M, Itoh K and Fukuyama A 1998 J. Phys. Soc. Jpn. **67** 4080
[4.369] Toda S, Itoh S-I, Yagi M, Itoh K and Fukuyama A 1999 J. Phys. Soc. Jpn. **68** 3520
[4.370] Callen J D and Kissick M W 1997 Plasma Phys. Contr. Fusion **39** B173
[4.371] Rosenbluth M N and Liu C S 1976 Phys. Fluids **19** 815
[4.372] Lazzara A and Putterman S 1986 Phys. Rev. Lett. **57** 2810
[4.373] Hazeltine R D 1999 J. Plasma Fusion Res. series **2** 12
[4.374] Iwasaki T. Itoh S-I. Yagi M. Itoh K and Stroth U 1999 J. Phys. Soc. Jpn. **68** 478
[4.375] Iwasaki T, Toda S. Itoh S-I, Yagi M and Itoh K 1999 Nucl. Fusion **39** 2127
[4.376] Parail V V et al. 1997 Nucl. Fusion **32** 1985
[4.377] Parail V V et al. 1998 Plasma Physics Contr. Fusion **40** 805
[4.378] Diamond P H and Hahm T S 1995 Phys. Plasmas **2** 3640
[4.379] Krommes J A 2000 Phys. Plasmas **7** 1064
[4.380] Lin Z, Hahm T S, Lee W W, Tang W M and Diamond P H 1999 Phys. Rev. Lett. **83** 3645
[4.381] Hinton F L and Rosenbluth M N 1999 Plasma Phys. Contr. Fusion **41** A653
[4.382] Garbet X and Waltz R E 1996 Phys. Plasma **3** 1898; 1998 Phys. Plasmas **5** 2836
[4.383] Carreras B A et al. 1996 Phys. Plasmas **3** 2903
[4.384] Sarazin Y and Ghendrih Ph 1998 Phys. Plasmas **5** 4214
[4.385] Naulin V, Nycander J and Rasmussen J J 1998 Phys. Rev. Lett. **81** 4148
[4.386] Beyer P, Sarazin Y, Garbet X, Ghendrih P and Benkadda S 1999 Plasma Phys. Contr. Fusion **41** A757
[4.387] Thyagaraja A 2000 Plasma Phys. Contr. Fusion **42** B255
[4.388] Thyagaraja A 1994 Plasma Phys. Contr. Fusion **36** 1037
[4.389] Yagi M 1999 J. Plasma Fusion Research **75** 1097 (in Japanese)
[4.390] Yagi M, Itoh S-I, Itoh K and Fukuyama A 2000 Plasma Phys. Contr. Fusion **42** A133
[4.391] Kubota T, Itoh S-I, Yagi M and Itoh K 1998 J. Phys. Soc. Jpn. **67** 3100
[4.392] Matsukawa S, Itoh S-I and Yagi M 2000 Contrib. Plasma Phys. **40** 381
[4.393] Newmann D E, Carreras B A, Diamond P H and Hahm T S 1996 Phys. Plasmas **3** 1858
[4.394] Dendy R O and Helander P 1997 Plasma Phys. Contr. Fusion **39** 1947
[4.395] Bak P, Tang C and Wiesenfeld K 1987 Phys. Rev. Lett. **59** 381
[4.396] Carreras B A et al. 1998 Phys. Plasmas **5** 3632
[4.397] Carreras B A et al. 1999 Phys. Plasmas **6** 1885
[4.398] Krommes J A 2000 Phys. Plasmas **7** 1752

5. Summary

Theoretical methods for fluid and plasma turbulence have made remarkable progress in this century. Understanding of turbulence has become mature in various aspects: the excitation of fluctuations by instabilities that are caused by inhomogeneities, the energy partition via cascade and enhanced dissipation, the formation of meso-scale structures by the inverse cascade or parametric excitation, the transport and destruction of inhomogeneous structure by fluctuations, the suppression of turbulence by inhomogeneity, and the subcritical excitation due to nonlinear instabilities. These processes are either cooperating or competing with each other, and constitute the dynamics of turbulence. The subject of this review article is the illustration of turbulence theories which have given analytic insights into these essential features of highly-fluctuating media.

Among various nonlinearly interacting dynamics in fluids and plasmas, turbulence is characterized by a large number of degrees of freedom. One of the main advances is seen in the statistical description of turbulence, which is discussed in this review. Contrary to the case of media in or near the thermodynamical equilibrium, which is described by well-established statistical laws (Maxwell–Boltzmann statistics, Fermi–Dirac statistics or Bose–Einstein statistics), a turbulent state is in a far-non-equilibrium state. Statistical theories have been developed, and various useful closure models have been investigated. On this basis, hierarchical modelling like the TSDIA and mean-field approaches like the K–ε model are developed. The renormalized dielectric tensor is derived in plasma turbulence theories, which describe self-consistent systems of equations for the turbulent spectrum. These methods allow one to investigate the dynamics of generation and nonlinear decorrelation of turbulence, providing a key to the understanding of turbulence and turbulent transport. At the same time, the statistical physics of a non-equilibrium state is generalized. Various theoretical formulae are surveyed.

Another outstanding progress in turbulence theories is the understanding of the mutual interactions between perturbations and inhomogeneities with various length scales. This mechanism introduces a variety of characteristics of turbulent media. Inhomogeneous structures (e.g., sheared flow, pressure gradient, localized electromagnetic fields, etc.) generate fluctuations so that ordered structures are destroyed through turbulent transport. Simultaneously, global or ordered structures are generated from the nonlinear interactions among turbulent fluctuations. Theories have shown that these two competing processes (i.e., the destruction and production mechanisms) are equally important, providing an explanation to the question: Why is nature full of observable structures although Reynolds numbers are extremely large so that fully developed turbulence might erase inhomogeneities? Structural transitions of turbulent media, of which the H-mode transition is the leading example in plasma

physics, are described. The dynamo is another challenging example, theories for which are addressed.

In this review article, we have surveyed methods in turbulence theories. Much common physics has flourished in fluid dynamics and plasma physics. Therefore, emphasis is put on those plasma-turbulence theories that are based on a fluid description of plasmas, and little about kinetic-turbulence theories is discussed.

Another approach to investigate turbulence is direct nonlinear simulation. This approach is indispensable, and is complementary to the methods which were described in this article. Quantitative description requires direct nonlinear simulations, because exactly solvable systems are very limited in the field of turbulence problems. The description of direct numerical simulation is limited in this review. The turbulence theories may deepen further understanding of the physical mechanisms and provide laws that govern turbulent phenomena. Turbulence theories of fluid and plasma, cooperating with simulation methods, will continue to challenge the frontier of physics, i.e., the problem of the millenaries, '$\Pi\alpha\nu\tau\alpha\ \rho\epsilon\iota$ (all things flow)'.

Acknowledgments

Two of the authors (SII and KI) wish to acknowledge colleagues, in particular Prof. A. Fukuyama, Dr. M. Yagi, Prof. R. Balescu, Dr. J. W. Connor, and Dr. J. A. Krommes for useful discussions. This work is partly supported by the Grant-in-Aid for Scientific Research of Ministry of Education, Science, Sports and Culture Japan, by the collaboration programme of National Institute for Fusion Science and by the collaboration programme of the Research Institute for Applied Mechanics of Kyushu University.

Appendices

A. Quasi-linear theory of transport

Within the framework of the quasi-linear theory, which is briefly explained here, the reactions of turbulence on the mean distribution and global profile can be calculated [4.31]. The fluctuation-driven flux can be characterized by a transport matrix.

A.1. Reaction on mean distribution

The back-reaction of the linear response affects the average distribution function as

$$\frac{\partial}{\partial t}\bar{f} = \frac{e}{m}\left\langle \left(\tilde{\mathbf{E}} + \mathbf{v}\times\tilde{\mathbf{B}}\right)\cdot\frac{\partial}{\partial \mathbf{v}}\tilde{f}\right\rangle. \tag{A.1}$$

Upon substitution of the linear response function $\tilde{f}$ into Eq. (A.1), the evolution equation is obtained. The electrostatic limit, $\tilde{\mathbf{E}} = -\nabla\tilde{\phi}$, is shown for an illustration as

$$\frac{\partial}{\partial t}\bar{f} = \left(\frac{e}{m}\right)^2 \sum_{\mathbf{k}} |\phi_{\mathbf{k}}|^2\, \mathbf{k}\cdot\frac{\partial}{\partial \mathbf{v}}\Im\left(\frac{1}{\omega - \mathbf{k}\cdot\mathbf{v}}\right)\mathbf{k}\cdot\frac{\partial}{\partial \mathbf{v}}\bar{f}. \tag{A.2}$$

A diffusion equation in the phase space is obtained, with the diffusion coefficient being a quadratic function of the perturbation amplitude in the quasi-linear model. The influence of a strong magnetic field and finite-gyroradius effects has been extensively discussed in the literature.

A.2. Influence on the global profile and transport matrix

In inhomogeneous plasmas, diffusion in the phase space is also associated with transport in the real space.

The fluctuation-driven fluxes of particle, energy, and current have been calculated by use of the quasilinear theory. Fluxes are expressed in terms of a transport matrix. Similar to neoclassical transport, the transport matrix has been obtained for electron fluxes. In this appendix, by convention denotes the particle flux, not the decorrelation rate. An example is quoted from [4.38] as

$$\begin{pmatrix} \Gamma_r \\ \frac{q_{e,r}}{T_e} \\ \frac{J_\parallel}{T_e} \end{pmatrix} = -\begin{pmatrix} D & -\frac{3}{2}D & D_{31} \\ -\frac{3}{2}D & \frac{13}{4}D & -0.87D_{31} \\ D_{31} & -0.87D_{31} & -\frac{\sigma_{eC}}{T_e} \end{pmatrix}\begin{pmatrix} X_1 \\ X_2 \\ E_\parallel \end{pmatrix}, \tag{A.3}$$

where the driving forces are given as

$$X_1 = -\left\langle\frac{\omega}{m}\right\rangle\frac{eBr}{T_e} - \frac{T_i}{T_e}\frac{1}{p_i}\frac{dp_i}{dr} - \frac{e}{T_e}\frac{d\phi}{dr} + \frac{T_e + T_i}{T_e}\frac{1}{p}\frac{dp}{dr}, \tag{A.4a}$$

$$X_2 = \frac{1}{T_e}\frac{dT_e}{dr}, \tag{A.4b}$$

and the matrix elements are given as

$$D = \frac{\sqrt{\pi}}{4} n_{\rm e} \rho_{\rm pe}^2 \frac{v_{\rm the}}{qR} \sum_{m,n,\omega} \frac{m^2}{|m-nq|} \left(\frac{e\tilde{\phi}_{m,n,\omega}}{\sqrt{2}T_{\rm e}} \right)^2, \tag{A.5a}$$

$$D_{31} = \frac{\sqrt{\pi}}{2} \frac{n_{\rm e}}{\nu_{\rm ei} B_p} \frac{v_{\rm the}}{qR} \sum_{m,n,\omega} \frac{m(m-nq)}{|m-nq|} \left(\frac{e\tilde{\phi}_{m,n,\omega}}{\sqrt{2}T_{\rm e}} \right)^2, \tag{A.5b}$$

and

$$\sigma_{\rm e\zeta} = \sigma_{\rm c} \left[1 - 0.175 \frac{\sqrt{\pi} v_{\rm the}}{\nu_{\rm ei} qR} \sum_{m,n,\omega} |m-nq| \left(\frac{e\tilde{\phi}_{m,n,\omega}}{\sqrt{2}T_{\rm e}} \right)^2 \right], \tag{A.5c}$$

where the overline, which denotes the global (averaged) quantity, is suppressed for simplicity. In this expression, (m, n) are the poloidal and toroidal mode numbers, respectively, $\rho_{\rm pe}$ is the electron gyroradius in the poloidal magnetic field, and σ_c is the electrical conductivity (determined by the collisional processes). There are other anomalous fluxes, such as the ion energy flux $q_{{\rm i},r}$, electron–ion energy equipartition Q_{ei}, ion shear viscosity, etc. More complete transport matrices for the sets of fluxes $(\Gamma, q_{{\rm e},r}, q_{{\rm i},r}, J_\parallel)$ or $(\Gamma, q_{{\rm e},r}, q_{{\rm i},r}, Q_{ei})$ are explicitly given in [4.40]. A transport matrix that includes the ion shear viscosity is discussed in [4.39].

The transport matrix is a quadratic function of the fluctuation amplitude. The fluctuation level is not determined in this framework, and must be given by other theoretical considerations. An order-of-magnitude estimate of the flux is often made by employing the fluctuation level of $e\tilde{\phi}/T \sim 1/(kL_n)$. However, that level is sufficiently high that the assumption of quasilinear response is violated, as is noted in §4.1.3.

A.3. On the inward pinch

In addition to the off-diagonal terms of the transport matrix, which are associated with pinch terms, an additional mechanism exists that causes particle and energy pinches. Specifically, fluctuation-driven flux caused by the inhomogeneity of the magnetic field has been analyzed. This flux is seen as a pinch.

The linear response of the distribution function to the electric-field perturbation is calculated in a toroidal geometry. By use of a simplified equation, i.e., the gyrokinetic equation [see, e.g., Eq. (2.28)], one has the response as

$$\tilde{f} = \frac{-i}{\omega - k_\parallel v_\parallel - \omega_{\rm M}} \left(\tilde{\mathbf{V}}_{E\times B} \cdot \nabla \bar{f} - \frac{e}{T} v_\parallel \tilde{E}_\parallel \bar{f} - \frac{v_\perp^2 + 2v_\parallel^2}{v_{\rm th}^2} \tilde{\mathbf{V}}_{E\times B} \cdot \frac{\nabla \bar{B}}{\bar{B}} \bar{f} \right), \tag{A.6}$$

where $\tilde{\mathbf{V}}_{E\times B} = \tilde{\mathbf{E}} \times \mathbf{b}/\bar{B}$ and $\omega_M = (v_\perp^2 + 2v_\parallel^2)\omega_c^{-1}\mathbf{k}\cdot(\mathbf{b}\times\nabla\bar{B})\bar{B}^{-1}$ is the magnetic drift frequency ($\bar{B} = |\bar{\mathbf{B}}|$) [4.173]. The particle flux, which is caused by the fluctuating $E\times B$ drift, is given as

$$\Gamma = \left\langle \tilde{\mathbf{V}}_{E\times B}\tilde{n} \right\rangle = \left\langle \tilde{\mathbf{V}}_{E\times B} \int d\mathbf{v}\tilde{f}(\mathbf{v}) \right\rangle. \tag{A.7}$$

There thus appears a term proportional to the gradient of the magnetic field [the third term on the right-hand side of Eq. (A.6)]. The third term, which is a diffusion in phase space, is associated with a plasma flux directed to the region of higher magnetic field. Note that the origin of this third term in Eq. (A.6) is the gradient- B drift term in the gyrokinetic equation Eq. (2.28) [the second term of $\mathbf{v}_D$, which is explicitly given after Eq. (2.28)].

This flux can cause the pinch in tokamaks. It is in the direction of the major radius for tokamak configurations, so the component of this flux across the magnetic surface has a poloidal dependence of $\cos\theta$, where θ is the poloidal angle. As has been discussed in the case of collisional transport (Pfirsch–Schlüter diffusion), the surface area has a dependence as $1+(r/R)\cos\theta$, and is larger in the lower-field side. As a result, an inward pinch is induced. Upon comparing the first term and the third term on the right-hand side, one has an order-of-magnitude estimate

$$\frac{\text{flux by the third term}}{\text{flux by the first term}} \cong \frac{-D_{\mathrm{QL}} r R^{-2} n}{-D_{\mathrm{QL}}\nabla n}. \tag{A.8}$$

From this estimate one has the particle and heat fluxes, Γ and q_r, as

$$\Gamma \cong -D_{\mathrm{QL}}\nabla n - D_{\mathrm{QL}}\frac{r}{R^2}n \tag{A.9a}$$

and

$$q_r \cong -\chi_{\mathrm{QL}}\nabla\bar{p} - \chi_{\mathrm{QL}}\frac{r}{R^2}\bar{p}, \tag{A.9b}$$

where D_{QL} and χ_{QL} are the quasi-linear diffusion coefficient and quasilinear thermal diffusion coefficient, respectively. If the gradient is weak, the pinch term can be effective. The pinch term vanishes near the magnetic axis $r = 0$, because the poloidal-angle dependence of the surface element vanishes there. If the fluctuation amplitude is not constant on the magnetic surface, like the case of ballooning instabilities, the pinch term could be larger.

B. Thermodynamical equilibrium and statistical property

B.1. Thermodynamical equilibrium

In the fluid dynamics of the invicid limit, the Hopf solution for the characteristic function $\Phi(u_k)$ is known as

$$\Phi(u_k) = \exp\left[-\frac{k_B T}{2}\int d\mathbf{k} u_{-k.a}(\delta_{ab} - k_a k_b k^{-2}) u_{k.b}\right]. \tag{B.1}$$

This solution corresponds to a state that all the modes are equally excited satisfying the equipartition law as

$$E(k) = 4\pi k_B T k^2. \tag{B.2}$$

Some particular solutions of the plasma equations are obtained in the thermodynamical equations.

The equilibrium properties of the Hasegawa–Mima (HM) equation have been studied. In the state that a large number of modes are excited, equipartition is sometimes assumed. A function which is expressed in terms of constants of motion is a particular solution of the Liouville equation. For the HM equation, the energy and enstrophy are conserved. In the Fourier representation, they are given as

$$\mathcal{E} = (1/2)\sum_k (1 + k_\perp^2)\phi_k^2,$$

$$\mathcal{U} = (1/2)\sum_k k_\perp^2 (1 + k_\perp^2)\phi_k^2.$$

In thermodynamical equilibrium, the Boltzmann distribution is sometimes assumed and the probability density function (PDF) given as [B.1, B.2]

$$P[\{\phi_k\}] \propto \exp(-\alpha\mathcal{E} - \beta\mathcal{U}) = \prod_k \exp\left[-\left(\frac{\alpha}{2} + \frac{\beta}{2}k_\perp^2\right)(1 + k_\perp^2)\phi_k^2\right]. \tag{B.3}$$

The statistical averages of Fourier components of the fluctuation potential, energy, and enstrophy are given as

$$\langle \phi_k^2 \rangle = \frac{1}{(1 + k_\perp^2)(\alpha + \beta k_\perp^2)}, \tag{B.4a}$$

$$\langle \mathcal{E}_k \rangle = \frac{L^2}{2\pi}\frac{k}{(\alpha + \beta k_\perp^2)}, \tag{B.4b}$$

$$\langle \mathcal{U}_k \rangle = \frac{L^2}{2\pi}\frac{k(1 + k_\perp^2)}{(\alpha + \beta k_\perp^2)}, \tag{B.4c}$$

where L^2 is the plasma volume per unit length in the $\hat{z}$-direction (ignorable coordinate). The energy is larger in the longer-wavelength region, and the enstrophy is dominant

in the shorter-wavelength region. In the limit of strong collisions, two equations in the Hasegawa–Wakatani (HW) equations become decoupled. In such a limit, the internal energy

$$\mathcal{E}^{(n)} = (1/2)\sum_k n_k^2$$

and the cross-correlation between the density and the vorticity,

$$\mathcal{C} = (1/2)\sum_k k_\perp^2 n_k \phi_k,$$

become an additional integral of motion. The thermodynamical equilibrium distribution function is given as

$$P[\{\phi_k\}] \propto \exp\left(-\alpha\mathcal{E} - \beta\mathcal{U} - \alpha'\mathcal{E}^{(n)} - \beta'\mathcal{C}\right). \tag{B.5}$$

In this case, the functional dependence of $\langle\mathcal{E}_k\rangle$ and $\langle\mathcal{U}_k\rangle$ on $k_\perp^2$ is similar to the one in Eqs. (B.4b) and (B.4c), and an asymptotic dependence is unchanged, i.e.,

$$\langle\mathcal{E}_k\rangle \propto k_\perp^{-1} \quad \text{and} \quad \langle\mathcal{U}_k\rangle \propto k_\perp$$

in the large-$k_\perp^2$ limit. It is noted by [B.3] that the 'temperature' of quasi-particle could become negative if one employs the Gibbs canonical ensemble. Instead, the microcanonical ensemble is used in [4.46]. The particular solution Eq. (B.3) is divergent in the short-wavelength limit. That is, it is not a physically observable state. However, it would give some insight for the property of the plasma dynamics.

Equation (B.3) is expressed in terms of Fourier space. The choice of other functional spaces is possible. The Beltrami field

$$\nabla \times \mathbf{u} = \chi\mathbf{u}, \tag{B.6}$$

where $\{\mathbf{u}\}$ constitutes a complete set of orthogonal eigenfunctions, has been used to analyze the thermodynamical equilibrium [B.4]. In this study, the distribution function is expressed in terms of energy and helicity. A similar power-law distribution is obtained.

A large amplitude in the long-wavelength region is often called the 'inverse-cascade of energy'. In other words, the system of equations has a property of anti-shielding. Consider the situation there are many clusters of charge. One might call them vortices, or quasi-particles, or clumps. The dominance of fluctuation energy in the long-wavelength region means that a positive vortex is surrounded mainly by positive vortices: a negative one is mainly by negative ones. The correlation function of the vorticity is obtained by use of the microcanonical ensemble as

$$\langle\rho(0)\rho(\ell)\rangle \propto K_0\left[\frac{\ell}{\ell_s}\exp\left(-\frac{1}{2}\frac{\mathcal{E}}{Ne^2}\right)\right], \tag{B.7}$$

where K_0 is the zeroth-order modified Bessel function of the second kind, ℓ_s is the screening length in the HM equation, N and e are the number and charge of quasi-particles (vortices), respectively, and $\mathcal{E}$ is the total Coulomb energy among interacting quasi-particles. The correlation function $\langle\rho(0)\rho(\ell)\rangle$ decays at the distance

$$\ell \cong \ell_s \exp[\mathcal{E}/(2Ne^2)]. \tag{B.8}$$

This length is considered to be the size of a vortex (clump) in thermodynamical equilibrium. As the total interacting energy $\mathcal{E}$ becomes larger, the correlation length (clump size) becomes exponentially longer.

B.2. Propagating solitary structure

The other solution of interest is a solitary structure which moves with constant velocity. In an atmospheric application, a solution like a 'typhoon' has been obtained as

$$\phi(x,y,t) = \phi(\hat{y}) \quad \text{and} \quad \hat{y} = \sqrt{x^2 + (y - v_{**}t)^2} \tag{B.9}$$

with the asymptotic form

$$\phi(\zeta) \to \exp(-\hat{y}/\ell_s) \tag{B.10}$$

[B.5]. The drift-wave vortex, which has a similar form as Eq. (B.9), has also been obtained [B.6, B.7]. The vortex is either propagating in the direction of the ion diamagnetic drift (ion modon) or in the direction of the electron diamagnetic dirft (electron modon). The velocity of the drift-wave vortex (electron modon), v_{**}, is faster than the drift velocity V_d. Influences of drift-wave vortex on transport in nonlinear simulation have been discussed in, e.g., [B.8].

B.3. Comparison of cases for strong turbulence and thermodynamical equilibrium

In the usual thermodynamical-equilibrium statistics, the principle of 'minimum entropy production rate' is employed [B.9]. The cascade of enstrophy takes place in turbulence. In fluids, the cascade process is dominant in the inertial range and an ansatz of 'minimum enstrophy' was proposed. For the interaction of charged clumps (vortex, quasi-particle) in plasmas, an inverse cascade of energy and a cascade of enstrophy occur. The 'maximum energy/enstrophy' hypothesis is referred to for the thermodynamical-equilibrium limit.

The strong turbulence in plasmas is not in thermodynamical equilibrium. The strong pumping of fluctuation exists, and equipartition is not established. In case that the excitation and nonlinear damping balance, the power-law dependence

$$\langle\phi_k^2\rangle \propto k_\perp^{-6}, \quad \text{i.e.,} \quad \langle\mathcal{E}_k\rangle \propto k_\perp^{-3} \tag{B.11}$$

has been obtained in many cases (see, e.g., [4.13]). A principle for strong turbulence was proposed as the minimum of the effective potential $S(\mathcal{E})$, which is given as an integral of renormalized dissipation [Eq. (4.329)] as

$$S(\mathcal{E}) = \int_0^{\mathcal{E}} \frac{4\Lambda\mathcal{E}}{\mathcal{G}^2} d\mathcal{E}, \tag{B.12}$$

where Λ is the nonlinear damping rate of the dressed test mode (quasi-particle) and $\mathcal{G}^2 = \sum_k \mathcal{S}_k^2 k_\perp^4 \phi_k^2$ stands for the statistical noise-source term. The statistical noise-source term $\mathcal{G}^2$ is induced by the excited turbulent fluctuations. The instability mechanism and the turbulent decorrelation are included in the nonlinear damping rate Λ. It has been shown that the 'minimum of $S(\mathcal{E})$' reduces to the minimum of the entropy production rate, if one takes the thermodynamical-equilibrium limit of Eq. (B.11). The minimum principle for $S(\mathcal{E})$ is a generalization of the thermodynamical principle to the turbulence counterpart. The comparison between the statistical principle for turbulence and the principle of thermodynamical equilibrium is summarized in Table B1.

References

[B.1] Fyfe D and Montgomery D 1979 Phys. Fluids **22** 246

[B.2] Gang F Y et al. 1989 Phys. Fluids B **1** 1331

[B.3] Edwards S F and Taylor J B 1974 Proc. R. Soc. A **336** 257

[B.4] Ito N and Yoshida Z 1996 Phys. Rev. E **53** 5200

[B.5] Flierl G R et al. 1980 Dyn. Atmos. Oceans **5** 1

[B.6] Makino M, Kamimura T and Taniuti T 1981 J. Phys. Soc. Jpn. **50** 980

[B.7] Meiss J D and Horton C W 1983 Phys. Fluids **26** 990

[B.8] Koniges A E, Crotinger J A and Diamond P H 1992 Phys. Fluids B **4** 2785

[B.9] Prigogine I 1961 *Introduction to Thermodynamics of Irreversible Processes* 2nd ed. (Interscience Publishers, New York)

Table B.1. Principles of statistical theory for strong plasma turbulence are compared to the principles of thermodynamical equilibrium. (Example of CDIM/CDBM turbulence [4.98. 4.99, 4.365, 4.366].)

	Near Thermodynamical Equilibrium	**Far-Non-Equilibrium**
Basic assumption	Stosszahl Ansats; $1/\Omega$-expansion	Large number of degrees of freedom with positive Lyapunov exponents
Damping	Molecular viscosity $\gamma_c = \mu_c k_\perp^2$	Nonlinear (eddy) damping $\gamma_N \sim \tilde{\phi} k_\perp^2 / B$
Micro vs Macro	$\mu_{micro} = \mu_{macro}$ Onsager's Ansatz	Scale-dependent
Excitation		
(random)	Thermal excitation	Nonlinear drive
(coherent)	(none)	Instability drive
Decorrelation rate	γ_c	Nonlinear decorrelation λ_1
Balance	Fluctuation–dissipation (FD) theorem	Extended FD theorem
	Einstein's relation	$I \sim \frac{nonlinear\ noise}{nonlinear\ decorrelation}$
Partition	Equipartition $E_k \sim Tk$	Nonlinear Balance $E_k \sim \lvert\nabla p_0\rvert k^{-3}$
Probability density function	Boltzmann $P(\mathcal{E}) \sim \exp[-\mathcal{E}/(k_B T)]$	Integral of renorm. dissipation $P(\mathcal{E}) \sim \exp[-S(\mathcal{E})]/g$ power-law tail
Min. / Max. principle	Maximum entropy/ Minimum entropy-production rate	$S(\mathcal{E})$ minimum
Phase boundary	Maxwell's construction	$S(\mathcal{E}_A) = S(\mathcal{E}_B)$
Transition probability	$\ln(K) \sim -\Delta Q/T$ Arrhenius law	$K \propto \exp[-S(\mathcal{E}_{saddle})]$ power law
Transport matrix	Onsager's symmetry	Not necessarily symmetric
Interface of fluxes	Curie's principle	Interfaces between heat, particles, and momentum
Transport coefficients	Independent of gradient	Depend on gradient

C. Clumps

The contribution of ballistic terms in the response function is discussed in [4.57, 4.58, C.1, C.2]. A brief explanation of the concept is made after ref. [4.58]. A more thorough survey of the clump theories is given in [1.34].

In deriving Eq. (A.2) from Eq. (A.1), the wavelike solution of the linearlized Vlasov equation has been substituted. However, the solution of the linearlized equation

$$[(\partial/\partial t) + \mathbf{v}\cdot\nabla]\tilde{f} = -(ie/m)\tilde{\phi}[\mathbf{k}\cdot(\partial/\partial\mathbf{v})]\bar{f}$$

is a sum of the wavelike solution and that of the homogeneous equation as

$$\tilde{f} = \frac{e}{m}\frac{\tilde{\phi}}{\omega - \mathbf{k}\cdot\mathbf{v}}\mathbf{k}\cdot\frac{\partial}{\partial\mathbf{v}}\bar{f} + \tilde{f}_{\mathrm{cl}}, \tag{C.1}$$

where $\tilde{f}_{\mathrm{cl}}$ is a solution of the homogeneous equation

$$(\omega - \mathbf{k}\cdot\mathbf{v})\tilde{f}_{\mathrm{cl}} = 0.$$

Here, the suffix cl denotes clump. The self-consistent electric field that is induced by this clump is

$$\tilde{\phi} = \frac{-1}{\varepsilon}\frac{e}{\varepsilon_0 k^2}\int dv\tilde{f}_{\mathrm{cl}}, \tag{C.2}$$

where ε is the dielectric constant [see Eq. (4.34)]. The clump in the phase space $\tilde{f}_{\mathrm{cl}}$ and this induced electric field cooperatively introduce the evolution of the averaged distribution function. Substituting Eqs. (C.1) and (C.2) into Eq. (A.1), one has

$$\frac{\partial}{\partial t}\bar{f} = \frac{e^2}{m^2}\int\left(\frac{e}{\varepsilon\varepsilon_0 k}\right)^2\mathbf{k}\cdot\frac{\partial}{\partial\mathbf{v}}H\left[\bar{f}(\mathbf{v}),\bar{f}(\mathbf{v}')\right]d\mathbf{v}'d\mathbf{v}''d\mathbf{k}d\omega, \tag{C.3}$$

$$\begin{aligned} H\left[\bar{f}(\mathbf{v}),\bar{f}(\mathbf{v}')\right] = \Bigg[&\left\langle\tilde{f}_{\mathrm{cl}}(\mathbf{v}')\tilde{f}^*_{\mathrm{cl}}(\mathbf{v}'')\right\rangle_{k\omega}\delta(\omega - \mathbf{k}\cdot\mathbf{v})\mathbf{k}\cdot\frac{\partial}{\partial\mathbf{v}}\bar{f}(\mathbf{v}) \\ &-\left\langle\tilde{f}_{\mathrm{cl}}(\mathbf{v}'')\tilde{f}^*_{\mathrm{cl}}(\mathbf{v})\right\rangle_{k\omega}\delta(\omega - \mathbf{k}\cdot\mathbf{v}')\mathbf{k}\cdot\frac{\partial}{\partial\mathbf{v}'}\bar{f}(\mathbf{v}')\Bigg] \end{aligned} \tag{C.4}$$

with the two-point correlation function

$$\begin{aligned} &\left\langle\tilde{f}_{\mathrm{cl}}(\mathbf{r}+\mathbf{r}',\mathbf{v}',t+\tau)\tilde{f}_{\mathrm{cl}}(\mathbf{r},\mathbf{v},t)\right\rangle \\ &\quad = \int\left\langle\tilde{f}_{\mathrm{cl}}(\mathbf{v})\tilde{f}_{\mathrm{cl}}(\mathbf{v}')\right\rangle_{k\omega}\exp(i\mathbf{k}\cdot\mathbf{r}' - i\omega\tau)d\mathbf{k}d\omega. \end{aligned} \tag{C.5}$$

This contribution of clumps in Eq. (C.3) could contribute to the relaxation in the non-wave region where the dielectric constant ε does not vanish. The correlation of the clumps is proportional to $\delta(\omega - \mathbf{k}\cdot\mathbf{v})$, and remains finite in a small interval $\Delta r\Delta v$ in

the phase space. The interval must satisfy $\Delta r \ll v_{\rm th}/\omega_{\rm p}$ and $\Delta v \ll v_{\rm th}$. The correlation relation is approximated as

$$\left\langle \tilde{f}_{\rm cl}(\mathbf{v})\tilde{f}_{\rm cl}(\mathbf{v}')\right\rangle_{k\omega} = A(\Delta r \Delta v)^3 \delta(\omega - \mathbf{k}\cdot\mathbf{v})\delta(\mathbf{v}-\mathbf{v}'), \tag{C.6}$$

where A is an amplitude given by the initial condition. Notice that the enhancement factor $Q^2 \equiv (\Delta r \Delta v)^3$ indicates that the contribution of the relaxation is due to a macro particle with charge Qe. Since the binary collision frequency is proportional to the square of the charge of particle, the formation of the clump is influential in accelerating the relaxation.

An example is the case where an initial distribution function is given by such a model that $\bar{f} = 1$ if $\bar{f} \neq 0$ (like a spinodal decomposition) [4.58]. With this initial condition, the coefficient A is approximated as $A = (1-\bar{f})\bar{f}$. An accelerated relaxation to the Fermi distribution is shown. It has been pointed out that the interactions with collective modes can give rise to a high energy tail. Also note that the initial memory of the clump decays in time. Therefore the acceleration of the relaxation is effective when the initial distribution function deviates substantially from the equilibrium distribution function.

A quantitative analysis has been developed for the study of the clump correlation function in, e.g., [4.269, C.1 - C.3]. The method of deriving the two-point correlation has been extended to pressure-driven turbulence, e.g., [4.45, 4.75, 4.138, 4.253]. More extensive discussion on the clump algorithm as applied to fluid problems is given in [1.34].

References

[C.1] Dupree T H 1972 Phys. Fluids **15** 334
[C.2] Dupree T H 1983 Phys. Fluids **26** 2460
[C.3] Boutros-Ghali T, Dupree T H 1981 Phys. Fluids **24** 1839

D. Rigorous upper bounds for transport

In some cases, a rigorous upper bound for the turbulent transport can be obtained. The analysis of an upper bound has been explored in, e.g., [4.67, 4.78, D.1, D.2]. A brief survey of the concept is explained here; details are given in [1.34]. Let us take an equation of, say, temperature

$$\left(\frac{\partial}{\partial t}+\tilde{u}\frac{\partial}{\partial x}-\chi_{\rm c}\frac{\partial^2}{\partial x^2}\right)T(x,t)=0 \tag{D.1}$$

where $\tilde{u}$ is a turbulent velocity field and $\chi_{\rm c}$ stands for the molecular thermal diffusivity that is caused by binary particle collisions. The total flux $Q_{\rm tot}$ is composed of the turbulent transport Q and by the collisional transport $Q_{\rm c}$ as $Q_{\rm tot}=Q+Q_{\rm c}$, where $Q=\langle\tilde{u}T(x,t)\rangle$ and $Q_{\rm c}=-\chi_{\rm c}(\partial/\partial x)T$ hold.

When the statistics of the turbulent velocity field $\tilde{u}$ are specified, being independent of the response of the temperature fluctuation, the problem is called passive. When the dynamics of $\tilde{u}$ is determined by the dynamics of plasmas or fluids (e.g., through the MHD equations or the Navier–Stokes equation), the problem is called self-consistent.

The structure of the theory is explained by taking an example from the passive problem, following [4.67]. The system of Eq. (D.1) may be normalized as follows: length to L (the distance between the two boundaries), temperature to ΔT (the temperature difference between the two boundaries), fluctuating velocity to the average $\bar{\tilde{u}}=\langle\tilde{u}^2\rangle^{1/2}$, and time to $\tau_{\rm L}=L/\bar{\tilde{u}}$ (the macroscopic eddy-turnover time). Under this normalization, the characteristic parameters are the Reynolds number Re and the Kubo number $\mathcal{K}$, which are given as

$$Re=\bar{\tilde{u}}L/\chi_{\rm c}\quad\text{and}\quad\mathcal{K}=\bar{\tilde{u}}\tau_{\rm ac}/L, \tag{D.2}$$

where $\tau_{\rm ac}$ is the auto-correlation time of the fluctuating filed $\tilde{u}$. In a passive problem, Re and $\mathcal{K}$ are given parameters.

The maximum of the possible turbulent flux is discussed with the boundary condition $Q(0)=Q(1)=0$. As is discussed in §4.1.4 [e.g., Eqs. (4.48) and (4.49)], a quadratic form in perturbed quantities can be obtained from Eq. (D.1). The space average like $\overline{\overline{Q}}=\int_0^1 dxQ(x)$ is employed. In a stationary state, one has

$$\overline{\overline{-Q(x)\frac{\partial}{\partial x}\langle T(x)\rangle}}=Re^{-1}\overline{\overline{\left(\frac{d\delta T}{dx}\right)^2}} \tag{D.3}$$

where the deviation of temperature profile is denoted as $\delta T(x)$, with respect to which the turbulence-driven flux Q is maximized. Equation (D.3) is rewritten as

$$\overline{\overline{Q}}=Re\overline{\overline{\left(Q-\overline{\overline{Q}}\right)^2}}+Re^{-1}\overline{\overline{\left(\frac{d\delta T}{dx}\right)^2}}. \tag{D.4}$$

The variational principle is stated as:

$$\begin{aligned} &\text{Maximize the functional } \overline{\overline{Q}}[\delta T] \\ &\quad \text{subject to the constraint, Eq. (D.4).} \end{aligned} \tag{D.5}$$

This maximum principle is well-posed. One has the Schwartz inequality

$$\overline{\overline{Q}} = \overline{\overline{\langle \delta u \delta T \rangle}} \leq \overline{\overline{\langle \delta u^2 \rangle^{1/2}}}\ \overline{\overline{\langle \delta T^2 \rangle^{1/2}}}.$$

That is, the left-hand side of Eq. (D.4) is linear (at most) in the temperature perturbation, while the right-hand side of Eq. (D.4) is quadratic. The constraint Eq. (D.4) bounds the domain of δT, and confirms the presence of the upper-bound of the left-hand side, $\overline{\overline{Q}}[\delta T]$.

Several cases has been studied [4.67]. In the limit of large Kubo number, $\mathcal{K} \to \infty$, i.e., the perturbation is static, the upper bound of the flux is given as

$$\overline{\overline{Q}}_{\rm ub} = \overline{\overline{Q}}_{\infty}(Re) = Re^{-1}\left[\frac{1}{2} Re \coth\left(\frac{1}{2} Re\right) - 1\right]. \tag{D.6}$$

In the limit of small Kubo number (i.e., very short auto-correlation time of fluctuations), the result is obtained as $\overline{\overline{Q}} = \overline{\overline{Q}}_{\rm ql}(\mathcal{K})$. It was pointed out that in order to achieve proper quasi-linear scaling, a two-time constraint is necessary in addition to the constraint, Eq. (D.4). See [4.67] for details. An upper bound is given for an arbitrary Kubo number as

$$\overline{\overline{Q}}_{\rm ub} = \frac{\overline{\overline{Q}}_{\rm ql}(\mathcal{K})\overline{\overline{Q}}_{\infty}(Re)}{\overline{\overline{Q}}_{\rm ql}(\mathcal{K}) + \overline{\overline{Q}}_{\infty}(Re)}. \tag{D.7}$$

Application has also been made to a self-consistent problem in plasma turbulence theories. The MHD equation has been analyzed for the turbulent resistivity of the reversed-field pinch (RFP), and an upper bound for the volume-averaged turbulent resistivity $\eta^{\rm ub}_{\rm turb}$ has been obtained [D.2]. An energy-stability criterion for the turbulence, below which $\eta^{ub}_{\rm turb} = 0$ holds, i.e., any (subcritical as well as supercritical excitation) perturbation is predicted to decay in time, is also obtained.

References

[D.1] Busse F H 1978 Adv. Appl. Mech. **18** 77

[D.2] Krommes J A 1990 Phys. Fluids B **2** 1331

Recent Issues of NIFS Series

NIFS-668 T Muton, R Kumazawa, T Seki, K Saito, Y Torii, F Shimpo, G Nomura, T Watari, D A Hartmann, M Yokota, K Akaishi, N Ashikawa, P deVries, M Emoto, H Funaba, M Goto, K Ida, H Idei, K Ikeda, S Inagaki, N Inoue, M Isobe, O Kaneko, K Kawahata, A Komori, T Kobuchi, S Kubo, S Masuzaki, T Morisaki, S Morita, J Miyazawa, S Murakami, T Minami, S Muto, Y Nagayama, Y Nakamura, H Nakanishi, K Narihara, N Noda, K Nishimura, K Ohkubo, N Ohyabu, S Ohdachi, Y Oka, M Osakabe, T Ozaki, B J Peterson, A Sagara, N Sato, S Sakakibara, R Sakamoto, H Sasao, M Sasao, M Sato, T Shimozuma, M Shoji, S Sudo, H Suzuki, Y Takeiri, K Tanaka, K Toi, T Tokuzawa, K Tsumori, K Y Watanabe, T Watanabe, H Yamada, I Yamada, S Yamaguchi, K Yamazaki, M Yokoyama, Y Yoshimura, Y. Hamada, O Motojima, M Fujiwara,
Fast- and Slow-Wave Heating of Ion Cyclotron Range of Frequencies in the Large Helical Device: Nov 2000

NIFS-669 K Mima, M S Jovanovic, Y Sentoku, Z-M Sheng, M M Skoric and T Sato,
Stimulated Photon Cascade and Condensate in Relativistic Laser-plasma Interaction Nov 2000

NIFS-670 L Hadzievski, M.M Skoric and T Sato,
On Origin and Dynamics of the Discrete NLS Equation Nov 2000

NIFS-671 K Ohkubo, S Kubo, H Idei, T Shimozuma, Y Yoshimura, F Leuterer, M Sato and Y Takita,
Analysis of Oversized Sliding Waveguide by Mode Matching and Multi Mode Network Theory Dec 2000

NIFS-672 C Das, S Kida and S Goto,
Overall Self-Similar Decay of Two-Dimensional Turbulence Dec 2000

NIFS-673 L A Bureyeva, T Kato, V S Lisitsa and C Namba
Quasiclassical Representation of Autoionization Decay Rates in Parabolic Coordinates Dec 2000

NIFS-674 L A Bureyeva, V S Lisitsa and C Namba,
Radiative Cascade Due to Dielectronic Recombination Dec 2000

NIFS-675 M FHeyn, S V Kasilof, W Kernbichler, K Matsuoka, V V Nemov, S Okamura, O S. Pavlichenko,
Configurational Effects on Low Collision Plasma Confinement in CHS Heliotron/Torsatron, Jan 2001

NIFS-676 K Itoh
A Prospect at 11th International Toki Conference - Plasma physics, quo vadis? Jan 2001

NIFS-677 S Satake, H Sugama, M Okamoto and M Wakatani,
Classification of Particle Orbits near the Magnetic Axis in a Tokamak by Using Constants of Motion, Jan 2001

NIFS-678 M Tanaka and A Yu Grosberg,
Giant Charge Inversion of a Macroion Due to Multivalent Counterions and Monovalent Coions Molecular Dynamics Studyn, Jan 2001

NIFS-679 K. Akaishi, M Nakasuga, H Suzuki, M Iima, N Suzuki, A Komori, O Motojima and Vacuum Engineering Group,
Simulation by a Diffusion Model for the Variation of Hydrogen Pressure with Time between Hydrogen Discharge Shots in LHD, Feb 2001

NIFS-680 A Yoshizawa, N Yokoi, S Nisizima, S -I Itoh and K Itoh
Variational Approach to a Turbulent Swirling Pipe Flow with the Aid of Helicity, Feb 2001

NIFS-681 Alexander A Shishkin
Estafette of Drift Resonances, Stochasticity and Control of Particle Motion in a Toroidal Magnetic Trap, Feb 2001

NIFS-682 H Momota and G H Miley,
Virtual Cathode in a Spherical Inertial Electrostatic Confinement Device, Feb 2001

NIFS-683 K Saito, R Kumazawa, T Mutoh, T Seki, T Watari, Y Torii, D A Hartmann, Y Zhao, A Fukuyama, F Shimpo, G Nomura, M Yokota, M Sasao, M Isobe, M Osakabe, T Ozaki, K Narihara, Y Nagayama, S Inagaki, K Itoh, S Morita, A V Krasilnikov, K Ohkubo, M Sato, S Kubo, T Shimozuma, H. Idei, Y Yoshimura, O Kaneko, Y Takeiri, Y Oka, K Tsumori, K Ikeda, A Komori, H Yamada, H Funaba, K Y Watanabe, S Sakakibara, M Shoji, R Sakamoto, J Miyazawa, K Tanaka, B J Peterson, N Ashikawa, S Murakami, T Minami, S Ohakachi, S Yamamoto, S Kado, H Sasao, H Suzuki, K Kawahata, P deVries, M Emoto, H Nakanishi, T Kobuchi, N Inoue, N Ohyabu, Y Nakamura, S Masuzaki, S Muto, K Sato, T Morisaki, M Yokoyama, T Watanabe, M Goto, I Yamada, K Ida, T Tokuzawa, , N Noda, S Yamaguchi, K Akaishi, A Sagara, K Toi, K Nishimura, K Yamazaki, S Sudo, Y Hamada, O Motojima, M Fujiwara,
Ion and Electron Heating in ICRF Heating Experiments on LHD Mar 2001

NIFS-684 S Kida and S Goto
Line Statistics Stretching Rate of Passive Lines in Turbulence Mar 2001

NIFS-685 R Tanaka, T Nakamura and T. Yabe,
Exactly Conservative Semi-Lagrangian Scheme (CIP-CSL) in One-Dimension Mar 2001

NIFS-686 S Toda and K Itoh,
Analysis of Structure and Transition of Radial Electric Field in Helical Systems Mar 2001

NIFS-687 T Kuroda and H. Sugama,
Effects of Multiple-Helicity Fields on Ion Temperature Gradient Modes Apr 2001

NIFS-688 M Tanaka,
The Origins of Electrical Resistivity in Magnetic Reconnection Studies by 2D and 3D Macro Particle Simulations Apr 2001

NIFS-689 A Maluckov, N Nakajima, M Okamoto, S Murakami and R Kanno,
Statistical Properties of the Neoclassical Radial Diffusion in a Tokamak Equilibrium. Apr 2001

NIFS-690 Y Matsumoto, T Nagaura, Y Itoh, S-I Okawa and T Watanabe
LHD Type Proton-Boron Reactor and the Control of its Peripheral Potential Structure Apr 2001

NIFS-691 A Yoshizawa, S -I Itoh, K Itoh and N Yokoi,
Turbulence Theories and Modelling of Fluids and Plasmas Apr 2001